Consideration of high-order boundary conditions and numerical analysis of diffusion problems on curved meshes using high-order finite elements.

Joyce Ghantous

UNIVERSITÉ DE PAU ET DES PAYS DE L'ADOUR

THÈSE DE DOCTORAT EN MATHÉMATIQUES

Par

Joyce Ghantous

Prise en compte de conditions aux bords d'ordre élevé et analyse numérique de problèmes de diffusion sur maillages courbes à l'aide d'éléments finis d'ordre élevé

ÉCOLE DOCTORALE N° 211
Sciences Exactes et ses Applications
Thèse présentée et soutenue à Pau, le 23 septembre 2024

Unité de recherche : LMAP - UMR CNRS 5142

Composition du jury :

Président :	Julien Diaz	Directeur de Recherche, INRIA Bordeaux Sud-Ouest
Rapporteurs :	Thomas Ranner	Lecturer, University of Leeds
	Stéphanie Salmon	Professeure des Universités, Université de Reims Champagne-Ardenne
Examinateurs :	Claire Chainais-Hillairet	Professeure des Universités, Université de Lille
	Alexandre Ern	Professeur des Universités, École des Ponts
	Flore Nabet	Maîtresse de Conférences, École polytechnique
Directeurs de thèse :	Fabien Caubet	Maître de Conférences HDR, Université de Pau et des Pays de l'Adour
	Charles Pierre	Ingénieur de Recherche CNRS, Université de Pau et des Pays de l'Adour

Acknowledgement

I would like to extend my deepest gratitude to my PhD supervisors, Charles and Fabien, whose guidance, wisdom, and unwavering support have been instrumental in the completion of this work. Your mentorship has been inspiring, and I will forever be thankful for the opportunities and insights you have provided. I also wish to sincerely thank my friends and colleagues, whose encouragement and camaraderie made this journey more fulfilling and joyful. To my family, your constant love and belief in me have been my greatest source of strength. Without your support, this achievement would not have been possible. Thank you for being by my side every step of the way.

To my dearest sister, Jessica, words cannot fully express how grateful I am for your unwavering love and support throughout this journey. You have been my constant source of strength, always ready with words of encouragement or simply a listening ear when I needed it most. Your belief in me, even during times when I doubted myself, has meant more than you'll ever know. Thank you for standing by me, for celebrating my victories, and for lifting me up when the challenges seemed insurmountable. This achievement is as much yours as it is mine, and I'm so blessed to have you in my life.

Table of Contents

INTRODUCTION GÉNÉRALE

Cette thèse de doctorat s'inscrit dans le domaine des mathématiques connu sous le nom de **l'analyse numérique**. Plus précisément, dans ce qui suit, nous nous concentrerons sur l'analyse d'erreur des **Equations aux Dérivées Partielles (EDP) avec des conditions aux limites d'ordre élevé**. Tout au long de cette introduction, nous tenterons de répondre aux questions suivantes :

1. dans un contexte général, quelles sont les principales étapes dans une analyse d'erreur ? Et quels sont les outils mathématiques utilisés ?
2. quelles sont les motivations derrière le choix des problèmes étudiés dans cette thèse ?
3. quelles sont les nouvelles étapes à suivre pour prendre en compte la complexité des problèmes étudiés dans le contexte de cette thèse ?
4. l'obtention d'une estimation d'erreur pour un problème n'est pas un nouveau défi, ce qui soulève la question de ce qui distingue cette thèse des travaux précédemment réalisés sur ce sujet : qu'apporte-t-elle de nouveau à la littérature existante ?

Nous procéderons par étapes en répondant à ces questions dans leur ordre respectif.

Les éléments essentiels d'une analyse d'erreur dans un cadre général

Généralement, nous considérons un problème bien posé ayant une solution unique que nous cherchons à approximer. La méthode traditionnelle est de **discrétiser le domaine**, de **choisir une méthode numérique** pour approcher la solution et enfin de **calculer la différence entre la solution exacte et son approximation**.

Définition d'un maillage. Suivant la définition 1.49 dans [45], soit Ω un domaine borné dans $\mathbb{R}^d$ $(d = 2, 3)$. On définit un **maillage** comme une union d'un nombre fini N d'ensembles compacts, connexes et lipschitzien avec un intérieur non vide tel

que $\{T_m\}_{m=1}^N$ forme une partition de Ω, c'est-à-dire,

$$\bar{\Omega} = \bigcup_{m=1}^{N} T_m \quad \text{et} \quad \overset{\circ}{T}_m \cap \overset{\circ}{T}_n = \emptyset \quad \text{pour} \quad m \neq n.$$

Les sous-ensembles T_m sont appelés les **éléments du maillage** ou les **cellules du maillage** (ou simplement **éléments** lorsqu'il n'y a pas d'ambiguïté).

Tout au long de ce travail, nous considérons des éléments simpliciaux, c'est-à-dire des **triangles** en 2D et des **tétraèdres** en 3D, comme illustré dans la figure 2.3. De plus, dans la section suivante, nous donnerons la définition des **éléments courbes**, que nous allons utiliser dans cette thèse.

Figure 1 – Représentation d'un élément de maillage triangulaire en 2D et d'un élément de maillage tétraédrique en 3D.

La méthode des éléments finis. La méthode des éléments finis est une approche numérique utilisée pour obtenir des solutions approchées pour des problèmes de type EDP. Elle est utilisée en ingénierie, physique et mathématiques appliquées pour résoudre des problèmes complexes de mécanique des structures, de mécanique des fluides, de transfert de chaleur, etc. Les origines de cette méthode remontent aux années 1950 ([8]) lorsque des ingénieurs ont commencé à résoudre numériquement des problèmes de mécanique des structures en aéronautique. Nous faisons aussi référence à [45, 20, 32, 30, 79, 60] pour plus de détails sur la méthode des éléments finis. En utilisant cette méthode, nous pouvons établir une estimation de l'erreur produite lors de l'approximation de la solution d'un problème noté u, typiquement une EDP, par son approximation par éléments finis notée u_h.

Tout au long de ce travail, nous utiliserons **la méthode des éléments finis de Lagrange** $\mathbb{P}^k$, avec un degré $k \geq 1$.

Estimation d'erreur. Il existe deux types d'estimation d'erreur : les estimations a priori et les estimations a posteriori. L'objectif d'une **estimation d'erreur a priori** est d'évaluer l'erreur $\|u-u_h\|$ dans une norme donnée par rapport au pas du maillage h, aux données du problème et à la solution exacte u (voir, par exemple, [45, 20, 61]). En revanche, une estimation a posteriori dépend de h et de la solution calculée u_h, mais pas de u (voir par exemple [1, 55]). L'analyse d'erreur a priori est principalement orientée vers la qualification théorique, tandis que l'analyse d'erreur a posteriori est plus à visée pratique.

À partir de maintenant, nous nous concentrerons sur les estimations d'erreur a priori.

Motivation des problèmes étudiés

Motivation. Dans cette thèse, nous nous concentrerons sur l'obtention d'estimations d'erreur a priori d'une EDP avec des conditions aux limites d'ordre élevé. En effet, ce travail fait partie du programme de recherche RODAM [1], qui étudie des problèmes d'optimisation de forme (voir, par exemple, [59, 3] pour des généralités sur l'optimisation de forme) en mécanique des structures dans un contexte industriel. En particulier, une des thématiques concerne l'étude des propriétés vibratoires de structures élastiques entourées par une **couche mince** (qui peut provenir d'un traitement de surface ou d'une couche de corrosion, par exemple). L'objectif principal est d'utiliser l'optimisation de forme pour améliorer la structure de ces pièces mécaniques en vue de réduire leur masse tout en conservant leurs propriétés mécaniques.

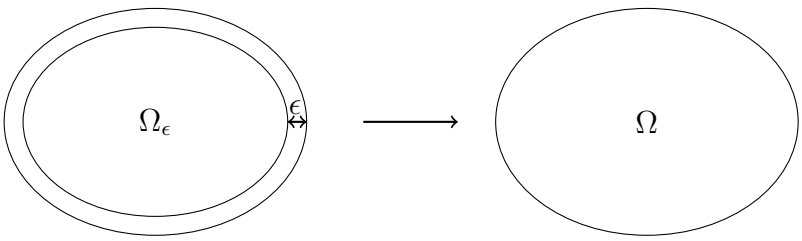

Figure 2 – Approximation d'un domaine ayant une couche mince l'entourant (à gauche) par un domaine équipé de conditions aux limites d'ordre élevé (à droite).

D'un point de vue numérique, la prise en compte des couches minces autour d'un

1. *Robust Optimal Design under Additive Manufacturing constraints*: `https://lma-umr5142.univ-pau.fr/en/scientific-activities/scientific-challenges/rodam.html`

domaine, comme illustré dans la figure 2, présente des défis particuliers, notamment la discrétisation du domaine qui nécessite un maillage adapté avec un pas de maillage réduit dans la couche mince. Afin d'éviter cette difficulté, le domaine et la solution du problème considéré peuvent être approchés à l'aide d'un développement asymptotique : ainsi la couche mince est modélisée par des conditions aux limites adaptées (voir par exemple [17, 16, 77, 54, 52]). Plus précisément, le domaine approché n'est plus entouré par une couche mince ; à la place, il est muni de conditions aux limites du second ordre appelées **conditions de Ventcel**, également connues sous le nom de **conditions de Robin généralisées**. Ces conditions découlent des travaux pionniers de Ventcel dans [75, 76] et sont également étudiées dans le contexte des problèmes de diffusion autour d'obstacles, comme décrit dans [18]. De plus, la prise en compte des couches minces est essentielle en aéroacoustique, où les conditions aux limites d'Ingard-Myers sont utilisées pour modéliser la présence d'un matériau absorbant sur la surface d'un conduit (voir [66]). Nous mentionnons enfin les travaux dans [64] qui étudient l'analyse numérique de problèmes paraboliques avec des conditions aux limites dynamiques.

Pour donner une idée de la définition de ces conditions aux limites, nous considérons l'équation de Poisson dans le cadre scalaire : dans ce cas, les conditions aux limites de Ventcel sont données par,

$$-\Delta_\Gamma u + \partial_{\mathrm{n}} u + u = 0 \quad \text{sur } \partial\Omega,$$

où $\partial_{\mathrm{n}} u$ est la dérivée normale d'une solution u et où Δ_Γ est l'**opérateur de Laplace-Beltrami**. Cet opérateur d'ordre deux, également connu sous le nom de **laplacien tangentiel**, est défini comme suit pour toute fonction suffisamment régulière u,

$$\Delta_\Gamma u := \mathrm{div}_\Gamma(\nabla_\Gamma u),$$

où ∇_Γ est le gradient tangentiel et div_Γ est la divergence tangentielle définie dans la Définition 1.1.1 ci-dessous. Pour plus de détails, nous faisons référence à [59].

Les problèmes étudiés. Le problème physique d'origine visant à étudier les propriétés vibratoires des structures mécaniques est d'abord simplifié en considérant des **problèmes de diffusion scalaires** avant de passer à l'étude du problème dans le cadre de l'**élasticité linéaire vectorielle**. Nous présentons les trois problèmes étudiés dans cette thèse.

Soit Ω un domaine borné, non vide et connexe de $\mathbb{R}^d$, où $d = 2$ ou 3, avec un bord lisse $\Gamma := \partial\Omega$, et soient α, $\beta > 0$. Le chapitre 1 présente les trois systèmes étudiés équipés des **conditions de Ventcel**, donnés comme suit.

1. Dans le cas scalaire, nous considérons d'abord le problème classique avec des termes sources avant d'étudier le problème spectral :
   — le *problème de Poisson-Ventcel*,

$$\begin{cases} -\Delta u + \kappa u &= f \quad \text{dans } \Omega, \\ -\beta\Delta_\Gamma u + \partial_{\mathrm{n}} u + \alpha u &= g \quad \text{sur } \Gamma, \end{cases} \tag{1}$$

   où f et g sont des termes sources suffisamment réguliers et $\kappa \geq 0$;
   — le *problème spectral avec des conditions aux limites de Ventcel,*

$$\begin{cases} -\Delta u = \lambda u \quad \text{dans } \Omega, \\ -\beta\Delta_\Gamma u + \partial_{\mathrm{n}} u + \alpha u = 0 \quad \text{sur } \Gamma. \end{cases} \tag{2}$$

2. Dans le cas vectoriel, nous considérons le *problème d'élasticité linéaire avec des conditions aux limites de Ventcel*,

$$\begin{cases} -\mathrm{div}(\mathbf{A}_\Omega e(\boldsymbol{u})) = \boldsymbol{f} \quad \text{dans } \Omega, \\ -\beta\mathrm{div}_\Gamma(\mathbf{A}_\Gamma e_\Gamma(\boldsymbol{u})) + \mathbf{A}_\Omega e(\boldsymbol{u})\mathbf{n} + \alpha\boldsymbol{u} = \boldsymbol{g} \quad \text{sur } \Gamma, \end{cases} \tag{3}$$

   où $\boldsymbol{f}$ et $\boldsymbol{g}$ sont des termes sources suffisamment réguliers, où $\mathbf{A}_\Omega$ et $\mathbf{A}_\Gamma$ sont des *tenseurs de Hooke* et où $e(\boldsymbol{u})$ et $e_\Gamma(\boldsymbol{u})$ sont des *tenseurs de déformation* (voir la section 1.2 pour des détails).

Sous des hypothèses adéquates, ces trois problèmes sont bien posés : le problème (1) (resp. le problème (3)) admet une solution unique u (resp. $\boldsymbol{u}$) et le problème spectral (2) admet un nombre infini de valeurs propres positives, de multiplicités finies, formant une suite croissante qui tend vers l'infini.

Difficultés techniques dans l'analyse d'erreur des problèmes de Ventcel. L'objectif principal est d'établir une analyse d'erreur des problèmes définis précédemment, en suivant les étapes principales présentées ci-dessus : en particulier, on discrétisera le domaine considéré et on utilisera la méthode des éléments finis pour approximer la solution exacte des problèmes continus.

Afin que les conditions d'ordre deux précédentes aient un sens, le domaine considéré doit être supposé lisse. En effet, cette hypothèse de régularité est imposée pour pouvoir appliquer la formule d'intégration par parties sur la frontière du domaine dans le chapitre 1 pour obtenir les formulations variationnelles des problèmes considérés. Ainsi, nous faisons face à des problèmes où le domaine physique et le domaine du maillage diffèrent, impliquant ainsi une **erreur géométrique** intrinsèque, comme détaillé ci-après.

Les outils mathématiques fondamentaux utilisés pour traiter les problèmes de Ventcel

L'analyse d'erreur de chacun des trois problèmes de Ventcel exposés ci-dessus présente ses propres difficultés. Cependant, ils ont tous une difficulté en commun : le domaine physique Ω a un bord lisse et ne peut pas être exactement recouvert par un maillage. Cela implique les deux principaux problèmes suivants :

— (P1) : un écart entre Ω et le domaine du maillage est mis en avant. Cette différence est appelée l'**erreur géométrique**. **Comment pouvons-nous réduire cette erreur ?**

— (P2) : les fonctions discrètes appartenant à l'espace des éléments finis sont définies sur le domaine du maillage, qui diffère du domaine physique. Cela soulève la question suivante : **comment pouvons-nous estimer l'erreur entre la solution exacte et la solution discrète, qui ne sont pas définies sur le même domaine ?**

Solution de (P1) : les maillages courbes. Pour réduire l'erreur géométrique, nous utiliserons des **maillages courbes**, notés $\mathcal{T}_h^{(r)}$, avec un **ordre géométrique** $r \geq 1$. Ces maillages ont été étudiés et définis dans de nombreux travaux tels que [32, 33, 42, 43]. Cependant, l'utilisation de maillages courbes d'ordre r n'implique pas que l'écart entre le domaine Ω et le domaine du maillage noté $\Omega_h^{(r)}$ est nul. La seule chose que nous pouvons espérer est que plus l'ordre géométrique du maillage r est élevé, plus l'erreur géométrique va diminuer. Par conséquent, en utilisant des maillages courbes, nous visons à améliorer le comportement asymptotique de l'erreur totale, qui dépend partiellement de l'erreur géométrique, par rapport au pas du maillage h. Au chapitre 2,

la définition des maillages courbes est détaillée avec des exemples explicatifs en 2D et en 3D.

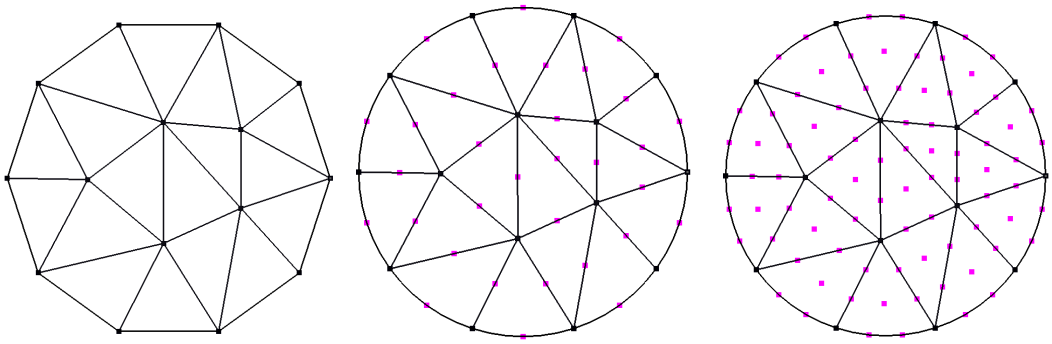

Figure 3 – Un maillage linéaire ($r = 1$), un maillage quadratique ($r = 2$) et un maillage cubique ($r = 3$) du disque unité.

Dans la figure 3, sont respectivement affichés un maillage linéaire ($r = 1$), un maillage quadratique ($r = 2$) et un maillage cubique ($r = 3$) du disque unité. Tous ces maillages ne correspondent pas exactement au disque unité, même si nous ne voyons aucune différence entre le disque et le domaine du maillage quadratique (resp. cubique) : le cercle ne peut pas être paramétré localement à l'aide de polynômes. Dans la littérature, il est connu qu'un élément de maillage linéaire est construit à l'aide d'une transformation affine et à partir du triangle de référence (voir par exemple [33, 32]). Les maillages courbes sont quant à eux construits à l'aide d'une transformation polynomiale $F_T^{(r)}$ de degré r, définie au chapitre 2. Nous soulignons qu'en 2D, un élément de maillage affine possède 3 nœuds (les 3 sommets du triangle), un élément quadratique possède 6 nœuds (les 3 sommets du triangle et les 3 points milieux des arêtes) et un élément cubique possède 10 nœuds (les 3 sommets du triangle, les 6 points sur les arêtes et le centre du triangle).

Il faut noter que, dans l'analyse d'erreur à venir, les maillages quadratiques se comportent comme si $r = 3$ et présentent une **super-convergence** : en effet, sur ces maillages, les erreurs présentent de meilleurs ordres de convergence que prévu, ayant des valeurs similaires à celles obtenues dans le cas cubique. Une observation similaire est mise en avant dans l'analyse d'erreur du problème spectral de l'opérateur de Laplace-Beltrami sur une surface dans [15] en 2018. Même si aucune explication théorique n'est encore donnée, nous avons remarqué que cette super-convergence n'est

pas liée au problème ni au domaine considéré. Une étude numérique approfondie est présentée dans la section 4.4, sur diverses géométries en 2D et 3D.

Par ailleurs, dans toutes les simulations numériques présentées dans cette thèse, les erreurs numériques sur les maillages cubiques présenteront une perte dans l'ordre de convergence. Une étude est alors faite dans la section 4.5, conduisant à la conclusion suivante : ce défaut est lié à l'erreur d'interpolation des éléments finis.

Solution de (P2) : l'opérateur de lift. La solution pour estimer l'erreur entre la solution exacte et la solution discrète (qui ne sont pas définies sur le même domaine) est la première nouveauté présentée dans ce manuscrit : l'**opérateur de lift**. Cet opérateur nous permet de *lifter* (ou de relever) une fonction définie sur le domaine du maillage $\Omega_h^{(r)}$ pour la définir sur le domaine physique Ω. En effet, à toute fonction u_h définie sur $\Omega_h^{(r)}$ est associée son lift, notée u_h^ℓ, définie sur Ω, grâce à la transformation $G_h^{(r)}$ définie de $\Omega_h^{(r)}$ vers Ω et illustrée dans la figure 4.

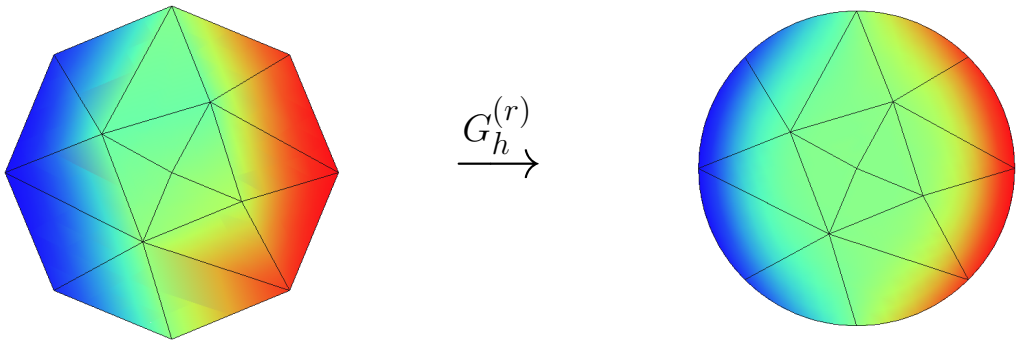

Figure 4 – La transformation de lift $G_h^{(r)} : \Omega_h^{(r)} \to \Omega$.

Le lift est utile dans l'analyse d'erreur, où au lieu d'estimer la différence entre la solution exacte u et la solution discrète u_h, nous estimons l'erreur entre u et le lift u_h^ℓ définies sur Ω.

Dans les années 1970, l'idée de lifter une fonction a été introduite par de nombreux auteurs dans le but de comparer une fonction à une autre qui n'est pas définie sur le même domaine (voir, par exemple, [38, 65, 69, 73, 80, 81]). Dans les travaux de Dubois [38] dans les années 1990, l'auteur a défini un lift utilisant la projection orthogonale sur le bord Γ. Ce même outil mathématique est utilisé en 1988 par Dzuik dans [40] pour définir un **lift surfacique** sur un maillage affine surfacique. Cette

définition du lift surfacique a été généralisée en 2009 par Demlow dans [36] pour des maillages surfaciques d'ordre élevé où une estimation d'erreur a priori sur une surface est établie. De plus, avec un raisonnement similaire, la définition d'un lift volumique a été présentée dans le contexte des maillages courbes afin d'améliorer la régularité de cet opérateur par Elliott et Ranner dans [43] en 2013. Ils ont défini une nouvelle transformation du lift basée sur les coordonnées barycentriques, la projection orthogonale sur Γ et un paramètre de régularité.

Au chapitre 3, nous définissons une version modifiée du lift défini dans [43] pour des raisons de régularité et pour améliorer les estimations d'erreur. En effet, d'une part, cette modification dans la définition du lift a un impact important sur l'approximation des erreurs comme observé dans les simulations numériques au chapitre 5. D'autre part, comme expliqué dans la proposition 3.1.4, la définition modifiée du lift garantit la **propriété de la trace**. Cette propriété stipule que, pour toute fonction u_h définie sur le domaine de maillage $\Omega_h^{(r)}$, nous avons,

$$\left(u_{h|_{\partial\Omega_h^{(r)}}}\right)^\ell = \left(u_h^\ell\right)_{|\Gamma}.$$

Cette propriété n'était pas toujours satisfaite auparavant dans la littérature. Dans un contexte différent, on fait référence à [44] où un lift est défini, satisfaisant la propriété de trace.

Résultats principaux : les estimations d'erreur

Les principales nouveautés de cette thèse par rapport à la littérature existante sont les estimations d'erreur a priori établies pour les trois problèmes présentés ci-dessus. Les erreurs sont calculées et exprimées à la fois en termes de l'erreur d'approximation de la méthode des éléments finis et de l'erreur géométrique, respectivement associées au degré des éléments finis $k \geq 1$ et à l'ordre du maillage $r \geq 1$. Nous considérons un cadre général, sans prendre nécessairement une approche isoparamétrique $k = r$, sur des maillages courbes et en utilisant l'opérateur de lift.

L'approche isoparamétrique/non-isoparamétrique. Dans les travaux existants, l'approche usuelle consiste à considérer $k = r$: c'est l'approche isoparamétrique (voir, par exemple, [32, 58]). Dans le travail récent d'Edelmann en 2021 [42], des estimations

d'erreur d'un problème de diffusion avec des conditions aux limites de Ventcel ont été établies en utilisant le lift défini par Elliott et Ranner dans [43] en 2013. De même, dans [43], une analyse d'erreur approfondie est réalisée sur un problème avec des conditions de Ventcel dans un cadre isoparamétrique.

Bien que l'approche non-isoparamétrique ne soit pas la plus courante dans la littérature, elle est utilisée dans de nombreux travaux de Demlow et al. [15, 36, 37] sur l'analyse d'erreur des problèmes surfaciques en utilisant un lift surfacique. L'avantage de considérer une telle méthode est de pouvoir choisir un ordre géometrique et un degré pour la méthode des éléments finis adaptés afin d'optimiser les résultats numériques en termes d'efficacité et de précision. Cela sera visible à travers nos simulations numériques dans les chapitres 5 et 6.

Estimations d'erreur du problème de Poisson-Ventcel. Dans le chapitre 5, les estimations d'erreur a priori relatives au problème (1) sont étudiées. Dans le théorème 5.3.1, il est prouvé qu'il existe une constante indépendante du maillage $c > 0$ telle que, pour un pas de maillage $h > 0$ suffisamment petit, on ait,

$$\|u - u_h^\ell\|_{\mathrm{L}^2(\Omega,\Gamma)} \leq c(h^{k+1} + h^{r+1}) \quad \text{et} \quad \|u - u_h^\ell\|_{\mathrm{H}^1(\Omega,\Gamma)} \leq c(h^k + h^{r+1/2}), \tag{4}$$

où u est la solution exacte du problème (1), u_h^ℓ est le lift de la solution approchée de (1), et les normes correspondent aux normes classiques de L^2 et de H^1 sur Ω et Γ, respectivement (voir Section 1.1.1).

Estimations d'erreur du problème spectral de Ventcel. Dans le chapitre 6, on démontre les estimations d'erreur a priori relatives au problème (2), résumées comme suit (voir le théorème 6.3.1). Soit $i \in \mathbb{N}^*$ avec λ_i une valeur propre de multiplicité N avec ses fonctions propres correspondantes, $\{u_j\}_{j\in \mathrm{J}}$, où $\mathrm{J} = \{i, ..., i+N-1\}$, relativement au problème (2). Alors, il existe une constante indépendante du maillage $c_{\lambda_i} > 0$, telle que pour tout $j \in \mathrm{J}$ et pour un $h > 0$ suffisamment petit, on ait,

$$|\lambda_j - \Lambda_j| \leq c_{\lambda_i}(h^{2k} + h^{r+1}), \tag{5}$$

$$\inf_{U\in\mathbb{F}_h^\ell} \|u_j - U\|_{\mathrm{L}^2(\Omega)} \leq c_{\lambda_i}(h^{k+1} + h^{r+1/2}), \tag{6}$$

$$\inf_{U\in\mathbb{F}_h^\ell} \|u_j - U\|_{\mathrm{H}^1(\Omega,\Gamma)} \leq c_{\lambda_i}(h^{k} + h^{r+1/2}), \tag{7}$$

où Λ_j est la valeur propre de la discrétisation de (2) de rang $j \in \mathrm{J}$, $\mathbb{F}_h$ est l'espace généré par les fonctions propres discrètes associées à $\{\Lambda_j\}_{j\in\mathrm{J}}$, et $\mathbb{F}_h^\ell$ est le lift de $\mathbb{F}_h$ composé des fonctions propres discrètes liftées définies sur Ω.

Estimations d'erreur du problème d'élasticité linéaire avec conditions aux limites de Ventcel. Le chapitre 7 traite l'analyse d'erreur du problème d'élasticité (3) où le résultat principal est le théorème 7.3.2, qui peut être énoncé comme suit. Soit $\boldsymbol{u}$ la solution de (3) et soit $\boldsymbol{u}_h$ la solution du problème discret avec son lift $\boldsymbol{u}_h^\ell$. Il existe une constante indépendante du maillage $c > 0$, telle que les inégalités suivantes sont vérifiées pour un $h > 0$ suffisamment petit,

$$\|\boldsymbol{u} - \boldsymbol{u}_h^\ell\|_{\mathbf{H}^1(\Omega,\Gamma)} \leq c(h^k + h^r) \quad \text{et} \quad \|\boldsymbol{u} - \boldsymbol{u}_h^\ell\|_{\mathbf{L}^2(\Omega,\Gamma)} \leq c(h^{k+1} + h^r),$$

où $\mathbf{H}^1(\Omega,\Gamma)$ et $\mathbf{L}^2(\Omega,\Gamma)$ sont respectivement les espaces vectoriels de Sobolev et de Lebesgue sur Ω et Γ (voir Section 1.2 pour plus de détails).

Éléments principaux des preuves : l'erreur des éléments finis et l'erreur géométrique. Dans toutes les estimations d'erreur présentées ci-dessus, l'erreur est contrôlée par deux composants principaux :

— **l'erreur des éléments finis** produite lors de l'approximation de la solution exacte par une fonction éléments finis $\mathbb{P}^k$. Cette erreur est visible à travers l'inégalité d'interpolation, qui fait intervenir l'opérateur de lift. Cette estimation est établie dans le cadre scalaire et le cadre vectoriel dans le chapitre 4 ;

— **l'erreur géométrique**, comme son nom l'indique, est liée à l'ordre géométrique du maillage considéré. En effet, il s'agit de l'erreur produite lors de l'approximation du domaine lisse par un maillage courbe d'ordre $r \geq 1$.

Il faut souligner que la preuve de chaque problème étudié présente ses propres difficultés :

— en traitant le problème de Poisson-Ventcel (1), la principale difficulté consiste à trouver un lift adéquat qui vérifie toutes les propriétés essentielles pour une analyse d'erreur ;

— la preuve du problème spectral est établie progressivement en trois étapes principales : d'abord une estimation preliminaire de l'erreur des valeurs propres est nécessaire avant d'estimer la différence entre les fonctions propres exactes et

leurs projections sur l'espace des fonctions propres discrètes liftées, pour enfin améliorer l'estimation d'erreur des valeurs propres ;

— les résultats dans le cas scalaire doivent être étendus au cas vectoriel pour traiter le problème d'élasticité (3). Cela présente ses propres difficultés liées à l'utilisation des fonctions vectorielles.

Les simulations numériques

Pour valider les estimations d'erreur présentées ci-dessus, de nombreux outils numériques sont nécessaires, comme le choix d'une bibliothèque d'éléments finis pour résoudre le problème avec un solveur linéaire adéquat sur des domaines 2D et 3D, la génération de maillages courbes, la mise en place du lift et le calcul de l'erreur. Pour cela, la bibliothèque CUMIN (voir [71]) est entièrement adaptée. Elle contenait déjà certains outils essentiels et au cours de ma thèse, j'ai ajouté de nouveaux outils nécessaires pour calculer numériquement les erreurs, comme le lift défini dans ce travail et les maillages courbes générés à l'aide de GMSH.

Dans la section 4.3, nous abordons la résolution de problèmes connus dans la littérature afin de valider l'implémentation des éléments de code ajoutés à CUMIN, tels que l'assemblage de matrice de masse et de raideur sur la surface et l'analyse d'erreur en utilisant l'opérateur de lift. Nous avons calculé les quatre erreurs suivantes :

$$\int_\Omega |\nabla u - \nabla u_h^\ell|^2 \,\mathrm{d}x, \quad \int_\Omega |u - u_h^\ell|^2 \,\mathrm{d}x, \quad \int_\Gamma |\nabla_\Gamma u - \nabla_\Gamma u_h^\ell|^2 \,\mathrm{d}s \quad \text{et} \quad \int_\Gamma |u - u_h^\ell|^2 \,\mathrm{d}s.$$

Notons que le domaine d'intégration ici est soit le domaine exact Ω ou soit la surface Γ, et non le domaine du maillage $\Omega_h^{(r)}$ ou le bord du maillage $\Gamma_h^{(r)}$.

Bien que la plupart des résultats coïncident avec la littérature existante, les simulations que j'ai menées ont mis en évidence un phénomène intéressant : **la super-convergence de l'erreur sur les maillages quadratiques**, où l'ordre de convergence de l'erreur présente des résultats similaires à ceux du cas cubique. Étant donné que ce comportement est observé dans toutes les simulations numériques réalisées sur des problèmes surfaciques et volumiques, la section 4.4 est consacrée à l'investigation de l'origine de cette super-convergence. Diverses simulations sont effectuées sur différents problèmes et géométries, indiquant que ce phénomène n'est pas spécifique au problème étudié ni à la géométrie du domaine considéré. Un autre phénomène intéressant est

observé dans la section 4.3 et tout au long de la partie III : c'est la perte du taux de convergence de l'erreur d'interpolation sur les maillages cubiques. C'est le principal sujet de discussion dans la section 4.5, où de nombreuses expériences sont réalisées sur différents domaines en 2D et 3D.

Ensuite, dans la section 5.4, je mets en évidence numériquement l'**optimalité des estimations d'erreur** (4) sur des domaines en 2D et en 3D même si des observations similaires à celles faites dans la section 4.3 sont aussi présentes ici : le phénomène de super-convergence sur les maillages quadratiques est également observé et une perte dans le taux de convergence de l'erreur d'interpolation est mise en évidence sur les maillages cubiques. De même, pour le problème spectral, des expériences numériques sont menées sur diverses géométries en 2D et 3D où des résultats similaires au cas du problème de Poisson-Ventcel sont observés. On remarque une sous-optimalité dans l'estimation d'erreur en norme L^2 des fonctions propres (6), pour laquelle une conjecture est proposée. Je tiens à souligner que les estimations d'erreur en norme H^1 des fonctions propres (7) et des valeurs propres (5) sont toutes les deux optimales selon les expériences effectuées.

Enfin, je précise que toutes les simulations numériques présentées tout au long de cette thèse peuvent être entièrement reproduites à l'aide des codes sources dédiés disponibles sur le GitLab de CUMIN [2].

Le fruit de mon travail. Cette thèse a conduit aux deux publications suivantes :

- *Finite element analysis of a spectral problem on curved meshes occurring in diffusion with high order boundary conditions,* F. Caubet, J. Ghantous et C. Pierre (soumis et disponible sur HAL [3]) ;
- *A priori error estimations of a diffusion equation with Ventcel boundary conditions on curved meshes,* SIAM Journal on Numerical Analysis, F. Caubet, J. Ghantous et C. Pierre (publié en 2024 et disponible sur le site du journal [4]) ;

et à la publication d'un acte de conférence :

- *Numerical study of a diffusion equation with Ventcel boundary condition using curved meshes,* Monografías Matemáticas García de Galdeano, F. Caubet, J.

2. CUMIN GitLab deposit, `https://plmlab.math.cnrs.fr/cpierre1/cumin`
3. `https://hal.science/hal-04552691`
4. `https://epubs.siam.org/doi/10.1137/23M1582497`

Ghantous et C. Pierre (publié en 2023 et disponible sur HAL [5]).

5. `https://hal.science/hal-03972051`

GENERAL INTRODUCTION

This PhD thesis is part of the mathematical field known as **numerical analysis**. More precisely, in what follows, we will focus on the error analysis of **Partial Differential Equations (PDE) with high order boundary conditions**. Throughout this introduction, we will try to answer the following essential questions:

1. in a general context, what are the main steps in an error analysis? And what are the classical mathematical tools used?
2. what are the motivations behind the particular choice of the problems studied in this thesis?
3. positioning ourselves in the present context of this thesis, what are the new steps that need to be followed in order to accommodate the particularity of the problems under consideration?
4. establishing an error estimation of a problem is not a new dilemma, hence, one might ask what does this thesis differ from the existing works on such subject? And what does it add to the existing literature?

We proceed step by step responding to these inquiries by their respective orders.

The key ingredients of an error analysis in a general context

Generally, we consider a well-posed problem having a unique solution, which we aim to approximate. The classical way to proceed is to **discretize the domain**, **choose a numerical method** to approach the solution and lastly **compute the difference between the exact solution and its approximation.**

Mesh definition. Following Definition 1.49 in [45], let Ω be a bounded domain in $\mathbb{R}^d$ $(d = 2, 3)$. A *mesh* is a union of a finite number N of compact, connected, Lipschitz

sets T_m with non-empty interior such that $\{T_m\}_{m=1}^N$ forms a partition of Ω, i.e.,

$$\bar{\Omega} = \bigcup_{m=1}^{N} T_m \quad \text{and} \quad \mathring{T}_m \cap \mathring{T}_n = \emptyset \quad \text{for} \quad m \neq n.$$

The subsets T_m are called *mesh cells* or *mesh elements* (or simply *elements* when there is no ambiguity).

Throughout this work, we consider simplicial elements i.e. **triangles** in 2D and **tetrahedral** in 3D, as displayed in Figure 2.3. Additionally, in the upcoming section, we will give the definition of **curved mesh elements**, which are used in this thesis.

Figure 5 – Display of a triangle mesh element in 2D and tetrahedral mesh element in 3D.

The finite element method. The finite element method is a numerical method for finding approximate solutions to boundary value problems for PDE. It is widely used in engineering, physics, and applied mathematics for solving complex problems involving structures, fluid dynamics, heat transfer, etc. The origins of this method (see [8]) can be traced back to the 1950s when engineers started to solve numerically structural mechanics problems in aeronautics. We also refer to [45, 20, 32, 30, 79, 60] for details on the finite element method. A key point in the analysis of this method is to obtain an estimate of the error produced while approximating the solution of a problem denoted u, typically a PDE, by its finite element approximation denoted u_h.

Throughout this work, we will rely on **the $\mathbb{P}^k$ Lagrange finite element method,** where $k \geq 1$ is the degree of the method.

Error estimation. There exists two types of error estimation either an a priori or an a posteriori estimation. The goal of an **a priori error estimation** is to assess the error $\|u - u_h\|$ in a given norm in terms of the mesh size h, the problem data, and the exact solution u (see, e.g. [45, 20, 61]). Conversely, an a posteriori estimation

depends on h and the computed solution u_h, but not on u (see e.g. [1, 55]). Altogether, the a priori error analysis is mainly oriented for theoretical qualification, while the a posteriori error analysis serves practical purposes. Together these approaches provide a broad view on the reliability of the approximation method considered.

From this point forward, we will focus on a priori error estimations.

Motivation behind the studied problems

Motivation. In this thesis we will focus on obtaining a priori error estimations of a PDE with high order boundary conditions. Indeed, this work is part of the RODAM research program [6], which studies **shape optimisation problems** (see, e.g., [59, 3] for generalities on shape optimisation) in structural mechanics within an industrial context. In particular, one of the questions concerns the study of vibrational properties of elastic structures, especially when they have **a thin layer** (which may come from surface treatment or corrosion, for example). The main objective is to use shape optimisation for a better understanding of these mechanical parts and to improve their design with the aim of minimizing the mass of the structure while maintaining the mechanical properties.

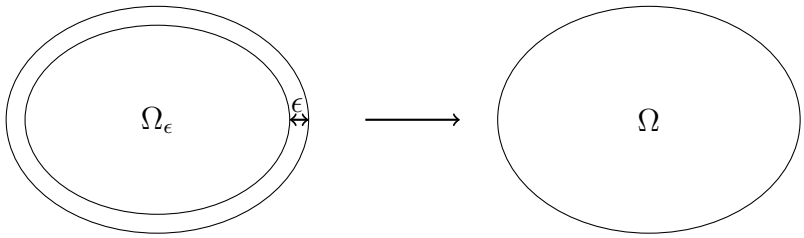

Figure 6 – Approximation of a domain having a thin layer surrounding it (on the left) by a domain equipped with high order boundary conditions (on the right).

From a numerical perspective, considering the thin layers around mechanical parts, as displayed in Figure 6, poses specific challenges, particularly in discretizing the domain with a mesh size adapted to the thin layer. To overcome these difficulties, the domain and solution of the considered problem can be approximated using an asymptotic expansion: the thin layer is modeled by adapted boundary conditions (see e.g. [16, 77, 54, 52]). In other words, the approximated domain is not be surrounded by a

6. *Robust Optimal Design under Additive Manufacturing constraints*: `https://lma-umr5142.univ-pau.fr/en/scientific-activities/scientific-challenges/rodam.html`

thin layer, but it is equipped with second order boundary conditions such as **Ventcel conditions**, also known as **generalized Robin conditions**. These conditions derive from the pioneering works of Ventcel in [75, 76]. They are also studied in obstacle scattering problems like in [18]. We also mention the need to take thin layers into account in the context of aeroacoustics where the so-called Ingard-Myers boundary conditions are used to model the presence of a liner located on the surface of a duct (see [66]). For the sake of completeness, we also refer to [64] that deals with the numerical analysis of parabolic problems that are subject to dynamic boundary conditions.

To give the readers an idea of the definition of these boundary conditions, we here give an example in a classical case, when considering the Poisson equation in the scalar case: in this case, the Ventcel boundary conditions are given by,

$$-\Delta_\Gamma u + \partial_{\mathrm{n}} u + u = 0 \quad \text{ on } \partial\Omega,$$

where $\partial_{\mathrm{n}} u$ is the normal derivative of a solution u and where Δ_Γ is the **Laplace-Beltrami operator**. This second order operator, also known as the **tangential Laplacian**, is defined as follows for any sufficiently regular function u,

$$\Delta_\Gamma u := \mathrm{div}_\Gamma(\nabla_\Gamma u),$$

where ∇_Γ is the tangential gradient and div_Γ is the tangential divergence defined in Definition 1.1.1 below. For more details, we refer to [59].

The studied Ventcel problems. The original physical problem of studying the vibrational properties of mechanical structures is first simplified considering **scalar diffusion problems** before passing to the study of **the vector linear elasticity framework**. We present the following three studied problems through this thesis.

Let Ω be a nonempty bounded connected domain in $\mathbb{R}^d$, $d = 2, 3$, with a **smooth boundary** $\Gamma := \partial\Omega$ and let α, $\beta > 0$. Motivated by generalized impedance boundary conditions, in Chapter 1 are presented the three studied systems equipped with Ventcel boundary conditions, given as follows.

1. In the scalar case, we firstly consider the typical problem with source terms before passing to the spectral problem:

— the *Poisson-Ventcel problem*,

$$\begin{cases} -\Delta u + \kappa u &= f \quad \text{in } \Omega, \\ -\beta \Delta_\Gamma u + \partial_{\mathrm{n}} u + \alpha u &= g \quad \text{on } \Gamma, \end{cases} \tag{8}$$

where f and g are sufficiently regular source terms and $\kappa \geq 0$;

— the *spectral problem with Ventcel boundary conditions*,

$$\begin{cases} -\Delta u = \lambda u \quad \text{in } \Omega, \\ -\beta \Delta_\Gamma u + \partial_{\mathrm{n}} u + \alpha u = 0 \quad \text{on } \Gamma. \end{cases} \tag{9}$$

2. In the vectorial case, we consider the *linear elasticity problem with Ventcel boundary conditions*,

$$\begin{cases} -\mathrm{div}(\mathbf{A}_\Omega e(\boldsymbol{u})) = \boldsymbol{f} \quad \text{in } \Omega, \\ -\beta \mathrm{div}_\Gamma(\mathbf{A}_\Gamma e_\Gamma(\boldsymbol{u})) + \mathbf{A}_\Omega e(\boldsymbol{u})\mathbf{n} + \alpha \boldsymbol{u} = \boldsymbol{g} \quad \text{on } \Gamma, \end{cases} \tag{10}$$

where $\mathbf{n}$ denotes the external unit normal to Γ, where $\boldsymbol{f}$ and $\boldsymbol{g}$ are sufficiently regular source terms, where $\mathbf{A}_\Omega$ and $\mathbf{A}_\Gamma$ are *Hooke tensors* and where $e(\boldsymbol{u})$ and $e_\Gamma(\boldsymbol{u})$ are *strain tensors* (see Section 1.2 for details).

Under the adequate hypothesis imposed, these three problems are well-posed: Problem (8) (resp. Problem (10)) admits a unique solution u (resp. $\boldsymbol{u}$) and the spectral problem (9) admits an infinite number of positive eigenvalues, with finite multiplicities, forming an increasing sequence tending to infinity.

Technical complications in the error analysis of the Ventcel problems. Now, the main objective is to establish an error analysis of the previously defined problems, following the main steps presented above: in particular we will discretize the considered domain and use the finite element method to approximate the exact solution of the continuous problems.

The price to pay for these second order conditions to make sense is that we have to consider a smooth domain. Indeed, this regularity assumption is imposed to be able to use the integration by part formula on the boundary of the domain in Chapter 1 to obtain the variational formulations of the considered problems. Thus, we face problems where the physical domain and the mesh domain differ, putting forward an intrinsic **geometric error**, as will be detailed in the following.

Essential mathematical tools used to accommodate the Ventcel problems

The error analysis of each previous Ventcel problem presents its proper difficulties. However they all share a common problem: as mentioned above, the physical domain Ω has a smooth boundary and can not be exactly fitted by a mesh. This puts forward the following two main issues.

— (P1): a gap between Ω and the mesh domain is highlighted and is refereed to as a geometric error. **How can we decrease this error?**

— (P2): the discrete functions belonging to the finite element space are defined on the mesh domain, which defer from the physical one. This raises the following question: **How can we estimate the error between the exact solution and the discrete one, which are not defined on the same domain?**

Solution to (P1): curved meshes. To decrease the geometric error, we will resort to **curved meshes**, denoted $\mathcal{T}_h^{(r)}$, with a **geometric order** $r \geq 1$. These meshes were studied and defined in many works such as [32, 33, 42, 43]. However, using curved meshes of order r, does not imply that the gap between the domain Ω and the mesh domain denoted $\Omega_h^{(r)}$ is reduced to nothing. The only thing that we can gather is that the higher the geometric mesh order r is, the lower the geometric error will be. Consequently, using curved meshes, we aim to improve the asymptotic behavior of the total error with respect to the mesh size h that partially depends on the geometric error. In Chapter 2, the definition of curved meshes is detailed and explanatory examples are displayed in 2D and 3D.

In Figure 7, a linear mesh ($r = 1$), a quadratic mesh ($r = 2$), and a cubic mesh ($r = 3$) of the unit disk are displayed, respectively. All these meshes do not fit exactly the unit disk: even though we do not visibly see any difference between the disk and the quadratic (resp. cubic) mesh domain, the circle can not be locally parameterized using polynomials. Throughout the literature, it is known that an affine mesh element is constructed with help of an affine transformation from the reference triangle (see e.g. [33, 32]). As for the curved mesh elements, they are constructed with the help of a polynomial transformation $F_T^{(r)}$ of order r, defined in Chapter 2. We point out that in 2D an affine mesh element has 3 nodes (the 3 vertices of the triangle), a quadratic element has 6 nodes (the 3 vertices of the triangle and the 3 edge mid-points) and a

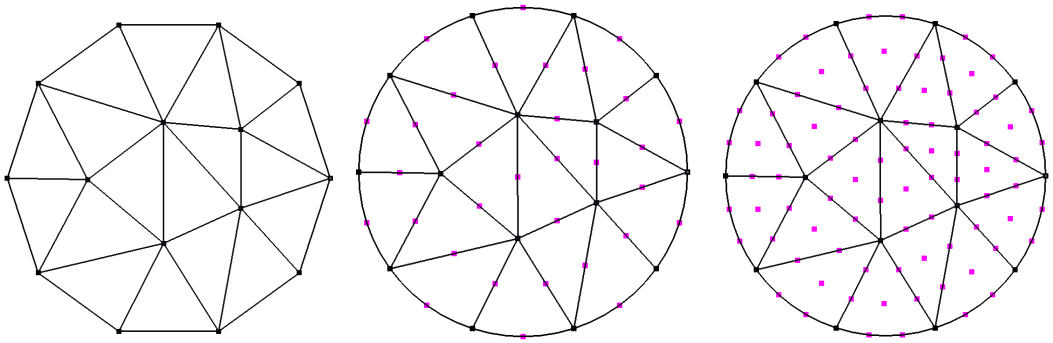

Figure 7 – Linear mesh ($r = 1$), quadratic mesh ($r = 2$) and cubic mesh ($r = 3$) of the unit disk.

cubic element has 10 nodes (the 3 vertices of the triangle, the 6 edge points and the center of the triangle).

We have to note that, in the upcoming error analysis, the quadratic meshes behave as if $r = 3$ and exhibit a **super-convergent** behavior: on these meshes the errors will always present better convergence rates than expected, having similar values as in the cubic case. A similar observation is highlighted in the error analysis of the spectral problem of the Laplace-Beltrami on a surface in [15] in 2018. Even though, no theoretical explanation is found yet, we came to the following conclusion during our investigations: this super-convergence phenomena is not related to the considered problem nor the considered domain. A thorough study is presented in Section 4.4, on various geometries in 2D and 3D.

Moreover, in all the numerical simulations presented in this thesis, the numerical errors on the cubic meshes will be subjected to a loss in the convergence rate. A detailed investigation was made in Section 4.5, leading to the following assumption: this default is tied to the finite element interpolation error.

Solution to (P2): the lift operator. The solution in order to estimate the error between the exact solution and the discrete one (not defined on the same domain) is the first main novelty presented in this manuscript: **the lift operator**. This operator allows us to redefine or *"lift"* a function defined on the mesh domain $\Omega_h^{(r)}$ to be defined onto the physical domain Ω. Indeed, to any function u_h defined on $\Omega_h^{(r)}$ is associated its lift denoted u_h^ℓ defined on Ω, through a transformation $G_h^{(r)}$ defined from $\Omega_h^{(r)}$ to Ω, as displayed in Figure 8.

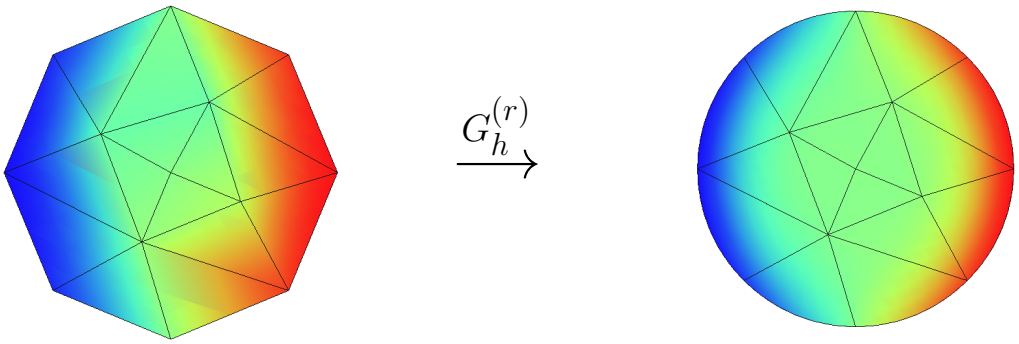

Figure 8 – Display of the lift transformation $G_h^{(r)} : \Omega_h^{(r)} \to \Omega$.

The lift comes in handy in the error analysis, where instead of estimating the difference between the exact solution u and the discrete solution u_h, we estimate the error between two functions defined over Ω: u and u_h^ℓ.

In the 1970s, the idea of lifting a function was introduced by many authors for the similar purpose of comparing a function to another one not defined on the same domain (see, e.g., [38, 65, 69, 73, 80, 81]). In the work [38] of Dubois in the 1990's, the author defined a lift using the orthogonal projection onto the boundary Γ. This same mathematical tool is used in 1988 by Dzuik in [40] to define **a surface lift** for an affine surface mesh. This surface lift definition was generalised in 2009 by Demlow in [36] for high order surface meshes where a surface a priori error estimation is established. Furthermore, following a similar reasoning, the volume lift definition was modified in the context of curved meshes in order to improve its regularity by Elliott and Ranner in [43] in 2013. They defined a new lift transformation based on the barycentric coordinates, the orthogonal projection onto Γ and a regularity parameter.

In Chapter 3, we define a **modified version of the lift** defined in [43] for a regularity purpose and to sharpen the error estimates. Indeed, on one hand, this modification in the lift definition has a big impact on the error approximation as is observed in the numerical simulations in Chapter 5. On another hand, as will be explained in Proposition 3.1.4, the modified lift definition guarantees the so-called **trace property**. This property states that, for any function u_h defined on the mesh domain $\Omega_h^{(r)}$, we have,

$$\left(u_{h|_{\partial\Omega_h^{(r)}}}\right)^\ell = \left(u_h^\ell\right)_{|\Gamma}.$$

This property was not always satisfied formerly in the literature. However, in the

context of evolving bulk-surface problems, we refer to [44], where an adapted lift is defined that satisfies the trace property.

Main results: the error estimations

The main novelty of this thesis with regards to the existing literature is the a priori error estimations established for the three problems presented above. The errors are computed and expressed both in terms of finite element approximation error and of geometrical error, respectively, associated to the finite element degree $k \geq 1$ and to the mesh order $r \geq 1$. We proceeded in a **non-isoparametric setting**, where k and r can differ from one another, while working on curved meshes and using the lift operator.

The isoparametric/non-isoparametric approach. Ordinarily, in the existing works, researchers chose to consider the more classical approach taking $k = r$: the isoparametric approach (see e.g. [32, 58]). In the recent work of Edelmann in 2021 [42], error estimations of a diffusion problem with Ventcel boundary conditions were established using the lift defined by Elliott and Ranner in [43] in 2013. Similarly in [43], while also taking an isoparametric approach, a thorough error analysis is made on a coupled bulk–surface partial differential equation with Ventcel boundary conditions.

Even though the non-isoparametric approach is not the most common throughout the literature, it is used in the many works of Demlow *et al.* [15, 36, 37] on the error analysis of surface problems using a surface lift. The purpose of considering such method is that one can choose the adequate geometric order and the degree of the finite element method used in order to optimise the computational result in terms of efficiency and sharpness. This will be clearly visible through our numerical simulations in Chapter 5 and Chapter 6.

Error estimations of the Poisson-Ventcel problem. In Chapter 5, the a priori error estimations relative to Problem (8) are studied. In Theorem 5.3.1, it is proven that there exists a mesh independent constant $c > 0$ such that, for a sufficiently small mesh size $h > 0$,

$$\|u - u_h^\ell\|_{\mathrm{L}^2(\Omega,\Gamma)} \leq c(h^{k+1} + h^{r+1}) \quad \text{and} \quad \|u - u_h^\ell\|_{\mathrm{H}^1(\Omega,\Gamma)} \leq c(h^k + h^{r+1/2}), \tag{11}$$

where u is the exact solution of (8), where u_h^ℓ is the lift of the approximated solution of (8) and where the $\mathrm{L}^2(\Omega,\Gamma)$ norm (resp. $\mathrm{H}^1(\Omega,\Gamma)$ norm) corresponds to the sum between the classical L^2 (resp. H^1) norms on Ω and Γ respectively (see Section 1.1.1).

Error estimations of the spectral Ventcel problem. In Chapter 6, we prove the a priori error estimations relative to Problem (9), which are summarised as follows (see Theorem 6.3.1 for a precise statement). Let λ_j be an eigenvalue of multiplicity N with its corresponding eigenfunctions, $\{u_j\}_{j\in \mathrm{J}}$, where $\mathrm{J} = \{i, ..., i+N-1\}$, relatively to Problem (9). Then, there exists a mesh independent constant $c_{\lambda_i} > 0$, such that, for any $j \in \mathrm{J}$, for a sufficiently small $h > 0$,

$$
\begin{aligned}
|\lambda_j - \Lambda_j| &\leq c_{\lambda_i}(h^{2k} + h^{r+1}), && (12)\\
\inf_{U\in\mathbb{F}_h^\ell} \|u_j - U\|_{\mathrm{L}^2(\Omega)} &\leq c_{\lambda_i}(h^{k+1} + h^{r+1/2}), && (13)\\
\inf_{U\in\mathbb{F}_h^\ell} \|u_j - U\|_{\mathrm{H}^1(\Omega,\Gamma)} &\leq c_{\lambda_i}(h^{k} + h^{r+1/2}), && (14)
\end{aligned}
$$

where Λ_j is the eigenvalue of the discretization of (9) of rank $j \in \mathrm{J}$, $\mathbb{F}_h$ is the space generated by the discrete eigenfunctions associated to $\{\Lambda_j\}_{j\in\mathrm{J}}$, and $\mathbb{F}_h^\ell$ is the lift of $\mathbb{F}_h$ made of the lifted discrete eigenfunctions defined on Ω.

Error estimations of the linear elasticity problem with Ventcel boundary conditions. Chapter 7 deals with the error analysis of the elasticity problem (10) where the main results is Theorem 7.3.2, which can be stated as follows. Let $\boldsymbol{u}$ be the solution of (10) and let $\boldsymbol{u}_h$ be the solution of the discrete problem with $\boldsymbol{u}_h^\ell$ as its lift. There exists a mesh independent constant $c > 0$, such that the following inequalities stand for a sufficiently small $h > 0$,

$$
\|\boldsymbol{u} - \boldsymbol{u}_h^\ell\|_{\mathbf{H}^1(\Omega,\Gamma)} \leq c(h^k + h^r) \quad \text{and} \quad \|\boldsymbol{u} - \boldsymbol{u}_h^\ell\|_{\mathbf{L}^2(\Omega,\Gamma)} \leq c(h^{k+1} + h^r),
$$

where $\mathbf{H}^1(\Omega,\Gamma)$ and $\mathbf{L}^2(\Omega,\Gamma)$ are respectively the Sobolev and Lebesgue vector spaces over Ω and Γ (see Section 1.2 for details).

Main proof elements: the finite element error and the geometric error. In all the error estimations presented above, the error is controlled by two main components:

— **the finite element error** produced when approximating the exact solution by a $\mathbb{P}^k$ finite element function. This error is rendered visible through the classical interpolation inequality, which is lifted on Ω with the help of the lift operator. This estimation is established for the scalar and vectorial cases in Chapter 4;

— **the geometric error**, as its given name indicates, is related to the geometric order and the domain considered. Indeed, it is the error produced when approximating the smooth domain by a curved mesh of order $r \geq 1$.

It is worth pointing out that the proof of each studied problem presents its proper difficulties:

— when dealing with the Poisson-Ventcel problem (8), the main difficulty was finding an adequate lift that checks all the desired boxes for an error analysis;

— the proof of the spectral problem is not obvious nor direct, it is established gradually in three main steps: preliminary an eigenvalue error estimation is needed before we estimate the difference between the exact eigenfunctions and their projections onto the space of the lifted discrete eigenfunctions, then the eigenvalue error estimation can be improved;

— the results already established in the scalar case have to be extended to the vectorial case in order to deal with the elasticity problem (10). This comes with its proper difficulties related to the use of vector valued functions.

The discussion of the numerical simulations

In order to validate the error estimation presented above, many requirement are needed like choosing a finite element library to solve the problem with an adequate linear solver on 2D and 3D domains, generating curved meshes, implementing the lift and computing the error. This is where the finite element library CUMIN (see [71]) came in handy. It already contained some essential computational tools and throughout my thesis I added other tools that are needed to numerically compute the errors, like the lift defined in this work and the curved meshes generated using the curved mesh generator GMSH.

In Section 4.3, we consider the resolution of problems documented in the literature aimed to validate the code implementation added to CUMIN: surface matrix assembling

and error analysis using the lift operator. We computed the following four errors:

$$\int_\Omega |\nabla u - \nabla u_h^\ell|^2 \,\mathrm{d}x, \quad \int_\Omega |u - u_h^\ell|^2 \,\mathrm{d}x, \quad \int_\Gamma |\nabla_\Gamma u - \nabla_\Gamma u_h^\ell|^2 \,\mathrm{d}s \quad \text{and} \quad \int_\Gamma |u - u_h^\ell|^2 \,\mathrm{d}s.$$

Note that the integration domain here is either the exact domain Ω or the exact surface Γ and not the mesh domain $\Omega_h^{(r)}$ neither the mesh surface $\Gamma_h^{(r)}$.

While most results coincided with the existing literature, the simulations I led had put forward an interesting phenomena: **the super-convergence of the error on quadratic meshes,** where the convergence rate of error present similar results as if $r = 3$. Since this pattern is observed in all the numerical simulations made on surface and volume problems, Section 4.4 is dedicated to the investigation of the source of this super-convergence. Various simulations are made on different problems and geometries, implying the non dependency of this phenomena to the studied problem and to the considered geometry of the domain. Another interesting phenomena is observed in Section 4.3 and all throughout Part III: the loss in the convergence rate of the interpolation error on cubic meshes. This is the main topic of discussion of Section 4.5, where many experiments are made on different domains in 2D and 3D.

Then, in Section 5.4, I highlight numerically **the optimality of the error estimates** (11) on 2D and 3D domains. Notice that the same numerical observations are made as in Section 4.3: the super-convergence phenomena on the quadratic meshes is also observed and a loss in the convergence rate of the interpolation error is highlighted on cubic meshes. Similarly for the spectral problem, numerical experiments are established on various geometries in 2D and 3D where similar patterns are depicted as in the case of the Poisson-Ventcel problem. One notices a sub-optimality in the L^2 eigenfunction error estimate (13), where a conjecture is proposed. I have to point out that the H^1 eigenfunction error (14) and the eigenvalue error estimations (12) are both optimal following the observations made.

Finally I mention that all numerical results presented throughout this work can be fully reproduced using dedicated source codes available on CUMIN Gitlab [7].

The fruits of my labor. This thesis led to the two following publications:

— *Finite element analysis of a spectral problem on curved meshes occurring in diffusion with high order boundary conditions,* F. Caubet, J. Ghantous et C. Pierre

7. CUMIN GitLab deposit, `https://plmlab.math.cnrs.fr/cpierre1/cumin`

(submitted and available on HAL [8]);

— *A priori error estimations of a diffusion equation with Ventcel boundary conditions on curved meshes,* SIAM Journal on Numerical Analysis, F. Caubet, J. Ghantous et C. Pierre (published in 2024 and available on the journal's page [9]);

and to the published conference proceeding:

— *Numerical study of a diffusion equation with Ventcel boundary condition using curved meshes,* Monografías Matemáticas García de Galdeano, F. Caubet, J. Ghantous et C. Pierre (published in 2023 and available on HAL [10]).

8. https://hal.science/hal-04552691
9. https://epubs.siam.org/doi/10.1137/23M1582497
10. https://hal.science/hal-03972051

GENERAL NOTATIONS

$\mathbb{R}$	The set of real numbers
$\mathbb{R}_+^*$	The set of positive real numbers
d	The dimension, $d \in \{2, 3\}$
Ω	Nonempty bounded connected open subset of $\mathbb{R}^d$ with a smooth boundary
Γ	The boundary of Ω
α	A strictly positive constant
β	A strictly positive constant
κ	A non-negative constant
c	Strictly positive mesh independent constant
d	The signed distance function relative to Γ
$\mathbf{n}$	The outward-pointing unit normal vector to Γ
I_d	The identity matrix of dimension $d \times d$
P	The orthogonal projection onto the tangential space of Γ, given by $\mathrm{P} = \mathrm{I}_d - \mathbf{n} \otimes \mathbf{n}$
b	The orthogonal projection onto Γ
$\partial_{\mathrm{n}} u$	The normal derivative of u
∇_Γ	The tangential gradient
div_Γ	The tangential divergence
$\mathrm{H}^1(\Omega, \Gamma)$	The Sobolev space composed of functions in $\mathrm{H}^1(\Omega)$ such that their restrictions to the boundary belong to $\mathrm{H}^1(\Gamma)$
λ	An exact eigenvalue of the spectral problem presented in Chapter 1
c_λ	A strictly positive mesh independent constant that dependents on the eigenvalue λ
$\mathbf{H}^1(\Omega)$	The Sobolev space composed of vector functions belonging to $\mathrm{H}^1(\Omega, \mathbb{R}^d)$

$\mathbf{H}^1(\Gamma)$	The Sobolev space composed of vector functions belonging to $\mathrm{H}^1(\Gamma, \mathbb{R}^d)$
M^T	The transpose of a matrix M
e	The strain tensor defined by $e(\boldsymbol{u}) := \frac{1}{2}\left(\nabla \boldsymbol{u} + (\nabla \boldsymbol{u})^\mathsf{T}\right)$ for all $\boldsymbol{u} \in \mathbf{H}^1(\Omega)$
e_Γ	The tangential strain tensor defined by $e_\Gamma(\boldsymbol{u}) := \frac{1}{2}\left(\nabla_\Gamma \boldsymbol{u} + (\nabla_\Gamma \boldsymbol{u})^\mathsf{T}\right)$ for all $\boldsymbol{u} \in \mathbf{H}^1(\Gamma)$
$\mathbf{A}_\Omega$	The stiffness tensor (see Chapter 1)
$\mathbf{A}_\Gamma$	The surface stiffness tensor (see Chapter 1)
$\mathbf{V}_\Gamma$	The Sobolev space composed of vector functions $\boldsymbol{u}$ in $\mathbf{L}^2(\Gamma)$ such that $e_\Gamma(\boldsymbol{u})$ belongs to $\mathrm{L}^2(\Gamma)$
$\mathbf{H}_{(\Omega,\Gamma)}$	The Sobolev space composed of vector functions belonging to $\mathbf{H}^1(\Omega)$ such that their restriction to the boundary belong to $\mathbf{V}_\Gamma$
$\hat{T}$	The reference simplex of dimension d
$\mathcal{T}_h^{(1)}$	Affine mesh, with a mesh domain $\Omega_h^{(1)}$
$\mathcal{T}_h^{(r)}$	Curved mesh, with a mesh domain $\Omega_h^{(r)}$
$\mathcal{T}_h^{(e)}$	Exact mesh, with a mesh domain equal to Ω
r	The goemetric order of the mesh $\Omega_h^{(r)}$
h	The mesh step
$G_h^{(r)}$	The lift transformation (see Chapter 3)
u_h^ℓ	The lift of the finite element function u_h by $u_h^\ell \circ G_h^{(r)} = u_h$
$\boldsymbol{u}_h^\ell$	The lift of the finite element vector function $\boldsymbol{u}_h$ by $\boldsymbol{u}_h^\ell \circ G_h^{(r)} = \boldsymbol{u}_h$
k	The degree of the finite element method
$\mathbb{P}^k$	The set of polynomials in $\mathbb{R}^d$ of degree k or less
$\mathbb{V}_h$	The $\mathbb{P}^k$ finite element space
$\mathbb{V}_h^\ell$	The lifted finite element space
$\boldsymbol{V}_h$	The $\mathbb{P}^k$ finite element vector space
$\boldsymbol{V}_h^\ell$	The lifted finite element vector space

Part I

The continuous problems and curved meshes definition

The first part of this thesis is composed of two chapters. In Chapter 1, we present some needed mathematical tools and notations used all through this manuscript and the three main problems studied. These problems are equipped with second order boundary conditions called the *Ventcel boundary conditions*. These boundary conditions model the physical aspect of having a thin layer surrounding the domain (see [16, 77, 52, 18, 28, 78]). Before proceeding with the numerical analysis of such problems, we recall in Chapter 1 the variational formulations of the continuous problems.

Note that in order for the boundary condition to make sense, the physical domain is assumed to have a smooth boundary (at least $\mathcal{C}^2$). Consequently, some technical difficulties arise in the numerical study: indeed, the computational domain does not have a globally $\mathcal{C}^2$ boundary but a piece-wise smooth (polynomial) boundary. Consequently, any mesh of the exact domain does not exactly fit it and a default between the mesh domain and the physical one is produced, called the *geometric error*. As we plan to conduct an error analysis in the following parts, it is crucial to minimize this error, as it directly impacts the total error between the exact solution of a given problem and its approximation. In Chapter 2, we define *higher-order curved meshes*, which help reduce this geometric error. Indeed, they are one of the key tools used in the upcoming chapters.

Chapter 1

THE CONTINUOUS PROBLEMS

In this chapter are presented the three studied problems in this thesis equipped with boundary conditions of order two, known as the Ventcel boundary conditions. As previously mentioned, for these boundary conditions to make sense, the physical domain Ω on which our problem is defined needs to satisfy a regularity assumption: its boundary, denoted Γ, is assumed to be smooth (at least $\mathcal{C}^2$). Moreover, this regularity ensures that the integration by part formula on the boundary Γ can be applied in each problem case.

We start by studying the scalar case with the following two problems: the *Poisson-Ventcel problem* with source terms and the *spectral Ventcel problem*. Afterwards, we pass on to the vectorial case, studying the linear elasticity equations with associated Ventcel boundary conditions. Before proceeding with the error analysis in the following chapters of this thesis, we claim the well-posedness of these three problems in each section. For the sake of completeness, the notations and some essential mathematical tools used throughout this manuscript are presented in the beginning of each section.

1.1 The scalar case

1.1.1 Notations and needed mathematical tools

Throughout this work, Ω is a nonempty bounded connected open subset of $\mathbb{R}^d$ ($d = 2, 3$) with a smooth (at least $\mathcal{C}^2$) boundary $\Gamma := \partial\Omega$. The unit normal to Γ pointing outwards is denoted by $\mathbf{n}$ and $\partial_{\mathrm{n}} u$ is the normal derivative of a function u. We denote respectively by $\mathrm{L}^2(\Omega)$ and $\mathrm{L}^2(\Gamma)$ the usual Lebesgue spaces endowed with their standard norms on Ω and Γ. Moreover, for $k \geq 0$, $\mathrm{H}^{k+1}(\Omega)$ denotes the usual Sobolev space endowed with its standard norm (see [46, 21]). We also consider the Sobolev spaces $\mathrm{H}^{k+1}(\Gamma)$ on the boundary as defined e.g. in [62, §2.3]. It is recalled that the norm on $\mathrm{H}^1(\Gamma)$ is: $\|u\|^2_{\mathrm{H}^1(\Gamma)} := \|u\|^2_{\mathrm{L}^2(\Gamma)} + \|\nabla_\Gamma u\|^2_{\mathrm{L}^2(\Gamma)}$, where ∇_Γ is the tangential

gradient defined below; and that $\|u\|^2_{\mathrm{H}^{k+1}(\Gamma)} := \|u\|^2_{\mathrm{H}^k(\Gamma)} + \|\nabla_\Gamma u\|^2_{\mathrm{H}^k(\Gamma)}$. Throughout the scalar case, we rely on the following Hilbert space (see [62]),

$$\mathrm{H}^1(\Omega,\Gamma) := \{u \in \mathrm{H}^1(\Omega),\ u_{|\Gamma} \in \mathrm{H}^1(\Gamma)\},$$

equipped with the norm $\|u\|^2_{\mathrm{H}^1(\Omega,\Gamma)} := \|u\|^2_{\mathrm{H}^1(\Omega)} + \|u\|^2_{\mathrm{H}^1(\Gamma)}$. More generally, for any $k \geq 0$, we consider the Hilbert space $\mathrm{H}^{k+1}(\Omega,\Gamma) := \{u \in \mathrm{H}^{k+1}(\Omega),\ u_{|\Gamma} \in \mathrm{H}^{k+1}(\Gamma)\}$ (see [62, §2.3] for more details on these spaces and norms). Additionally, we define the following norm, used in Part III, $\|u\|^2_{\mathrm{L}^2(\Omega,\Gamma)} := \|u\|^2_{\mathrm{L}^2(\Omega)} + \|u\|^2_{\mathrm{L}^2(\Gamma)}$. This norm is well defined for $u \in \mathrm{H}^1(\Omega,\Gamma)$ (and more generally for any function on $\overline{\Omega}$ such that $u \in \mathrm{L}^2(\Omega)$ and $u_\Gamma \in \mathrm{L}^2(\Gamma)$).

For the sake of completeness, we recall the definition of the tangential operators involved in this work. For exhaustive details, we refer to [59, pages 192-196].

Definition 1.1.1. *Let $w \in \mathrm{H}^1(\Gamma)$, $W \in \mathrm{H}^1(\Gamma,\mathbb{R}^d)$ and $u \in \mathrm{H}^2(\Gamma)$. Then the following operators are defined on Γ:*

- *the tangential gradient of w given by $\nabla_\Gamma w := \nabla\tilde{w} - (\nabla\tilde{w}\cdot\mathbf{n})\mathbf{n}$, where $\tilde{w} \in \mathrm{H}^1(\mathbb{R}^d)$ is any extension of w;*
- *the tangential divergence of W given by $\mathrm{div}_\Gamma W := \mathrm{div}\tilde{W} - (\mathrm{D}\tilde{W}\mathbf{n})\cdot\mathbf{n}$, where $\tilde{W} \in \mathrm{H}^1(\mathbb{R}^d,\mathbb{R}^d)$ is any extension of W;*
- *the Laplace-Beltrami operator of u given by $\Delta_\Gamma u := \mathrm{div}_\Gamma(\nabla_\Gamma u)$.*

1.1.2 The Poisson-Ventcel problem

Considering the source terms $f \in \mathrm{L}^2(\Omega)$ and $g \in \mathrm{L}^2(\Gamma)$, as well as some given constants $\kappa \geq 0$, α, $\beta > 0$, the *Poisson-Ventcel problem* is given by,

$$\begin{cases} -\Delta u + \kappa u = & f \quad \text{in } \Omega, \\ -\beta\Delta_\Gamma u + \partial_{\mathrm{n}} u + \alpha u = & g \quad \text{on } \Gamma. \end{cases} \tag{1.1}$$

Following the notations presented previously, the variational formulation of Problem (1.1) is obtained using the *integration by parts formulas* (see [4, Theorem 4.4.7 p.104] and [59]). We recall that, for any $\phi \in \mathrm{H}^1(\Omega)$ and any $\sigma \in [\mathrm{L}^2(\Omega)]^d$ such that $\mathrm{div}(\sigma) \in \mathrm{L}^2(\Omega)$, we have,

$$\int_\Omega \mathrm{div}(\sigma)\phi\,\mathrm{d}x + \int_\Omega \sigma\cdot\nabla\phi\,\mathrm{d}x = \int_\Gamma (\sigma\cdot\mathbf{n})\,\phi\,\mathrm{d}s. \tag{1.2}$$

We also recall that for any $\phi, \psi \in \mathrm{H}^1(\Gamma)$,

$$-\int_\Gamma \mathrm{div}_\Gamma(\nabla_\Gamma \psi)\, \phi \, \mathrm{d}s = \int_\Gamma \nabla_\Gamma \psi \cdot \nabla_\Gamma \phi \, \mathrm{d}s. \tag{1.3}$$

Thus by applying (1.2) and (1.3), we obtain the following variational formulation of Problem (1.1),

$$\begin{cases} \text{find } u \in \mathrm{H}^1(\Omega, \Gamma), \ \text{ such that,} \\ a(u, v) = l(v), \ \forall\ v \in \mathrm{H}^1(\Omega, \Gamma), \end{cases} \tag{1.4}$$

where the bilinear form a, defined on $\mathrm{H}^1(\Omega, \Gamma) \times \mathrm{H}^1(\Omega, \Gamma)$, is given by,

$$a(u, v) := \int_\Omega \nabla u \cdot \nabla v \, \mathrm{d}x + \kappa \int_\Omega uv \, \mathrm{d}x + \beta \int_\Gamma \nabla_\Gamma u \cdot \nabla_\Gamma v \, \mathrm{d}s + \alpha \int_\Gamma uv \, \mathrm{d}s,$$

and the linear form l, defined on $\mathrm{H}^1(\Omega, \Gamma)$, is given by,

$$l(v) := \int_\Omega fv \, \mathrm{d}x + \int_\Gamma gv \, \mathrm{d}s.$$

The following theorem claims the well-posedness of Problem (1.4) and establishes the solution regularity proved in [62, §3]. Throughout this work, we extended the proof of the well-posedness to the particular case where κ vanishes. The following theorem is published in the proceeding [23]:

— F. Caubet, J. Ghantous, C. Pierre, *Numerical study of a diffusion equation with Ventcel boundary condition using curved meshes,* published in Monografías Matemáticas García de Galdeano, 2023.

For the sake of completeness, we present the proof of the well-posedness.

Theorem 1.1.2. *Let Ω and $\Gamma = \partial\Omega$ be as stated previously. Let α, $\beta > 0$, $\kappa \geq 0$, and $f \in \mathrm{L}^2(\Omega)$, $g \in \mathrm{L}^2(\Gamma)$. Then there exists a unique solution $u \in \mathrm{H}^1(\Omega, \Gamma)$ to Problem* (1.4).

Moreover, for $k \geq 1$, if Γ is of class $\mathcal{C}^{k+1}$, and $f \in \mathrm{H}^{k-1}(\Omega)$, $g \in \mathrm{H}^{k-1}(\Gamma)$, then the solution u of (1.4) *belongs to $\mathrm{H}^{k+1}(\Omega, \Gamma)$ and is a strong solution of the Ventcel problem* (1.1). *Additionally, there exists $c > 0$ such that the following inequality holds,*

$$\|u\|_{\mathrm{H}^{k+1}(\Omega,\Gamma)} \leq c\, (\|f\|_{\mathrm{H}^{k-1}(\Omega)} + \|g\|_{\mathrm{H}^{k-1}(\Gamma)}).$$

Proof of the well-posedness. The proof relies on the Lax-Milgram theorem. The linear form $l(\cdot)$ and the bilinear form $a(\cdot, \cdot)$ in (1.4) being continuous respectively on $\mathrm{H}^1(\Omega, \Gamma)$

and on $\mathrm{H}^1(\Omega,\Gamma)\times\mathrm{H}^1(\Omega,\Gamma)$, it remains to show that a is coercive. We must distinguish between two cases.

1) If $\kappa\neq 0$. The result is obvious for all $u\in\mathrm{H}^1(\Omega,\Gamma)$,

$$a(u,u)\geq\min\{1,\kappa,\alpha,\beta\}\|u\|^2_{\mathrm{H}^1(\Omega,\Gamma)}.$$

2) If $\kappa=0$. We proceed by contradiction assuming that there exists a sequence $(u_n)_{n\in\mathbb{N}^*}$ in $\mathrm{H}^1(\Omega,\Gamma)$ such that for all $n\geq 1$,

$$a(u_n,u_n)=\|\nabla u_n\|^2_{\mathrm{L}^2(\Omega)}+\beta\|\nabla_\Gamma u_n\|^2_{\mathrm{L}^2(\Gamma)}+\alpha\|u_n\|^2_{\mathrm{L}^2(\Gamma)}<\frac{1}{n}\Big(\|u_n\|^2_{\mathrm{H}^1(\Omega)}+\|u_n\|^2_{\mathrm{H}^1(\Gamma)}\Big).$$

It follows that $u_n\neq 0$ for all $n\geq 1$. Thus u_n can be normalized such that,

$$\|u_n\|_{\mathrm{H}^1(\Omega,\Gamma)}=1\qquad\text{and}\qquad\|\nabla u_n\|^2_{\mathrm{L}^2(\Omega)}+\beta\|\nabla_\Gamma u_n\|^2_{\mathrm{L}^2(\Gamma)}+\alpha\|u_n\|^2_{\mathrm{L}^2(\Gamma)}<\frac{1}{n}.$$

Therefore, we notice that,

$$\nabla u_n\to 0\quad\text{in }\mathrm{L}^2(\Omega),\quad\nabla_\Gamma u_n\to 0\quad\text{in }\mathrm{L}^2(\Gamma)\quad\text{and}\quad u_n\to 0\quad\text{in }\mathrm{L}^2(\Gamma).\tag{1.5}$$

Since $(u_n)_n$ is bounded in $\mathrm{H}^1(\Omega,\Gamma)$, there exists $u\in\mathrm{H}^1(\Omega,\Gamma)$ such that $u_n\rightharpoonup u$ in $\mathrm{H}^1(\Omega,\Gamma)$, and since $\mathrm{H}^1(\Omega,\Gamma)\hookrightarrow\mathrm{L}^2(\Omega,\Gamma)$ is a compact injection, the following convergence stands,

$$u_n\to u\ \text{ in }\ \mathrm{L}^2(\Omega,\Gamma).\tag{1.6}$$

Passing to the limit in the following equation,

$$\|u_n\|^2_{\mathrm{H}^1(\Omega,\Gamma)}=\|\nabla u_n\|^2_{\mathrm{L}^2(\Omega)}+\|\nabla_\Gamma u_n\|^2_{\mathrm{L}^2(\Gamma)}+\|u_n\|^2_{\mathrm{L}^2(\Gamma)}+\|u_n\|^2_{\mathrm{L}^2(\Omega)}=1,$$

and using the convergences given in (1.5) and (1.6), we obtain $\|u\|^2_{\mathrm{L}^2(\Omega,\Gamma)}=1$. However, since $\nabla u_n\rightharpoonup\nabla u$ in $\mathrm{L}^2(\Omega)$, employing (1.5) and the uniqueness of the limit we obtain $\nabla u=0$. Additionally, since Ω is a connected set, it follows that $u=C\in\mathbb{R}$. Finally, recalling that $u_n\to u$ in $\mathrm{L}^2(\Gamma)$ and also $u_n\to 0$ in $\mathrm{L}^2(\Gamma)$, these two points yield that $u=0=C$ which contradicts $\|u\|_{\mathrm{L}^2(\Omega,\Gamma)}=1$ and concludes the proof of the coercivity.

□

1.1.3 The spectral Ventcel problem

Let $\alpha, \beta > 0$. In the following, we will also focus on the numerical analysis of the *spectral problem with Ventcel boundary conditions* given by,

$$\begin{cases} -\Delta u = \lambda u & \text{in } \Omega, \\ -\beta \Delta_\Gamma u + \partial_{\mathrm{n}} u + \alpha u = 0 & \text{on } \Gamma. \end{cases} \tag{1.7}$$

The variational formulation of the studied problem (1.7) is classically obtained, using the integration by parts formula (1.2) and (1.3) and it is then given by,

$$\begin{cases} \text{find } (\lambda, u) \in \mathbb{R} \times \mathrm{H}^1(\Omega, \Gamma), \quad \text{such that,} \\ a(u, v) = \lambda\, m(u, v), \quad \forall\, v \in \mathrm{H}^1(\Omega, \Gamma), \end{cases}$$

where a is the bilinear form, defined on $\mathrm{H}^1(\Omega, \Gamma) \times \mathrm{H}^1(\Omega, \Gamma)$, given by,

$$a(u, v) := \int_\Omega \nabla u \cdot \nabla v \, \mathrm{d}x + \beta \int_\Gamma \nabla_\Gamma u \cdot \nabla_\Gamma v \, \mathrm{d}s + \alpha \int_\Gamma uv \, \mathrm{d}s,$$

and m is the bilinear form, defined on $\mathrm{H}^1(\Omega, \Gamma) \times \mathrm{H}^1(\Omega, \Gamma)$, given by,

$$m(u, v) := \int_\Omega uv \, \mathrm{d}x.$$

The bilinear form a, being symmetric and continuous, is also coercive with respect to the norm over $\mathrm{H}^1(\Omega, \Gamma)$, as proved in Theorem 1.1.2. The second bilinear form m is none other than the scalar product on the space $\mathrm{L}^2(\Omega)$. Then by a classical spectral result (see [4, Theorem 7.3.2]), the spectrum of the problem is made of positive eigenvalues of finite multiplicity, moreover there exists an orthonormal Hilbert basis of $\mathrm{L}^2(\Omega)$ made of eigenfunctions denoted u_n with an associated eigenvalue λ_n ordered such that,

$$0 < \lambda_0 \leq ... \leq \lambda_n \to +\infty$$

satisfying,

$$u_n \in \mathrm{H}^1(\Omega, \Gamma), \text{ and } a(u_n, v) = \lambda_n m(u_n, v), \quad \forall\, v \in \mathrm{H}^1(\Omega, \Gamma).$$

Remark 1.1.3. *We point out that in Section 6.4, an alternative problem is studied, where instead of having λu on Ω in the right hand side of Problem* (1.7)*, it is positioned*

on the boundary Γ. *This other spectral problem also admits a spectrum consisting of positive eigenvalues of finite multiplicities. Moreover, there exists an orthonormal Hilbert basis of* $\mathrm{L}^2(\Gamma)$ *composed of eigenfunctions associated with these eigenvalues.*

1.2 The vectorial case

1.2.1 Notations and needed mathematical tools

In the following, spaces of vector functions will be denoted by boldface letters. Thus, we denote $\mathbf{L}^2(\Omega) := [\mathrm{L}^2(\Omega)]^d$ and $\mathbf{L}^2(\Gamma) := [\mathrm{L}^2(\Gamma)]^d$. Similarly, for any $k \geq 0$, we have $\mathbf{H}^{k+1}(\Omega) := [\mathrm{H}^{k+1}(\Omega)]^d$ and $\mathbf{H}^{k+1}(\Gamma) := [\mathrm{H}^{k+1}(\Gamma)]^d$. We denote by I_d the $d \times d$ identity matrix. Finally, for two square real valued matrices A and B of same size $d \times d$, $A : B$ denotes the term by term product $A : B = \mathrm{Tr}(A^{\mathsf{T}} B) = \sum_{1 \leq i,j \leq d} a_{ij}\, b_{ij}$, also known as the Frobenius inner product. The symbol $\otimes$ represents the tensor product: for two vectors $a, b \in \mathbb{R}^d$, $a \otimes b = ab^{\mathsf{T}}$ (vectors here are in column form).

Let us now introduce some other notations (see e.g. [39, 27, 56]). For any smooth vector field $\boldsymbol{u}$, $\nabla \boldsymbol{u}$ is the matrix whose i^{th} row is the gradient of the i^{th} component of $\boldsymbol{u}$. For any smooth surface vector field $\boldsymbol{v}$, $\nabla_\Gamma \boldsymbol{v}$ is the matrix whose i^{th} row is the tangential gradient of the i^{th} component of $\boldsymbol{v}$ (see Definition 1.1.1 for the expression of the tangential gradient of a scalar function). Note that for any smooth vector field $\boldsymbol{v} = (v_i)_{i=1}^d$, we have by definition of the tangential gradient that $\mathrm{P}\, \nabla_\Gamma v_i = \nabla_\Gamma v_i$, which implies that $\nabla_\Gamma \boldsymbol{v}\, \mathrm{P} = \nabla_\Gamma \boldsymbol{v}$, where $\mathrm{P}(x) := \mathrm{I}_d - (\mathbf{n} \otimes \mathbf{n})(x)$ is the orthogonal projection over the tangential space of Γ at x. We underline the symmetry of P which will be used in the sequel: $\mathrm{P} = \mathrm{P}^{\mathsf{T}}$.

Let S be a smooth matrix function on Ω with values in $\mathbb{R}^{d \times d}$, with rows S_j for $j = 1, \ldots, d$, then the divergence of S is $\mathrm{div} S : \Omega \to \mathbb{R}^d$ given by $\mathrm{div}(S)_j = \mathrm{div}(S_j)$, for $j = 1, \ldots, d$. In a similar manner, one defines the tangential divergence of S by, $\mathrm{div}_\Gamma(S)_j = \mathrm{div}_\Gamma(S_j)$ for $j = 1, \ldots, d$ (see Definition 1.1.1 for the expression of the tangential divergence of a vector function).

For any vector field $\boldsymbol{u} = (u_i)_{i=1,\ldots,d} \in \mathbf{H}^1(\Omega)$, the *strain tensor*, defined by,

$$e(\boldsymbol{u}) := \frac{1}{2}(\nabla \boldsymbol{u} + (\nabla \boldsymbol{u})^{\mathsf{T}}), \tag{1.8}$$

is the symmetric part of the Jacobian matrix $\nabla \boldsymbol{u}$. In a similar manner, for any vector

field $\boldsymbol{u} = (u_i)_{i=1,\dots,d} \in \mathbf{H}^1(\Gamma)$, the *tangential strain tensor* is given by,

$$e_\Gamma(\boldsymbol{u}) := \frac{1}{2}\mathrm{P}(\nabla_\Gamma \boldsymbol{u} + (\nabla_\Gamma \boldsymbol{u})^\mathsf{T})\mathrm{P}. \tag{1.9}$$

Note that the following equality also holds,

$$e_\Gamma(\boldsymbol{u}) = \frac{1}{2}(\mathrm{P}\nabla_\Gamma \boldsymbol{u} + (\mathrm{P}\nabla_\Gamma \boldsymbol{u})^\mathsf{T}), \tag{1.10}$$

where we used the fact that $\nabla_\Gamma \boldsymbol{u}\,\mathrm{P} = \nabla_\Gamma \boldsymbol{u}$.

Next, we present an interesting remark used throughout Chapter 7.

Remark 1.2.1. *For $\boldsymbol{u} \in \mathbf{H}^1(\Omega)$ and $\boldsymbol{v} \in \mathbf{H}^1(\Gamma)$, we have,*

$$\mathrm{div}(\boldsymbol{u}) = \mathrm{Tr}(e(\boldsymbol{u})) \quad \text{and} \quad \mathrm{div}_\Gamma(\boldsymbol{v}) = \mathrm{Tr}(e_\Gamma(\boldsymbol{v})). \tag{1.11}$$

To prove the left hand side of (1.11)*, we need to notice that* $\mathrm{Tr}(\nabla \boldsymbol{u}) = \mathrm{Tr}((\nabla \boldsymbol{u})^\mathsf{T})$*. Thus,*

$$\mathrm{Tr}(e(\boldsymbol{u})) = \frac{1}{2}\Big(\mathrm{Tr}(\nabla \boldsymbol{u}) + \mathrm{Tr}((\nabla \boldsymbol{u})^\mathsf{T})\Big) = \mathrm{Tr}(\nabla \boldsymbol{u}) = \mathrm{div}(\boldsymbol{u}).$$

To prove the other equation of (1.11)*, we proceed in a similar manner using* (1.10) *as follows,*

$$\mathrm{Tr}(e_\Gamma(\boldsymbol{u})) = \mathrm{Tr}(\mathrm{P}\,\nabla_\Gamma \boldsymbol{u}) = \mathrm{Tr}(\nabla_\Gamma \boldsymbol{u}\,\mathrm{P}) = \mathrm{Tr}(\nabla_\Gamma \boldsymbol{u}) = \mathrm{div}_\Gamma(\boldsymbol{u}),$$

where we used that $\mathrm{Tr}(AB) = \mathrm{Tr}(BA)$ *for any two square real valued matrices A and B of same size $d \times d$ and that* $\nabla_\Gamma \boldsymbol{u}\,\mathrm{P} = \nabla_\Gamma \boldsymbol{u}$*.*

Here, we assume that Ω is an elastic body and we consider an isotropic elastic medium with *Lamé coefficients* $\mu_\Omega > 0$ and $\lambda_\Omega > 0$, which are considered as constants for more simplicity in this study (possible extension to variable coefficients will be discussed later on see Remark 7.1.1), and associated *elastic or Hooke tensor* $\mathbf{A}_\Omega$ given by,

$$\mathbf{A}_\Omega \xi := 2\mu_\Omega \xi + \lambda_\Omega \mathrm{Tr}(\xi)\mathrm{I}_d, \tag{1.12}$$

for all symmetric matrices $\xi \in \mathbb{R}^d \times \mathbb{R}^d$, with Tr denoting the matrix trace. We refer to [47, 31] for more details.

Additionally, we assume that the body Ω is surrounded by a *thin layer* with another

Hooke tensor given for $x \in \Gamma$ by,

$$\mathbf{A}_\Gamma \xi(x) := 2\mu_\Gamma \xi(x) + \lambda_\Gamma \mathrm{Tr}(\xi(x))\mathrm{P}(x), \tag{1.13}$$

for all symmetric matrices ξ, where $\mu_\Gamma > 0$ and $\lambda_\Gamma > 0$ are some (modified) *Lamé constants* which correspond to a coating (the thin layer) and which are considered as constants (see Remark 7.1.1) and where, for any $x \in \Gamma$, $\mathrm{P}(x) = \mathrm{I}_d - (\mathbf{n} \otimes \mathbf{n})(x)$ is the orthogonal projection over the tangential space of Γ at x.

Now, we define the following Hilbert space,

$$\mathbf{V}_\Gamma := \{\boldsymbol{v} \in \mathbf{L}^2(\Gamma),\, e_\Gamma(\boldsymbol{v}) \in [\mathrm{L}^2(\Gamma)]^{d\times d}\},$$

endowed with the norm, $\|\boldsymbol{v}\|^2_{\mathbf{V}_\Gamma} := \|\boldsymbol{v}\|^2_{\mathbf{L}^2(\Gamma)} + \|e_\Gamma(\boldsymbol{v})\|^2_{[\mathrm{L}^2(\Gamma)]^{d\times d}}$. Throughout the vectorial case in Chapter 7, we rely on the following Hilbert space,

$$\mathbf{H}_{(\Omega,\Gamma)} := \{\boldsymbol{v} \in \mathbf{H}^1(\Omega);\, \boldsymbol{v}_{|_\Gamma} \in \mathbf{V}_\Gamma\},$$

endowed with the norm, $\|\boldsymbol{v}\|^2_{\mathbf{H}_{(\Omega,\Gamma)}} := \|\boldsymbol{v}\|^2_{\mathbf{H}^1(\Omega)} + \|\boldsymbol{v}\|^2_{\mathbf{V}_\Gamma}$.

A classical tool when dealing with a linear elasticity problem is *Korn's inequality* (see, e.g., [29, Theorem 6.3-4]): let Ω be an open, connected domain in $\mathbb{R}^d$, $d \geq 2$. There exists a constant $C > 0$, known as the *Korn constant* of Ω, such that, for all $\boldsymbol{v} \in \mathbf{H}^1(\Omega)$,

$$\|\boldsymbol{v}\|^2_{\mathbf{H}^1(\Omega)} \leq C\Big(\|\boldsymbol{v}\|^2_{\mathbf{L}^2(\Omega)} + \|e(\boldsymbol{v})\|^2_{[\mathrm{L}^2(\Omega)]^{d\times d}}\Big).$$

In this work, a Korn inequality with surface norms and the symmetrized tangential gradient is needed. Under the adequate hypothesis, there exists a constant $C > 0$ depending on Γ, such that, for all $\boldsymbol{v} \in \mathbf{V}_\Gamma$,

$$\|\boldsymbol{v}\|^2_{\mathbf{H}^1(\Gamma)} \leq C\Big(\|\boldsymbol{v}\|^2_{\mathbf{L}^2(\Gamma)} + \|e_\Gamma(\boldsymbol{v})\|^2_{[\mathrm{L}^2(\Gamma)]^{d\times d}}\Big) = C\|\boldsymbol{v}\|^2_{\mathbf{V}_\Gamma}. \tag{1.14}$$

For the sake of completeness, we give a brief explanation on how to obtain this surface Korn inequality (1.14). Indeed, using the formulas given in [31, page 88], one can check that the operator $\boldsymbol{u} \in \mathbf{V}_\Gamma \to e_\Gamma(\boldsymbol{u}) \in \mathbf{L}^2(\Gamma)$ corresponds to the operator $\gamma_{\alpha\beta}$ defined in [31, Theorem 2.7.1]. Then, we can derive a Korn-type inequality on 2-dimensional compact manifolds without boundary from [31, Theorem 2.7.1] ensuring that there exists a constant $C > 0$ depending on Γ such that for any $\boldsymbol{v} \in \mathbf{V}_\Gamma$ Inequality (1.14)

holds.

Furthermore, the two spaces $\mathbf{H}_{(\Omega,\Gamma)}$ and $\mathbf{H}^1(\Omega,\Gamma)$ coincide and have equivalent norms satisfying the following inequality for any $\boldsymbol{v} \in \mathbf{H}_{(\Omega,\Gamma)}$,

$$c_1\|\boldsymbol{v}\|_{\mathbf{H}^1(\Omega,\Gamma)} \leq \|\boldsymbol{v}\|_{\mathbf{H}_{(\Omega,\Gamma)}} \leq c_2\|\boldsymbol{v}\|_{\mathbf{H}^1(\Omega,\Gamma)}, \tag{1.15}$$

where $\|\boldsymbol{v}\|^2_{\mathbf{H}^1(\Omega,\Gamma)} := \|\boldsymbol{v}\|^2_{\mathbf{H}^1(\Omega)} + \|\boldsymbol{v}_{|\Gamma}\|^2_{\mathbf{H}^1(\Gamma)}$ and c_1, c_2 are positive constants. The right hand side of (1.15) is quite natural and it is classically obtained by definition of each norm. The left hand side of (1.15) is a consequence of the korn inequality (1.14). This norm equivalence (1.15) will be used multiple times throughout the proofs of Chapter 7.

Next, we present the following equalities used in Chapter 7.

Lemma 1.2.2. *For any $\boldsymbol{u}, \boldsymbol{v} \in \mathbf{H}_{(\Omega,\Gamma)}$, we have,*

$$\mathbf{A}_\Omega(e(\boldsymbol{u})) : \nabla\boldsymbol{v} = \mu_\Omega\Big(\nabla\boldsymbol{u} : \nabla\boldsymbol{v} + (\nabla\boldsymbol{u})^{\mathsf{T}} : \nabla\boldsymbol{v}\Big) + \lambda_\Omega \mathrm{div}(\boldsymbol{u})\,\mathrm{div}(\boldsymbol{v}), \tag{1.16}$$

$$\mathbf{A}_\Gamma(e_\Gamma(\boldsymbol{u})) : \nabla_\Gamma\boldsymbol{v} = \mu_\Gamma\Big(\mathrm{P}\,\nabla_\Gamma\boldsymbol{u} : \nabla_\Gamma\boldsymbol{v} + (\nabla_\Gamma\boldsymbol{u})^{\mathsf{T}} : \nabla_\Gamma\boldsymbol{v}\Big) + \lambda_\Gamma\,\mathrm{div}_\Gamma(\boldsymbol{u})\,\mathrm{div}_\Gamma(\boldsymbol{v}). \tag{1.17}$$

Proof. To prove (1.16), we use the definition of the Hooke tensor in (1.12) and of the strain tensor in (1.8) as follows,

$$\begin{aligned}
\mathbf{A}_\Omega(e(\boldsymbol{u})) : \nabla\boldsymbol{v} &= 2\mu_\Omega\, e(\boldsymbol{u}) : \nabla\boldsymbol{v} + \lambda_\Omega\,\mathrm{Tr}(\nabla\boldsymbol{u})\,\mathrm{I}_d : \nabla\boldsymbol{v} \\
&= \mu_\Omega\Big(\nabla\boldsymbol{u} : \nabla\boldsymbol{v} + (\nabla\boldsymbol{u})^{\mathsf{T}} : \nabla\boldsymbol{v}\Big) + \lambda_\Omega\,\mathrm{Tr}(\nabla\boldsymbol{u})\,\mathrm{Tr}(\nabla\boldsymbol{v}) \\
&= \mu_\Omega\Big(\nabla\boldsymbol{u} : \nabla\boldsymbol{v} + (\nabla\boldsymbol{u})^{\mathsf{T}} : \nabla\boldsymbol{v}\Big) + \lambda_\Omega\,\mathrm{div}(\boldsymbol{u})\,\mathrm{div}(\boldsymbol{v}).
\end{aligned}$$

Similarly, by definition of the Hooke tensor in (1.13) and by applying the expression of the strain tensor in (1.10), Equation (1.17) can be easily explained as follows,

$$\begin{aligned}
\mathbf{A}_\Gamma(e_\Gamma(\boldsymbol{u})) : \nabla_\Gamma\boldsymbol{v} &= 2\mu_\Gamma\, e_\Gamma(\boldsymbol{u}) : \nabla_\Gamma\boldsymbol{v} + \lambda_\Gamma\,\mathrm{Tr}(\nabla_\Gamma\boldsymbol{u})\,\mathrm{P} : \nabla_\Gamma\boldsymbol{v} \\
&= \mu_\Gamma\Big(\mathrm{P}\,\nabla_\Gamma\boldsymbol{u} : \nabla_\Gamma\boldsymbol{v} + (\mathrm{P}\nabla_\Gamma\boldsymbol{u})^{\mathsf{T}} : \nabla_\Gamma\boldsymbol{v}\Big) + \lambda_\Gamma\,\mathrm{Tr}(\nabla_\Gamma\boldsymbol{u})\,\mathrm{Tr}(\nabla_\Gamma\boldsymbol{v}\,\mathrm{P}) \\
&= \mu_\Gamma\Big(\mathrm{P}\,\nabla_\Gamma\boldsymbol{u} : \nabla_\Gamma\boldsymbol{v} + (\nabla_\Gamma\boldsymbol{u})^{\mathsf{T}}\mathrm{P} : \nabla_\Gamma\boldsymbol{v}\Big) + \lambda_\Gamma\,\mathrm{Tr}(\nabla_\Gamma\boldsymbol{u})\mathrm{Tr}(\nabla_\Gamma\boldsymbol{v}),
\end{aligned}$$

where we used that $\nabla_\Gamma \boldsymbol{v}\,\mathrm{P} = \nabla_\Gamma \boldsymbol{v}$. Then, by definition of div_Γ, we get,

$$\begin{aligned}\mathbf{A}_\Gamma(e_\Gamma(\boldsymbol{u})) : \nabla_\Gamma \boldsymbol{v} &= \mu_\Gamma\Big(\mathrm{P}\,\nabla_\Gamma \boldsymbol{u} : \nabla_\Gamma \boldsymbol{v} + (\nabla_\Gamma \boldsymbol{u})^{\mathsf{T}} : \nabla_\Gamma \boldsymbol{v}\,\mathrm{P}\Big) + \lambda_\Gamma\,\mathrm{div}_\Gamma(\boldsymbol{u})\,\mathrm{div}_\Gamma(\boldsymbol{v}) \\ &= \mu_\Gamma\Big(\mathrm{P}\,\nabla_\Gamma \boldsymbol{u} : \nabla_\Gamma \boldsymbol{v} + (\nabla_\Gamma \boldsymbol{u})^{\mathsf{T}} : \nabla_\Gamma \boldsymbol{v}\Big) + \lambda_\Gamma\,\mathrm{div}_\Gamma(\boldsymbol{u})\,\mathrm{div}_\Gamma(\boldsymbol{v}),\end{aligned}$$

where we used that $AB^{\mathsf{T}} : C = A : CB$ for any square real valued matrices A, B and C of same size $d \times d$. □

1.2.2 The elasticity module with Ventcel boundary conditions

Let $\boldsymbol{f} \in \mathbf{L}^2(\Omega)$, $\boldsymbol{g} \in \mathbf{L}^2(\Gamma)$. Given $\alpha, \beta > 0$ two real numbers, we consider the following *linear elasticity problem with Ventcel boundary condition*,

$$\begin{cases} -\mathrm{div}(\mathbf{A}_\Omega e(\boldsymbol{u})) = \boldsymbol{f} & \text{in } \Omega, \\ -\beta \mathrm{div}_\Gamma(\mathbf{A}_\Gamma e_\Gamma(\boldsymbol{u})) + \mathbf{A}_\Omega e(\boldsymbol{u})\mathbf{n} + \alpha \boldsymbol{u} = \boldsymbol{g} & \text{on } \Gamma. \end{cases} \tag{1.18}$$

For more details, we refer to [26], where an asymptotic analysis is used to derive the elasticity problem (1.18).

Following the notations presented previously, the variational formulation of Problem (1.18) is obtained using the *integration by parts formulas with vector valued functions* (see [4, Theorem 4.4.7 p.104], [59] and [46]). For the sake of completeness, we recall the integration formulas respectively on the domain Ω and on the surface Γ. For any $\phi \in \mathbf{H}^1(\Omega)$ and $\sigma \in [\mathbf{L}^2(\Omega)]^{d\times d}$ a square real valued matrix function such that $\mathrm{div}(\sigma) \in \mathbf{L}^2(\Omega)$, we have,

$$\int_\Omega \mathrm{div}(\sigma) \cdot \phi \,\mathrm{d}x + \int_\Omega \sigma : \nabla \phi \,\mathrm{d}x = \int_\Gamma (\sigma\,\mathbf{n}) \cdot \phi \,\mathrm{d}s. \tag{1.19}$$

We also have for any $\phi \in \mathbf{H}^1(\Gamma)$ and $\sigma \in [\mathbf{L}^2(\Gamma)]^{d\times d}$ a square real valued matrix function such that $\mathrm{div}_\Gamma(\sigma) \in \mathbf{L}^2(\Gamma)$,

$$-\int_\Gamma \mathrm{div}_\Gamma(\sigma) \cdot \phi \,\mathrm{d}s + \int_\Gamma \mathrm{H}\,\phi \cdot (\sigma\mathbf{n})\,\mathrm{d}s = \int_\Gamma \sigma : \nabla_\Gamma \phi \,\mathrm{d}s,$$

where H is the mean curvature of Γ (see Proposition 5.4.9 in [59]). In particular, by denoting $\sigma_\Gamma := \sigma\mathrm{P}$ the tangential part of σ, the previous formula can be written as follows:

$$-\int_\Gamma \mathrm{div}_\Gamma(\sigma_\Gamma) \cdot \phi \,\mathrm{d}s = \int_\Gamma \sigma_\Gamma : \nabla_\Gamma \phi \,\mathrm{d}s. \tag{1.20}$$

We also notice that $\mathbf{A}_\Gamma e_\Gamma(\boldsymbol{u})\,\mathrm{P} = \mathbf{A}_\Gamma e_\Gamma(\boldsymbol{u})$. Indeed, by using the definition of the tangential strain tensor in (1.9) and the idempotence property of the orthogonal projection P, we get the following equality,

$$\begin{aligned}\mathbf{A}_\Gamma e_\Gamma(\boldsymbol{u})\,\mathrm{P} &= 2\mu_\Gamma e_\Gamma(\boldsymbol{u})\,\mathrm{P} + \lambda_\Gamma \mathrm{Tr}(e_\Gamma(\boldsymbol{u}))\,\mathrm{P}^2 \\ &= 2\mu_\Gamma e_\Gamma(\boldsymbol{u}) + \lambda_\Gamma \mathrm{Tr}(e_\Gamma(\boldsymbol{u}))\,\mathrm{P} = \mathbf{A}_\Gamma e_\Gamma(\boldsymbol{u}).\end{aligned}$$

Thus, applying (1.19) and (1.20), the variational formulation is given by,

$$\begin{cases} \text{find } \boldsymbol{u} \in \mathbf{H}_{(\Omega,\Gamma)}, \quad \text{such that,} \\ a(\boldsymbol{u},\boldsymbol{v}) = l(\boldsymbol{v}),\ \forall\ \boldsymbol{v} \in \mathbf{H}_{(\Omega,\Gamma)}, \end{cases} \tag{1.21}$$

where the bilinear form a, defined on $\mathbf{H}_{(\Omega,\Gamma)} \times \mathbf{H}_{(\Omega,\Gamma)}$, is given by,

$$a(\boldsymbol{u},\boldsymbol{v}) = \int_\Omega \mathbf{A}_\Omega(e(\boldsymbol{u})) : \nabla \boldsymbol{v}\,\mathrm{d}x + \beta \int_\Gamma \mathbf{A}_\Gamma(e_\Gamma(\boldsymbol{u})) : \nabla_\Gamma \boldsymbol{v}\,\mathrm{d}s + \alpha \int_\Gamma \boldsymbol{u}\cdot\boldsymbol{v}\,\mathrm{d}s.$$

The linear form l in (1.21), defined on $\mathbf{H}_{(\Omega,\Gamma)}$, is given by,

$$l(\boldsymbol{v}) := \int_\Omega \boldsymbol{f}\cdot\boldsymbol{v}\,\mathrm{d}x + \int_\Gamma \boldsymbol{g}\cdot\boldsymbol{v}\,\mathrm{d}s.$$

The following theorem claims the well-posedness of Problem (1.21). We refer to [26, Proposition A.1] for its full proof.

Theorem 1.2.3. *Let Ω and $\Gamma = \partial\Omega$ be as stated previously. Let $\alpha,\ \beta > 0$ and $\boldsymbol{f} \in \mathbf{L}^2(\Omega)$, $\boldsymbol{g} \in \mathbf{L}^2(\Gamma)$. Then there exists a unique solution $\boldsymbol{u} \in \mathbf{H}_{(\Omega,\Gamma)}$ to Problem (1.21). Additionally, there exists $c > 0$ such that the following inequality holds,*

$$\|\boldsymbol{u}\|_{\mathbf{H}_{(\Omega,\Gamma)}} \leq c\,(\|\boldsymbol{f}\|_{\mathbf{L}^2(\Omega)} + \|\boldsymbol{g}\|_{\mathbf{L}^2(\Gamma)}).$$

Remark 1.2.4. *We need to point out that in [26], the well-posedness of the weak formulation* (1.21) *is proved using the following bilinear form,*

$$\tilde{a}(\boldsymbol{u},\boldsymbol{v}) := \int_\Omega \mathbf{A}_\Omega(e(\boldsymbol{u})) : e(\boldsymbol{v})\,\mathrm{d}x + \beta \int_\Gamma \mathbf{A}_\Gamma(e_\Gamma(\boldsymbol{u})) : e_\Gamma(\boldsymbol{v})\,\mathrm{d}s + \alpha \int_\Gamma \boldsymbol{u}\cdot\boldsymbol{v}\,\mathrm{d}s.$$

Furthermore, we have $\tilde{a}(\boldsymbol{u},\boldsymbol{v}) = a(\boldsymbol{u},\boldsymbol{v})$, for any $\boldsymbol{u},\boldsymbol{v} \in \mathbf{H}_{(\Omega,\Gamma)}$, by applying the follow-

ing equations,

$$\mathbf{A}_\Omega(e(\boldsymbol{u})) : e(\boldsymbol{v}) = \mathbf{A}_\Omega(e(\boldsymbol{u})) : \nabla \boldsymbol{v}, \quad \mathbf{A}_\Gamma(e_\Gamma(\boldsymbol{u})) : e_\Gamma(\boldsymbol{v}) = \mathbf{A}_\Gamma(e_\Gamma(\boldsymbol{u})) : \nabla_\Gamma \boldsymbol{v}. \quad (1.22)$$

Now we prove the equations stated in (1.22)*. By definition of the strain tensor defined in* (1.8)*, we have,*

$$\begin{aligned}\mathbf{A}_\Omega(e(\boldsymbol{u})) : e(\boldsymbol{v}) &= \frac{1}{2}\Big(\mathbf{A}_\Omega(e(\boldsymbol{u})) : \nabla \boldsymbol{v} + \mathbf{A}_\Omega(e(\boldsymbol{u})) : (\nabla \boldsymbol{v})^{\mathsf{T}}\Big) \\ &= \frac{1}{2}\Big(\mathbf{A}_\Omega(e(\boldsymbol{u})) : \nabla \boldsymbol{v} + (\mathbf{A}_\Omega(e(\boldsymbol{u})))^{\mathsf{T}} : \nabla \boldsymbol{v}\Big).\end{aligned}$$

Since $(\mathbf{A}_\Omega(e(\boldsymbol{u})))^{\mathsf{T}} = \mathbf{A}_\Omega(e(\boldsymbol{u}))$ *for any* $\boldsymbol{u} \in \mathbf{H}_{(\Omega,\Gamma)}$*, we obtain the equation on the left hand side of* (1.22)*.*

In a similar manner, one obtains the following equation while using the expression of the tangential strain tensor in (1.10)*,*

$$\mathbf{A}_\Gamma(e_\Gamma(\boldsymbol{u})) : e_\Gamma(\boldsymbol{v}) = \mathbf{A}_\Gamma(e_\Gamma(\boldsymbol{u})) : \mathrm{P}\nabla_\Gamma \boldsymbol{v} = \mathrm{P}\mathbf{A}_\Gamma(e_\Gamma(\boldsymbol{u})) : \nabla_\Gamma \boldsymbol{v}, \quad (1.23)$$

where we used that $A : B^{\mathsf{T}} C = BA : C$*. Moreover, using* (1.10)*, we have,*

$$\begin{aligned}\mathrm{P}\, e_\Gamma(\boldsymbol{u}) = \frac{1}{2}(\mathrm{P}^2\, \nabla_\Gamma \boldsymbol{u} + \mathrm{P}\,(\mathrm{P}\, \nabla_\Gamma \boldsymbol{u})^{\mathsf{T}}) &= \frac{1}{2}(\mathrm{P}\, \nabla_\Gamma \boldsymbol{u} + (\mathrm{P}\, \nabla_\Gamma \boldsymbol{u}\, \mathrm{P})^{\mathsf{T}}) \\ &= \frac{1}{2}(\mathrm{P}\, \nabla_\Gamma \boldsymbol{u} + (\mathrm{P}\, \nabla_\Gamma \boldsymbol{u})^{\mathsf{T}}) = e_\Gamma(\boldsymbol{u}),\end{aligned}$$

since $\mathrm{P}^2 = \mathrm{P}$ *and* $\nabla_\Gamma \boldsymbol{u}\, \mathrm{P} = \nabla_\Gamma \boldsymbol{u}$*. Finally, using* (1.13) *with the latter equation, we have,*

$$\begin{aligned}\mathrm{P}\, \mathbf{A}_\Gamma(e_\Gamma(\boldsymbol{u})) &= 2\mu_\Gamma \mathrm{P}\, e_\Gamma(\boldsymbol{u}) + \lambda_\Gamma \mathrm{Tr}(e_\Gamma(\boldsymbol{u}))\mathrm{P}^2 \\ &= 2\mu_\Gamma e_\Gamma(\boldsymbol{u}) + \lambda_\Gamma \mathrm{Tr}(e_\Gamma(\boldsymbol{u}))\mathrm{P} = \mathbf{A}_\Gamma(e_\Gamma(\boldsymbol{u})).\end{aligned}$$

Replacing this equality in (1.23)*, we obtain the equation on the right hand side of* (1.22)*.*

Chapter 2

Curved meshes

In this chapter we recall the construction of curved meshes of geometrical order $r \geq 1$ of the domain Ω and introduce some notations.

Context and state of the art. The first prerequisite in the error analysis is to discretize the domain. As previously mentioned, due to the presence of the second order term in the Ventcel boundary conditions of the problems (1.1), (1.7), and (1.18), the domain Ω is assumed to be smooth. Thus, the physical domain Ω being non-polygonal can not be exactly fitted by an affine mesh domain Ω_h, i.e. $\Omega_h \neq \Omega$. This gap between Ω and Ω_h produces a *geometric error*. When using classical meshes made of triangles (affine meshes), this geometric error induces a saturation of the error at order 2, independently of the considered finite element order. To overcome this issue, we will resort to *curved meshes*, following the work of many authors (see, e.g., [32, 33, 42, 43]). We need to point out that the domain of the mesh of order r, denoted $\Omega_h^{(r)}$, does not fit the domain Ω. However, the numerical results are expected to be more accurate for $r \geq 2$ than for *standard affine meshes* (with $r = 1$) as will be exposed in Chapters 5, 6 and 7.

For $r \geq 1$, the set of polynomials in $\mathbb{R}^d$ of order r or less is denoted by $\mathbb{P}^r$. From now on, $\hat{T}$ denotes the reference simplex of dimension d. In a nutshell, since the domain Ω is smooth (at least $\mathcal{C}^{r+2}$), the way to proceed is the following.

1. Construct *an affine mesh* $\mathcal{T}_h^{(1)}$ of Ω composed of simplices T and define the affine transformation $F_T : \hat{T} \to T := F_T(\hat{T})$ associated to each simplice T.
2. For each simplex $T \in \mathcal{T}_h^{(1)}$, a mapping $F_T^{(e)} : \hat{T} \to T^{(e)} := F_T^{(e)}(\hat{T})$ is designed and the resulting *exact elements* $T^{(e)}$ will form *an exact curved mesh* $\mathcal{T}_h^{(e)}$ of Ω where its domain exactly fits Ω.
3. For each $T \in \mathcal{T}_h^{(1)}$, the mapping $F_T^{(r)}$ is the $\mathbb{P}^r$ interpolant of $F_T^{(e)}$. *The curved mesh* $\mathcal{T}_h^{(r)}$ of order r is composed of the elements $T^{(r)} := F_T^{(r)}(\hat{T})$.

The constructions of these meshes are based on the following fundamental result that may be found in [35] and [51, §14.6]. They rely on the geometrical properties of the tubular neighborhood and the orthogonal projection defined in Proposition 2.0.1. For more exhaustive details we refer to [36, 37, 41].

Proposition 2.0.1. *Let Ω and $\Gamma = \partial\Omega$ be as stated previously. Let $\mathrm{d} : \mathbb{R}^d \to \mathbb{R}$ be the signed distance function with respect to Γ defined by,*

$$\mathrm{d}(x) := \begin{cases} -\mathrm{dist}(x,\Gamma) & \text{if } x \in \Omega, \\ 0 & \text{if } x \in \Gamma, \\ \mathrm{dist}(x,\Gamma) & \text{otherwise,} \end{cases} \qquad \text{with} \quad \mathrm{dist}(x,\Gamma) := \inf\{|x-y|, \quad y \in \Gamma\}.$$

Then there exists a tubular neighborhood $\mathcal{U}_\Gamma$ of Γ where d is a $\mathcal{C}^2$ function. Its gradient $\nabla\mathrm{d}$ is an extension of the external unit normal $\mathbf{n}$ to Γ. Additionally, in this neighborhood $\mathcal{U}_\Gamma$, the orthogonal projection b onto Γ is uniquely defined and given by

$$b \; : \; x \in \mathcal{U}_\Gamma \longmapsto b(x) := x - \mathrm{d}(x)\nabla\mathrm{d}(x) \in \Gamma.$$

2.1 Affine mesh $\mathcal{T}_h^{(1)}$

Let $\mathcal{T}_h^{(1)}$ be a polyhedral mesh of Ω made of simplices of dimension d (triangles or tetrahedra). The mesh domain is denoted by $\Omega_h^{(1)} := \cup_{T\in\mathcal{T}_h^{(1)}} T$. Its boundary denoted by $\Gamma_h^{(1)} := \partial\Omega_h^{(1)}$ is composed of $(d-1)$-dimensional simplices (edges or triangles) that form a mesh of $\Gamma = \partial\Omega$.

Assumption. The vertices of $\Gamma_h^{(1)}$ are assumed to lie on Γ. This assumption will be assumed to be fulfilled by all the meshes in this work.

The *mesh size* is defined as follows, $h := \max\{\mathrm{diam}(T);\ T \in \mathcal{T}_h^{(1)}\}$, where $\mathrm{diam}(T)$ is the diameter of T. The mesh $\mathcal{T}_h^{(1)}$ is chosen as *quasi-uniform* and henceforth *shape-regular*, hence there exists a constant $c > 0$ such that,

$$h \leq c \min\{\mathrm{diam}(\mathcal{B}_T), T \in \mathcal{T}_h^{(1)}\},$$

where $\mathcal{B}_T$ is the biggest ball or disk that is contained in T (see [19, Definition 4.4.13] for more details).

Definition 2.1.1. *In a mesh we define two types of elements:*

— *an internal mesh element having at most one vertex on the domain's boundary* Γ*;*

— *a non-internal mesh element that has a least two vertices on* Γ*.*

Remark 2.1.2. *Note that for a sufficiently small mesh size* h *and under the hypothesis of a quasi-uniform mesh* $\mathcal{T}_h^{(1)}$*, the mesh boundary satisfies* $\Gamma_h^{(1)} \subset \mathcal{U}_\Gamma$*, where* $\mathcal{U}_\Gamma$ *is the tubular neighborhood given in Proposition 2.0.1. This guaranties that the orthogonal projection* $b : \Gamma_h^{(1)} \to \Gamma$ *is one to one which is required for the construction of the exact mesh.*

Under the assumption of a quasi-uniformal mesh and for a sufficiently small mesh size h*, the non-internal mesh elements can not have all their vertices on the boundary* Γ*: in 2D, a triangle has at most 2 vertices on* Γ *and in 3D, a tetrahedral has at most 3 vertices on* Γ*.*

For $T \in \mathcal{T}_h^{(1)}$, we define an affine function that maps the reference element onto T,

$$F_T : \hat{T} \to T := F_T(\hat{T}).$$

Example 2.1.3. *In the two dimensional case, is displayed in Figure 2.1 the case of a triangle* $T \in \mathcal{T}_h^{(1)}$*, with* $T \cap \Gamma = \{v_2, v_3\}$*, together with the mapping* F_T *that maps* $\hat{T}$ *into* T*.*

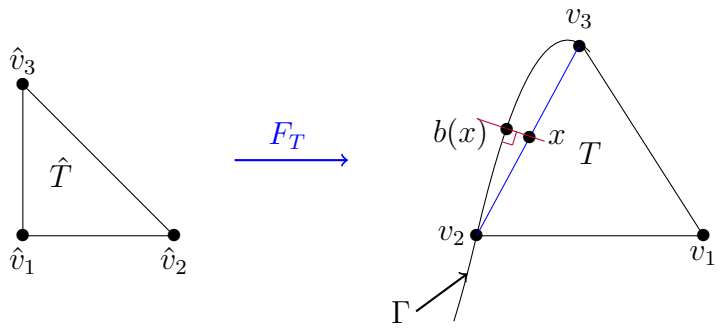

Figure 2.1 – Visualisation of $F_T : \hat{T} \to T$ and $b : [v_2, v_3] \to \Gamma$.

Notice that $[v_2, v_3] \subset \Gamma_h^{(1)} \subset \mathcal{U}_\Gamma$*, the orthogonal projection* $b(x)$ *of any point* $x \in [v_1, v_2]$ *is uniquely defined on the boundary* Γ*, by Proposition 2.0.1.*

2.2 Exact mesh $\mathcal{T}_h^{(e)}$

In this section, is recalled the definition of an exact transformation $F_T^{(e)}$ defined in the work of Elliott *et al.* in [43] in 2013, which is used throughout this work. For the sake of completeness, one needs to recall that in the 1970's, Scott gave an explicit construction of an exact triangulation in two dimensions in [73]. Later on, it was generalised by Lenoir in [65]. The present definition of an exact transformation $F_T^{(e)}$ combines the definitions found in [65, 73, 69, 12] with the orthogonal projection onto the domain's boundary b, defined in Proposition 2.0.1, first used to this aim by Dubois in [38] in the 1990's.

Following Remark 2.1.2, we recall that for a sufficiently small h, a mesh element $T \in \mathcal{T}_h^{(1)}$ cannot have $d+1$ vertices on the boundary Γ. In Definition 2.2.1, are given essential key elements for the construction of $F_T^{(e)}$.

Definition 2.2.1. *Let $T \in \mathcal{T}_h^{(1)}$ be a non-internal element (see Remark 2.1.1). Denote $v_i = F_T(\hat{v}_i)$ as its vertices, where $\hat{v}_i$ are the vertices of $\hat{T}$. We define $\varepsilon_i = 1$ if $v_i \in \Gamma$ and $\varepsilon_i = 0$ otherwise. To $\hat{x} \in \hat{T}$ is associated its barycentric coordinates λ_i associated to the vertices $\hat{v}_i$ of $\hat{T}$ and $\lambda^*(\hat{x}) := \sum_{i=1}^{d+1} \varepsilon_i \lambda_i$ (shortly denoted by λ^*). Finally, we define $\hat{\sigma} := \{\hat{x} \in \hat{T}; \lambda^*(\hat{x}) = 0\}$ and the function $\hat{y} := \dfrac{1}{\lambda^*} \sum_{i=1}^{d+1} \varepsilon_i \lambda_i \hat{v}_i \in \hat{T}$, which is well defined on $\hat{T} \backslash \hat{\sigma}$.*

Consider a non-internal mesh element $T \in \mathcal{T}_h^{(1)}$, with the affine transformation denoted F_T. In the two dimensional case, $F_T(\hat{\sigma})$ will consist of the only vertex of T that is not on the boundary Γ. As an illustration on Figure 2.2, $\hat{\sigma}$ is the vertex $\hat{v}_1$ of $\hat{T}$ and consequently $F_T(\hat{\sigma})$ is equal to v_1.

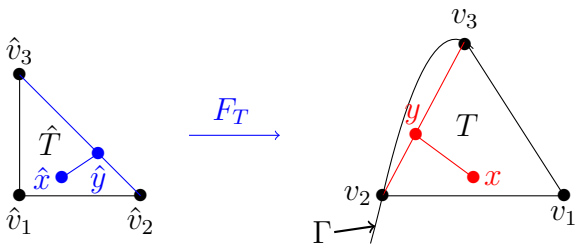

Figure 2.2 – Visualisation of the two functions $\hat{y} : \hat{T} \setminus \{\hat{v}_1\} \to [\hat{v}_2, \hat{v}_3]$ and $y : \hat{T} \backslash \{v_1\} \to [v_2, v_3]$ in Definition 2.2.2 in a 2D case

In the three dimensional case, the tetrahedral T either has 2 or 3 vertices on the boundary. In the case where T has 2 vertices on the boundary, $F_T(\hat{\sigma})$ is the edge of T

joining its two internal vertices as illustrated on the right side of Figure 2.3: $F_T(\hat{\sigma}) := [v_4, v_1]$ and $\hat{\sigma} := [\hat{v}_4, \hat{v}_1]$. In the case where T has 3 vertices on the boundary, $F_T(\hat{\sigma})$ is the unique vertex of T that is not on the boundary as illustrated on the left side of Figure 2.3: $F_T(\hat{\sigma}) := v_4$ and $\hat{\sigma} := \hat{v}_4$.

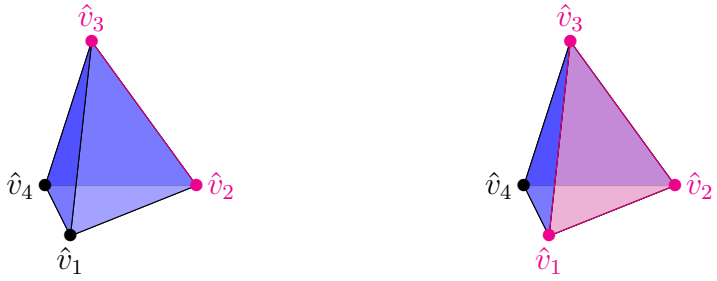

(a) The case where $\hat{\sigma} := [\hat{v}_4, \hat{v}_1]$. (b) The case where $\hat{\sigma} := \{\hat{v}_4\}$.

Figure 2.3 – Reference tetrahedral $\hat{T}$.

Definition 2.2.2. *We denote $\mathcal{T}_h^{(e)}$ the mesh consisting of all exact elements $T^{(e)} = F_T^{(e)}(\hat{T})$, where $F_T^{(e)} = F_T$ for all internal elements of $\mathcal{T}_h^{(1)}$, as for the case of non-internal elements $F_T^{(e)}$ is given by,*

$$\begin{aligned} F_T^{(e)} : \ \hat{T} &\longrightarrow T^{(e)} := F_T^{(e)}(\hat{T}) \\ \hat{x} &\longmapsto F_T^{(e)}(\hat{x}) := \begin{cases} x & \text{if } \hat{x} \in \hat{\sigma}, \\ x + (\lambda^*)^{r+2}(b(y) - y) & \text{if } \hat{x} \in \hat{T} \backslash \hat{\sigma}, \end{cases} \end{aligned} \tag{2.1}$$

with $x = F_T(\hat{x})$ and $y = F_T(\hat{y})$ and for an integer $r \geq 1$, the value of which is discussed in the following remark.

For extensive explication, a visualisation of $\hat{y} : \hat{T} \setminus \{\hat{v}_1\} \to [\hat{v}_2, \hat{v}_3]$ and $y : \hat{T} \backslash \{v_1\} \to [v_2, v_3]$ is given in Figure 2.2 in $\mathbb{R}^2$.

Remark 2.2.3 ($F_T^{(e)}$ regularity)**.** *It has been proven in [43] that the exact transformation $F_T^{(e)}$ is a $\mathcal{C}^1$-diffeomorphism and C^{r+1} regular on $\hat{T}$. Indeed for any $\hat{x} \in \hat{T} \backslash \hat{\sigma}$, the function $F_T^{(e)}(\hat{x}) = x + (\lambda^*)^s(b(y) - y)$ has an exponent $s = r + 2$ inherited from [43]: this exponent value guaranties the $\mathcal{C}^{r+1}$ regularity of the function $F_T^{(e)}$.*

Remark 2.2.4. *For $x \in T \cap \Gamma_h^{(1)}$, we have that $\lambda^* = 1$ and so $y = x$ inducing that $F_T^{(e)}(\hat{x}) = b(x)$. Then $F_T^{(e)} \circ F_T^{-1} = b$ on $T \cap \Gamma_h^{(1)}$.*

An example is provided to illustrate the effect of the exact transformation $F_T^{(e)}$ given in Definition 2.2.2 on the mesh elements.

Example 2.2.5. *Consider three triangles T_1, T_2 and T_3 in $\mathbb{R}^2$, with $(v_i)_{i=1}^5$ as there vertices, as displayed in Figure 2.4. For $i = 1, 2, 3$, the transformation $F_{T_i}^{(e)} \circ F_{T_i}^{-1}$ maps $T_i \in \mathcal{T}_h^{(1)}$ into $T_i^{(e)}$ as follows,*

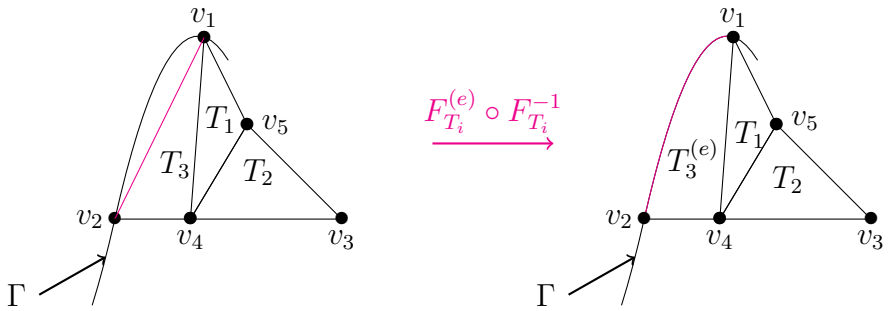

Figure 2.4 – Impact of $F_T^{(e)}$ on internal and non-internal mesh elements.

As displayed in Figure 2.4, T_1 and T_2 are internal elements of the mesh, having at most one vertex on Γ. Consequently, they remain unchanged by the transformations $F_{T_i}^{(e)} \circ F_{T_i}^{-1}$. Whereas T_3 is not internal having two vertices v_1, v_2 on Γ. Therefore this element is mapped into a curved triangle with an edge exactly fitting Γ.

2.3 Curved mesh $\mathcal{T}_h^{(r)}$ of order r

The exact mapping $F_T^{(e)}$, defined in (2.1), is interpolated as a polynomial of order $r \geq 1$ in the classical $\mathbb{P}^r$-Lagrange basis on $\hat{T}$, where $\mathbb{P}^r$ is the set of polynomials in $\mathbb{R}^d$ of order r or less. The interpolant, denoted $F_T^{(r)}$, is defined as follows. Let $T \in \mathcal{T}_h^{(1)}$ and let $\phi_1^r, ..., \phi_{n_r}^r$ be the Lagrangian basis functions of degree r on $\hat{T}$ corresponding to the nodal points $\hat{v}_1, ..., \hat{v}_{n_r}$, where n_r is the dimension of $\mathbb{P}^r$ (examples will be given late on), we define,

$$\begin{aligned} F_T^{(r)} : \ \hat{T} &\longrightarrow T^{(r)} := F_T^{(r)}(\hat{T}) \\ \hat{x} &\longmapsto F_T^{(r)}(\hat{x}) := \sum_{j=1}^{n_r} F_T^{(e)}(\hat{v}_j)\phi_j^r. \end{aligned}$$

Note that, for a sufficiently small mesh size h, $F_T^{(r)}$ is a $\mathcal{C}^1$-diffeomorphism and is in $\mathcal{C}^{r+1}(\hat{T})$ (see [32, chap. 4.3]). Additionally, by definition, $F_T^{(r)}$ and $F_T^{(e)}$ coincide on

all $\mathbb{P}^r$-Lagrange nodes, by definition of a $\mathbb{P}^r$-Lagrangien interpolation operator.

The *curved mesh of order* r is $\mathcal{T}_h^{(r)} := \{T^{(r)};\ T \in \mathcal{T}_h^{(1)}\}$, $\Omega_h^{(r)} := \cup_{T^{(r)} \in \mathcal{T}_h^{(r)}} T^{(r)}$ is the mesh domain and $\Gamma_h^{(r)} := \partial\Omega_h^{(r)}$ is its boundary. For more exhaustive details, we refer to [43, 33, 32, 58].

For the sake of completeness, we present an example of a quadratic mesh ($r = 2$) in 2D and an example of a cubic mesh ($r = 3$) in 2D.

Example 2.3.1. *Let $T^{(2)}$ be a non internal element of a quadratic mesh ($r = 2$) constructed from a reference element $\hat{T}$ with the help of the transformation $F_T^{(2)}$ (see Figure 2.5). The mappings $F_T^{(2)}$ and $F_T^{(e)}$ coincide at the $\mathbb{P}^2$-Lagrange nodes which are the three vertexes $\hat{v}_1, \hat{v}_2, \hat{v}_3$ and the three edge mid-points $\hat{v}_4, \hat{v}_5, \hat{v}_6$ of $\hat{T}$.*

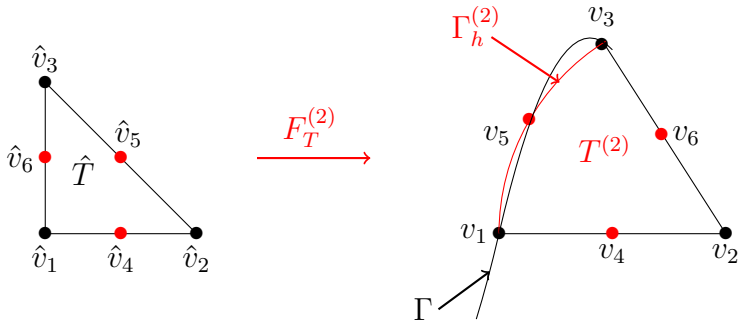

Figure 2.5 – Visualisation of $F_T^{(2)} : \hat{T} \to T^{(2)}$.

Comparing T to $T^{(2)}$ in Figures 2.1 and 2.5, one deduces that a quadratic element approximates Γ better than a simplex, which was our goal.

Example 2.3.2. *Let $T^{(3)}$ be a non internal element of a cubic mesh ($r = 3$) constructed from a reference element $\hat{T}$ with the help of the transformation $F_T^{(3)}$ (see Figure 2.6).*

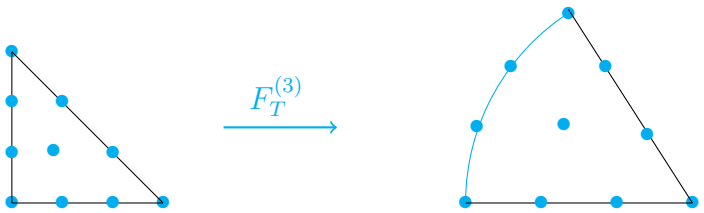

Figure 2.6 – Visualisation of $F_T^{(3)} : \hat{T} \to T^{(3)}$.

The mappings $F_T^{(3)}$ and $F_T^{(e)}$ coincide at the $\mathbb{P}^3$-Lagrange nodes of $\hat{T}$, which are the 10 nodes highlighted in cyan in Figure 2.6.

Example 2.3.3. *Next is presented a 3D example of the number of nodes of a curved mesh element of a quadratic (resp. cubic) mesh, as displayed in Figure 2.7.*

— *Let $T^{(2)}$ be a tetrahedral of a quadratic mesh ($r = 2$) in 3D. Then, $T^{(2)}$ has 10 nodes, comprising of its 4 vertices and of the 6 midpoints, one on each edge of the tetrahedral.*

— *Consider a tetrahedral $T^{(3)}$ within a cubic mesh ($r = 3$) in 3D. Then, $T^{(3)}$ has 20 nodes, consisting of its 4 vertices, of two nodes on each edge (at one third and at two third of the edge, with a total number equal to 12), and of the center of gravity of each face or triangle, which are a total of 4 nodes.*

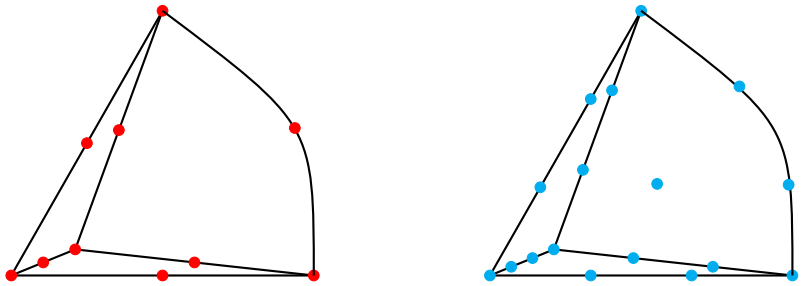

(a) The case where $r = 2$. (b) The case where $r = 3$.

Figure 2.7 – A curved tetrahedral.

Part II

Lift operator definition and numerical settings

With the aim of doing an error analysis in Part III on the three problems presented in Chapter 1, one needs to define the discrete solution relative to each of them. This solution will belong to the considered finite element space and it will be defined on the mesh domain. As stated before, the mesh domain differs from the physical domain, thus we proceed as follows.

— In Chapter 3, we put forward a key element of this thesis: the *lift operator.* This operator allows us to compare between the exact solution defined on Ω and the discrete one defined on the mesh domain Ω_h, by "lifting" or "transporting" the discrete solution onto Ω.

— In Chapter 4, is firstly presented the $\mathbb{P}^k$-Lagrangian finite element framework with its associated lifted version: indeed, with the help of the lift operator, we define the *lifted finite element space* with its associated *lifted interpolation operator*, which are used in Part III. Next, is discussed the numerical framework used in this manuscript. We explain the essential elements of the implementation, which are validated by reproducing known results in the literature. This part wraps up with discussions centered around unexpected results, which all the numerical simulations in this manuscript put forward: *the super-convergence phenomena of the error on quadratic meshes* and the *default or loss in the finite element convergence rate of the interpolation error on cubic meshes.*

Chapter 3

The lift operator

From this chapter are composed the sections dedicated to the *lift operator* in the following accepted article [25],

— F. Caubet, J. Ghantous, C. Pierre, *A priori error estimates of a poisson diffusion equation with ventcel boundary conditions on curved meshes,* published in SIAM J. Numer. Anal., 2024.

Motivation and state of the art. As previously highlighted, the curved mesh of order $r \geq 1$, denoted by $\Omega_h^{(r)}$, does not exactly fit the physical domain i.e. $\Omega_h^{(r)} \neq \Omega$. Then one can not directly compare the numerical solution u_h defined on $\Omega_h^{(r)}$ to the exact solution u defined on Ω. Thus, to obtain *a priori* error estimations, the notion of *lifting* a function from a domain onto another domain needs to be introduced. The *lift functional* was firstly introduced in the 1970s by many authors (see, e.g., [38, 65, 69, 73, 12, 80, 81]). Among them, in the 1990's, Dubois defined a lift based on the orthogonal projection onto the domain boundary Γ in [38]. The idea of relying on the orthogonal projection in the definition of a *surface lift* was proposed in the late 1980's by Dzuik in [40]. This was generalised in the case of lifting a function from higher order surface meshes onto a continuous surface in [36] by Demlow in 2009. In a context of error analysis, this surface lift was applied in some of Demlow's most recent work (see [36, 37, 15]). In the context of curved meshes with order $r \geq 2$, the definition of a *volume lift* required a higher regularity: in 2013, such an improvement was brought by Elliott *et al.* in [43], with a definition that also relies on the orthogonal projection.

However, the definition of the volume lift given in [43] did not fit the orthogonal projection on the computational domain's boundary, as will be highlighted later on in Remark 3.1.7. In the present work, we need this property which is crucialis crucial for the derivation of *a priori* error estimates in the following chapters.

Main novelties. In order to address this issue, an alternative definition to satisfy that property, as developed in Proposition 3.1.4, together with all the necessary regularity properties is introduced in this chapter. This modification in the former lift definition in [43] has a big impact on the error approximation as is discussed in-depth in the numerical examples in Chapter 5. This lift definition will be used to perform a numerical study of the computational error of the systems (1.1), (1.7), and (1.18).

Section 3.1 focuses on the lift operator in the scalar case. It is then extended to the vectorial case in Section 3.2 in order to address the linear elasticity problem. Following Section 2.3, $\mathcal{T}_h^{(r)}$ denotes the curved mesh of the physical domain Ω, with a geometrical order $r \geq 1$. We also recall that $\Omega_h^{(r)} = \cup_{T \in \mathcal{T}_h^{(r)}} T$ denotes the mesh domain and $\Gamma_h^{(r)}$ is its boundary.

3.1 The lift operator

3.1.1 Surface and volume lift definitions

With the help of transformations defined in Chapter 2, we define the *lift operator* that transports a scalar function from $\Omega_h^{(r)}$ (resp. $\Gamma_h^{(r)}$) onto Ω (resp. Γ). We start by recalling the *surface lift* definition as introduced by Demlow in [36].

Definition 3.1.1 (Surface lift)**.** *Let $u_h \in \mathrm{L}^2(\Gamma_h^{(r)})$. The surface lift $u_h^L \in \mathrm{L}^2(\Gamma)$ associated to u_h is defined by,*

$$u_h^L \circ b := u_h,$$

where $b : \Gamma_h^{(r)} \to \Gamma$ is the orthogonal projection, defined in Proposition 2.0.1. Likewise, to $u \in \mathrm{L}^2(\Gamma)$ is associated its inverse lift u^{-L} given by, $u^{-L} := u \circ b \in \mathrm{L}^2(\Gamma_h^{(r)})$.

The use of b the orthogonal projection on the boundary Γ to define the surface lift is natural since b is well defined on the tubular neighborhood $\mathcal{U}_\Gamma$ of Γ (see Proposition 2.0.1) and henceforth on $\Gamma_h^{(r)} \subset \mathcal{U}_\Gamma$ for sufficiently small mesh size h (see Remark 2.1.2 for more details).

The *volume lift* definition is a bit trickier: the orthogonal projection b cannot be used to define a volume lift. Thus, we define an adequate transformation that will play the same role as the orthogonal projection b while satisfying essential properties.

Following the notations presented in Definition 2.2.1, we introduce the transformation $G_h^{(r)} : \Omega_h^{(r)} \to \Omega$ given piecewise for all $T^{(r)} \in \mathcal{T}_h^{(r)}$ by,

$$G_h^{(r)}{}_{|_{T^{(r)}}} := F_{T^{(r)}}^{(e)} \circ (F_T^{(r)})^{-1}, \tag{3.1}$$

where the transformation $F_{T^{(r)}}^{(e)}$ is given as follows, for $\hat{x} \in \hat{T}$,

$$F_{T^{(r)}}^{(e)}(\hat{x}) := \begin{cases} x & \text{if } \hat{x} \in \hat{\sigma} \\ x + (\lambda^*)^{r+2}(b(y) - y) & \text{if } \hat{x} \in \hat{T} \backslash \hat{\sigma} \end{cases}, \tag{3.2}$$

with $x := F_T^{(r)}(\hat{x})$ and $y := F_T^{(r)}(\hat{y})$ (see Figure 2.2 for the affine case), where $F_T^{(r)}$ is defined in Section 2.3.

Notice that this definition implies that $G_h^{(r)}{}_{|_{T^{(r)}}} = id_{|_{T^{(r)}}}$, for any internal mesh element $T^{(r)} \in \mathcal{T}_h^{(r)}$. Note that, by construction, $G_h^{(r)}$ is globally continuous and piecewise differentiable on each mesh element. For the remainder of this chapter, the following notations are crucial: $\mathrm{D}G_h^{(r)}$ denotes the differential of $G_h^{(r)}$, $(\mathrm{D}G_h^{(r)})^{\mathsf{T}}$ is its transpose and J_h is its Jacobian.

For the sake of completeness, in the following example we illustrate the transformation $G_h^{(r)}$ on a quadratic mesh ($r = 2$).

Example 3.1.2. *We display in this example the effect of $G_h^{(r)}$ on the elements of the curved mesh $\mathcal{T}_h^{(r)}$, for $r = 2$. In Figure 3.1, we display the transformation $G_h^{(2)}$ that maps a curved element $T^{(2)} \in \mathcal{T}_h^{(2)}$ into an exact element $T^{(e)}$ (see Section 2.2).*

Definition 3.1.3 (Volume lift)**.** *Let $u_h \in \mathrm{L}^2(\Omega_h^{(r)})$. We define the volume lift associated to u_h, denoted $u_h^\ell \in \mathrm{L}^2(\Omega)$, by,*

$$u_h^\ell \circ G_h^{(r)} := u_h.$$

In a similar way, to $u \in \mathrm{L}^2(\Omega)$ is associated its inverse lift $u^{-\ell} \in \mathrm{L}^2(\Omega_h^{(r)})$ given by $u^{-\ell} := u \circ G_h^{(r)}$.

From this definition, we can prove the following property, which is important in the sequel.

Proposition 3.1.4. *The volume and surface lifts coincide on $\Gamma_h^{(r)}$, satisfying the trace property given by,*

$$\forall\ u_h \in \mathrm{H}^1(\Omega_h^{(r)}, \Gamma_h^{(r)}), \quad (\mathrm{Tr}\ u_h)^L = \mathrm{Tr}(u_h^\ell).$$

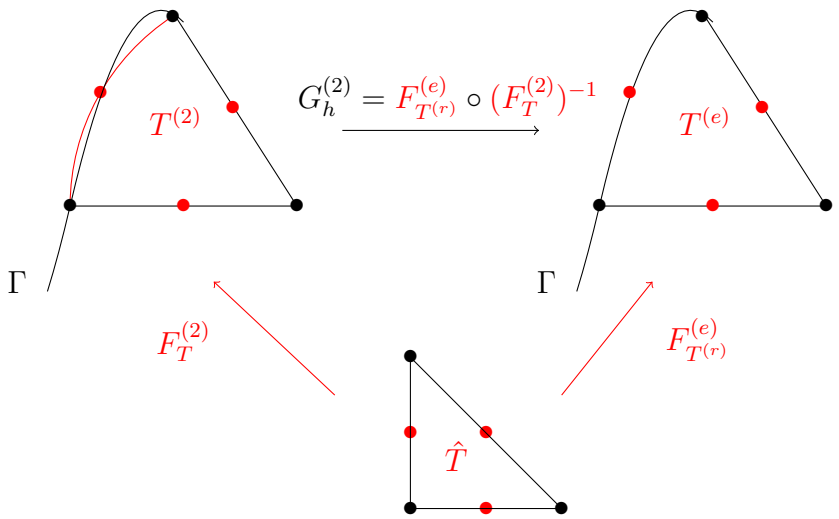

Figure 3.1 – Visualisation of $G_h^{(2)} : T^{(2)} \to T^{(e)}$ in a 2D case, in the quadratic case ($r = 2$).

Consequently, the surface lift v_h^L (resp. the inverse lift v^{-L}) will now be simply denoted by v_h^ℓ (resp. $v^{-\ell}$). Moreover, it follows that $(v^{-\ell})^\ell = v$.

Proof. Taking $x \in T^{(r)} \cap \Gamma_h^{(r)}$, $\hat{x} = (F_T^{(r)})^{(-1)}(x)$ satisfies $\lambda^* = 1$ and so $\hat{y} = \hat{x}$ and $y = x$. Thus $F_{T^{(r)}}^{(e)}(\hat{x}) = b(x)$, in other words,

$$G_h^{(r)}(x) = F_{T^{(r)}}^{(e)} \circ (F_T^{(r)})^{-1}(x) = b(x), \qquad \forall\, x \in T^{(r)} \cap \Gamma_h^{(r)}.$$

□

In the following proposition, are presented the essential properties of $G_h^{(r)}$ for the upcoming error estimation.

Proposition 3.1.5. *Let $T^{(r)} \in \mathcal{T}_h^{(r)}$ and let the domain Ω be smooth (at least $\mathcal{C}^{r+2}$ regular). Then the mapping $G_h^{(r)}{}_{|_{T^{(r)}}}$ is $\mathcal{C}^{r+1}(T^{(r)})$ regular and a $\mathcal{C}^1$-diffeomorphism from $T^{(r)}$ onto $T^{(e)}$. Additionally, for a sufficiently small mesh size h, there exists a constant $c > 0$, independent of h, such that,*

$$\forall\, x \in T^{(r)}, \qquad \|\mathrm{D}G_h^{(r)}(x) - \mathrm{I}_d\| \leq ch^r \qquad \text{and} \qquad |J_h(x) - 1| \leq ch^r, \tag{3.3}$$

where $G_h^{(r)}$ is defined in (3.1) *and J_h is its Jacobian.*

The full proof of this proposition is partially adapted from the work of Elliott *et al.* in [43] and is detailed in Subsection 3.1.4.

Remark 3.1.6 (Lift regularity)**.** *The lift transformation* $G_h^{(r)} : \Omega_h^{(r)} \to \Omega$ *defined in Equation* (3.1) *involves the function,*

$$\rho_{T^{(r)}}(\hat{x}) := \begin{cases} 0 & \text{if } \hat{x} \in \hat{\sigma} \\ (\lambda^*)^s (b(y) - y) & \text{if } \hat{x} \in \hat{T} \backslash \hat{\sigma} \end{cases},$$

with an exponent $s = r + 2$ *inherited from [43]: this exponent value guaranties the* $\mathcal{C}^{r+1}$ *piecewise regularity of the function* $G_h^{(r)}$ *on each mesh element. We have led numerical experiments in order to evaluate the impact of decreasing the value of* s*. We noticed that decreasing the value of* s *to* 2*, does not seem to have a big influence on the estimates in (3.3). This is unexpected since the estimations should not be make sense if* $s = 2$*. This is investigated in Section 5.5.1.*

Remark 3.1.7 (Former lift definition)**.** *The volume lift presented in Definition 3.1.3 is an adaptation of the lift definition in [43], which however does not fulfill Proposition 3.1.4. Precisely, in [43], to* $u_h \in \mathrm{L}^2(\Omega_h^{(r)})$ *is associated the lifted function* $u_h^{e\ell} \in \mathrm{L}^2(\Omega)$*, given by* $u_h^{e\ell} \circ G_h := u_h$*, where* $G_h : \Omega_h^{(r)} \to \Omega$ *is defined piecewise, for each mesh element* $T^{(r)} \in \mathcal{T}_h^{(r)}$*, by,*

$$G_{h|_{T^{(r)}}} := F_T^{(e)} \circ (F_T^{(r)})^{-1},$$

where T *is the affine element relative to* $T^{(r)}$*,* $F_T^{(e)}$ *is defined in* (2.1) *and* $F_T^{(r)}$ *is its* $\mathbb{P}^r$*-Lagrangian interpolation given in Section 2.3.*

However, this transformation does not coincide with the orthogonal projection over the boundary b*, on the mesh boundary* $\Gamma_h^{(r)}$*. Indeed, since* $F_T^{(e)} \circ F_T^{-1} = b$ *on* $T \cap \Gamma_h^{(1)}$ *(see Remark 2.2.4), we have,*

$$G_h(x) = b \circ F_T \circ (F_T^{(r)})^{-1}(x) \neq b(x), \quad \forall\, x \in \Gamma_h^{(r)} \cap T^{(r)}.$$

Consequently in this case, the trace property in Proposition 3.1.4 is not satisfied, since

$$(\mathrm{Tr}\ u_h)^L \neq \mathrm{Tr}(u_h^{e\ell}).$$

3.1.2 Lift of the variational formulation

The upcoming error analysis in chapters 5 and 6 requires a number of relationships between integrals defined on the physical domain and integrals defined on the mesh domain. With the help of the lift operator, one may express an integral over $\Gamma_h^{(r)}$ (resp. $\Omega_h^{(r)}$) with respect to one over Γ (resp. Ω), as will be discussed in this section.

Surface integrals. In this subsection, all results stated may be found alongside their proofs in the works of Demlow like in [36, 14], but we recall some necessary information for the sake of completeness. For extensive details, we also refer to [37, 41, 40].

Let J_b be the Jacobian of the orthogonal projection on the boundary b, defined in Proposition 2.0.1. Notice that J_b is bounded independently of h and its detailed expression may be found in [36, 37]. Consider also the lift of J_b given by $J_b^\ell \circ b = J_b$ (see Definition 3.1.1).

Let $u_h, v_h \in \mathrm{H}^1(\Gamma_h^{(r)})$ with $u_h^\ell, v_h^\ell \in \mathrm{H}^1(\Gamma)$ as their respected lifts. Then, one has,

$$\int_{\Gamma_h^{(r)}} u_h v_h \,\mathrm{d}s = \int_\Gamma u_h^\ell v_h^\ell \,\frac{\mathrm{d}s}{J_b^\ell}. \tag{3.4}$$

A similar equation may be written with tangential gradients. We start by recalling the following notations. We denote the outer unit normal vector over Γ by $\mathbf{n} = \nabla \mathrm{d}$, where d is the signed distance function to Gamma (see Proposition 2.0.1). The outer unit normal vector over $\Gamma_h^{(r)} = \partial\Omega_h^{(r)}$ is denoted by $\mathbf{n}_h$. Denote $\mathrm{P}(x) := \mathrm{I}_d - (\mathbf{n}\otimes\mathbf{n})(x)$ (resp. $\mathrm{P}_h := \mathrm{I}_d - (\mathbf{n}_h \otimes \mathbf{n}_h)(x)$) the orthogonal projection over the tangential space of Γ (resp. of $\Gamma_h^{(r)}$) at a given point $x \in \Gamma$ (resp. $x \in \Gamma_h^{(r)}$). Additionally, the Weingarten map $\mathcal{H} : \mathbb{R}^d \to \mathbb{R}^{d\times d}$ is given by $\mathcal{H} := \mathrm{D}^2\mathrm{d} = \mathrm{D}\mathbf{n}$. With the previous notations, we have,

$$\nabla_{\Gamma_h^{(r)}} v_h(x) = \mathrm{P}_h(\mathrm{I}_d - \mathrm{d}\mathcal{H})\mathrm{P}\nabla_\Gamma v_h^\ell(b(x)), \qquad \forall\, x \in \Gamma_h^{(r)}. \tag{3.5}$$

Taking advantage of (3.5), one may derive the following expression,

$$\int_{\Gamma_h^{(r)}} \nabla_{\Gamma_h^{(r)}} u_h \cdot \nabla_{\Gamma_h^{(r)}} v_h \,\mathrm{d}s = \int_\Gamma A_h^\ell \nabla_\Gamma u_h^\ell \cdot \nabla_\Gamma v_h^\ell \,\mathrm{d}s, \tag{3.6}$$

where A_h^ℓ is the lift of the matrix function A_h given by,

$$A_h(x) := \frac{1}{J_b(x)} \mathrm{P}(\mathrm{I}_d - \mathrm{d}\mathcal{H})\mathrm{P}_h(\mathrm{I}_d - \mathrm{d}\mathcal{H})\mathrm{P}(x), \qquad \forall\, x \in \Gamma_h^{(r)}. \tag{3.7}$$

Volume integrals. Similarly, consider $u_h, v_h \in \mathrm{H}^1(\Omega_h^{(r)})$ and let $u_h^\ell, v_h^\ell \in \mathrm{H}^1(\Omega)$ be their respected lifts, we have,

$$\int_{\Omega_h^{(r)}} u_h v_h \,\mathrm{d}x = \int_\Omega u_h^\ell v_h^\ell \frac{1}{J_h^\ell} \,\mathrm{d}x, \tag{3.8}$$

where J_h denotes the Jacobian of $G_h^{(r)}$ and J_h^ℓ is its lift given by $J_h^\ell \circ G_h^{(r)} = J_h$.

Additionally, the gradient can be written as follows, for any $x \in \Omega_h^{(r)}$,

$$\nabla v_h(x) = \nabla(v_h^\ell \circ G_h^{(r)})(x) = (\mathrm{D}G_h^{(r)})^\mathsf{T}(x)\,(\nabla v_h^\ell) \circ (G_h^{(r)}(x)).$$

Using a change of variables $z = G_h^{(r)}(x) \in \Omega$, one has, $(\nabla v_h)^\ell(z) = (\mathrm{D}G_h^{(r)})^\mathsf{T}(x)\,\nabla v_h^\ell(z)$. Finally, introducing the matrix function $\mathcal{G}_h^{(r)}$,

$$\mathcal{G}_h^{(r)}(z) := (\mathrm{D}G_h^{(r)})^\mathsf{T}(x), \tag{3.9}$$

one has,

$$\int_{\Omega_h^{(r)}} \nabla u_h \cdot \nabla v_h \,\mathrm{d}x = \int_\Omega \mathcal{G}_h^{(r)}(\nabla u_h^\ell) \cdot \mathcal{G}_h^{(r)}(\nabla v_h^\ell) \frac{1}{J_h^\ell} \,\mathrm{d}x. \tag{3.10}$$

3.1.3 Useful estimations

Surface estimations. A key point in the error estimation proofs is the ability to bound $A_h^\ell - \mathrm{P}$ and $J_b^\ell - 1$ with respect to the mesh size h and the geometrical order of the mesh r. Following the notations introduced in Section 3.1.2, we recall two important estimates proved in [36]: there exists a constant $c > 0$ independent of h such that,

$$\|A_h^\ell - \mathrm{P}\|_{\mathrm{L}^\infty(\Gamma)} \leq c h^{r+1} \qquad \text{and} \qquad \left\| 1 - \frac{1}{J_b^\ell} \right\|_{\mathrm{L}^\infty(\Gamma)} \leq c h^{r+1}, \tag{3.11}$$

where A_h^ℓ and J_b^ℓ are respectively the lifts of A_h defined in (3.7) and of J_b, the Jacobian of b the orthogonal projection on the boundary Γ.

Volume estimations. A direct consequence of Proposition 3.1.5 is that both $\mathrm{D}G_h^{(r)}$ and J_h are bounded on every $T^{(r)} \in \mathcal{T}_h^{(r)}$. As an extension of that, by Definition 3.1.3 of the lift, both $\mathcal{G}_h^{(r)}$ and J_h^ℓ are also bounded on $T^{(e)}$ (see Section 2.2 for the definition of an exact mesh element $T^{(e)}$). Moreover, the inequalities in (3.3) will not be directly

used in the error estimations in Part III, the following inequalities will be used instead,

$$\forall\, x \in T^{(e)}, \quad \|\mathcal{G}_h^{(r)}(x) - \mathrm{I}_d\| \leq ch^r \qquad \text{and} \qquad \left|\frac{1}{J_h^\ell(x)} - 1\right| \leq ch^r, \tag{3.12}$$

where $\mathcal{G}_h^{(r)}$ is given in Equation (3.9). These inequalities are a consequence of the lift applied on the inequalities (3.3).

Estimations near the boundary. From this point forward, we denote $B_h^\ell \subset \Omega$ as the union of all the non-internal elements of the exact mesh $\mathcal{T}_h^{(e)}$,

$$B_h^\ell := \{T^{(e)} \in \mathcal{T}_h^{(e)};\ T^{(e)} \text{ has at least two vertices on } \Gamma\}.$$

Note that, by definition of B_h^ℓ, we have,

$$\frac{1}{J_h^\ell} - 1 = 0 \quad \text{and} \quad \mathcal{G}_h^{(r)} - \mathrm{I}_d = 0 \quad \text{in } \Omega \backslash B_h^\ell. \tag{3.13}$$

The following corollary involving B_h^ℓ is a direct consequence of [43, Lemma 4.10] or [53, Theorem 1.5.1.10].

Corollary 3.1.8. *There exists $c > 0$ such that, for a sufficiently small h, the following inequalities hold for any $v \in \mathrm{H}^1(\Omega)$ and $w \in \mathrm{H}^2(\Omega)$,*

$$\|v\|_{\mathrm{L}^2(B_h^\ell)} \leq ch^{1/2}\|v\|_{\mathrm{H}^1(\Omega)} \qquad \textit{and} \qquad \|w\|_{\mathrm{H}^1(B_h^\ell)} \leq ch^{1/2}\|w\|_{\mathrm{H}^2(\Omega)}. \tag{3.14}$$

Norm equivalence using the lift operator. Let us emphasize that, through the lift operator, there exists an *"equivalence"* between the L^2 and H^1 norms over $\Omega_h^{(r)}$ (resp. $\Gamma_h^{(r)}$) and the L^2 and H^1 norms over Ω (resp. Γ).

We recall the work of Demlow in [36] regarding the surface norm: let $v_h \in \mathrm{H}^1(\Gamma_h^{(r)})$ and let $v_h^\ell \in \mathrm{H}^1(\Gamma)$ be its lift. Then, there exist constants $c_1, c_2, c_1', c_2' > 0$ independent of h such that, for a sufficiently small h, we have,

$$\begin{array}{rcccl} c_1\|v_h^\ell\|_{\mathrm{L}^2(\Gamma)} & \leq & \|v_h\|_{\mathrm{L}^2(\Gamma_h^{(r)})} & \leq & c_2\|v_h^\ell\|_{\mathrm{L}^2(\Gamma)}, \\ c_1'\|v_h^\ell\|_{\mathrm{H}^1(\Gamma)} & \leq & \|v_h\|_{\mathrm{H}^1(\Gamma_h^{(r)})} & \leq & c_2'\|v_h^\ell\|_{\mathrm{H}^1(\Gamma)}. \end{array} \tag{3.15}$$

Additionally, as proved in [36, page 7], for $v_h \in \mathrm{H}^s(\Gamma_h^{(r)})$ with $s \geq 2$, there exists a

constant mesh independent $c_3 > 0$ such that, for a sufficiently small h, we have,

$$\|v_h\|_{\mathrm{H}^s(\Gamma_h^{(r)})} \leq c_3 \|v_h^\ell\|_{\mathrm{H}^s(\Gamma)}.$$

Lemma 3.1.9. *Let $v_h \in \mathrm{H}^1(\Omega_h^{(r)})$ and let $v_h^\ell \in \mathrm{H}^1(\Omega)$ be its lift. Then, there exist mesh independent constants $c_4, c_5, c_4', c_5' > 0$ such that, for a sufficiently small h, we have,*

$$\begin{array}{rcccl} c_1\|v_h^\ell\|_{\mathrm{L}^2(\Omega)} & \leq & \|v_h\|_{\mathrm{L}^2(\Omega_h^{(r)})} & \leq & c_2\|v_h^\ell\|_{\mathrm{L}^2(\Omega)}, \\ c_1\|v_h^\ell\|_{\mathrm{H}^1(\Omega)} & \leq & \|v_h\|_{\mathrm{H}^1(\Omega_h^{(r)})} & \leq & c_2\|v_h^\ell\|_{\mathrm{H}^1(\Omega)}. \end{array} \tag{3.16}$$

Furthermore, let $T^{(r)}$ be a curved mesh element of $\mathcal{T}_h^{(r)}$ and let $v_h \in \mathrm{H}^s(T^{(r)})$ with $2 \leq s \leq r+1$. Then there exits $c_6 > 0$ such that, for a sufficiently small h, we have,

$$\|v_h\|_{\mathrm{H}^s(T^{(r)})} \leq c\|v_h^\ell\|_{\mathrm{H}^s(T^{(e)})}, \tag{3.17}$$

where $T^{(e)}$ is the exact mesh element associated with $T^{(r)}$ (see Section 2.2).

Proof. To prove the right hand side of the first inequality in (3.16), we use Equation (3.8), as follows,

$$\|v_h\|^2_{\mathrm{L}^2(\Omega_h^{(r)})} = \int_{\Omega_h^{(r)}} v_h^2 \,\mathrm{d}x = \int_\Omega (v_h^\ell)^2 \frac{1}{J_h^\ell} \,\mathrm{d}x \leq c_2\|v_h^\ell\|_{\mathrm{L}^2(\Omega)}.$$

The latter inequality holds due to the fact that $\frac{1}{J_h^\ell}$ is bounded independently of h. Similarly, one can prove the left hand side of the first inequality in (3.16).

To prove Inequality (3.16) with H^1 norms, one needs to apply Equation (3.10), while keeping in mind that $\mathcal{G}_h^{(r)}$ is also bounded independently of h.

Inequality (3.17) derives from a change of variables and the fact that, for $s \geq 2$, $\mathrm{D}^s(G_h^{(r)}) = \mathrm{I}_d + \mathrm{D}^s(\rho_{T^{(r)}} \circ (F_T^{(r)})^{-1})$ is bounded locally on each mesh element independently of h, which is easily proved using [33, page 19] and Inequality (3.24) proved in the following section. □

3.1.4 Proof of Proposition 3.1.5

Our main goal in this section is to prove Proposition 3.1.5. Following the notations given in Definition 2.2.1, we present the proof of this result which requires a series of

preliminary results given in Propositions 3.1.10, 3.1.12 and 3.1.13. The proofs of these propositions are inspired by the proofs of [12, Lemma 6.2], [43, Lemma 4.3] and [43, Proposition 4.4] respectively. However, these existing propositions in the literature are established for different functions than those presented and proved in this work.

For the sake of clarity and following Definition 2.2.1, we recall that $\lambda^* = \sum_{i=1}^{d+1} \varepsilon_i \lambda_i$, where $\varepsilon_i = 1$ if $v_i \in \Gamma$ or $\varepsilon_i = 0$ otherwise, and λ_i are the barycentric coordinates to the vertices $\hat{v}_i$ of the reference element $\hat{T}$. Moreover, we defined $\hat{\sigma} = \{\hat{x} \in \hat{T}; \lambda^*(\hat{x}) = 0\}$ and $\hat{y} = \dfrac{1}{\lambda^*} \sum_{i=1}^{d+1} \varepsilon_i \lambda_i \hat{v}_i \in \partial\hat{T}$.

Proposition 3.1.10. *The map $y : \hat{x} \in \hat{T} \backslash \hat{\sigma} \mapsto y := F_T^{(r)}(\hat{y}) \in \Gamma_h^{(r)}$ is a smooth function and for all $m \geq 1$, there exists a constant $c > 0$ independent of h such that,*

$$\|\mathrm{D}^m y\|_{\mathrm{L}^\infty(\hat{T}\backslash\hat{\sigma})} \leq \frac{ch}{(\lambda^*)^m}. \tag{3.18}$$

Remark 3.1.11. *The proof of this proposition and of the next one rely on the formula of Faà di Bruno (see [12, equation 2.9]). This formula states that for two functions f and g, which are of class $\mathcal{C}^m$, such that $f \circ g$ is well defined, the derivative of order m of the composition $f \circ g$ may be written as follows,*

$$\mathrm{D}^m(f \circ g) = \sum_{p=1}^{m} \Big(\mathrm{D}^p(f) \sum_{i \in E(m,p)} c_i \prod_{q=1}^{m} \mathrm{D}^q g^{i_q} \Big), \tag{3.19}$$

where $E(m,p) := \{i \in \mathbb{N}^m; \sum_{q=1}^m i_q = p \text{ and } \sum_{q=1}^m q i_q = m\}$ and c_i are positives constants, for all $i \in E(m,p)$.

Proof of Proposition 3.1.10. We detail the proof in the 2 dimensional case, the 3D case can be proved in a similar way.

As displayed in Figure 3.2, we consider the reference triangle $\hat{T}$ with the usual orientation. Its vertices are denoted $(\hat{v}_i)_{i=1}^3$ and the associated barycentric coordinates respectively are: $\lambda_1 = 1 - x_1 - x_2$, $\lambda_2 = x_2$ and $\lambda_3 = x_1$. Consider a non-internal mesh element $T^{(r)}$ such that, without loss of generality, $v_1 \notin \Gamma$. In such a case, depicted in Figure 3.2, $\varepsilon_1 = 0$ and $\varepsilon_2 = \varepsilon_3 = 1$, since $v_2, v_3 \in \Gamma \cap T^{(r)}$. This implies that $\lambda^* = \lambda_2 + \lambda_3 = x_2 + x_1$ and,

$$\hat{y} = \frac{1}{\lambda^*}(\lambda_2 \hat{v}_2 + \lambda_3 \hat{v}_3) = \frac{1}{x_2 + x_1}(x_2 \hat{v}_2 + x_1 \hat{v}_3). \tag{3.20}$$

In this case, $\hat{\sigma} = \{\hat{v}_1\}$ and $\hat{y}$ is defined on $\hat{T} \setminus \{\hat{v}_1\}$.

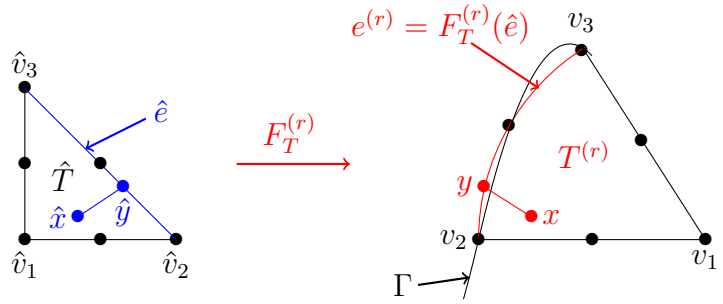

Figure 3.2 – Displaying $F_T^{(r)} : \hat{T} \to T^{(r)}$ in a 2D quadratic case (r=2).

By differentiating the expression (3.20) of $\hat{y}$ and using an induction argument, it can be proven that $\hat{y}$ is a smooth function on $\hat{T}\backslash\hat{\sigma}$ and there exists a constant $c > 0$, independent of h, such that,

$$\|\mathrm{D}^m \hat{y}\|_{\mathrm{L}^\infty(\hat{T}\backslash\hat{\sigma})} \leq \frac{c}{(\lambda^*)^m}, \qquad \text{for all } m \geq 1. \tag{3.21}$$

For $m = 1$, the first order derivative with respect to x_1 may be bounded as follows,

$$|\partial_{x_1}\hat{y}| = |\frac{x_2}{(x_2+x_1)^2}(\hat{v}_3 - \hat{v}_2)| \leq \frac{\lambda^*}{(\lambda^*)^2}|\hat{v}_3 - \hat{v}_2| \leq \frac{c}{\lambda^*}.$$

Similarly, $|\partial_{x_2}\hat{y}| = |\frac{x_1}{(x_2+x_1)^2}(\hat{v}_2 - \hat{v}_3)| \leq \frac{c}{\lambda^*}$. Taking $m = 2$, we estimate the second order derivatives of $\hat{y}$ as follows,

$$|\partial^2_{x_1^2}\hat{y}| = |\frac{-2x_2}{(x_2+x_1)^3}(\hat{v}_3 - \hat{v}_2)| \leq \frac{2\lambda^*}{(\lambda^*)^3}|\hat{v}_3 - \hat{v}_2| \leq \frac{c}{(\lambda^*)^2}.$$

In a similar manner using Leibniz's formula, we obtain (3.21) for any $m \geq 1$.

Since $F_T^{(r)}$ is the $\mathbb{P}^r$-Lagrangian interpolant of $F_T^{(e)}$ on $\hat{T}$, then $y = F_T^{(r)} \circ \hat{y}$ is a smooth function on $\hat{T}\backslash\hat{\sigma}$. We now apply Inequality (3.19) for $y = F_T^{(r)} \circ \hat{y}$ to estimate its derivative's norm as follows, for all $m \geq 1$,

$$\|\mathrm{D}^m(y)\|_{\mathrm{L}^\infty(\hat{T}\backslash\hat{\sigma})} \leq \sum_{p=1}^{m} \left(\|\mathrm{D}^p(F_T^{(r)})\|_{\mathrm{L}^\infty(\hat{e})} \sum_{i \in E(m,p)} c_i \prod_{q=1}^{m} \|\mathrm{D}^q\hat{y}\|^{i_q}_{\mathrm{L}^\infty(\hat{T}\backslash\hat{\sigma})} \right),$$

where $\hat{e} := (F_T^{(r)})^{(-1)}(e^{(r)})$ and $e^{(r)} := \partial T^{(r)} \cap \Gamma_h^{(r)}$ are displayed in Figure 3.2. After-

wards, we decompose the sum into two parts, one part taking $p = 1$ and the second one for $p \geq 2$, and apply inequality (3.21),

$$\begin{aligned}
&\|\mathrm{D}^m(y)\|_{\mathrm{L}^\infty(\hat{T}\backslash\hat{\sigma})} \\
&\qquad \leq \|\mathrm{D}(F_T^{(r)})\|_{\mathrm{L}^\infty(\hat{e})} \sum_{i\in E(m,1)} \prod_{q=1}^{m} (\frac{c}{(\lambda^*)^q})^{i_q} + \sum_{p=2}^{m} \Big(\|\mathrm{D}^p(F_T^{(r)})\|_{\mathrm{L}^\infty(\hat{e})} \sum_{i\in E(m,p)} \prod_{q=1}^{m} (\frac{c}{(\lambda^*)^q})^{i_q} \Big) \\
&\qquad \leq ch\lambda^{*(-\sum_{q=1}^m qi_q)} + c\sum_{p=2}^{m} h^r \lambda^{*(-\sum_{q=1}^m qi_q)} \leq ch(\lambda^*)^{-m},
\end{aligned}$$

using that $\|\mathrm{D}(F_T^{(r)})\|_{\mathrm{L}^\infty(\hat{e})} \leq ch$ and $\|\mathrm{D}^p(F_T^{(r)})\|_{\mathrm{L}^\infty(\hat{e})} \leq ch^r$, for $2 \leq p \leq r+1$ (see [33, page 239]), where the constant $c > 0$ is independent of h. This concludes the proof. □

Using the previous proposition, we can prove the following result.

Proposition 3.1.12. *Assume that Γ is $\mathcal{C}^{r+2}$ regular. Then the mapping $b \circ y : \hat{x} \in \hat{T}\backslash\hat{\sigma} \mapsto b(y(\hat{x})) \in \Gamma$ is of class $\mathcal{C}^{r+1}$. Additionally, for any $1 \leq m \leq r+1$, there exists a constant $c > 0$ independent of h such that,*

$$\|\mathrm{D}^m(b(y) - y)\|_{\mathrm{L}^\infty(\hat{T}\backslash\hat{\sigma})} \leq \frac{ch^{r+1}}{(\lambda^*)^m}. \tag{3.22}$$

Proof. Since Γ is $\mathcal{C}^{r+2}$ regular, the orthogonal projection on the boundary b is a $\mathcal{C}^{r+1}$ function on a tubular neighborhood of Γ (see [41, Lemma 4.1] or [14]). Consequently, following Proposition 3.1.10, $b(y) - y$ is of class $\mathcal{C}^{r+1}$ on $\hat{T}\backslash\hat{\sigma}$.

Secondly, consider $1 \leq m \leq r+1$. Applying the Faà di Bruno formula (3.19) for the function $b(y) - y = (b - id) \circ y$, we have,

$$\|\mathrm{D}^m(b(y) - y)\|_{\mathrm{L}^\infty(\hat{T}\backslash\hat{\sigma})} \leq \sum_{p=1}^{m} \Big(\|\mathrm{D}^p(b - id)\|_{\mathrm{L}^\infty(e^{(r)})} \sum_{i\in E(m,p)} c_i \prod_{q=1}^{m} \|\mathrm{D}^q y\|^{i_q}_{\mathrm{L}^\infty(\hat{T}\backslash\hat{\sigma})} \Big), \tag{3.23}$$

where $e^{(r)} = \partial T^{(r)} \cap \Gamma_h^{(r)}$ is displayed in Figure 3.2. Notice that $b(v) = v$ for any $\mathbb{P}^r$-Lagrangian interpolation nodes $v \in \Gamma \cap e^{(r)}$. Then $id_{|_{e^{(r)}}}$ is the $\mathbb{P}^r$-Lagrangian interpolant of $b_{|_{e^{(r)}}}$. Consequently, the interpolation inequality can be applied as follows (see [45, 12]),

$$\forall z \in e^{(r)}, \quad \|\mathrm{D}^p(b(z) - z)\| \leq ch^{r+1-p}, \qquad \text{for any } 0 \leq p \leq r+1.$$

This interpolation result combined with (3.18) is replaced in (3.23) to obtain,

$$\begin{aligned}\|\mathrm{D}^m_{\hat{x}}(b(y)-y)\|_{\mathrm{L}^\infty(\hat{T}\backslash\hat{\sigma})} &\leq c\sum_{p=1}^{m}\Big(h^{r+1-p}\sum_{i\in E(m,p)}\prod_{q=1}^{m}(\frac{h}{(\lambda^*)^q})^{i_q}\Big)\\ &\leq c\sum_{p=1}^{m}\Big(h^{r+1-p}\frac{h^{\sum_{q=1}^m i_q}}{(\lambda^*)^{\sum_{q=1}^m qi_q}}\Big)\leq c\sum_{p=1}^{m}\Big(h^{r+1-p}\frac{h^p}{(\lambda^*)^m}\Big)\leq c\frac{h^{r+1}}{(\lambda^*)^m},\end{aligned}$$

where the constant $c>0$ is independent of h. This concludes the proof. □

Now, we introduce the mapping $\rho_{T^{(r)}}$, such that $F^{(e)}_{T^{(r)}} = F^{(r)}_T + \rho_{T^{(r)}}$ transforms $\hat{T}$ into the exact triangle $T^{(e)}$. We can prove the following proposition, which is a key point to prove Proposition 3.1.5, as will be shown afterwards in its proof.

Proposition 3.1.13. *Let $\rho_{T^{(r)}} : \hat{x}\in\hat{T}\mapsto\rho_{T^{(r)}}(\hat{x})\in\mathbb{R}^d$, be given by,*

$$\rho_{T^{(r)}}(\hat{x}) := \begin{cases} 0 & \text{if } \hat{x}\in\hat{\sigma},\\ (\lambda^*)^{r+2}(b(y)-y) & \text{if } \hat{x}\in\hat{T}\backslash\hat{\sigma}.\end{cases}$$

The mapping $\rho_{T^{(r)}}$ is of class $\mathcal{C}^{r+1}$ on $\hat{T}$ and there exist a constant $c>0$ independent of h such that,

$$\|\mathrm{D}^m\rho_{T^{(r)}}\|_{\mathrm{L}^\infty(\hat{T})}\leq ch^{r+1},\qquad \textit{for}\quad 0\leq m\leq r+1. \tag{3.24}$$

Proof. The mapping $\rho_{T^{(r)}}$ is of class $\mathcal{C}^{r+1}(\hat{T}\backslash\hat{\sigma})$, being the product of equally regular functions. Consider $0\leq m\leq r+1$. Applying the Leibniz formula, we have,

$$\begin{aligned}\mathrm{D}^m\rho_{T^{(r)}|_{\hat{T}\backslash\hat{\sigma}}} &= \mathrm{D}^m((\lambda^*)^{r+2}(b(y)-y))\\ &= \sum_{i=0}^{m}\binom{m}{i}(r+2)....(r+3-i)(\lambda^*)^{r+2-i}\mathrm{D}^{m-i}(b(y)-y).\end{aligned}$$

Then applying (3.22), we get, for $\hat{x}\in\hat{T}\backslash\hat{\sigma}$,

$$\|\mathrm{D}^m\rho_{T^{(r)}}(\hat{x})\|\leq c\sum_{i=0}^{m}(\lambda^*)^{r+2-i}\frac{ch^{r+1}}{(\lambda^*)^{m-i}}\leq ch^{r+1}(\lambda^*)^{r+2-m}.$$

Since $r+2-m>0$, $(\lambda^*)^{r+2-m}\underset{\hat{x}\to\hat{\sigma}}{\longrightarrow}0$. Consequently, $\mathrm{D}^m\rho_{T^{(r)}}$ can be continuously extended by 0 on $\hat{\sigma}$ when $0\leq m\leq r+1$. Thus $\rho_{T^{(r)}}\in\mathcal{C}^{r+1}$ and the latter inequality

ensures (3.24).

□

Example 3.1.14. *In this 2D example, is displayed the effect of $\rho_{T^{(r)}}$ on internal edges of a non-internal quadratic element of the mesh $\mathcal{T}_h^{(2)}$, $r = 2$.*

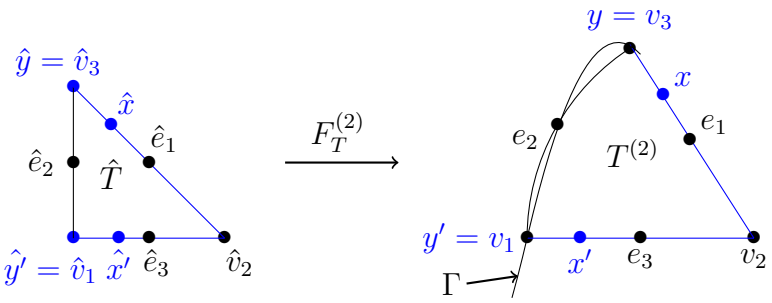

Figure 3.3 – Visualisation of the images via y of points on internal edges.

Notice that for any $\hat{x} \in [\hat{v}_2, \hat{v}_3]$, its associated $\hat{y} = \hat{v}_3$, since on this particular edge $\lambda_1 = 0$, and $\hat{y} = \dfrac{\lambda_1 \hat{v}_1 + \lambda_3 \hat{v}_3}{\lambda_1 + \lambda_3} = \hat{v}_3$. Consequently, its image by $F_T^{(2)}$ is $y = F_T^{(r)}(\hat{y}) = F_T^{(r)}(\hat{v}_3) = v_3$ as displayed above on the curved triangle $T^{(2)}$.

The point y, belonging to Γ, is equal to its image via the orthogonal projection b, i.e. $b(y) = y$. This implies that $\rho_{T^{(r)}}(\hat{x}) = (\lambda^*)^{r+2}(b(y) - y) = 0$, for any $\hat{x} \in [\hat{v}_2, \hat{v}_3]$. Similarly, $\rho_{T^{(r)}}(\hat{x}') = 0$, for any $\hat{x}' \in [\hat{v}_2, \hat{v}_2]$.

We can now prove Proposition 3.1.5: its proof relies on the previous proposition.

Proof of Proposition 3.1.5. Let $T^{(r)} \in \mathcal{T}_h^{(r)}$ be a non-internal element. Let $x = F_T^{(r)}(\hat{x}) \in T^{(r)}$ where $\hat{x} \in \hat{T}$. Following the equation (3.2), we recall that, $F_{T^{(r)}}^{(e)}(\hat{x}) = x + \rho_{T^{(r)}}(\hat{x})$. Then $G_h^{(r)}$ can be written as follows,

$$G_h^{(r)}{}_{|_{T^{(r)}}} = F_{T^{(r)}}^{(e)} \circ (F_T^{(r)})^{-1} = (F_T^{(r)} + \rho_{T^{(r)}}) \circ (F_T^{(r)})^{-1} = id_{|_{T^{(r)}}} + \rho_{T^{(r)}} \circ (F_T^{(r)})^{-1}.$$

Firstly, with Proposition 3.1.13, $\rho_{T^{(r)}}$ is of class $\mathcal{C}^{r+1}(\hat{T})$ and $F_T^{(r)}$ is a polynomial, then $G_h^{(r)}$ is also $\mathcal{C}^{r+1}(T^{(r)})$.

Secondly, $F_T^{(r)}$ is a $\mathcal{C}^1$-diffeomorphism and there exists a constant $c > 0$ independent of h such that (see [33, page 239]),

$$\|\mathrm{D}(F_T^{(r)})^{-1}\| \leq \frac{c}{h}. \tag{3.25}$$

Additionally, by applying (3.24) and (3.25), the following inequality holds,

$$\|\mathrm{D}(\rho_{T^{(r)}})\|_{\mathrm{L}^\infty(\hat{T})}\|\mathrm{D}((F_T^{(r)})^{-1})\|_{\mathrm{L}^\infty(T^{(r)})} \leq ch^{r+1}\frac{c}{h} = ch^r < 1. \tag{3.26}$$

Then by applying [33, Theorem 3], $F_T^{(r)} + \rho_{T^{(r)}}$ is a $\mathcal{C}^1$-diffeomorphism, being the sum of a $\mathcal{C}^1$-diffeomorphism and a $\mathcal{C}^1$ mapping, which satisfy (3.26). Therefore, $G_h^{(r)} = (F_T^{(r)} + \rho_{T^{(r)}}) \circ (F_T^{(r)})^{-1}$ is a $\mathcal{C}^1$-diffeomorphism.

To obtain the first inequality of (3.3), we differentiate the latter expression,

$$\mathrm{D}G_h^{(r)}{}_{|_{T^{(r)}}} - \mathrm{I}_{d|_{T^{(r)}}} = \mathrm{D}(\rho_{T^{(r)}} \circ (F_T^{(r)})^{-1}) = \mathrm{D}(\rho_{T^{(r)}}) \circ ((F_T^{(r)})^{-1})\mathrm{D}(F_T^{(r)})^{-1}.$$

Using (3.24) and (3.25), we obtain,

$$\|\mathrm{D}G_h^{(r)}{}_{|_{T^{(r)}}} - \mathrm{I}_{d|_{T^{(r)}}}\|_{\mathrm{L}^\infty(T^{(r)})} \leq \|\mathrm{D}(\rho_{T^{(r)}})\|_{\mathrm{L}^\infty(\hat{T})}\|\mathrm{D}((F_T^{(r)})^{-1})\|_{\mathrm{L}^\infty(T^{(r)})} \leq ch^r,$$

where the constant $c > 0$ is independent of h. Lastly, the second inequality of (3.3) comes as a consequence of the first one, by definition of a Jacobian. □

3.2 Extension to the vectorial case

3.2.1 Lift operator of vector functions

In the vectorial case, we define a lift for vector-valued functions similarly to the Definition 3.1.3 for scalar functions. Indeed, we employ the same transformation $G_h^{(r)}$, defined in (3.1) such that,

$$G_h^{(r)} : \Omega_h^{(r)} \to \Omega; \quad G_h^{(r)}{}_{|_{\Gamma_h^{(r)}}} = b,$$

where b is the orthogonal projection on the boundary Γ defined in Proposition 2.0.1.

Definition 3.2.1. *To any vector field $\boldsymbol{u}_h \in \mathbf{H}^1(\Omega_h^{(r)}, \Gamma_h^{(r)})$ is associated its lift, denoted $\boldsymbol{u}_h^\ell \in \mathbf{H}^1(\Omega, \Gamma)$, given component wise by,*

$$\boldsymbol{u}_h^\ell \circ G_h^{(r)} = (\boldsymbol{u}_{h1}^\ell \circ G_h^{(r)}, \dots, \boldsymbol{u}_{hd}^\ell \circ G_h^{(r)}) := \boldsymbol{u}_h.$$

Similarly, to any vector field $\boldsymbol{u} \in \mathbf{H}^1(\Omega, \Gamma)$, we can define its inverse lift, $\boldsymbol{u}^{-\ell} \in$

$\mathbf{H}^1(\Omega_h^{(r)}, \Gamma_h^{(r)})$, *given by,*

$$\boldsymbol{u}^{-\ell} := \boldsymbol{u} \circ G_h^{(r)} = (\boldsymbol{u}_1 \circ G_h^{(r)}, \dots, \boldsymbol{u}_d \circ G_h^{(r)}).$$

Remark 3.2.2. *The lift satisfies the trace property, which is an essential key ingredient in the error analysis in Chapter 7. Similarly to Proposition 3.1.4, this property states that, for any vector field* $\boldsymbol{u}_h \in \mathbf{H}^1(\Omega_h^{(r)})$*, the following equality stands,*

$$\left(\boldsymbol{u}_{hi}|_{\Gamma_h^{(r)}}\right)^{\ell} = \left(\boldsymbol{u}_{hi}^{\ell}\right)_{|\Gamma}, \quad \forall\, i = 1, \dots, d.$$

3.2.2 Lift properties for the linear elasticity problem

Similarly to the scalar case, integrals over $\Gamma_h^{(r)}$ (resp. $\Omega_h^{(r)}$) are expressed with respect to ones over Γ (resp. Ω), in the context of the elasticity problem (1.18) using the lift operator given in Definition 3.2.1. These integral expressions are essential in the error analysis exhibited in Chapter 7.

Surface integrals. Let $\boldsymbol{u}_h, \boldsymbol{v}_h \in \mathbf{H}^1(\Gamma_h^{(r)})$ with $\boldsymbol{u}_h^{\ell}, \boldsymbol{v}_h^{\ell} \in \mathbf{H}^1(\Gamma)$ as their respected lifts. Then, one has,

$$\int_{\Gamma_h^{(r)}} \boldsymbol{u}_h \cdot \boldsymbol{v}_h \, \mathrm{d}s = \int_{\Gamma} \boldsymbol{u}_h^{\ell} \cdot \boldsymbol{v}_h^{\ell} \frac{1}{J_b^{\ell}} \, \mathrm{d}s, \tag{3.27}$$

where J_b denotes the Jacobian of b the orthogonal projection on the boundary Γ defined in Proposition 2.0.1, and J_b^{ℓ} is its lift.

Next, to establish a relationship between an integral over $\Gamma_h^{(r)}$ and an integral over Γ involving the Hooke tensor in Lemma 3.2.3, we need to define the surface Hooke tensor over $\Gamma_h^{(r)}$ given for $x \in \Gamma_h^{(r)}$ by,

$$\mathbf{A}_{\Gamma_h^{(r)}}(\xi(x)) := 2\mu_{\Gamma}\xi(x) + \lambda_{\Gamma}\mathrm{Tr}(\xi(x))\mathrm{P}_h(x), \tag{3.28}$$

for any symmetric matrix $\xi \in \mathbb{R}^d \times \mathbb{R}^d$, where $\mathrm{P}_h(x)$ is the orthogonal projection over the tangential space of $\Gamma_h^{(r)}$ at point $x \in \Gamma_h^{(r)}$ and where μ_{Γ} and λ_{Γ} are the Lamé constants. For the readers' convenience, we recall that all the Lamé coefficients are taken as constants.

Additionally, we also define the tangential strain tensor over $\Gamma_h^{(r)}$ as follows,

$$e_{\Gamma_h^{(r)}}(\boldsymbol{u}_h) := \frac{1}{2}\,\mathrm{P}_h(\nabla_{\Gamma_h^{(r)}}\boldsymbol{u}_h + (\nabla_{\Gamma_h^{(r)}}\boldsymbol{u}_h)^{\mathsf{T}})\mathrm{P}_h = \frac{1}{2}\,(\mathrm{P}_h\nabla_{\Gamma_h^{(r)}}\boldsymbol{u}_h + (\mathrm{P}_h\nabla_{\Gamma_h^{(r)}}\boldsymbol{u}_h)^{\mathsf{T}}), \tag{3.29}$$

for any $\boldsymbol{u}_h \in \mathbf{H}^1(\Gamma_h^{(r)})$.

For more simplicity, we define the following notations before proceeding with the following lemma,

$$\mathcal{D}_h(x) := \mathrm{P}(b(x))[\mathrm{I}_d - \mathrm{d}(x)\mathcal{H}(x)]\mathrm{P}_h(x), \quad \forall\, x \in \Gamma_h^{(r)}, \tag{3.30}$$

with its lift $\mathcal{D}_h^\ell$ given as follows,

$$\mathcal{D}_h^\ell\Big(b(x)\Big) := \mathcal{D}_h(x), \quad \forall\, x \in \Gamma_h^{(r)}. \tag{3.31}$$

Additionally, one needs to mention that the orthogonal projections P and P_h are symmetric. This will come in handy in the following lemma.

Lemma 3.2.3. *Let $\boldsymbol{u}_h, \boldsymbol{v}_h \in \mathbf{H}^1(\Gamma_h^{(r)})$ and let $\boldsymbol{u}_h^\ell, \boldsymbol{v}_h^\ell \in \mathbf{H}^1(\Gamma)$ be their respective lifts. The following equation holds,*

$$\begin{aligned}
&\int_{\Gamma_h^{(r)}} \mathbf{A}_{\Gamma_h^{(r)}}(e_{\Gamma_h^{(r)}}(\boldsymbol{u}_h)) : \nabla_{\Gamma_h^{(r)}} \boldsymbol{v}_h \,\mathrm{d}s = \mu_\Gamma \int_\Gamma (\mathrm{P}_h^\ell \nabla_\Gamma \boldsymbol{u}_h^\ell A_h^\ell) : \nabla_\Gamma \boldsymbol{v}_h^\ell \,\mathrm{d}s \\
&+ \mu_\Gamma \int_\Gamma (\nabla_\Gamma \boldsymbol{u}_h^\ell \mathcal{D}_h^\ell)^\mathsf{T} : (\nabla_\Gamma \boldsymbol{v}_h^\ell \mathcal{D}_h^\ell) \frac{1}{J_b^\ell} \,\mathrm{d}s + \lambda_\Gamma \int_\Gamma \mathrm{Tr}(\nabla_\Gamma \boldsymbol{u}_h^\ell \mathcal{D}_h^\ell)\, \mathrm{Tr}(\nabla_\Gamma \boldsymbol{v}_h^\ell \mathcal{D}_h^\ell) \frac{1}{J_b^\ell} \,\mathrm{d}s,
\end{aligned} \tag{3.32}$$

where A_h^ℓ is the lift of the matrix A_h defined in (3.7).

Proof. Consider $\boldsymbol{v}_h = (v_{hi})_{i=1}^d \in \mathbf{H}^1(\Gamma_h^{(r)})$. The tangential gradient of each component of $\boldsymbol{v}_h$ can be expressed as follows by applying (3.5), for all $i = 1, \ldots, d$ and $x \in \Gamma_h^{(r)}$,

$$\nabla_{\Gamma_h^{(r)}} v_{hi}(x) = \mathrm{P}_h(x)[(\mathrm{I}_d - \mathrm{d}\mathcal{H})(x)]\mathrm{P}(b(x))\, \nabla_\Gamma v_{hi}^\ell\,(b(x)) = \Big(\mathcal{D}_h(x)\Big)^\mathsf{T} \nabla_\Gamma v_{hi}^\ell\,(b(x)),$$

where we used the notation of $\mathcal{D}_h$ in (3.30). By definition of the lift, we get the following expression by applying (3.31),

$$(\nabla_{\Gamma_h^{(r)}} v_{hi})^\ell = (\mathcal{D}_h^\ell)^\mathsf{T}\, \nabla_\Gamma v_{hi}^\ell.$$

Thus, the lifted tangential gradient of $\boldsymbol{v}_h$ can be written by,

$$(\nabla_{\Gamma_h^{(r)}} \boldsymbol{v}_h)^\ell = \nabla_\Gamma({\boldsymbol{v}_h}^\ell)\, \mathcal{D}_h^\ell. \tag{3.33}$$

Using the expression of the tensors $\mathbf{A}_{\Gamma_h^{(r)}}$ and $e_{\Gamma_h^{(r)}}(\boldsymbol{u}_h)$ defined in (3.28) and in (3.29),

we can decompose the integral into three terms,

$$\int_{\Gamma_h^{(r)}} \mathbf{A}_{\Gamma_h^{(r)}}(e_{\Gamma_h^{(r)}}(\boldsymbol{u}_h)) : \nabla_{\Gamma_h^{(r)}} \boldsymbol{v}_h \,\mathrm{d}s = \mu_\Gamma I_1 + \mu_\Gamma I_2 + \lambda_\Gamma I_3, \tag{3.34}$$

where,

$$\begin{aligned} I_1 &:= \int_{\Gamma_h^{(r)}} (\mathrm{P}_h \nabla_{\Gamma_h^{(r)}} \boldsymbol{u}_h) : (\nabla_{\Gamma_h^{(r)}} \boldsymbol{v}_h) \,\mathrm{d}s, \\ I_2 &:= \int_{\Gamma_h^{(r)}} (\mathrm{P}_h \nabla_{\Gamma_h^{(r)}} \boldsymbol{u}_h)^{\mathsf{T}} : (\nabla_{\Gamma_h^{(r)}} \boldsymbol{v}_h) \,\mathrm{d}s, \\ I_3 &:= \int_{\Gamma_h^{(r)}} \mathrm{Tr}(e_{\Gamma_h^{(r)}}(\boldsymbol{u}_h)) \,\mathrm{P}_h : \nabla_{\Gamma_h^{(r)}} \boldsymbol{v}_h \,\mathrm{d}s. \end{aligned}$$

We proceed by estimating each integral separately.

The first term can be written as follows using a change of variable and Equation (3.33),

$$I_1 = \int_{\Gamma_h^{(r)}} (\mathrm{P}_h \nabla_{\Gamma_h^{(r)}} \boldsymbol{u}_h) : (\nabla_{\Gamma_h^{(r)}} \boldsymbol{v}_h) \,\mathrm{d}s = \int_\Gamma (\mathrm{P}_h^\ell \nabla_\Gamma \boldsymbol{u}_h^\ell \mathcal{D}_h^\ell) : (\nabla_\Gamma \boldsymbol{v}_h^\ell \mathcal{D}_h^\ell) \,\frac{1}{J_b^\ell} \,\mathrm{d}s.$$

Noticing that by definition of A_h^ℓ in (3.7), it can be also written as follows $A_h^\ell = \left(\mathcal{D}_h^\ell \,(\mathcal{D}_h^\ell)^{\mathsf{T}}\right) \frac{1}{J_b^\ell}$. Thus we arrive at the following expression while using the matrix product property $A : BC = AC^{\mathsf{T}} : B$ for any real valued square matrices A, B and C of the same size $d \times d$,

$$I_1 \;=\; \int_\Gamma (\mathrm{P}_h^\ell \nabla_\Gamma \boldsymbol{u}_h^\ell A_h^\ell) : (\nabla_\Gamma \boldsymbol{v}_h^\ell) \,\mathrm{d}s.$$

As for the second term, we proceed as follows using again that $AB^{\mathsf{T}} : C = A : CB$,

$$\begin{aligned} I_2 = \int_{\Gamma_h^{(r)}} (\mathrm{P}_h \nabla_{\Gamma_h^{(r)}} \boldsymbol{u}_h)^{\mathsf{T}} : (\nabla_{\Gamma_h^{(r)}} \boldsymbol{v}_h) \,\mathrm{d}s &= \int_{\Gamma_h^{(r)}} \left((\nabla_{\Gamma_h^{(r)}} \boldsymbol{u}_h)^{\mathsf{T}} \mathrm{P}_h^{\mathsf{T}}\right) : (\nabla_{\Gamma_h^{(r)}} \boldsymbol{v}_h) \,\mathrm{d}s \\ &= \int_{\Gamma_h^{(r)}} (\nabla_{\Gamma_h^{(r)}} \boldsymbol{u}_h)^{\mathsf{T}} : (\nabla_{\Gamma_h^{(r)}} \boldsymbol{v}_h \,\mathrm{P}_h) \,\mathrm{d}s. \end{aligned}$$

Keeping in mind that that $\nabla_{\Gamma_h^{(r)}} \boldsymbol{v}_h \,\mathrm{P}_h = \nabla_{\Gamma_h^{(r)}} \boldsymbol{v}_h$ and applying a change of variable and (3.33), we obtain,

$$I_2 = \int_{\Gamma_h^{(r)}} (\nabla_{\Gamma_h^{(r)}} \boldsymbol{u}_h)^{\mathsf{T}} : (\nabla_{\Gamma_h^{(r)}} \boldsymbol{v}_h) \,\mathrm{d}s = \int_\Gamma (\nabla_\Gamma \boldsymbol{u}_h^\ell \mathcal{D}_h^\ell)^{\mathsf{T}} : (\nabla_\Gamma \boldsymbol{v}_h^\ell \mathcal{D}_h^\ell) \,\frac{1}{J_b^\ell} \,\mathrm{d}s.$$

Next, we apply the definition of the Frobenius inner product, which states that for any real valued square matrices A, B of dimension $d \times d$, $A : B = \mathrm{Tr}(BA^{\mathsf{T}})$, to obtain,

$$I_3 = \int_{\Gamma_h^{(r)}} \mathrm{Tr}(e_{\Gamma_h^{(r)}}(\boldsymbol{u}_h)) \, \mathrm{Tr}(\nabla_{\Gamma_h^{(r)}} \boldsymbol{v}_h \mathrm{P}_h^{\mathsf{T}}) \, \mathrm{d}s = \int_{\Gamma_h^{(r)}} \mathrm{Tr}(e_{\Gamma_h^{(r)}}(\boldsymbol{u}_h)) \, \mathrm{Tr}(\nabla_{\Gamma_h^{(r)}} \boldsymbol{v}_h \mathrm{P}_h) \, \mathrm{d}s,$$

where we used that $\mathrm{P}_h = \mathrm{P}_h^{\mathsf{T}}$. Since $\nabla_{\Gamma_h^{(r)}} \boldsymbol{v}_h \mathrm{P}_h = \nabla_{\Gamma_h^{(r)}} \boldsymbol{v}_h$ and $\mathrm{Tr}(e_{\Gamma_h^{(r)}}(\boldsymbol{u}_h)) = \mathrm{Tr}(\mathrm{P}_h \nabla_{\Gamma_h^{(r)}} \boldsymbol{u}_h) = \mathrm{Tr}(\nabla_{\Gamma_h^{(r)}} \boldsymbol{u}_h \mathrm{P}_h) = \mathrm{Tr}(\nabla_{\Gamma_h^{(r)}} \boldsymbol{u}_h)$, we get by a change of variable,

$$I_3 = \int_{\Gamma_h^{(r)}} \mathrm{Tr}(\nabla_{\Gamma_h^{(r)}} \boldsymbol{u}_h) \, \mathrm{Tr}(\nabla_{\Gamma_h^{(r)}} \boldsymbol{v}_h) \, \mathrm{d}s = \int_{\Gamma} \mathrm{Tr}(\nabla_{\Gamma} \boldsymbol{u}_h^{\ell} \mathcal{D}_h^{\ell}) \, \mathrm{Tr}(\nabla_{\Gamma} \boldsymbol{v}_h^{\ell} \mathcal{D}_h^{\ell}) \, \frac{1}{J_b^{\ell}} \, \mathrm{d}s.$$

Replacing the expressions of I_1, I_2 and I_3 in (3.34) concludes the proof. □

Volume integrals. Consider $\boldsymbol{u}_h, \boldsymbol{v}_h \in \mathbf{H}^1(\Omega_h^{(r)})$ and let $\boldsymbol{u}_h^{\ell}, \boldsymbol{v}_h^{\ell} \in \mathbf{H}^1(\Omega)$ be their respected lifts, we have,

$$\int_{\Omega_h^{(r)}} \boldsymbol{u}_h \cdot \boldsymbol{v}_h \, \mathrm{d}x = \int_{\Omega} \boldsymbol{u}_h^{\ell} \cdot \boldsymbol{v}_h^{\ell} \frac{1}{J_h^{\ell}} \mathrm{d}x, \tag{3.35}$$

where J_h denotes the Jacobian of $G_h^{(r)}$ and J_h^{ℓ} is its lift.

We proceed in a similar way by defining an expressing for the lift of the gradient of a discrete function. Note that for any $x \in \Omega_h^{(r)}$, using a change of variables $z = G_h^{(r)}(x) \in \Omega$, one has for all $i = 1, \ldots, d$, $(\nabla v_{hi})^{\ell}(z) = (\mathrm{D}G_h^{(r)})^{\mathsf{T}}(x) \nabla v_{hi}^{\ell}(z)$, where $(\mathrm{D}G_h^{(r)})^{\mathsf{T}}$ is the transpose of $\mathrm{D}G_h^{(r)}$. For simplicity, from here on now, we denote for $z \in \Omega$,

$$\mathcal{G}^{\mathsf{T}}(z) := (\mathcal{G}_h^{(r)})^{\mathsf{T}}(z) = (\mathrm{D}G_h^{(r)})(x). \tag{3.36}$$

Hence, one has,

$$(\nabla \boldsymbol{v}_h)^{\ell} = \left((\mathcal{G}_h^{(r)} \nabla v_{hi}^{\ell})^{\mathsf{T}} \right)_{i=1}^{d} = \nabla \boldsymbol{v}_h^{\ell} \mathcal{G}^{\mathsf{T}}. \tag{3.37}$$

Lemma 3.2.4. *Let $\boldsymbol{u}_h, \boldsymbol{v}_h \in \mathbf{H}^1(\Omega_h^{(r)})$ and let $\boldsymbol{u}_h^{\ell}, \boldsymbol{v}_h^{\ell} \in \mathbf{H}^1(\Omega)$. Following the notation in* (3.37)*, we have,*

$$\begin{aligned} \int_{\Omega_h^{(r)}} \mathbf{A}_{\Omega}(e(\boldsymbol{u}_h)) : \nabla \boldsymbol{v}_h \, \mathrm{d}x &= \mu_{\Omega} \int_{\Omega} (\nabla \boldsymbol{u}_h^{\ell} \mathcal{G}^{\mathsf{T}}) : (\nabla \boldsymbol{v}_h^{\ell} \mathcal{G}^{\mathsf{T}}) \, \frac{1}{J_h^{\ell}} \, \mathrm{d}x \\ &+ \mu_{\Omega} \int_{\Omega} (\nabla \boldsymbol{u}_h^{\ell} \mathcal{G}^{\mathsf{T}})^{\mathsf{T}} : (\nabla \boldsymbol{v}_h^{\ell} \mathcal{G}^{\mathsf{T}}) \, \frac{1}{J_h^{\ell}} \, \mathrm{d}x + \lambda_{\Omega} \int_{\Omega} \mathrm{Tr}(\nabla \boldsymbol{u}_h^{\ell} \mathcal{G}^{\mathsf{T}}) \, \mathrm{Tr}(\nabla \boldsymbol{v}_h^{\ell} \mathcal{G}^{\mathsf{T}}) \, \frac{1}{J_h^{\ell}} \, \mathrm{d}x, \end{aligned} \tag{3.38}$$

where $\mathbf{A}_\Omega$ *is the Hooke tensor given in* (1.12) *and where* J_h^ℓ *is the lift of the the Jacobian of* $G_h^{(r)}$.

Proof. The proof is similar as the proof of Lemma 3.2.3 by permuting the roles of $\mathcal{D}_h^\ell$ and $\mathcal{G}^\mathsf{T}$, it is however developed for the sake of completeness. Consider $\boldsymbol{u}_h, \boldsymbol{v}_h \in \mathbf{H}^1(\Omega_h^{(r)})$ and $\boldsymbol{u}_h^\ell, \boldsymbol{v}_h^\ell \in \mathbf{H}^1(\Omega)$. By definition of the Hooke tensor $\mathbf{A}_\Omega$ in (1.12), we can seperate the integrale into two terms as follows,

$$\int_{\Omega_h^{(r)}} \mathbf{A}_\Omega(e(\boldsymbol{u}_h)) : \nabla \boldsymbol{v}_h \,\mathrm{d}x = \mu_\Omega I_1 + \lambda_\Omega I_2, \tag{3.39}$$

where $I_1 = 2\int_{\Omega_h^{(r)}}(e(\boldsymbol{u}_h)) : (\nabla \boldsymbol{v}_h)\,\mathrm{d}x$ and $I_2 = \int_{\Omega_h^{(r)}} \mathrm{Tr}(e(\boldsymbol{u}_h))\,\mathrm{Tr}(\nabla \boldsymbol{v}_h)\,\mathrm{d}x$. We proceed by estimating each integral separately.

For the first term, we use the expression of $e(\boldsymbol{u}_h)$ in (1.8) as follows,

$$I_1 \;=\; \int_{\Omega_h^{(r)}} (\nabla \boldsymbol{u}_h) : (\nabla \boldsymbol{v}_h)\,\mathrm{d}x + \int_{\Omega_h^{(r)}} (\nabla \boldsymbol{u}_h)^\mathsf{T} : (\nabla \boldsymbol{v}_h)\,\mathrm{d}x.$$

Using a change of variable and Equation (3.37), we have,

$$I_1 \;=\; \int_\Omega (\nabla \boldsymbol{u}_h^\ell \mathcal{G}^\mathsf{T}) : (\nabla \boldsymbol{v}_h^\ell \mathcal{G}^\mathsf{T})\,\frac{1}{J_h^\ell}\,\mathrm{d}x + \int_\Omega (\nabla \boldsymbol{u}_h^\ell \mathcal{G}^\mathsf{T})^\mathsf{T} : (\nabla \boldsymbol{v}_h^\ell \mathcal{G}^\mathsf{T})\,\frac{1}{J_h^\ell}\,\mathrm{d}x.$$

As for the second term, we take advantage of the fact that $\mathrm{Tr}(e(\boldsymbol{u}_h)) = \mathrm{Tr}(\nabla \boldsymbol{u}_h)$ and we proceed in a similar manner using a change of variable and applying Equation (3.37) as follows,

$$\begin{aligned} I_2 = \int_{\Omega_h^{(r)}} \mathrm{Tr}(e(\boldsymbol{u}_h))\,\mathrm{Tr}(\nabla \boldsymbol{v}_h)\,\mathrm{d}x &= \int_{\Omega_h^{(r)}} \mathrm{Tr}(\nabla \boldsymbol{u}_h)\,\mathrm{Tr}(\nabla \boldsymbol{v}_h)\,\mathrm{d}x \\ &= \int_\Omega \mathrm{Tr}(\nabla \boldsymbol{u}_h^\ell \mathcal{G}^\mathsf{T})\,\mathrm{Tr}(\nabla \boldsymbol{v}_h^\ell \mathcal{G}^\mathsf{T})\,\frac{1}{J_h^\ell}\,\mathrm{d}x. \end{aligned}$$

Replacing the expression of I_1 and I_2 in (3.39) concludes the proof. □

Estimations near the boundary. For the sake of completeness, we extend Corollary 3.1.8 to a vectorial setting as follows. The proof of the following inequalities derives from Inequality (3.14).

Corollary 3.2.5. *There exists* $c > 0$*, for a sufficiently small* h*, such that the following*

inequalities hold for any $\boldsymbol{v} \in \mathbf{H}^1(\Omega)$ *and* $\boldsymbol{w} \in \mathbf{H}^2(\Omega)$,

$$\|\boldsymbol{v}\|_{\mathbf{L}^2(B_h^\ell)} \leq ch^{1/2}\|\boldsymbol{v}\|_{\mathbf{H}^1(\Omega)} \qquad \textit{and} \qquad \|\boldsymbol{w}\|_{\mathbf{H}^1(B_h^\ell)} \leq ch^{1/2}\|\boldsymbol{w}\|_{\mathbf{H}^2(\Omega)}, \tag{3.40}$$

where $B_h^\ell = \{T^{(e)} \in \mathcal{T}_h^{(e)};\ T^{(e)}$ *has at least 2 verticies on* $\Gamma\}$.

Chapter 4

Finite element approximation and implementation settings

In this chapter, we firstly present the $\mathbb{P}^k$-Lagrange finite element framework used in the error analysis in Chapters 5, 6 and 7. In the present context, the finite element functions are defined on the mesh domain, hence they will be lifted onto Ω through the lift operator in order to approximate the exact solution of the continuous problem in the upcoming chapters.

In Section 4.2, we present the main key implementation elements in the finite element library CUMIN used throughout all the numerical experiments. A validation of the added numerical tools to CUMIN, such as the lift operator and the surface integrals, is established by reproducing known results in the literature. A *super-convergence* of the error on the quadratic meshes in the numerical simulations is depicted and investigated in Section 4.4. In Section 4.5, we inquire into the loss in the convergence rate on cubic meshes we experienced in the volume errors of the Poisson-Neumann test.

4.1 Finite element approximation

Let $k \geq 1$ be the degree of the finite element method, given a curved mesh $\mathcal{T}_h^{(r)}$ of geometric order $r \geq 1$, with Ω_h as the mesh domain and Γ_h its boundary. We start by introducing the finite element method in a scalar setting before passing on to the vectorial setting. We refer to [45, 32] for more details on finite element methods.

4.1.1 The scalar case

The $\mathbb{P}^k$-*Lagrangian finite element space* is given by,

$$\mathbb{V}_h := \{\chi \in C^0(\Omega_h);\ \chi_{|_T} = \hat{\chi} \circ (F_T^{(r)})^{-1},\ \hat{\chi} \in \mathbb{P}^k(\hat{T}),\ \forall\ T \in \mathcal{T}_h^{(r)}\}. \tag{4.1}$$

Let the $\mathbb{P}^r$-*Lagrangian interpolation operator* be denoted by $\mathcal{I}^{(r)} : v \in \mathcal{C}^0(\Omega_h) \mapsto \mathcal{I}^{(r)}(v) \in \mathbb{V}_h$ classically defined with the values of the function v at the nodal points of the $\mathbb{P}^r$-Lagrange finite element.

The *lifted finite element space* is defined by,

$$\mathbb{V}_h^\ell := \{v_h^\ell;\ v_h \in \mathbb{V}_h\} \subset \mathcal{C}^0(\Omega). \tag{4.2}$$

Its associated *lifted interpolation operator* $\mathcal{I}^\ell$ is defined with the help of the lift operator as follows,

$$\begin{array}{rccl} \mathcal{I}^\ell : & \mathcal{C}^0(\Omega) & \longrightarrow & \mathbb{V}_h^\ell \\ & v & \longmapsto & \mathcal{I}^\ell(v) := \Big(\mathcal{I}^{(r)}(v^{-\ell})\Big)^\ell. \end{array} \tag{4.3}$$

It is important to notice that since Ω is an open subset of $\mathbb{R}^2$ or $\mathbb{R}^3$, then we have the following Sobolev embedding $\mathrm{H}^{k+1}(\Omega) \hookrightarrow \mathcal{C}^0(\Omega)$, for $k \geq 1$. Thus, any function $w \in \mathrm{H}^{k+1}(\Omega)$ has an interpolant $\mathcal{I}^\ell(w) \in \mathbb{V}_h^\ell$.

The lifted interpolation operator $\mathcal{I}^\ell$ plays a key part in the error estimation throughout the following interpolation inequality.

Proposition 4.1.1. *There exists a constant $c > 0$ independent of h such that the interpolation operator $\mathcal{I}^\ell$ satisfies the following inequality for $2 \leq m \leq k+1$,*

$$\|v - \mathcal{I}^\ell v\|_{\mathrm{L}^2(\Omega,\Gamma)} + h\|v - \mathcal{I}^\ell v\|_{\mathrm{H}^1(\Omega,\Gamma)} \leq ch^m \|v\|_{\mathrm{H}^m(\Omega,\Gamma)}, \quad \forall\, v \in \mathrm{H}^{k+1}(\Omega,\Gamma).$$

Proof. Let $2 \leq m \leq k+1$ and $v \in \mathrm{H}^{k+1}(\Omega,\Gamma)$. We start by proving the estimation for the L^2 volume norm. Using the norm equivalence (3.16) with the lift operator, we have,

$$\begin{aligned} \|v - \mathcal{I}^\ell v\|^2_{\mathrm{L}^2(\Omega)} \leq c\|v^{-\ell} - \mathcal{I}^{(r)}(v^{-\ell})\|^2_{\mathrm{L}^2(\Omega_h)} &= c \sum_{T^{(r)} \in \mathcal{T}_h^{(r)}} \|v^{-\ell} - \mathcal{I}^{(r)}(v^{-\ell})\|^2_{\mathrm{L}^2(T^{(r)})} \\ &\leq c \sum_{T^{(r)} \in \mathcal{T}_h^{(r)}} h^m \|v^{-\ell}\|^2_{\mathrm{H}^m(T^{(r)})}, \end{aligned}$$

where the latter inequality is a consequence of the classical interpolation inequality applied to $\mathcal{I}^{(r)}$ (see e.g. [32, 19]).

Then, we apply Inequality (3.17) for H^m norms as follows,

$$\|v - \mathcal{I}^\ell v\|^2_{\mathrm{L}^2(\Omega)} \leq ch^m \sum_{T^{(e)} \in \mathcal{T}_h^{(e)}} \|v\|^2_{\mathrm{H}^m(T^{(e)})} = ch^m \|v\|^2_{\mathrm{H}^m(\Omega)},$$

where under the assumption of a quasi-uniform mesh, the final result derives from given interpolation theory, see [12, Corollary 4.1] and [19] for norms over Ω.

In a similar manner, we prove the estimation with the $\mathrm{H}^1(\Omega)$ norm. As for the proof of the interpolation inequality in surface norms over Γ, we refer to [36, 37]. □

Lemma 4.1.2 (The continuity property of the interpolation operator)**.** *There exists a mesh independent constant $c > 0$ such that,*

$$\|\mathcal{I}^\ell(v)\|_{\mathrm{H}^1(\Omega,\Gamma)} \leq c\|v\|_{\mathrm{H}^2(\Omega,\Gamma)}, \qquad \forall\, v \in \mathrm{H}^2(\Omega,\Gamma). \tag{4.4}$$

Proof. Let $v \in \mathrm{H}^2(\Omega,\Gamma)$. Using Proposition 4.1.1, we obtain Inequality (4.4) as follows,

$$\begin{aligned}
\|\mathcal{I}^\ell(v)\|_{\mathrm{H}^1(\Omega,\Gamma)} &\leq \|\mathcal{I}^\ell(v) - v\|_{\mathrm{H}^1(\Omega,\Gamma)} + \|v\|_{\mathrm{H}^1(\Omega,\Gamma)} \\
&\leq ch\|v\|_{\mathrm{H}^2(\Omega,\Gamma)} + c\|v\|_{\mathrm{H}^2(\Omega,\Gamma)} \\
&\leq c\|v\|_{\mathrm{H}^2(\Omega,\Gamma)}.
\end{aligned}$$

□

4.1.2 The vectorial case

The $\mathbb{P}^k$*-Lagrangian finite element vector space* is given by,

$$\boldsymbol{V}_h := [\mathbb{V}_h]^d = \{\chi \in [C^0(\Omega_h)]^d;\ \chi_{|_T} = \hat{\chi} \circ (F_T^{(r)})^{-1},\ \hat{\chi} \in [\mathbb{P}^k(\hat{T})]^d,\ \forall\, T \in \mathcal{T}_h^{(r)}\}. \tag{4.5}$$

The lifted finite element space is defined by,

$$\boldsymbol{V}_h^\ell := [\mathbb{V}_h^\ell]^d = \{\boldsymbol{v}_h^\ell;\ \boldsymbol{v}_h \in \boldsymbol{V}_h\}. \tag{4.6}$$

Its associated lifted interpolation operator $\boldsymbol{I}^{\ell}$ is given by,

$$\begin{array}{rccl} \boldsymbol{I}^{\ell}: & [\mathcal{C}^0(\Omega)]^d & \longrightarrow & \boldsymbol{V}_h^{\ell} \\ & \boldsymbol{v}=(\boldsymbol{v}_i)_{i=1}^d & \longmapsto & \boldsymbol{I}^{\ell}(\boldsymbol{v}) := \left(\mathcal{I}^{\ell}(\boldsymbol{v}_i)\right)_{i=1}^d, \end{array}$$

where $\mathcal{I}^{\ell}$ is the scalar lifted interpolation operator defined in (4.3). Similarly to the scalar case, any vector valued function $\boldsymbol{w} \in \mathbf{H}^{k+1}(\Omega) \subset [\mathcal{C}^0(\Omega)]^d$ has an interpolant $\boldsymbol{I}^{\ell}(\boldsymbol{w}) \in \boldsymbol{V}_h^{\ell}$.

We present the following interpolation inequality associated with $\boldsymbol{I}^{\ell}$, which plays a key part in the error estimation. It derives from Proposition 4.1.1 for scalar norms over Ω and Γ.

Proposition 4.1.3. *There exists a constant $c > 0$ independent of h, such that the following interpolation inequality holds for any $\boldsymbol{v} \in \mathbf{H}^{k+1}(\Omega,\Gamma) := \{u \in \mathbf{H}^{k+1}(\Omega),\ u_{|\Gamma} \in \mathbf{H}^{k+1}(\Gamma)\}$ and any $2 \leq m \leq k+1$,*

$$\|\boldsymbol{v} - \boldsymbol{I}^{\ell}\boldsymbol{v}\|_{\mathbf{L}^2(\Omega,\Gamma)} + h\|\boldsymbol{v} - \boldsymbol{I}^{\ell}\boldsymbol{v}\|_{\mathbf{H}^1(\Omega,\Gamma)} \leq ch^m\|\boldsymbol{v}\|_{\mathbf{H}^m(\Omega,\Gamma)}.$$

Similarly to the scalar case, we present the continuity property of the interpolation operator. The proof of this lemma derives from Inequality (4.4) using the definitions of vector norms.

Lemma 4.1.4 (The continuity property of the interpolation operator)**.** *There exists a constant $c > 0$ mesh independent such that,*

$$\|\boldsymbol{I}^{\ell}(\boldsymbol{v})\|_{\mathbf{H}^1(\Omega,\Gamma)} \leq c\|\boldsymbol{v}\|_{\mathbf{H}^2(\Omega,\Gamma)}, \qquad \forall\, \boldsymbol{v} \in \mathbf{H}^2(\Omega,\Gamma). \tag{4.7}$$

4.2 Implementation

Throughout this manuscript, many numerical experiments are needed in order to validate the theoretical results obtained. These simulations are led by the code CUMIN [71], which is a library standard FORTRAN 90 comprising of many essential existing tools for this work, such as,

— $\mathbb{P}^k$ finite elements of high order;

— curved meshes of the domain Ω of geometrical order $1 \leq r \leq 3$ generated using the software GMSH [1] (see the reference manual for more details [49]);

— solvers for diffusion problem such as the direct solver MUMPS [2](MUltifrontal Massively Parallel sparse direct Solver) which allows fast computations in 2D;

— solvers for linear elasticity PDE's like GMRES (Generalized minimal residual method), which is an iterative method for the numerical solution of a sparse linear system (see [72, Chapter 6.5]);

— eigenvalue problem solvers, such as ARPACK [3], which is a numerical software library for solving large scale eigenvalue problems.

All numerical results presented throughout this work can be fully reproduced using dedicated source codes available on CUMIN Gitlab [4].

In order to numerically solve the systems (1.1), (1.7) and (1.18) presented in Chapter 1, some additional computational key elements are needed to be present in the code. Firstly, we needed to assemble the surface stiffness matrix S_s and the surface mass matrix M_s, which are present in the three studies problem throughout this manuscript. Considering a canonical basis of $\mathbb{V}_h$, we identify a finite element function u_h with its vectorial representation $U \in \mathbb{R}^N$, where N is the number of degrees of freedom (the dimension of $\mathbb{V}_h$). Thus, the matrices are given respectively by,

$$(u_h, v_h) \to \int_{\Gamma_h} \nabla_{\Gamma_h} u_h \cdot \nabla_{\Gamma_h} v_h \, \mathrm{d}s = U^T S_s V,$$

$$(u_h, v_h) \to \int_{\Gamma_h} u_h \, v_h \, \mathrm{d}s = U^T M_s V.$$

We need to point out that all integral computations are performed on the reference simplex using changes of coordinates, considering the lift transformation $G_h^{(r)} : \Omega_h \to \Omega$ defined in (3.1), and the orthogonal projection $b : \Gamma_h \to \Gamma$ onto Γ defined in Proposition 2.0.1. These changes of coordinates are made on each element of the underlying mesh that is considered: either an affine mesh $\mathcal{T}_h^{(1)}$, a curved mesh $\mathcal{T}_h^{(r)}$ or an exact mesh $\mathcal{T}_h^{(e)}$. Additionally, on the reference simplex, high order quadrature methods are used such that the integration error is of lower order than the approximation errors:

1. `https://gmsh.info/`
2. https://mumps-solver.org/index.php
3. https://www.arpack.fr/
4. CUMIN GitLab deposit, `https://plmlab.math.cnrs.fr/cpierre1/cumin`

it has systematically been verified that the integration errors have negligible influence over the forthcoming numerical results.

Since it is not only used in theory but in practice too, we implemented the volume lift given in Definition 3.1.3. From the numerical point of view, the lift operator intervenes at two main steps: in the definition of the right hand side of the problem and in the post-processing of the error. Additionally, we also defined the former lift given in [43] to compare the efficiency and the impact of each lift on the numerical error as it is discussed in Section 5.4. For the sake of completeness, a surface lift is put in place to be applied in the case of surface problems, using the orthogonal projection on the boundary b.

4.3 Code validation: Laplace equation

In this section, we consider the resolution of classical problems aimed to validate the code implementation: matrix assembling and error analysis using the lift operator. We aim to recover the correct method's convergence rate as predicted by the theory.

4.3.1 On a surface

In order to validate the code CUMIN used in all our computations, we first draw our attention towards the Laplace-Beltrami equation on a smooth surface $\Gamma \subset \mathbb{R}^3$,

$$-\Delta_\Gamma u + u = \tilde{g},$$

where $\tilde{g}$ is a smooth enough source term. In the works of Demlow [36, 37], the error analysis of this problem was studied on curved surface meshes using the finite element method.

To begin with, let $\mathcal{T}_h^{(r)}$ be a high order surface mesh of Γ, with Γ_h as its domain. Following the finite element space definition (4.1), the $\mathbb{P}^k$-Lagrange finite element space on Γ_h is given by,

$$W_h := \left\{ u \in \mathrm{C}^0(\Gamma_h),\ \forall\, T \in \mathcal{T}_h^{(r)},\ u_{|T} \circ F_T^{(r)} \in \mathbb{P}^k(\hat{T}) \right\}.$$

In this instance, the discrete problem is given by,

$$\begin{cases} \text{find } u_h \in W_h, \quad \text{such that,} \\ \displaystyle\int_{\Gamma_h} \nabla_{\Gamma_h} u_h \cdot \nabla_{\Gamma_h} v_h \,\mathrm{d}s + \int_{\Gamma_h} u_h\, v_h \,\mathrm{d}s = \int_{\Gamma_h} v_h\, \tilde{g}^{-\ell}\, J_b \,\mathrm{d}s, \quad \forall\ v_h \in W_h, \end{cases}$$

where $\tilde{g}^{-\ell}$ is the inverse lift of $\tilde{g}$ given in Definition 3.1.3 and J_b is the jacobian of the orthogonal projection on the boundary b (which is defined on a tubular defined in Proposition 2.0.1).

The *a priori* error estimates for this problem developed by Demlow read,

$$\|u - u_h^\ell\|_{\mathrm{L}^2(\Gamma)} = O(h^{k+1} + h^{r+1}), \qquad \|\nabla_\Gamma (u - u_h^\ell)\|_{\mathrm{L}^2(\Gamma)} = O(h^k + h^{r+1}). \tag{4.8}$$

Numerical experiment with CUMIN. We set Γ to the unit sphere and the source term to $\tilde{g}(x, y, z) = (y + 2)y\mathrm{e}^y$. The sphere is discretized using linear, quadratic and cubic meshes by GMSH. In Figure 4.1, are displayed the numerical solutions associated to this problem on an affine and a quadratic coarse mesh. As for the exact solution u of the Laplace-Beltrami problem, it is approximated using a finite element method of degree $k = 1, \ldots, 4$.

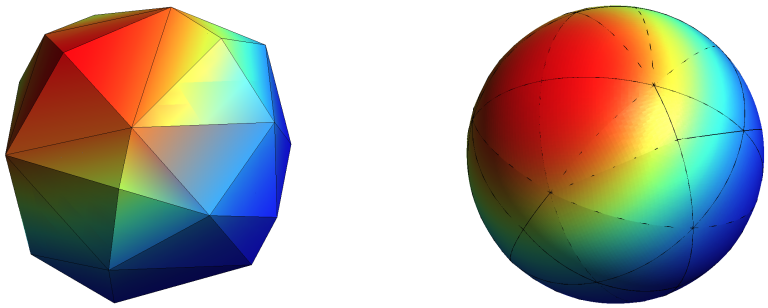

Figure 4.1 – Numerical solution of the Laplace-Beltrami equation on a sphere with affine and quadratic meshes.

The following numerical errors are computed on series of successively refined meshes, where each mesh counts $20 \times 2^{n-1}$ edges on the domain boundary, for $n = 1, \ldots, 5$. Additionally, we note that the refined meshes are not sub-meshes of the coarser ones. Thus on respectively affine, quadratic and cubic, of Γ and for $\mathbb{P}^k$, with $k = 1, \ldots, 4$, we compute,

$$\|u - u_h^\ell\|_{\mathrm{L}^2(\Gamma)} \quad \text{and} \quad \|\nabla_\Gamma (u - u_h^\ell)\|_{\mathrm{L}^2(\Gamma)}.$$

In each case, the mesh size is halved successively to observe the convergence behavior. The measured convergence orders of each of the previous errors are reported in Table 4.1. They are evaluated from the error ratio between two successive meshes.

	$\|u - u_h^\ell\|_{\mathrm{L}^2(\Gamma)}$				$\|u - u_h^\ell\|_{\mathrm{H}^1(\Gamma)}$			
	$\mathbb{P}^1$	$\mathbb{P}^2$	$\mathbb{P}^3$	$\mathbb{P}^4$	$\mathbb{P}^1$	$\mathbb{P}^2$	$\mathbb{P}^3$	$\mathbb{P}^4$
Affine mesh (r=1)	1.96	1.96	1.96	1.96	0.99	1.96	1.96	1.96
Quadratic mesh (r=2)	1.98	2.95	3.92	3.92	0.98	1.97	3.00	3.91
Cubic mesh (r=3)	1.98	2.94	3.95	3.92	0.98	1.96	2.96	3.95

Table 4.1 – Convergence order for the Laplace equation on a sphere (Figures in blue represent a super-convergence in the convergence rate).

On an affine mesh ($r = 1$), the computed errors behave exactly as expected following Inequalities (4.8): the convergence order of the $\mathrm{L}^2(\Gamma)$ error is always equal to 2. Indeed, the order stops at the geometric error order equal to $r + 1$. Similarly, the order of the $\mathrm{H}^1(\Gamma)$ error for any $k \geq 2$ is equal to the geometric error order equal to $r + 1 = 2$.

In turn, quadratic meshes ($r = 2$) produce unexpected convergence rates, which are highlighted in blue in Table 4.1: a *super-convergence* of the two errors is observed. Quadratic meshes display a geometrical error of order 4 instead of the expected order equal to 3 and thus behave as if $r = 3$. In the following section 4.4, this behavior is further investigated to better understand its origin.

On a cubic mesh ($r = 3$), the computed errors follow Inequalities (4.8). For a $\mathbb{P}^1$ (resp. $\mathbb{P}^2$) method, the convergence order of the $\mathrm{L}^2(\Gamma)$ error is equal to the finite element convergence rate, which is equal to 2 (resp. 3). For a $\mathbb{P}^k$ method with $k \geq 3$, the L^2 error rate is equal to $4 = r+1$ (the geometric error rate). The order of the $\mathrm{H}^1(\Gamma)$ error for a $\mathbb{P}^k$ method with $1 \leq k \leq 4$ is equal to the finite element error convergence order equal to k, which in each case is less than (or equal to) $4 = r + 1$.

4.3.2 In the volume

Now, we consider a volume problem to test the accuracy of the volume lift operator implemented. Thus we study a Poisson-Neuman problem on the unit disk, given as follows,

$$\begin{cases} -\Delta u + u &= \tilde{f} \quad \text{in } \Omega, \\ \partial_{\mathrm{n}} u &= \tilde{g} \quad \text{on } \Gamma, \end{cases} \tag{4.9}$$

where we chose $\tilde{f}(x,y) = -7y\,\mathrm{e}^{(x^2+y^2)} - 4y(x^2+y^2)\,\mathrm{e}^{(x^2+y^2)}$ and $\tilde{g}(x,y) = (2x^2y + 2y^3 + y)\,\mathrm{e}^{(x^2+y^2)}$. The analytical solution of Problem (4.9) on the unit disk is given by $u(x,y) = y\,\mathrm{e}^{(x^2+y^2)}$.

To begin with, let $\mathcal{T}_h^{(r)}$ be a curved mesh of Ω, with Ω_h as its domain and Γ_h is its boundary. Let $\mathbb{V}_h$ be the finite element space defined in (4.1), the discrete problem is given by,

$$\begin{cases} \text{find } u_h \in \mathbb{V}_h, \text{ such that,} \\ \displaystyle\int_{\Omega_h} \nabla u_h \cdot \nabla v_h \,\mathrm{d}x + \int_{\Omega_h} u_h\, v_h \,\mathrm{d}x = \int_{\Omega_h} v_h\, \tilde{f}^{-\ell}\, J_h \,\mathrm{d}x + \int_{\Gamma_h} v_h\, \tilde{g}^{-\ell}\, J_b \,\mathrm{d}s, \quad \forall\ v_h \in \mathbb{V}_h, \end{cases}$$

where $\tilde{f}^{-\ell}$ (resp. $\tilde{g}^{-\ell}$) is the inverse lift of $\tilde{f}$ (resp. $\tilde{g}$) and J_h (resp. J_b) is the jacobian of the lift transformation $G_h^{(r)}$, defined in (3.1) (resp. of the orthogonal projection on the boundary b, which is defined on a tubular defined in Proposition 2.0.1).

Taking an isoparametric approach, i.e. taking $k = r$, these estimations are well known in the literature and are given as follows (see [32])

$$\|u - u_h^\ell\|_{\mathrm{L}^2(\Omega)} = O(h^{k+1}), \qquad \|\nabla(u - u_h^\ell)\|_{\mathrm{L}^2(\Omega)} = O(h^k).$$

However in this work, we extended them to a non-isoparametric setting, taking $k \neq r$. The *a priori* error estimates for this problem read,

$$\|u - u_h^\ell\|_{\mathrm{L}^2(\Omega)} = O(h^{k+1} + h^{r+1}), \qquad \|\nabla(u - u_h^\ell)\|_{\mathrm{L}^2(\Omega)} = O(h^k + h^{r+1/2}). \tag{4.10}$$

Inequalities (4.10) can be proven following the same methodology considered in Chapter 5, while considering the constants $\beta = \alpha = 0$ and $\kappa = 1$ (see Theorem 5.3.1).

Hence, the following numerical errors have been computed on series of successively refined meshes, respectively affine, quadratic and cubic, of Ω and with $\mathbb{P}^k$ methods, with $k = 1, \ldots, 4$,

$$\|u - u_h^\ell\|_{\mathrm{L}^2(\Omega)} \quad \text{and} \quad \|\nabla(u - u_h^\ell)\|_{\mathrm{L}^2(\Omega)}.$$

The measured convergence orders of each of the previous errors are reported in Table 4.2. They are evaluated from the error ratio between two successive meshes.

On an affine mesh ($r = 1$), the computed errors behave exactly as expected following Inequalities (4.10): the convergence order of the $\mathrm{L}^2(\Omega)$ error is always equal to $2 = r+1$. Similarly, the order of the $\mathrm{H}_0^1(\Omega)$ error for any $k \geq 2$ is equal to the geometric error

	$\|u - u_h^\ell\|_{L^2(\Omega)}$				$\|\nabla(u - u_h^\ell)\|_{L^2(\Omega)}$			
	$\mathbb{P}^1$	$\mathbb{P}^2$	$\mathbb{P}^3$	$\mathbb{P}^4$	$\mathbb{P}^1$	$\mathbb{P}^2$	$\mathbb{P}^3$	$\mathbb{P}^4$
Affine mesh (r=1)	1.99	1.98	1.98	1.98	0.99	1.49	1.46	1.46
Quadratic mesh (r=2)	2.02	3.02	4.08	4.01	1.01	2.02	3.06	3.65
Cubic mesh (r=3)	2.05	2.5	3.32	4.35	1.05	1.53	2.33	3.41

Table 4.2 – Convergence order (Figures in red represent a loss in the convergence rate and figures in blue represent the super-convergence of the error).

order equal to $r + 1/2 = 1.5$.

Similarly to the previous surface problem, quadratic meshes ($r = 2$) produce the same *super-convergence* of the error rates, which are highlighted in blue in Table 4.2. Hence, the same observation seems to hold for volume and surface errors: quadratic meshes display a geometrical error of order 4 behaving as if $r = 3$. This is discussed in Section 4.4 with more details.

On a cubic mesh ($r = 3$), the computed errors follow Inequalities (4.10), for a $\mathbb{P}^1$ (resp. $\mathbb{P}^4$) method. For $\mathbb{P}^2$ and $\mathbb{P}^3$ methods, a loss in the convergence rate for both the L^2 and H_0^1 errors is highlighted in red. The L^2 error rate is equal to 2.5 (resp. 3.32) for a $\mathbb{P}^2$ (resp. $\mathbb{P}^3$) method, which is less than the expected value of 3 (resp. 4). Similarly, the order of the $H_0^1(\Omega)$ error is equal to 1.5 (resp. 2.33) for a $\mathbb{P}^2$ (resp. $\mathbb{P}^3$) method instead of 2 (resp. 3). This default is present in all the numerical error estimations in volume norms presented throughout this work, thus it is investigated with exhaustive details in Section 4.5.

4.4 Super-convergence on quadratic meshes

On quadratic meshes of geometric order $r = 2$, a super-convergence of the computed error was depicted in the previous section for a surface and a volume problem. In the context of surface error estimations for a spectral problem, the same super-convergence was also observed in the work of Bonito *et al.* [15] on quadratic meshes. Moreover, this super-convergence is also present on all the numerical experiments led in this thesis. In Part III, it is also observed throughout all the numerical evaluation of the error of volume problems in both volume norms and surface norms alike in 2D and 3D. We also point out that even when estimating the eigenvalue and the eigenfunction errors in Chapter 6, a super-convergence is depicted on various geometries. It does not seem to

depend on the specific domains considered in the previously introduced test cases, nor on the considered problems. However, to my knowledge, no theoretical explanation is given for such behavior.

To illustrate that the super convergence is not related with the domain geometry, the considered problem and the dimension, we numerically study the convergence of the following error in 2D and 3D. Given a function $\phi : \mathbb{R}^d \to \mathbb{R}$, we compute the difference between its integral on the mesh domain Ω_h and the value of its integral on the physical domain Ω. Hence, we are estimating the following error,

$$\mathrm{Err}_\phi := \left| \int_\Omega \phi \, \mathrm{d}x - \int_{\Omega_h} \phi \, \mathrm{d}x \right|. \tag{4.11}$$

4.4.1 Investigation on the unit disk

Let Ω be the unit disk, discretized using quadratic meshes. For the readers' convenience, on the right hand side of Figure 4.2, is displayed a quadratic mesh of the disk having 40 edges on the domain boundary. In order to compute the error Err_ϕ in (4.11), we consider the following function,

$$\phi(x, y) = \cos(x^2 + y^2).$$

The error Err_ϕ is computed on a series of successively refined meshes: each mesh counts $10 \times 2^{n-1}$ edges on the domain boundary, for $n = 1, \ldots, 7$. On the left hand side of Figure 4.2, is displayed the plot of Err_ϕ on successively refined quadratic and cubic meshes.

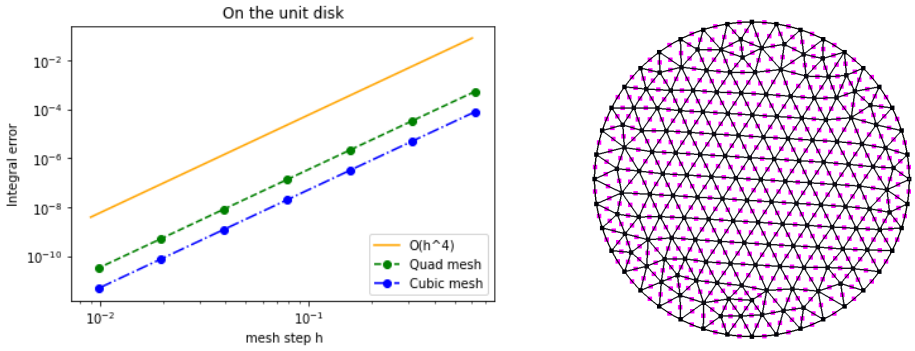

Figure 4.2 – Plot of Err_ϕ on successively refined quadratic and cubic meshes (left) and a quadratic mesh of the unit disk (right).

One quickly notice that the graphs of the error Err_ϕ, respectively on the quadratic meshes (in green) and on the cubic meshes (in blue) both follow the same graph (in yellow) representing a convergence order of 4. This indicates that the quadratic meshes seem to act as if $r = 3$, in the sense that the orders of convergence seem to be the same, even-though the errors in the cubic case are sharper than the ones in the quadratic case.

One might link this super-convergence to the geometry of the considered domain, especially since we are working on a symmetric domain: the unit disk. For this reason, we attempt to estimate the error Err_ϕ in (4.11) on non-symmetric domains in the following part.

4.4.2 Investigation on 2 dimensional non-symmetrical domains

In this section, we constructed non-symmetric smooth domains defined as the interior of a Jordan curve, denoted γ. The curve γ has been set in such a way to have a smooth and connex domain, which moreover is non-convex with no symmetries.

Indeed, the domain Ω is the interior of the Jordan curve $\gamma : \theta \in [0, 2\pi] \to \gamma(\theta) \in \mathbb{R}^2$ satisfying $\gamma(0) = \gamma(2\pi)$. For any $\theta \in [0, 2\pi]$, the function gamma is given by,

$$\gamma(\theta) = (\kappa(\theta)\cos\theta, \kappa(\theta)\sin\theta).$$

In this case, we compute the error relative to the volume of this constructed domain, i.e. we estimate,

$$\mathrm{Err}_{\mathrm{vol}} := \left| \int_\Omega \mathrm{d}x - \int_{\Omega_h} \mathrm{d}x \right|.$$

In my first attempt, we considered,

$$\kappa(\theta) := 1 + \alpha\cos(\theta) + \alpha\cos(5\theta) + \alpha\sin(2\theta) - \alpha\sin(5\theta),$$

where $\alpha = 0.1$. In Figure 4.3 on the left, are displayed the plots of the errors on successively refined quadratic and cubic meshes (see Figure 4.3 on the right for a quadratic mesh having 40 edges on the domain boundary).

Similarly to the case of the disk, the errors on the quadratic meshes, in Figure 4.3, behave the same as on the cubic meshes: in both cases the error has a convergence

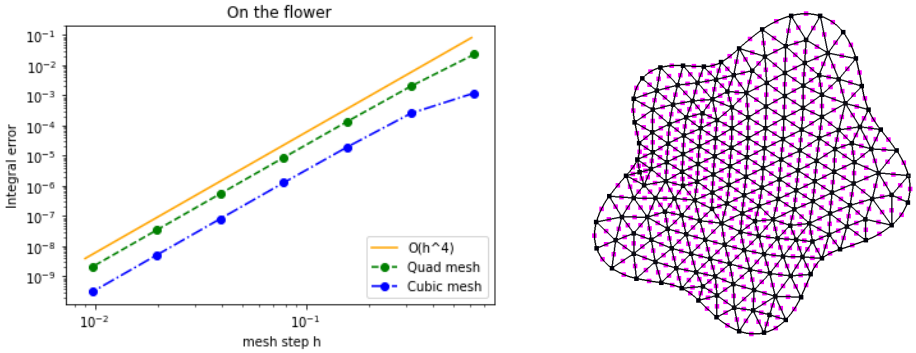

Figure 4.3 – Plots of $\mathrm{Err}_{\mathrm{vol}}$ on successively refined quadratic and cubic meshes (left) and a quadratic meshes a non-symmetrical domain (right).

order equal to 4. This drove us to believe that the super-convergence might not be dependent on the geometry of the domain.

To confirm this hypothesis, a different smooth domain is constructed as the interior of a Jordan curve, with the same approach, taking a different function $\kappa(\theta)$ defined as follows,

$$\kappa(\theta) := 1 + \alpha\cos(\theta) + \beta\sin(\theta) + \frac{\beta}{2}\sin(3\theta),$$

where $\beta = 0.4$ and $\alpha = 0.3$. We also compute the previous volume error $\mathrm{Err}_{\mathrm{vol}}$ on a series of quadratic and cubic refined meshes displayed on the left hand side of Figure 4.4. As observed on the right side of Figure 4.4, the domain is not even remotely close to have a particular symmetry.

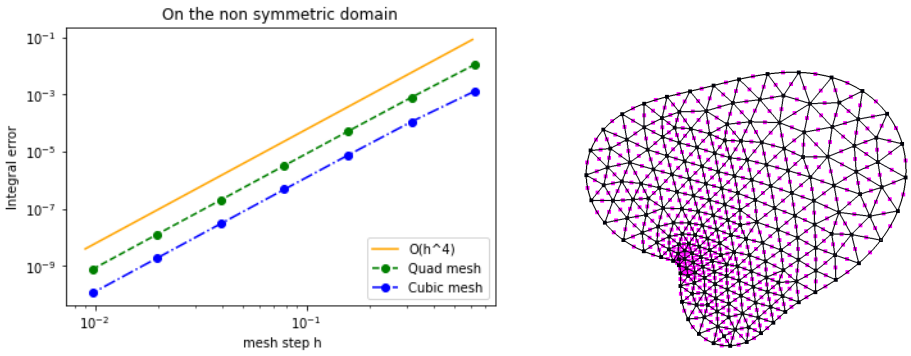

Figure 4.4 – Plots of $\mathrm{Err}_{\mathrm{vol}}$ on successively refined quadratic and cubic meshes (left) and a quadratic meshes of two non-symmetrical domains (right).

From the results displayed in Figure 4.4, the same pattern is observed: the computed errors on quadratic meshes and on cubic meshes (in green and in blue) are in $O(h^4)$. This seems to indicate that the super-convergence of the geometric error for quadratic meshes does not depend on the domain geometry.

4.4.3 Investigation on a 3 dimensional domain: the unit ball

Now, we estimate the error Err_ϕ, defined in (4.11), on a 3D domain to see if the same pattern persists. We compute the error on the unit ball with the following function,

$$\phi(x, y, z) = xyz.$$

The computed errors on meshes of order $r = 2, 3$ are displayed on the left of Figure 4.5. The blue and green plots, representing respectively the errors on quadratic and cubic meshes, follow the same yellow plot representing a convergence order equal to 4. This highlights the presence of the super-convergence phenomena on a 3D domain.

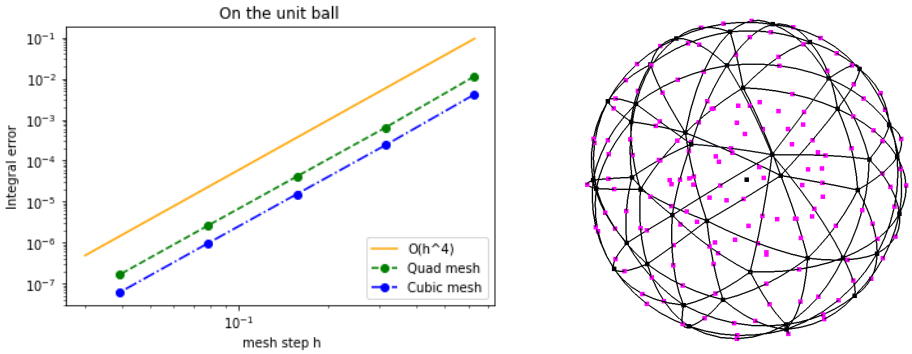

Figure 4.5 – Plot of Err_ϕ on successively refined quadratic and cubic meshes (left) and a quadratic mesh of the unit ball (right).

Remark 4.4.1. *In Figure 4.5, is displayed a quadratic mesh of the unit ball. It is quick interesting to highlight that in some spots one can clearly see that the mesh domain does not form exactly a ball: some curved edges seem too tight or too loose to exactly fit onto the sphere. Furthermore from the mathematical point of view, the unit sphere can not be locally parameterized by polynomial functions.*

4.5 The loss in the convergence order on cubic meshes

As highlighted in Section 4.3, a loss of $-1/2$ in the convergence order of the error on the cubic meshes is depicted when considering a Poisson problem with Newman boundary conditions on the unit disk. This default is highlighted in red in Table 4.2 where the convergence orders of the $\mathrm{L}^2(\Omega)$ and $\mathrm{H}^1(\Omega)$ errors are displayed. Furthermore, no loss was depicted in the numerical surface error of the Laplace-Beltrami surface problem on the unit sphere. Indeed, the errors computed in $\mathrm{L}^2(\Gamma)$ and $\mathrm{H}^1(\Gamma)$ norms in Table 4.1 show the expected convergence rate on cubic meshes. Hence, this loss seems to be only related to "volume" norms. Moreover, we have to point out that the same pattern also appears when estimating the errors of the Poisson-Ventcel problem in Chapter 5 and of the spectral Ventcel problem in Chapter 6 in 2D and in 3D: a loss in the convergence rate is depicted for the volume norms of the errors with no default in the convergence rates of surface errors. This indicates that this default on the cubic mesh is not problem dependent.

To better understand the reason behind this loss in volume norms, we investigated different elements that might affect the computed errors. In the following, we will see that this loss is independent of the lift operator used and of the geometric error. This pattern seems to only appear on the interpolation error with a $\mathbb{P}^k$ method with $k \geq 2$: it is associated with the difference between a smooth function u and its finite element interpolent $\mathcal{I}u \in \mathbb{V}_h$. Typically for a $\mathbb{P}^k$ finite element method with $k \geq 1$, the interpolation errors read (see e.g. [32, 45, 19]),

$$\|\mathcal{I}u - u\|_{\mathrm{L}^2(\Omega_h)} = O(h^{k+1}) \quad \text{and} \quad \|\mathcal{I}u - u\|_{\mathrm{H}^1_0(\Omega_h)} = O(h^k). \tag{4.12}$$

In the following experiments, we will deduce that these estimates are not satisfied on cubic meshes and a default of $-1/2$ appears in each norm estimation. To do that, we compute the following interpolation errors on various domains in 2D and 3D for a smooth function $u : \mathbb{R}^d \to \mathbb{R}$ using a $\mathbb{P}^k$ method with $k \geq 1$,

$$\mathrm{Err}_{\mathrm{L}^2} := \|\mathcal{I}u - u_{|\Omega_h}\|_{\mathrm{L}^2(\Omega_h)} \quad \text{and} \quad \mathrm{Err}_{\mathrm{H}^1_0} := \|\mathcal{I}u - u_{|\Omega_h}\|_{\mathrm{H}^1_0(\Omega_h)}.$$

When estimating these errors, we exclude the possibility of having an error coming from the use of the lift.

This chapter wraps up with an estimation of the interpolation errors on the unit

sphere. This test reinforced the particular relation between the default and the volume norms, since in the case of the unit sphere, no loss is detected.

Complementary experiments revealed how the interpolation error on cubic meshes is tied to the placement of the central node of each curved element (see the central blue node C in Figure 4.6).

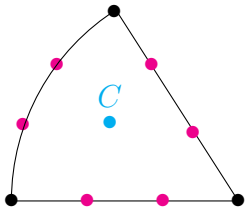

Figure 4.6 – Visualisation of a cubic element $T^{(3)}$ in 2D.

The interpolation error: on the unit disk. Let Ω be the unit disk, discretized using cubic meshes. For the readers' convenience, in Figure 4.7, is displayed a cubic mesh of the disk having 10 edges on the domain boundary: in black are the vertices of each triangle and in pink are the other cubic nodes. We compute the interpolation errors $\mathrm{Err}_{\mathrm{L}^2}$ and $\mathrm{Err}_{\mathrm{H}^1}$ relative to the following function,

$$u(x, y) = \sin(y)\, \mathrm{e}^x, \quad \forall\, (x, y) \in \mathbb{R}^2.$$

In Figure 4.8, the L^2 and H^1 errors are computed on a series of successively refined meshes: each mesh counts $10 \times 2^{n-1}$ edges on the domain boundary, for $n = 1, \ldots, 7$, using $\mathbb{P}^1$, $\mathbb{P}^2$, $\mathbb{P}^3$ and $\mathbb{P}^4$ methods.

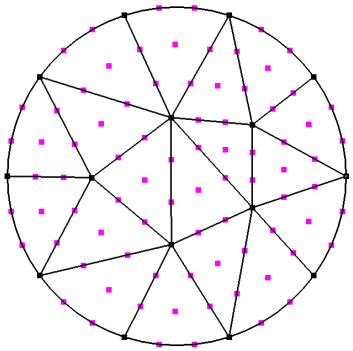

Figure 4.7 – Coarse cubic mesh of the unit disk.

From Figure 4.8, a default of $-1/2$ is depicted for the L^2 (resp. H^1) error using a $\mathbb{P}^k$ method with $k \geq 2$: in the $\mathbb{P}^2$ case, the L^2 (resp. H^1) convergence rate is equal to 2.5 (resp. 1.5), which is less than the expected value equal to 3 (resp. 2). Similarly with the $\mathbb{P}^3$ and $\mathbb{P}^4$ method, the error $\mathrm{Err}_{\mathrm{L}^2}$ (resp. $\mathrm{Err}_{\mathrm{H}^1}$) is in $O(h^{3.5})$ and $O(h^{4.5})$ (resp. $O(h^{2.5})$ and $O(h^{3.5})$). However, with a $\mathbb{P}^1$ method, the L^2 and H^1 errors follow Inequalities (4.12): the convergence rate of $\mathrm{Err}_{\mathrm{L}^2}$ and $\mathrm{Err}_{\mathrm{H}^1}$ is respectively equal to 2 and 1.

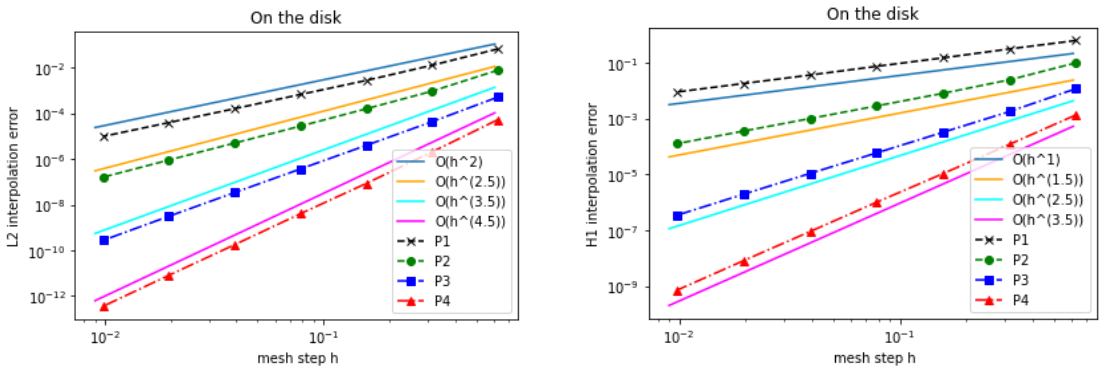

Figure 4.8 – Plots of $\mathrm{Err}_{\mathrm{L}^2}$ (left) and of $\mathrm{Err}_{\mathrm{H}^1}$ (right) on successively refined cubic of the unit disk.

The interpolation error: on the unit ball. We then tested if this loss will persist on a 3D domain. Thus we consider the unit ball. In Figure 4.9, is displayed a coarse cubic mesh of the ball having 10 edges on the equator circle. We computed the interpolation errors with the following function,

$$u(x, y, z) = \sin(y)\cos(z)\,\mathrm{e}^x \quad \forall\,(x, y, z) \in \mathbb{R}^3.$$

The interpolation error is computed on a series of 5 successively refined meshes, using $\mathbb{P}^1$, $\mathbb{P}^2$ and $\mathbb{P}^3$ methods.

As displayed in Figure 4.10, similar results as in the case of the disk are observed. Indeed, with a $\mathbb{P}^2$ or $\mathbb{P}^3$ method, both errors present a default of $-1/2$: the L^2 error is in $O(h^{2.5})$ and $O(h^{3.5})$, as for the H^1 error it is in $O(h^{1.5})$ and $O(h^{2.5})$. No loss in the convergence rate of the errors is detected with a $\mathbb{P}^1$ method.

The interpolation error: on a water-drop shaped domain. Taking it a step further, we construct a domain parameterized by a cubic curve in the form of a water

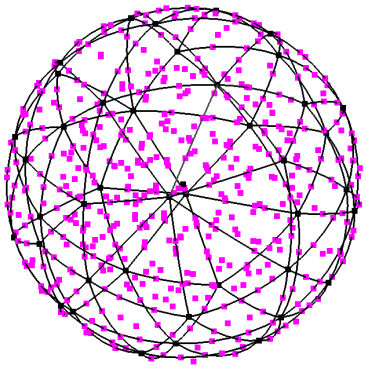

Figure 4.9 – Coarse cubic mesh of the unit ball.

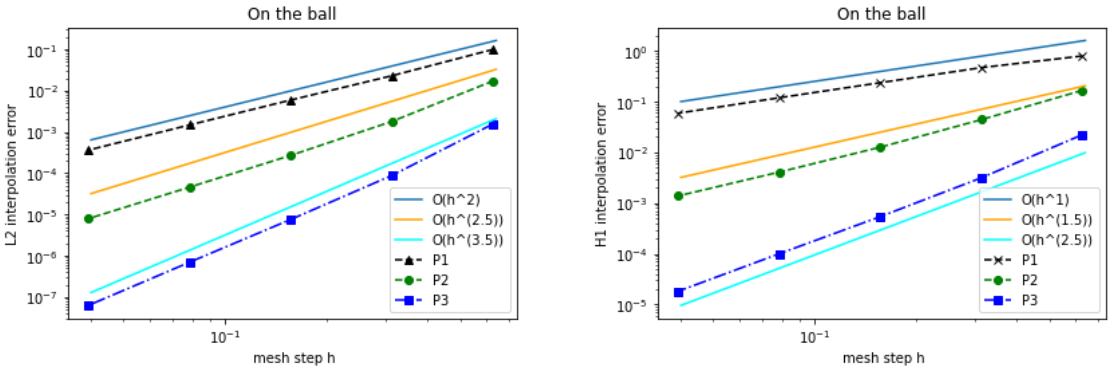

Figure 4.10 – Plots of $\mathrm{Err}_{\mathrm{L}^2}$ (left) and of $\mathrm{Err}_{\mathrm{H}^1}$ (right) on successively refined cubic meshes of the unit ball (right).

drop (see Figure 4.11). On such domain, we excluded the possibility of having a geometric error while using a cubic mesh: the cubic mesh domain will be exactly equal to the physical domain, with $\Omega_h = \Omega$.

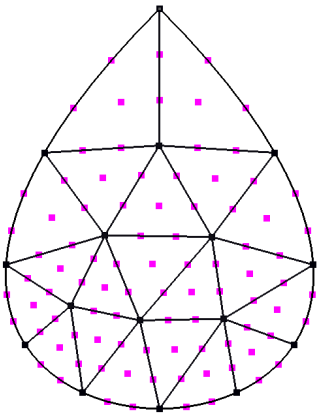

Figure 4.11 – Coarse exact cubic mesh of the domain.

We compute the interpolation errors using the following function,

$$u(x, y) = \cos(x)\,\sin(y), \quad \forall\,(x, y) \in \mathbb{R}^2.$$

Plots of the L^2 and H^1 errors using $\mathbb{P}^k$ methods with $k \geq 1$ are displayed in Figure 4.12. Interestingly enough, even when we excluded the possibility of having a geometric error, the same loss is depicted for the L^2 and H^1 errors with a $\mathbb{P}^k$ method, $k \geq 2$. This implies that the default is solely related to the interpolation errors. No other source of error seem to intervene in this case.

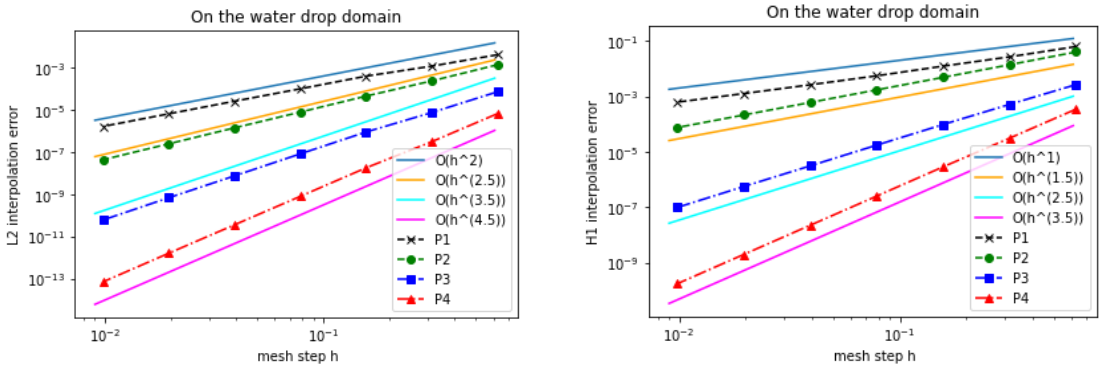

Figure 4.12 – Plot of $\mathrm{Err}_{\mathrm{L}^2}$ (left) and of $\mathrm{Err}_{\mathrm{H}^1}$ (right) on successively refined cubic meshes.

The interpolation error: on the unit sphere. Lastly, we consider the same interpolation problem on a surface in $\mathbb{R}^3$: the unit sphere. The objective of this last

test is to see if the same interpolation loss will be present with surface norms. So we consider the following function,

$$u(x, y, z) = \sin(y)\cos(z)\mathrm{e}^x, \quad \forall\,(x, y, z) \in \mathbb{R}^3.$$

As the previous tests, the sphere is discretized with a cubic surface mesh and the interpolation errors $\mathrm{Err}_{\mathrm{L}^2}$ and $\mathrm{Err}_{\mathrm{H}^1}$ are computed using $\mathbb{P}^k$ finite element methods with $1 \leq k \leq 3$.

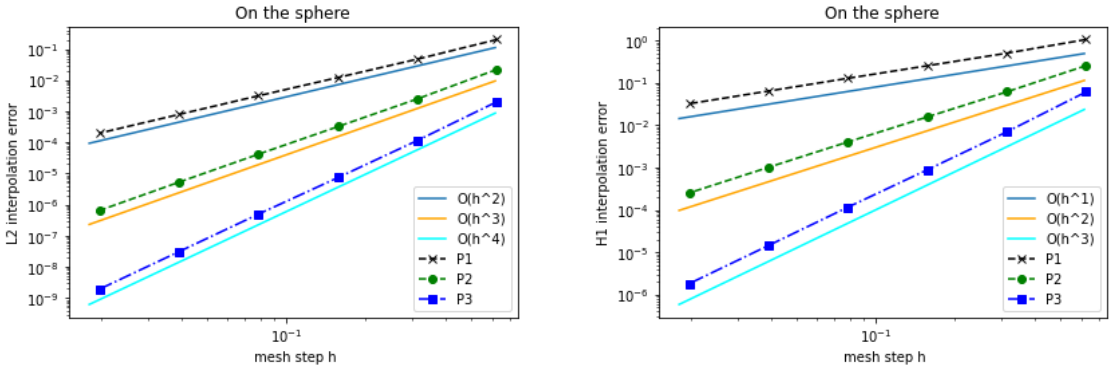

Figure 4.13 – Plot of $\mathrm{Err}_{\mathrm{L}^2}$ (left) and of $\mathrm{Err}_{\mathrm{H}^1}$ (right) on successively refined cubic meshes on the unit sphere.

In Figure 4.13, the L^2 and H^1 interpolation errors follow exactly Inequalities (4.12), for all $\mathbb{P}^k$ methods: indeed the L^2 convergence order is always equal to $k+1$ and the H^1 convergence order is always equal to k, for $k = 1, 2, 3$. This justifies our intuition that this loss is only related to the interpolation error on "volume" norms.

Part III

Error analysis of problems equipped with Ventcel boundary conditions

In this Part, we tackle the error analysis of the problems equipped with Ventcel boundary conditions: in Chapters 5 and 6, are presented and proved the error estimates for respectively the Poisson problem with Ventcel boundary conditions (1.1) and the spectral Ventcel problem (1.7) on curved meshes of order $r \geq 1$ using the $\mathbb{P}^k$ finite element method, with $k \geq 1$. In each case, the error estimates are validated in various numerical experiments in 2D and 3D.

The study in the scalar case is essential for the transition to a more realistic case. As explained in the introduction of this manuscript, our goal is to optimise the eigenvalues of the spectral elasticity problem with Ventcel boundary conditions. For this purpose, in Chapter 7, we present the error analysis of the linear elasticity problem with Ventcel boundary conditions, which comes as a prerequisite to the optimisation problem. In this case, we rely on the same key ingredients as for the scalar problems, such as the lift and the curved meshes, while extending the results to the vectorial case.

Chapter 5

The Poisson-Ventcel problem

From the content of this chapter is composed the following journal paper [25],

— F. Caubet, J. Ghantous, C. Pierre, *A priori error estimates of a poisson diffusion equation with ventcel boundary conditions on curved meshes,* published in SIAM J. Numer. Anal., 2024.

In a nutshell, in this chapter, we aim to do an error analysis of the Poisson-Ventcel problem (1.1), using curved meshes and the lift operator.

5.1 The continuous problem and main novelties

The Poisson-Ventcel problem. We recall that Ω is a nonempty bounded connected domain in $\mathbb{R}^d$, $d = 2$, 3, with a smooth boundary $\Gamma = \partial\Omega$ and we also recall that α, $\beta > 0$, $\kappa \geq 0$ are some given constants, with $f \in \mathrm{H}^{k-1}(\Omega)$, $g \in \mathrm{H}^{k-1}(\Gamma)$ as source terms, with $k \geq 1$. Following Theorem 1.1.2, the Poisson-Ventcel problem given by,

$$\left\{\begin{array}{rcll} -\Delta u + \kappa u & = & f & \text{in } \Omega, \\ -\beta\Delta_\Gamma u + \partial_{\mathrm{n}} u + \alpha u & = & g & \text{on } \Gamma, \end{array}\right. \tag{5.1}$$

admits a unique solution $u \in \mathrm{H}^{k+1}(\Omega, \Gamma)$, which we aim to approximate. Moreover u is also the unique solution to the variational formulation of Problem (5.1) given by,

$$\left\{\begin{array}{l} \text{find } u \in \mathrm{H}^1(\Omega, \Gamma), \ \text{ such that,} \\ a(u, v) = l(v), \ \forall\ v \in \mathrm{H}^1(\Omega, \Gamma), \end{array}\right. \tag{5.2}$$

where the bilinear form a, defined on $\mathrm{H}^1(\Omega, \Gamma) \times \mathrm{H}^1(\Omega, \Gamma)$, is given by,

$$a(u, v) = \int_\Omega \nabla u \cdot \nabla v \, \mathrm{d}x + \kappa \int_\Omega uv \, \mathrm{d}x + \beta \int_\Gamma \nabla_\Gamma u \cdot \nabla_\Gamma v \, \mathrm{d}s + \alpha \int_\Gamma uv \, \mathrm{d}s,$$

and the linear form l, defined on $\mathrm{H}^1(\Omega, \Gamma)$, is given by,

$$l(v) = \int_\Omega fv \,\mathrm{d}x + \int_\Gamma gv \,\mathrm{d}s.$$

As a prerequisite for the error estimation, the domain Ω is discretized using curved meshes of geometrical order $r \geq 1$, denoted $\mathcal{T}_h^{(r)}$. The mesh domain is denoted by Ω_h and its boundary is denoted by Γ_h. The $\mathbb{P}^k$ finite element method is used to define the discrete formulation of the problem, given in (5.3), that admits a unique discrete solution defined on Ω_h. In order to estimate the difference between the exact and discrete solution, the lift operator defined in Chapter 3 is employed.

Main novelties. The main novelty of this chapter with regards to the existing literature is the a priori error estimations, which are computed and expressed both in terms of finite element approximation error and of geometrical error, respectively, associated to the finite element degree $k \geq 1$ and to the mesh order $r \geq 1$. This follows the works of Demlow *et al.* [15, 36, 37] on surface problems, where a non isoparametric approach was considered in the error analysis using a surface lift, where k and r can differ from one another,. In the existing works like in the work of Edelmann [42], error estimates of Problem (5.1) were established using the lift defined by Elliott *et al.* in [43], while considering an isoparametric approach i.e. taking $k = r$. In [43], while also taking an isoparametric approach, a thorough error analysis is made on a coupled bulk–surface partial differential equation with Ventcel boundary conditions.

The main result is the following a priori error estimations, which will be explained in details and proved in Section 5.3:

$$\|u - u_h^\ell\|_{\mathrm{L}^2(\Omega,\Gamma)} = O(h^{k+1} + h^{r+1}) \quad \text{and} \quad \|u - u_h^\ell\|_{\mathrm{H}^1(\Omega,\Gamma)} = O(h^k + h^{r+1/2}),$$

where h is the mesh size and u_h^ℓ denotes the lift of u_h.

We validate these estimations in several numerical experiments presented in 2D and 3D respectively in Section 5.4.1 and in Section 5.4.2. Notice that the same superconvergence of the error rate on the quadratic meshes is depicted, following Section 4.4. Eventually, in Section 5.5.2, this chapter also brings to the fore a comparison between the lift defined in this manuscript and the former lift in [43].

5.2 The finite element approximation

Discrete formulation. We denote $\mathbb{V}_h$ the $\mathbb{P}^k$-Lagrangian finite element space given in (4.1). Following [43, 36], we begin by defining the following linear form l_h on $\mathbb{V}_h$ by,

$$l_h(v_h) := \int_{\Omega_h} v_h f^{-\ell} J_h \,\mathrm{d}x + \int_{\Gamma_h} v_h g^{-\ell} J_b \,\mathrm{d}s, \quad \forall\, v_h \in \mathbb{V}_h,$$

where J_h (resp. J_b) is the Jacobian of the lift transformation $G_h^{(r)}$ given in (3.1) (resp. the orthogonal projection b given in Proposition 2.0.1). With this definition, $l_h(v_h) = l(v_h^\ell)$, for any $v_h \in \mathbb{V}_h$, where l is the right hand side in the formulation (5.2). This can be explained as follows by applying the integral expressions (3.8) and (3.4),

$$\begin{aligned} l(v_h^\ell) = \int_\Omega f v_h^\ell \,\mathrm{d}x + \int_\Gamma g v_h^\ell \,\mathrm{d}s &= \int_\Omega (f^{-\ell} J_h)^\ell (v_h)^\ell \frac{\mathrm{d}x}{J_h^\ell} + \int_\Gamma (g^{-\ell} J_b)^\ell (v_h)^\ell \frac{\mathrm{d}s}{J_b^\ell} \\ &= \int_{\Omega_h} f^{-\ell} J_h v_h \,\mathrm{d}x + \int_{\Gamma_h} g^{-\ell} J_b v_h \,\mathrm{d}s = l_h(v_h). \end{aligned}$$

Hence, the approximation problem is given by,

$$\begin{cases} \text{find } u_h \in \mathbb{V}_h, \text{ such that,} \\ a_h(u_h, v_h) = l_h(v_h),\ \forall\, v_h \in \mathbb{V}_h, \end{cases} \tag{5.3}$$

where a_h is the following bilinear form, defined on $\mathbb{V}_h \times \mathbb{V}_h$ as follows,

$$\begin{aligned} a_h(u_h, v_h) := \int_{\Omega_h} \nabla u_h \cdot \nabla v_h \,\mathrm{d}x + \kappa \int_{\Omega_h} u_h v_h \,\mathrm{d}x + \beta \int_{\Gamma_h} \nabla_{\Gamma_h} u_h \cdot \nabla_{\Gamma_h} v_h \,\mathrm{d}s \\ + \alpha \int_{\Gamma_h} u_h v_h \,\mathrm{d}s. \end{aligned}$$

We note that since a_h is bilinear symmetric positive definite on a finite dimensional space, then there exists a unique solution $u_h \in \mathbb{V}_h$ to the discrete problem (5.3).

Lifted discrete formulation. To begin with, we need to point out that the lifted finite element space $\mathbb{V}_h^\ell$, defined in (4.2), is embedded in the Sobolev space $\mathrm{H}^1(\Omega, \Gamma)$. Thus, the equations (3.10), (3.6), (3.8) and (3.4), where integrals on Ω_h (resp. Γ_h) are expressed in terms of integrals on Ω (resp. Γ), can be applied for lifted finite element functions in the following. We refer to Section 3.2 for exhaustive details.

We define the lifted discrete bilinear form a_h^ℓ, defined on $\mathbb{V}_h^\ell \times \mathbb{V}_h^\ell$, throughout,

$$a_h^\ell(u_h^\ell, v_h^\ell) = a_h(u_h, v_h), \quad \forall\, u_h, v_h \in \mathbb{V}_h.$$

Applying a change of variables along with the integral expressions (3.10), (3.8), (3.6) and (3.4), a_h^ℓ can be expressed as follows for any $u_h^\ell, v_h^\ell \in \mathbb{V}_h^\ell$,

$$a_h^\ell(u_h^\ell, v_h^\ell) = \int_\Omega \mathcal{G}_h^{(r)}(\nabla u_h^\ell) \cdot \mathcal{G}_h^{(r)}(\nabla v_h^\ell) \frac{\mathrm{d}x}{J_h^\ell} + \beta \int_\Gamma A_h^\ell \nabla_\Gamma u_h^\ell \cdot \nabla_\Gamma v_h^\ell \,\mathrm{d}s + \kappa \int_\Omega (u_h)^\ell (v_h)^\ell \frac{\mathrm{d}x}{J_h^\ell} + \alpha \int_\Gamma (u_h)^\ell (v_h)^\ell \frac{\mathrm{d}s}{J_b^\ell}.$$

Keeping in mind that u is the solution of (5.2) and u_h^ℓ is the lift of the discrete solution of (5.3), for any $v_h^\ell \in \mathbb{V}_h^\ell \subset \mathrm{H}^1(\Omega, \Gamma)$, we notice that,

$$a(u, v_h^\ell) = l(v_h^\ell) = l_h(v_h) = a_h(u_h, v_h) = a_h^\ell(u_h^\ell, v_h^\ell). \tag{5.4}$$

Using the previous points, we can also define the lifted formulation of the discrete problem (5.3) by,

$$\begin{cases} \text{find } u_h^\ell \in \mathbb{V}_h^\ell, \text{ such that,} \\ a_h^\ell(u_h^\ell, v_h^\ell) = l(v_h^\ell),\ \forall\, v_h^\ell \in \mathbb{V}_h^\ell, \end{cases}$$

This problem admits a unique solution $u_h^\ell \in \mathbb{V}_h^\ell$, which is the lift of the discrete solution u_h of Problem (5.3).

5.3 Error analysis

Throughout this section, we consider that the mesh size h is sufficiently small (in particular so as to apply Remark 2.1.2) and that c refers to a positive constant independent of h. Our goal in this section is to prove the following theorem, where we estimate the error between the exact solution and the lift of the discrete solution, both defined on Ω.

Theorem 5.3.1. *Let $u \in \mathrm{H}^{k+1}(\Omega, \Gamma)$ be the solution of the variational problem* (5.2) *and $u_h \in \mathbb{V}_h$ be the solution of the finite element formulation* (5.3)*. There exists a*

mesh independent constant $c > 0$ such that for a sufficiently small mesh size h,

$$\|u - u_h^\ell\|_{\mathrm{H}^1(\Omega,\Gamma)} \leq c(h^k + h^{r+1/2}) \quad \textit{and} \quad \|u - u_h^\ell\|_{\mathrm{L}^2(\Omega,\Gamma)} \leq c(h^{k+1} + h^{r+1}). \tag{5.5}$$

The error in both the L^2 and H^1 norm in Theorem 5.3.1 is composed of two main components: the geometrical error and the finite element error. To prove these error bounds, we proceed as follows:

1. estimate the geometric error: we bound the difference between the exact bilinear form a and the lifted bilinear form a_h^ℓ;
2. bound the H^1 error using the geometric and interpolation error estimation, proving the left hand side of Inequality (5.5);
3. an Aubin-Nitsche argument helps us prove the right hand side of Inequality (5.5).

5.3.1 Geometric error

The geometric error is the error produced while approximating a domain by a mesh of order $r \geq 1$. In order to theoretically estimate this error, we compute the difference between the bilinear forms a and a_h^ℓ defined previously in the following proposition.

Proposition 5.3.2. *There exists $c > 0$, such that, for a sufficiently small h, the following geometric error estimation holds for all $v, w \in \mathbb{V}_h^\ell$,*

$$|a(v,w) - a_h^\ell(v,w)| \leq ch^r \|\nabla v\|_{\mathrm{L}^2(B_h^\ell)} \|\nabla w\|_{\mathrm{L}^2(B_h^\ell)} + ch^{r+1} \|v\|_{\mathrm{H}^1(\Omega,\Gamma)} \|w\|_{\mathrm{H}^1(\Omega,\Gamma)}. \tag{5.6}$$

The following proof is inspired by [43, Lemma 6.2]. The main difference is the use of the lift given in Definition 3.1.3 and the corresponding transformation $G_h^{(r)}$ alongside its associated matrix $\mathcal{G}_h^{(r)}$, defined in (3.9).

Proof. Let $v, w \in \mathbb{V}_h^\ell$. By the definitions of the bilinear forms a and a_h^ℓ, we have,

$$|a(v,w) - a_h^\ell(v,w)| \leq a_1(v,w) + \kappa a_2(v,w) + \beta a_3(v,w) + \alpha a_4(v,w),$$

where the terms a_i, defined on $\mathbb{V}_h^\ell \times \mathbb{V}_h^\ell$, are respectively given by,

$$
\begin{aligned}
a_1(v,w) &:= \left| \int_\Omega \nabla w \cdot \nabla v - (\mathcal{G}_h^{(r)} \nabla w) \cdot (\mathcal{G}_h^{(r)} \nabla v) \, \frac{1}{J_h^\ell} \, \mathrm{d}x \right|, \\
a_2(v,w) &:= \left| \int_\Omega wv \, (1 - \frac{1}{J_h^\ell}) \, \mathrm{d}x \right|, \\
a_3(v,w) &:= \left| \int_\Gamma \left((A_h^\ell - \mathrm{I}_d) \nabla_\Gamma w \right) \cdot \nabla_\Gamma v \, \mathrm{d}s \right|, \\
a_4(v,w) &:= \left| \int_\Gamma wv \, (1 - \frac{1}{J_b^\ell}) \, \mathrm{d}s \right|.
\end{aligned}
$$

The next step is to bound each a_i, for $i = 1, 2, 3, 4$, while using (3.12) and (3.11).

First of all, notice that $a_1(v,w) \leq Q_1 + Q_2 + Q_3$, where,

$$
\begin{aligned}
Q_1 &:= \left| \int_\Omega \left((\mathcal{G}_h^{(r)} - \mathrm{I}_d) \, \nabla w \right) \cdot (\mathcal{G}_h^{(r)} \nabla v) \, \frac{1}{J_h^\ell} \, \mathrm{d}x \right|, \\
Q_2 &:= \left| \int_\Omega \nabla w \cdot \left((\mathcal{G}_h^{(r)} - \mathrm{I}_d) \nabla v \right) \frac{1}{J_h^\ell} \, \mathrm{d}x \right|, \\
Q_3 &:= \left| \int_\Omega \nabla w \cdot \nabla v \left(\frac{1}{J_h^\ell} - 1 \right) \mathrm{d}x \right|.
\end{aligned}
$$

We recall that $\mathcal{G}_h^{(r)} - \mathrm{I}_d = 0$, and $\frac{1}{J_h^\ell} - 1 = 0$ in $\Omega \backslash B_h^\ell$ where B_h^ℓ is the union of all the non-internal elements of the exact mesh $\mathcal{T}_h^{(e)}$, as mentioned in (3.13). Taking advantage of these equations, we apply the inequalities in (3.12) to estimate each Q_j as follows,

$$
\begin{aligned}
Q_1 &= \left| \int_{B_h^\ell} \left((\mathcal{G}_h^{(r)} - \mathrm{I}_d) \, \nabla w \right) \cdot (\mathcal{G}_h^{(r)} \nabla v) \, \frac{1}{J_h^\ell} \, \mathrm{d}x \right| \leq c h^r \|\nabla w\|_{\mathrm{L}^2(B_h^\ell)} \|\nabla v\|_{\mathrm{L}^2(B_h^\ell)}, \\
Q_2 &= \left| \int_{B_h^\ell} \nabla w \cdot \left((\mathcal{G}_h^{(r)} - \mathrm{I}_d) \nabla v \right) \frac{1}{J_h^\ell} \, \mathrm{d}x \right| \leq c h^r \|\nabla w\|_{\mathrm{L}^2(B_h^\ell)} \|\nabla v\|_{\mathrm{L}^2(B_h^\ell)}, \\
Q_3 &= \left| \int_{B_h^\ell} \nabla w \cdot \nabla v \, (\frac{1}{J_h^\ell} - 1) \, \mathrm{d}x \right| \leq c h^r \|\nabla w\|_{\mathrm{L}^2(B_h^\ell)} \|\nabla v\|_{\mathrm{L}^2(B_h^\ell)}.
\end{aligned}
$$

Summing up the latter terms, we get, $a_1(v,w) \leq c h^r \|\nabla w\|_{\mathrm{L}^2(B_h^\ell)} \|\nabla v\|_{\mathrm{L}^2(B_h^\ell)}$.

Similarly, to bound a_2, we proceed by using (3.13) and (3.12) as follows,

$$
a_2(v,w) = \left| \int_{B_h^\ell} wv \, (1 - \frac{1}{J_h^\ell}) \, \mathrm{d}x \right| \leq c h^r \|w\|_{\mathrm{L}^2(B_h^\ell)} \|v\|_{\mathrm{L}^2(B_h^\ell)}.
$$

Since $v, w \in \mathbb{V}_h^\ell \subset \mathrm{H}^1(\Omega, \Gamma)$, we use (3.14) to get,

$$a_2(v, w) \leq ch^{r+1} \|w\|_{\mathrm{H}^1(\Omega)} \|v\|_{\mathrm{H}^1(\Omega)}.$$

Before estimating a_3, we need to notice that, by definition of the tangential gradient over Γ (see Def. 1.1.1), $\mathrm{P}\nabla_\Gamma = \nabla_\Gamma$ where $\mathrm{P}(x) = \mathrm{I}_d - (\mathbf{n} \otimes \mathbf{n})(x)$ is the orthogonal projection over the tangential spaces of Γ at a point $x \in \Gamma$. With the estimate (3.11), we get,

$$\begin{aligned} a_3(v, w) &= \left| \int_\Gamma \left((A_h^\ell - \mathrm{P})\ \nabla_\Gamma w \right) \cdot \nabla_\Gamma v \, \mathrm{d}s \right| \\ &\leq \|A_h^\ell - \mathrm{P}\|_{\mathrm{L}^\infty(\Gamma)} \|w\|_{\mathrm{H}^1(\Gamma)} \|v\|_{\mathrm{H}^1(\Gamma)} \leq ch^{r+1} \|w\|_{\mathrm{H}^1(\Gamma)} \|v\|_{\mathrm{H}^1(\Gamma)}. \end{aligned}$$

Then, using (3.11), we estimate a_4 as follows,

$$a_4(v, w) = \left| \int_\Gamma wv \left(1 - \frac{1}{J_b^\ell} \right) \mathrm{d}s \right| \leq ch^{r+1} \|w\|_{\mathrm{L}^2(\Gamma)} \|v\|_{\mathrm{L}^2(\Gamma)}.$$

Inequality (5.6) is easily obtained when summing up a_i, for all $i = 1, 2, 3, 4$. □

Remark 5.3.3. *Let us point out that the solution u of Problem* (5.2) *and the solution u of the discrete problem* (5.3) *satisfy the following inequality,*

$$\|u_h^\ell\|_{\mathrm{H}^1(\Omega,\Gamma)} \leq c \|u\|_{\mathrm{H}^1(\Omega,\Gamma)}, \tag{5.7}$$

where $c > 0$ is independent with respect to h. In fact, a relatively easy way to prove this inequality is by employing the geometrical error estimation (5.6)*, as follows,*

$$c_c \|u_h^\ell\|^2_{\mathrm{H}^1(\Omega,\Gamma)} \leq a(u_h^\ell, u_h^\ell) \leq a(u_h^\ell, u_h^\ell) - a(u, u_h^\ell) + a(u, u_h^\ell),$$

where c_c is the coercivity constant. Using (5.4)*, we have,*

$$c_c \|u_h^\ell\|^2_{\mathrm{H}^1(\Omega,\Gamma)} \leq a(u_h^\ell, u_h^\ell) - a_h^\ell(u_h^\ell, u_h^\ell) + a(u, u_h^\ell) = (a - a_h^\ell)(u_h^\ell, u_h^\ell) + a(u, u_h^\ell).$$

Thus applying the estimation (5.6) *along with the continuity of* a*, we get,*

$$\begin{aligned}\|u_h^\ell\|^2_{\mathrm{H}^1(\Omega,\Gamma)} &\leq ch^r\|\nabla u_h^\ell\|^2_{\mathrm{L}^2(B_h^\ell)} + ch^{r+1}\|u_h^\ell\|^2_{\mathrm{H}^1(\Omega,\Gamma)} + c\|u\|_{\mathrm{H}^1(\Omega,\Gamma)}\|u_h^\ell\|_{\mathrm{H}^1(\Omega,\Gamma)}\\ &\leq ch^r\|u_h^\ell\|^2_{\mathrm{H}^1(\Omega,\Gamma)} + c\|u\|_{\mathrm{H}^1(\Omega,\Gamma)}\|u_h^\ell\|_{\mathrm{H}^1(\Omega,\Gamma)}.\end{aligned}$$

Thus, we have,

$$(1-ch^r)\|u_h^\ell\|^2_{\mathrm{H}^1(\Omega,\Gamma)} \leq c\|u\|_{\mathrm{H}^1(\Omega,\Gamma)}\|u_h^\ell\|_{\mathrm{H}^1(\Omega,\Gamma)}.$$

For a sufficiently small h*, we have* $1-ch^r \geq \epsilon$*, for a given* $\epsilon > 0$*, which concludes the proof.*

5.3.2 Proof of the H^1 error bound in Theorem 5.3.1

Now, we proceed in proving the H^1 error norm. To begin with, we use the coercivity of the bilinear form a to obtain, denoting c_c as the coercivity constant,

$$\begin{aligned}c_c\|\mathcal{I}^\ell u - u_h^\ell\|^2_{\mathrm{H}^1(\Omega,\Gamma)} &\leq a(\mathcal{I}^\ell u - u_h^\ell, \mathcal{I}^\ell u - u_h^\ell) = a(\mathcal{I}^\ell u, \mathcal{I}^\ell u - u_h^\ell) - a(u_h^\ell, \mathcal{I}^\ell u - u_h^\ell)\\ &= a_h^\ell(u_h^\ell, \mathcal{I}^\ell u - u_h^\ell) - a(u_h^\ell, \mathcal{I}^\ell u - u_h^\ell) + a(\mathcal{I}^\ell u, \mathcal{I}^\ell u - u_h^\ell) - a_h^\ell(u_h^\ell, \mathcal{I}^\ell u - u_h^\ell),\end{aligned}$$

where in the latter equation, we added and subtracted $a_h^\ell(u_h^\ell, \mathcal{I}^\ell u - u_h^\ell)$. Thus,

$$c_c\|\mathcal{I}^\ell u - u_h^\ell\|^2_{\mathrm{H}^1(\Omega,\Gamma)} \leq \Big(a_h^\ell - a\Big)(u_h^\ell, \mathcal{I}^\ell u - u_h^\ell) + a(\mathcal{I}^\ell u, \mathcal{I}^\ell u - u_h^\ell) - a_h^\ell(u_h^\ell, \mathcal{I}^\ell u - u_h^\ell).$$

Applying (5.4) with $v = \mathcal{I}^\ell u - u_h^\ell \in \mathbb{V}_h^\ell$, we have,

$$c_c\|\mathcal{I}^\ell u - u_h^\ell\|^2_{\mathrm{H}^1(\Omega,\Gamma)} \leq |(a_h^\ell - a)(u_h^\ell, \mathcal{I}^\ell u - u_h^\ell)| + |a(\mathcal{I}^\ell u - u, \mathcal{I}^\ell u - u_h^\ell)|.$$

Taking advantage of the continuity of a (denoting c_{cont} the continuity constant) and the estimate (5.6), we obtain,

$$\begin{aligned}&c_c\|\mathcal{I}^\ell u - u_h^\ell\|^2_{\mathrm{H}^1(\Omega,\Gamma)}\\ &\quad\leq c\Big(h^r\|\nabla u_h^\ell\|_{\mathrm{L}^2(B_h^\ell)}\|\nabla(\mathcal{I}^\ell u - u_h^\ell)\|_{\mathrm{L}^2(B_h^\ell)} + h^{r+1}\|u_h^\ell\|_{\mathrm{H}^1(\Omega,\Gamma)}\|\mathcal{I}^\ell u - u_h^\ell\|_{\mathrm{H}^1(\Omega,\Gamma)}\Big)\\ &\qquad\quad + c_{cont}\|\mathcal{I}^\ell u - u\|_{\mathrm{H}^1(\Omega,\Gamma)}\|\mathcal{I}^\ell u - u_h^\ell\|_{\mathrm{H}^1(\Omega,\Gamma)}\\ &\quad\leq c\Big(h^r\|\nabla u_h^\ell\|_{\mathrm{L}^2(B_h^\ell)} + h^{r+1}\|u_h^\ell\|_{\mathrm{H}^1(\Omega,\Gamma)} + c_{cont}\|\mathcal{I}^\ell u - u\|_{\mathrm{H}^1(\Omega,\Gamma)}\Big)\|\mathcal{I}^\ell u - u_h^\ell\|_{\mathrm{H}^1(\Omega,\Gamma)}.\end{aligned}$$

Then, dividing by $\|\mathcal{I}^\ell u - u_h^\ell\|_{\mathrm{H}^1(\Omega,\Gamma)}$, we have,

$$\|\mathcal{I}^\ell u - u_h^\ell\|_{\mathrm{H}^1(\Omega,\Gamma)} \leq c\left(h^r\|\nabla u_h^\ell\|_{\mathrm{L}^2(B_h^\ell)} + h^{r+1}\|u_h^\ell\|_{\mathrm{H}^1(\Omega,\Gamma)} + \|\mathcal{I}^\ell u - u\|_{\mathrm{H}^1(\Omega,\Gamma)}\right).$$

To conclude, we use the latter inequality in the following estimate as follows,

$$\begin{aligned}\|u - u_h^\ell\|_{\mathrm{H}^1(\Omega,\Gamma)} &\leq \|u - \mathcal{I}^\ell u\|_{\mathrm{H}^1(\Omega,\Gamma)} + \|\mathcal{I}^\ell u - u_h^\ell\|_{\mathrm{H}^1(\Omega,\Gamma)}\\ &\leq c\left(h^r\|\nabla u_h^\ell\|_{\mathrm{L}^2(B_h^\ell)} + h^{r+1}\|u_h^\ell\|_{\mathrm{H}^1(\Omega,\Gamma)} + \|\mathcal{I}^\ell u - u\|_{\mathrm{H}^1(\Omega,\Gamma)}\right).\end{aligned}$$

Using the interpolation inequality in Proposition 4.1.1 and the inequalities in (3.14), we have,

$$\begin{aligned}&\|u - u_h^\ell\|_{\mathrm{H}^1(\Omega,\Gamma)}\\ &\leq ch^r(\|\nabla(u_h^\ell - u)\|_{\mathrm{L}^2(B_h^\ell)} + \|\nabla u\|_{\mathrm{L}^2(B_h^\ell)}) + ch^{r+1}\|u_h^\ell\|_{\mathrm{H}^1(\Omega,\Gamma)} + ch^k\|u\|_{\mathrm{H}^{k+1}(\Omega,\Gamma)}\\ &\leq ch^r(\|u_h^\ell - u\|_{\mathrm{H}^1(\Omega,\Gamma)} + h^{1/2}\|u\|_{\mathrm{H}^2(\Omega)}) + ch^{r+1}\|u_h^\ell\|_{\mathrm{H}^1(\Omega,\Gamma)} + ch^k\|u\|_{\mathrm{H}^{k+1}(\Omega,\Gamma)}.\end{aligned}$$

Hence we get,

$$(1 - ch^r)\|u - u_h^\ell\|_{\mathrm{H}^1(\Omega,\Gamma)} \leq c\left(h^{r+1/2}\|u\|_{\mathrm{H}^2(\Omega)} + h^k\|u\|_{\mathrm{H}^{k+1}(\Omega,\Gamma)} + h^{r+1}\|u_h^\ell\|_{\mathrm{H}^1(\Omega,\Gamma)}\right).$$

For a sufficiently small h, we arrive at,

$$\|u - u_h^\ell\|_{\mathrm{H}^1(\Omega,\Gamma)} \leq c\left(h^{r+1/2}\|u\|_{\mathrm{H}^2(\Omega,\Gamma)} + h^k\|u\|_{\mathrm{H}^{k+1}(\Omega,\Gamma)} + h^{r+1}\|u_h^\ell\|_{\mathrm{H}^1(\Omega,\Gamma)}\right).$$

This provides the desired result using Inequality (5.7).

5.3.3 Proof of the L^2 error bound in Theorem 5.3.1

To estimate the L^2 norm of the error, we start by defining the functional F_h by,

$$\begin{aligned}F_h: \ \mathrm{H}^1(\Omega,\Gamma) &\longrightarrow \mathbb{R}\\ v &\longmapsto F_h(v) = a(u - u_h^\ell, v).\end{aligned}$$

We bound $|F_h(v)|$ for any $v \in \mathrm{H}^2(\Omega,\Gamma)$ in Lemma 5.3.4. Afterwards an Aubin-Nitsche argument is applied to bound the L^2 norm of the error. We also mention that the constant c in the following lemma will depend on the norm of the exact solution u.

Lemma 5.3.4. *For a sufficiently small h, there exists $c > 0$ independent of h such that the following inequality holds for all $v \in \mathrm{H}^2(\Omega, \Gamma)$,*

$$|F_h(v)| \leq c(h^{k+1} + h^{r+1})\|v\|_{\mathrm{H}^2(\Omega,\Gamma)}. \tag{5.8}$$

Remark 5.3.5. *To prove Lemma 5.3.4, some key points for a function $v \in \mathrm{H}^2(\Omega, \Gamma)$ are presented. Firstly, Inequality* (3.14) *states that,*

$$\forall\, v \in \mathrm{H}^2(\Omega, \Gamma), \quad \|\nabla v\|_{\mathrm{L}^2(B_h^\ell)} \leq ch^{1/2}\|v\|_{\mathrm{H}^2(\Omega)}. \tag{5.9}$$

Secondly, the interpolation inequality in Proposition 4.1.1 implies that,

$$\forall\, v \in \mathrm{H}^2(\Omega, \Gamma), \quad \|\mathcal{I}^\ell v - v\|_{\mathrm{H}^1(\Omega,\Gamma)} \leq ch\|v\|_{\mathrm{H}^2(\Omega,\Gamma)}. \tag{5.10}$$

Applying Equality (5.4) *for $\mathcal{I}^\ell v \in \mathbb{V}_h^\ell$, we get,*

$$\forall\, v \in \mathrm{H}^2(\Omega, \Gamma), \quad a(u, \mathcal{I}^\ell v) = l(\mathcal{I}^\ell v) = a_h^\ell(u_h^\ell, \mathcal{I}^\ell v). \tag{5.11}$$

Proof of Lemma 5.3.4. Consider $v \in \mathrm{H}^2(\Omega, \Gamma)$. We may decompose $|F_h(v)|$ in two terms as follows,

$$|F_h(v)| = |a(u - u_h^\ell, v)| \leq |a(u - u_h^\ell, v - \mathcal{I}^\ell v)| + |a(u - u_h^\ell, \mathcal{I}^\ell v)| =: F_1 + F_2.$$

Firstly, to bound F_1, we take advantage of the continuity of the bilinear form a and apply the H^1 error estimation in (5.5), alongside Inequality (5.10) as follows,

$$\begin{aligned} F_1 = |a(u - u_h^\ell, v - \mathcal{I}^\ell v)| &\leq c_{cont}\, \|u - u_h^\ell\|_{\mathrm{H}^1(\Omega,\Gamma)}\|v - \mathcal{I}^\ell v\|_{\mathrm{H}^1(\Omega,\Gamma)} \\ &\leq c(h^k + h^{r+1/2})\, h\|v\|_{\mathrm{H}^2(\Omega,\Gamma)} \leq c(h^{k+1} + h^{r+3/2})\, \|v\|_{\mathrm{H}^2(\Omega,\Gamma)}. \end{aligned}$$

Secondly, to estimate F_2, we resort to Equation (5.11) and the geometric error estimation (5.6) as follows,

$$\begin{aligned} F_2 = |a(u, \mathcal{I}^\ell v) - a(u_h^\ell, \mathcal{I}^\ell v)| = |a_h^\ell(u_h^\ell, \mathcal{I}^\ell v) - a(u_h^\ell, \mathcal{I}^\ell v)| &= |(a_h^\ell - a)(u_h^\ell, \mathcal{I}^\ell v)| \\ \leq ch^r\|\nabla u_h^\ell\|_{\mathrm{L}^2(B_h^\ell)}\|\nabla(\mathcal{I}^\ell v)\|_{\mathrm{L}^2(B_h^\ell)} &+ ch^{r+1}\|u_h^\ell\|_{\mathrm{H}^1(\Omega,\Gamma)}\|\mathcal{I}^\ell v\|_{\mathrm{H}^1(\Omega,\Gamma)}. \end{aligned}$$

Next, we will treat the first term in the latter inequality separately. We have,

$$\begin{aligned} F_3 &:= h^r \|\nabla u_h^\ell\|_{\mathrm{L}^2(B_h^\ell)} \|\nabla(\mathcal{I}^\ell v)\|_{\mathrm{L}^2(B_h^\ell)} \\ &\leq h^r \Big(\|\nabla(u_h^\ell - u)\|_{\mathrm{L}^2(B_h^\ell)} + \|\nabla u\|_{\mathrm{L}^2(B_h^\ell)} \Big) \Big(\|\nabla(\mathcal{I}^\ell v - v)\|_{\mathrm{L}^2(B_h^\ell)} + \|\nabla v\|_{\mathrm{L}^2(B_h^\ell)} \Big) \\ &\leq h^r \Big(\|u_h^\ell - u\|_{\mathrm{H}^1(\Omega,\Gamma)} + \|\nabla u\|_{\mathrm{L}^2(B_h^\ell)} \Big) \Big(\|\mathcal{I}^\ell v - v\|_{\mathrm{H}^1(\Omega,\Gamma)} + \|\nabla v\|_{\mathrm{L}^2(B_h^\ell)} \Big). \end{aligned}$$

We now apply the H^1 error estimation in (5.5), Inequality (5.9) and the interpolation inequality (5.10), as follows,

$$\begin{aligned} F_3 &\leq c\, h^r \Big(h^k + h^{r+1/2} + h^{1/2} \|u\|_{\mathrm{H}^2(\Omega,\Gamma)} \Big) \Big(h \|v\|_{\mathrm{H}^2(\Omega,\Gamma)} + h^{1/2} \|v\|_{\mathrm{H}^2(\Omega,\Gamma)} \Big) \\ &\leq c\, h^r\, h^{1/2} \Big(h^{k-1/2} + h^r + \|u\|_{\mathrm{H}^2(\Omega,\Gamma)} \Big) \Big(h^{1/2} + 1 \Big) h^{1/2} \|v\|_{\mathrm{H}^2(\Omega,\Gamma)} \\ &\leq c\, h^{r+1} \Big(h^{k-1/2} + h^r + \|u\|_{\mathrm{H}^2(\Omega,\Gamma)} \Big) \Big(h^{1/2} + 1 \Big) \|v\|_{\mathrm{H}^2(\Omega,\Gamma)}. \end{aligned}$$

Noticing that $k - 1/2 > 0$ (since $k \geq 1$) and that $\Big(h^{k-1/2} + h^r + \|u\|_{\mathrm{H}^2(\Omega,\Gamma)} \Big) \Big(h^{1/2} + 1 \Big)$ is bounded by a constant independent of h, we obtain that

$$F_3 \leq c\, h^{r+1} \|v\|_{\mathrm{H}^2(\Omega,\Gamma)}.$$

Applying the latter inequality in the previous expression of F_2, we have,

$$F_2 \leq c h^{r+1} \|v\|_{\mathrm{H}^2(\Omega,\Gamma)} + c h^{r+1} \|u_h^\ell\|_{\mathrm{H}^1(\Omega,\Gamma)} \|\mathcal{I}^\ell v\|_{\mathrm{H}^1(\Omega,\Gamma)}.$$

Moreover, applying the continuity property of the interpolation operator $\mathcal{I}^\ell$ in (4.4), we get by using (5.7),

$$F_2 \leq c h^{r+1} \|v\|_{\mathrm{H}^2(\Omega,\Gamma)} + c h^{r+1} \|u_h^\ell\|_{\mathrm{H}^1(\Omega,\Gamma)} \|v\|_{\mathrm{H}^2(\Omega,\Gamma)} \leq c h^{r+1} \|v\|_{\mathrm{H}^2(\Omega,\Gamma)}.$$

We conclude the proof by summing the estimates of F_1 and F_2. □

Proof of the L^2 ***estimate*** (5.5)**.** Defining $e := u - u_h^\ell \in \mathrm{H}^1(\Omega, \Gamma)$, the aim is to estimate the following L^2 error norm: $\|e\|^2_{\mathrm{L}^2(\Omega,\Gamma)} = \|u - u_h^\ell\|^2_{\mathrm{L}^2(\Omega)} + \|u - u_h^\ell\|^2_{\mathrm{L}^2(\Gamma)}$. Applying Theorem 1.1.2 for $f = e$ and $g = e_{|\Gamma}$, which respectively belong to $\mathrm{L}^2(\Omega)$ and $\mathrm{L}^2(\Gamma)$, there exists a unique solution $z_e \in \mathrm{H}^2(\Omega, \Gamma)$ to (5.2), which satisfies the

following inequality,

$$\|z_e\|_{\mathrm{H}^2(\Omega,\Gamma)} \leq c\|e\|_{\mathrm{L}^2(\Omega,\Gamma)}. \tag{5.12}$$

Keeping in mind the definition of F_h, we obtain,

$$F_h(z_e) = a(e, z_e) = \|e\|^2_{\mathrm{L}^2(\Omega,\Gamma)}.$$

Applying Inequality (5.8) for $z_e \in \mathrm{H}^2(\Omega, \Gamma)$ and afterwards Inequality (5.12), we have,

$$\|e\|^2_{\mathrm{L}^2(\Omega,\Gamma)} = |F_h(z_e)| \leq c(h^{k+1} + h^{r+1})\|z_e\|_{\mathrm{H}^2(\Omega,\Gamma)} \leq c(h^{k+1} + h^{r+1})\|e\|_{\mathrm{L}^2(\Omega,\Gamma)},$$

which concludes the proof. □

5.4 Numerical experiments

In this section, numerical results in 2D and 3D are presented in order to illustrate the theoretical convergence results of Theorem 5.3.1. These experiments show in particular the optimality of the obtained estimates in (5.5). For the sake of completeness, we mention that the finite element space, the matrix assembling and the computation on curved surfaces in following examples are led using the finite element library CUMIN [71]. Additionally, the curved meshes of the domain Ω of geometrical order $1 \leq r \leq 3$ have been generated using the software GMSH [1]. For additional details we refer to Section 4.2.

5.4.1 Numerical study of the Poisson-Ventcel problem in the two dimensional case

In order to validate the error estimates (5.5), the Ventcel problem (5.1) is considered with $\alpha = \beta = \kappa = 1$ on the unit disk Ω,

$$\begin{cases} -\Delta u + u = f & \text{in } \Omega, \\ -\Delta_\Gamma u + \partial_{\mathrm{n}} u + u = g & \text{on } \Gamma, \end{cases}$$

with the source terms $f(x, y) = -y\mathrm{e}^x$ and $g(x, y) = y\mathrm{e}^x(3 + 4x - y^2)$ corresponding to the exact solution $u = -f$.

1. `https://gmsh.info/`

The numerical solutions u_h are computed for $\mathbb{P}^k$ finite elements, with $k = 1, \dots, 4$, on series of successively refined meshes of order $r = 1, \dots, 3$, as depicted on Figure 5.1 for coarse meshes (affine and quadratic). Each mesh counts $10 \times 2^{n-1}$ edges on the domain boundary, for $n = 1, \dots, 7$. On the most refined mesh using a $\mathbb{P}^4$ finite element method, we counted 10×2^6 boundary edges and approximately 75 500 triangles. The associated $\mathbb{P}^4$ finite element space has approximately 605 600 degrees of freedom. We mention that the computation time is very fast in the present case: total computations roughly last one minute on a simple laptop, which are made really efficient with the direct solver MUMPS for sparse linear systems.

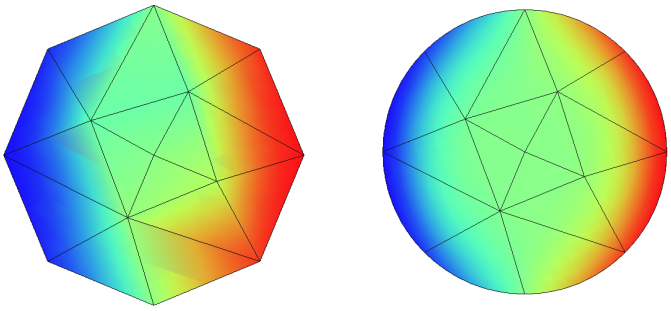

Figure 5.1 – Numerical solution of the Poisson-Ventcel problem on affine and quadratic meshes.

In order to validate numerically the estimates (5.5), for each mesh order r and each finite element degree k, the following numerical errors are computed on a series of refined meshes:

$$\|u - u_h^\ell\|_{\mathrm{L}^2(\Omega)}, \quad \|\nabla u - \nabla u_h^\ell\|_{\mathrm{L}^2(\Omega)}, \quad \|u - u_h^\ell\|_{\mathrm{L}^2(\Gamma)} \quad \text{and} \quad \|\nabla_\Gamma u - \nabla_\Gamma u_h^\ell\|_{\mathrm{L}^2(\Gamma)}.$$

The convergence orders of these errors, interpreted in terms of the mesh size, are reported in Table 5.1 and in Table 5.2. They are evaluated from the error ratio between two successive meshes. For readers' convenience, these four errors are plotted with respect to h in Figure 5.2 with volume norms and in Figure 5.3 with surface norms.

The convergence orders presented in Table 5.1 and in Figure 5.2, relatively to L^2 norms on Ω, deserve comments. In the affine case ($r = 1$), the figures are in perfect agreement with estimates (5.5): the L^2 error norm is in $O(h^{k+1} + h^2)$ and the L^2 norm of the gradient of the error is in $O(h^k + h^{1.5})$.

For quadratic meshes, following Section 4.4, the expected super-convergence phe-

	$\|u - u_h^\ell\|_{L^2(\Omega)}$				$\|\nabla u - \nabla u_h^\ell\|_{L^2(\Omega)}$			
	$\mathbb{P}^1$	$\mathbb{P}^2$	$\mathbb{P}^3$	$\mathbb{P}^4$	$\mathbb{P}^1$	$\mathbb{P}^2$	$\mathbb{P}^3$	$\mathbb{P}^4$
Affine mesh (r=1)	1.98	1.99	1.97	1.97	1.00	1.50	1.49	1.49
Quadratic mesh (r=2)	2.01	3.14	3.94	3.97	1.00	2.12	3.03	3.48
Cubic mesh (r=3)	2.04	2.45	3.44	4.04	1.02	1.47	2.42	3.46

Table 5.1 – Convergence orders, volume norms (Figures in red represent a loss in the convergence rate and figures in blue represent the super-convergence of the error).

nomena is observed in the geometric error, the case $r = 2$ behaves as if $r = 3$: the L^2 error norm is in $O(h^{k+1} + h^4)$ and the L^2 norm of the gradient of the error is in $O(h^k + h^{3.5})$. This is quite visible in Figure 5.2 (left) for the L^2 error: while using respectively a $\mathbb{P}^3$ and $\mathbb{P}^4$ method, the L^2 error graphs in both cases follow the same line representing $O(h^4)$. In the case of the L^2 gradient norm of the error, this super-convergence is depicted with a $\mathbb{P}^3$ (resp. $\mathbb{P}^4$) method: the convergence order is equal to 3 (resp. 3.5) surpassing the expected value of 2.5.

For the cubic case eventually, the L^2 error norm is expected to be in $O(h^{k+1} + h^4)$ and the L^2 norm of the gradient of the error in $O(h^{k+1/2} + h^{3.5})$. This is accurately observed for a $\mathbb{P}^1$ (resp. $\mathbb{P}^4$) method: the L^2 error is equal to 2.04 (resp. 4.04) and the L^2 gradient error is equal to 1.02 (resp. 3.46). However, a default of order -1/2 is observed on the convergence orders in the $\mathbb{P}^2$ and $\mathbb{P}^3$ case: the L^2 error is equal to 2.45 (resp. 3.44) instead of 3 (resp. 4) and the L^2 gradient error is equal to 1.47 (resp. 2.42) instead of 3 (resp. 3). Further experiments are led in Section 4.5, where we established the relation between this loss and the volume norms. This default is not observed when considering $L^2(\Gamma)$ errors as shown in Table 5.2.

	$\|u - u_h^\ell\|_{L^2(\Gamma)}$				$\|\nabla_\Gamma u - \nabla_\Gamma u_h^\ell\|_{L^2(\Gamma)}$			
	$\mathbb{P}^1$	$\mathbb{P}^2$	$\mathbb{P}^3$	$\mathbb{P}^4$	$\mathbb{P}^1$	$\mathbb{P}^2$	$\mathbb{P}^3$	$\mathbb{P}^4$
Affine mesh (r=1)	2.00	2.03	2.01	2.01	1.00	2.00	1.98	1.98
Quadratic mesh (r=2)	2.00	3.00	4.00	4.02	1.00	2.00	3.00	4.02
Cubic mesh (r=3)	2.00	3.00	4.00	4.21	1.00	2.00	3.00	3.98

Table 5.2 – Convergence orders, boundary norms (Figures in blue represent the super-convergence of the error).

Let us now discuss Table 5.2 and Figure 5.3, where the surface errors and their convergence rates are observed. The first interesting point is that the L^2 convergence towards the gradient of u is faster than expressed in (5.5): the error is in $O(h^k + h^{r+1})$

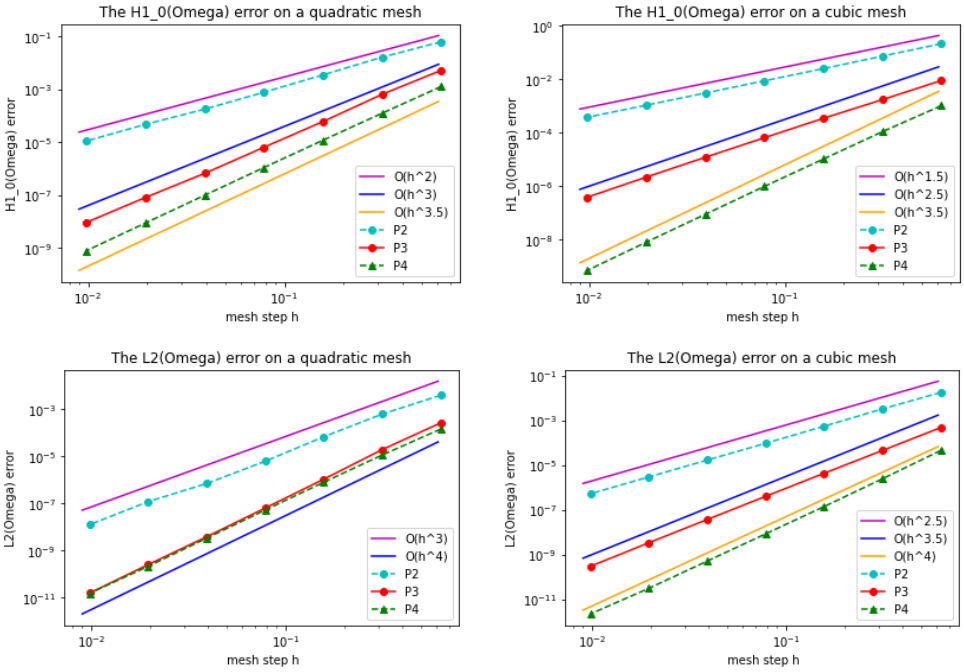

Figure 5.2 – Plots of the error in volume norms with respect to the mesh step h corresponding to the convergence order in Table 5.1: $\mathrm{H}_0^1(\Omega)$ norm (above) and $\mathrm{L}^2(\Omega)$ norm (below) for quadratic meshes (left) and cubic meshes (right).

instead of being in $O(h^k + h^{r+1/2})$, as expected. Indeed, this is observed on a cubic and quadratic mesh with a $\mathbb{P}^4$ method: the convergence rate is equal to 4 instead of 3.5. This does not contradict the optimality of the error estimations in Theorem 5.3.1, where the H_0^1 error is evaluated both on Ω and on Γ. This implies that the surface error norm is sharper than the $\mathrm{H}_0^1(\Omega)$ error and is thus hidden from the theoretical point of view. From the author's point of view, this improvement is related to the geometric error, which has a lower rate when estimating the error between volume integrals on Ω and Ω_h than when computing surface integral errors.

Meanwhile the L^2 convergence towards u behaves as expected. We note that the usual super-convergence associated to quadratic meshes previously described in Section 4.4 is also clearly visible in this case: if one simply compares the bottom two rows of Table 5.2 (for $r = 2$ and $r = 3$), it is easy to see that the convergence rates seem to be identical. As discussed in Section 4.5, the default of convergence of magnitude $-1/2$ for cubic meshes is absent in the case of the surface errors: the convergence rate of the errors correspond to the expected values following Theorem 5.3.1.

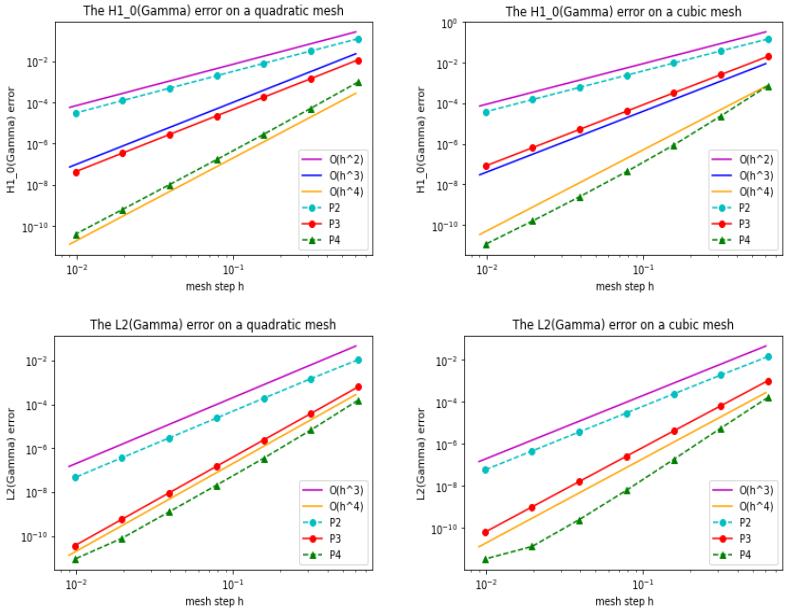

Figure 5.3 – Plots of the error in interior norms with respect to the mesh step h corresponding to the convergence order in Table 5.2: $\mathrm{H}_0^1(\Gamma)$ norm (above) and $\mathrm{L}^2(\Gamma)$ norm (below) for quadratic meshes (left) and cubic meshes (right).

5.4.2 Numerical study of the Poisson-Ventcel problem in the three dimensional case

In this section, the system (5.1) is considered on the unit ball $\Omega = \mathrm{B}(\mathrm{O}, 1) \subset \mathbb{R}^3$, with source terms $f = -(x+y)\mathrm{e}^z$ on the domain and $g = (x+y)(5z+z^2+3)\mathrm{e}^z$ on the boundary. The ball is discretized using curved meshes of order $r = 1, \ldots, 3$.

For each mesh order r and finite element degree k, we compute the error on a series of six successively refined meshes. Each mesh counts $10 \times 2^{n-1}$ edges on the equator circle, for $n = 1, \ldots, 6$. The most refined mesh has approximately $2,4 \times 10^6$ tetrahedra and the associated $\mathbb{P}^3$ finite element method counts 11×10^6 degrees of freedom. Consequently the matricial system of the spectral problem, which needs to be solved, has a size 11×10^6 with a rather large stencil. As a result, in the 3D case, the computations are much more demanding. The use of the direct solver MUMPS, as we did in the 2D case, is no longer an option due to memory limitation. Thus the inversion of the linear system is done using the conjugate gradient method with a Jacobi pre-conditioner. To handle these computations, we resorted to the UPPA

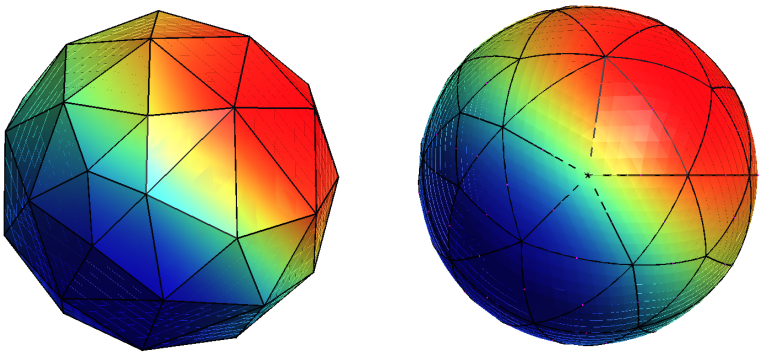

Figure 5.4 – Numerical solution of the Ventcel problem on affine and quadratic meshes.

research computer cluster PYRENE [2]. Using shared memory parallelism on a single CPU with 32 cores and 2 000 Mb of memory, the total time required is around 2 hours.

The following numerical errors are computed on a series of refined meshes,

$$\|u - u_h^\ell\|_{\mathrm{L}^2(\Omega)}, \quad \|\nabla u - \nabla u_h^\ell\|_{\mathrm{L}^2(\Omega)}, \quad \|u - u_h^\ell\|_{\mathrm{L}^2(\Gamma)} \quad \text{and} \quad \|\nabla_\Gamma u - \nabla_\Gamma u_h^\ell\|_{\mathrm{L}^2(\Gamma)}.$$

In Figure 5.5, is displayed a log–log graph of each of the surface errors in H_0^1 and L^2 norms on quadratic meshes, on the left, and on cubic meshes, on the right, using $\mathbb{P}^2$ and $\mathbb{P}^3$ finite element methods. For the H_0^1 (resp. L^2) error, the graphs on the right (for $r = 2$) and on the left (for $r = 3$) in Figure 5.5 have the same slope, even though the errors on the cubic meshes are sharper than those in the quadratic case. The usual super-convergence associated to quadratic meshes (discussed in Section 4.4) is also observed here for both norms. As observed in the case of the disk, the L^2 surface errors behave quite well following the inequalities in (5.5): the error is in $O(h^{k+1}+h^{r+1})$. The H^1 surface errors follow the same pattern as in the previous case: the error is in $O(h^k + h^{r+1})$ instead of $O(h^k + h^{r+1/2})$.

In Figure 5.6, the H_0^1 error in the volume is computed on quadratic meshes (left) and cubic meshes (right) with a $\mathbb{P}^2$ and $\mathbb{P}^3$ methods. In the quadratic case, the error has a convergence order of 2 (resp. 3) for a $\mathbb{P}^2$ (resp. $\mathbb{P}^3$) method, following Inequality (5.5). In the cubic case, the same phenomena is observed as in the case of the disk: a loss of $-1/2$ in the convergence rate is detected, and the error is in $O(h^{1.5})$ (resp. $O(h^{2.5})$)

2. PYRENE Mesocentre de Calcul Intensif Aquitain, https://git.univ-pau.fr/num-as/pyrene-cluster

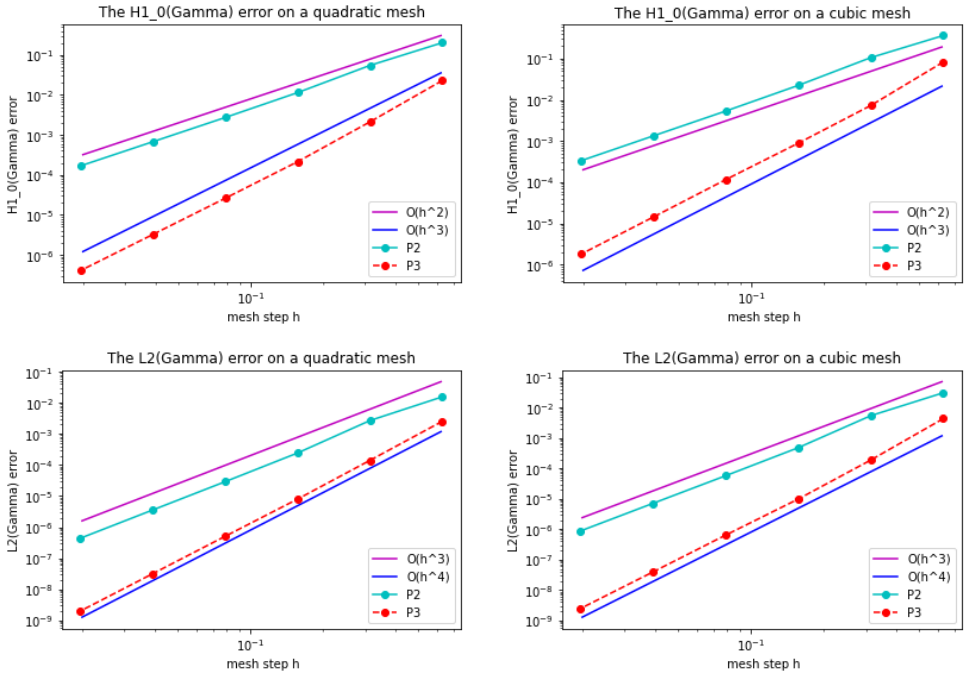

Figure 5.5 – 3D case: plots of the error in $\mathrm{H}_0^1(\Gamma)$ norm (above) and $\mathrm{L}^2(\Gamma)$ norm (below) and for quadratic meshes (left) and cubic meshes (right).

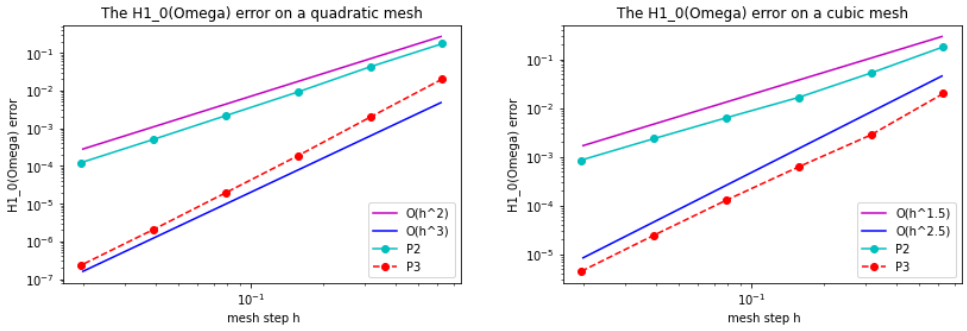

Figure 5.6 – 3D case: plots of the error in $\mathrm{H}_0^1(\Omega)$ norm for quadratic meshes (left) and cubic meshes (right).

for a $\mathbb{P}^2$ (resp. $\mathbb{P}^3$) method instead of being in $O(h^2)$ (resp. $O(h^3)$).

In Figure 5.7, the L^2 error in the volume is computed on quadratic meshes (left) and cubic meshes (right) with a $\mathbb{P}^2$ and $\mathbb{P}^3$ methods. In the quadratic case, the error has a convergence order of 3 for a $\mathbb{P}^2$ method. However, the convergence order of the L^2 error is equal to 4 for a $\mathbb{P}^3$ method, which is more than expected following the super-

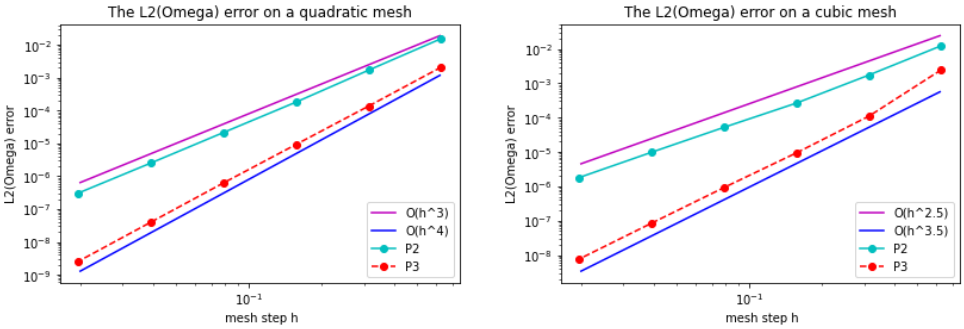

Figure 5.7 – 3D case: plots of the error in $\mathrm{L}^2(\Omega)$ norm for quadratic meshes (left) and cubic meshes (right).

convergence behavior of the quadratic meshes (see Section 4.4). In the cubic case, the same default of $-1/2$ in the convergence rate is visible as in the case of the disk: the graph of the error seems to have a slope of 2.5 (resp. 3.5) instead of 3 (resp. 4) for a $\mathbb{P}^2$ (resp. $\mathbb{P}^3$) method.

5.5 Additional numerical observations on the lift operator

In this section, we take it a step further first by investigating the impact of the regularity parameter "$s = r + 2$" in the expression of lift transformation in (3.1) on the error estimates, following Remark 3.1.6. Secondly, we estimate the error using the former lift defined in the work of Elliott *et al.* [43]. This helps us evaluate the impact of the choice of the lift used on the numerical results and furthermore show the efficiency of the new adapted lift presented in this work.

From this point forward, we place ourselves in the two dimensional case and consider the Poisson-Ventcel problem (5.1) on the unit disk with the same source terms as in Section 5.4.1.

5.5.1 Lift transformation regularity

In Remark 3.1.6 of Chapter 3, we discussed the dependency of the regularity of the lift transformation $G_h^{(r)} : \Omega_h \to \Omega$ with respect to the exponent s in the term $(\lambda^\star)^s$. According to the theory, the exponent s in $(\lambda^\star)^s$ needs to be set to $r + 2$ to ensure

that the transformation $G_h^{(r)}$ is piece-wise C^{r+1} on each element. In theory, it is thus necessary to set $s = r + 2$ for the estimates in Theorem 5.3.1 to hold.

Surprisingly, we have remarked that in practice, estimates in Theorem 5.3.1 still hold when decreasing the exponent of s of $(\lambda^\star)^s$. When setting $s = 2$, the results in Table 5.1 and in Table 5.2 remain unchanged. The plots of the errors are also the same as in Figure 5.2 and in Figure 5.3, with identical slopes. When setting $s = 1$, the same conclusion holds, though in this case $\mathrm{D}G_h^{(r)}$ has singularities on the non-internal elements. This is quite surprising since the estimate in (3.3), which is crucial for the error analysis, no longer holds. Beyond the convergence rate, we have also noticed that the accuracy itself is not damaged when decreasing the exponent s of $(\lambda^\star)^s$. A plausible reason for this is that the singular points of the derivatives of $G_h^{(r)}$ are always located at one element vertex or edge. They are "*not seen*", likely because they are away from the quadrature method nodes (used to approximate the integrals) that are located in the interior of considered element. Consequently, the singularities are not detected by this method.

5.5.2 Error analysis with the former lift operator

As developed in Remark 3.1.7, another lift transformation $G_h : \Omega_h \to \Omega$ had formerly been introduced in the work of Elliott *et al.* [43], with different properties on the boundary. In this section, we proceed by estimating the error between the exact solution u and the lifted discrete solution, denoted $u_h^{e\ell}$, using the former lift definition. We reported the convergence orders observed with this lift in Table 5.3 for volume and surface errors on quadratic and cubic meshes using $\mathbb{P}^k$ methods, where $1 \leq k \leq 4$.

	$\|u - u_h^{e\ell}\|_{\mathrm{L}^2(\Omega)}$				$\|\nabla u - \nabla u_h^{e\ell}\|_{\mathrm{L}^2(\Omega)}$			
	$\mathbb{P}^1$	$\mathbb{P}^2$	$\mathbb{P}^3$	$\mathbb{P}^4$	$\mathbb{P}^1$	$\mathbb{P}^2$	$\mathbb{P}^3$	$\mathbb{P}^4$
Quadratic mesh (r=2)	2.01	2.51	2.49	2.49	1.00	1.52	1.49	1.49
Cubic mesh (r=3)	2.04	2.50	2.48	2.49	1.03	1.51	1.49	1.49

	$\|u - u_h^{e\ell}\|_{\mathrm{L}^2(\Gamma)}$				$\|\nabla_\Gamma u - \nabla_\Gamma u_h^{e\ell}\|_{\mathrm{L}^2(\Gamma)}$			
	$\mathbb{P}^1$	$\mathbb{P}^2$	$\mathbb{P}^3$	$\mathbb{P}^4$	$\mathbb{P}^1$	$\mathbb{P}^2$	$\mathbb{P}^3$	$\mathbb{P}^4$
Quadratic mesh (r=2)	2.00	3.00	2.99	2.99	1.00	2.00	3.00	2.98
Cubic mesh (r=3)	2.00	3.00	2.99	2.98	1.00	2.00	3.00	2.98

Table 5.3 – Convergence orders for the errors using the lift defined in [43].

The first observation is that $\|u - u_h^{e\ell}\|_{\mathrm{L}^2(\Omega)}$ is at most in $O(h^{2.5})$ whereas $\|\nabla u - \nabla u_h^{e\ell}\|_{\mathrm{L}^2(\Omega)}$ is at most in $O(h^{1.5})$, resulting in a decrease in the error convergence rate as compared to Table 5.1. Similarly, $\|u - u_h^{e\ell}\|_{\mathrm{L}^2(\Gamma)}$ and $\|\nabla u - \nabla u_h^{e\ell}\|_{\mathrm{L}^2(\Gamma)}$ are at most in $O(h^3)$ whereas they could reach $O(h^4)$ as seen in Table 5.2.

Notice that the lift transformation intervenes at two different stages: for the right hand side definition in the discrete formulation (5.3) and for the error computation itself. We experienced the following. We set the lift for the right hand side computation to the one in [43] whereas the lift for the error computation is the one given in Definition 3.1.3 (so that the numerical solution u_h is the same as in Table 5.3, only its post treatment in terms of errors is different). Then we observed that the results are partially improved, for the $\mathbb{P}^4$ case on cubic meshes,

$$\|u - u_h^{e\ell}\|_{\mathrm{L}^2(\Omega)} = O(h^{3.0}) \quad \text{and} \quad \|\nabla u - \nabla u_h^{e\ell}\|_{\mathrm{L}^2(\Omega)} = O(h^{2.5}),$$

which remain lower than the convergence orders in Table 5.1.

Still considering the lift definition in [43], we also noticed that the exponent s in the term $(\lambda^\star)^s$ in the lift definition (see Remark 3.1.6) has an influence on the convergence rates. Surprisingly, the best convergence rates are obtained when setting $s = 1$: this case corresponds to the minimal regularity on the lift transformation G_h, the differential of which (as previously discussed) has singularities on the non-internal mesh elements. In that case however, the convergence rares goes up to $O(h^{3.5})$ and $O(h^{2.5})$ on quadratic and cubic meshes for $\|u - u_h^{e\ell}\|_{\mathrm{L}^2(\Omega)}$ and $\|\nabla u - \nabla u_h^{e\ell}\|_{\mathrm{L}^2(\Omega)}$ respectively. Meanwhile, it has been noticed that setting $s = 1$ somehow damages the quality of the numerical solution on the domain boundary: these last results are surprising and with no clear explanation. Eventually, when setting $s \geq 2$, the convergence rates are lower and identical to those in Table 5.3.

Chapter 6

The spectral problem with Ventcel boundary conditions

From the content of this chapter is composed of the following prepublication [24],

— F. Caubet, J. Ghantous, C. Pierre, *Finite element analysis of a spectral problem on curved meshes occurring in diffusion with high order boundary conditions,* submitted, 2024.

In this chapter, an error analysis of the spectral Ventcel problem (1.7) on curved meshes, using the lift operator is established from the theoretical and numerical point of view.

6.1 The continuous problem and main novelties

The spectral Ventcel problem. We recall that Ω is a nonempty bounded connected domain in $\mathbb{R}^d$, $d = 2$, 3, with a smooth boundary $\Gamma = \partial\Omega$ and we also recall that α, $\beta > 0$. We recall the following spectral problem with Ventcel boundary conditions,

$$\begin{cases} -\Delta u = \lambda u & \text{in } \Omega, \\ -\beta \Delta_\Gamma u + \partial_{\mathrm{n}} u + \alpha u = 0 & \text{on } \Gamma, \end{cases} \tag{6.1}$$

alongside its variational formulation given by,

$$\begin{cases} \text{find } (\lambda, u) \in \mathbb{R} \times \mathrm{H}^1(\Omega, \Gamma), \quad \text{such that,} \\ a(u, v) = \lambda\, m(u, v), \quad \forall\, v \in \mathrm{H}^1(\Omega, \Gamma), \end{cases} \tag{6.2}$$

where a is the bilinear form, defined on $\mathrm{H}^1(\Omega, \Gamma) \times \mathrm{H}^1(\Omega, \Gamma)$, given by,

$$a(u, v) = \int_\Omega \nabla u \cdot \nabla v \, \mathrm{d}x + \beta \int_\Gamma \nabla_\Gamma u \cdot \nabla_\Gamma v \, \mathrm{d}s + \alpha \int_\Gamma uv \, \mathrm{d}s,$$

and m is the bilinear form, defined on $\mathrm{H}^1(\Omega,\Gamma)\times\mathrm{H}^1(\Omega,\Gamma)$, given by,

$$m(u,v)=\int_\Omega uv\,\mathrm{d}x.$$

As discussed in Section 1.1.3, there exists an infinite number of eigenvalues with finite multiplicities to Problem (6.2), which form an increasing sequence $(\lambda_n)_{n\geq 1}\subset\mathbb{R}_+^*$ of positive real numbers, tending to infinity. Their associated eigenfunctions form an orthonormal Hilbert basis of $\mathrm{L}^2(\Omega)$, denoted $(u_n)_{n\geq 1}$ satisfying,

$$u_n\in\mathrm{H}^1(\Omega,\Gamma),\ \text{and}\ a(u_n,v)=\lambda_n m(u_n,v),\quad\forall\ v\ \in\ \mathrm{H}^1(\Omega,\Gamma).$$

Assuming that the eigenvalues are counted with their multiplicity and ordered increasingly, the aim of this work is to approximate an eigenvalue λ_i of finite multiplicity $N\geq 1$ and of rank $i\in\mathbb{N}^*$ on a curved mesh $\mathcal{T}_h^{(r)}$ of order $r\geq 1$. We denote Ω_h the mesh domain and Γ_h the boundary of Ω_h. In this chapter, we also aim to approximate the eigenfunctions $\{u_j\}_{j\in\mathrm{J}}$ associated to λ_i, where $\mathrm{J}:=\{i,...,i+N-1\}$ is the set of indices, using the $\mathbb{P}^k$ finite element method, with $k\geq 1$.

State of the art and main results. In 2018, error estimates for the surface Laplacian spectral problem on curved meshes have been carried out in [15] by Bonito *et al.* The ideas of [15] are adapted and extended in the present chapter in the case of a volume spectral problem, which is not a trivial. The main novelty is the use of the lift operator defined in Chapter 3 to estimate the eigenvalue and eigenfunction error both in terms of finite element approximation error and of geometric error, respectively, associated to the finite element degree $k\geq 1$ and to the mesh order $r\geq 1$. Let us also emphasize that the theoretical study and the numerical resolution of this spectral problem involve non-trivial difficulties compared with the analysis of the direct problem in Chapter 5. For the sake of completeness, we refer to [5] where an error estimation of the eigenvalues and eigenfunctions of the Steklov problem (with $\beta=0$) are established using the finite element method.

The main result of this chapter can be summarized as follows (see Theorem 6.3.1 for a precise statement). Let $i\in\mathbb{N}^*$, and let λ_i be an eigenvalue of multiplicity N with its corresponding eigenfunctions, $\{u_j\}_{j\in\mathrm{J}}$ relatively to Problem (6.1). Then, for a sufficiently small $h>0$, there exists a mesh independent constant $c_{\lambda_i}>0$, such that,

for any $j \in \mathrm{J}$,

$$\begin{aligned} |\lambda_j - \Lambda_j| &\leq c_{\lambda_i}(h^{2k} + h^{r+1}), \\ \inf_{U \in \mathbb{F}_h^\ell} \|u_j - U\|_{\mathrm{L}^2(\Omega)} &\leq c_{\lambda_i}(h^{k+1} + h^{r+1/2}), \\ \inf_{U \in \mathbb{F}_h^\ell} \|u_j - U\|_{\mathrm{H}^1(\Omega,\Gamma)} &\leq c_{\lambda_i}(h^{k} + h^{r+1/2}), \end{aligned}$$

where Λ_j is the eigenvalue of the discretization of (6.2) of rank $j \in \mathrm{J}$, $\mathbb{F}_h$ is the space generated by the discrete eigenfunctions associated to $\{\Lambda_j\}_{j\in\mathrm{J}}$, $\mathbb{F}_h^\ell$ is the lift of $\mathbb{F}_h$ made of functions defined on the physical domain Ω.

A prerequisite to the proof of the error estimations is the computation of the geometric error established in Proposition 6.4.3. Afterwards, the principal idea of the main proof of the error estimates is to proceed with a *bootstrap method*. A preliminary estimation of the eigenvalue error is needed in order to estimate the eigenfunction error in the $\mathrm{L}^2(\Omega)$ and $\mathrm{H}^1(\Omega, \Gamma)$ norms using orthogonal projections over the space $\mathbb{F}_h^\ell$. Lastly, we are able to obtain the adequate eigenvalue error estimation with respect to the finite element degree k and the geometric order of the mesh r using the obtained estimates on the eigenfunctions.

We also prove similar error estimations for a spectral Ventcel problem (6.45) having λu as a right hand side of the Ventcel boundary condition with a zero Laplace equation on Ω. We validate these estimations in several numerical experiments presented in two and three dimensions: on a non-symmetric, non convex domain and also on classical domains like the unit disk and the unit ball. As discussed in Section 4.4, a super-convergence of the error rate on the quadratic meshes is depicted similarly to the numerical results of Chapter 5. Furthermore, the loss of the convergence rate of the errors is highlighted throughout all the numerical experiments of this chapter, following Section 4.5.

6.2 Finite element approximation

Discrete formulation. We denote $\mathbb{V}_h$ the $\mathbb{P}^k$-Lagrangian finite element space given in (4.1). The approximation problem is given by,

$$\begin{cases} \text{find } (\Lambda, U) \in \mathbb{R} \times \mathbb{V}_h, \text{ such that,} \\ a_h(U, V) = \Lambda m_h(U, V), \, \forall \, V \in \mathbb{V}_h, \end{cases} \tag{6.3}$$

where a_h is the following bilinear form, defined on $\mathbb{V}_h \times \mathbb{V}_h$,

$$a_h(U, V) := \int_{\Omega_h} \nabla U \cdot \nabla V \mathrm{d}x + \beta \int_{\Gamma_h} \nabla_{\Gamma_h} U \cdot \nabla_{\Gamma_h} V \mathrm{d}s_h + \alpha \int_{\Gamma_h} UV \mathrm{d}s_h,$$

and m_h is the following bilinear form, defined on $\mathbb{V}_h \times \mathbb{V}_h$,

$$m_h(U, V) := \int_{\Omega_h} UV \mathrm{d}x.$$

The discrete problem (6.3) admits an increasing finite sequence of positive discrete eigenvalues $\Lambda_j \in \mathbb{R}_+^*$. There exists a basis of $\mathbb{V}_h$ made of discrete eigenfunctions $\{U_j\}_{j=1}^{\dim(\mathbb{V}_h)}$, which are m_h-orthogonal (see [4, Lemma 7.4.1]).

Lifted discrete formulation. We define the lifted bilinear form a_h^ℓ, defined on $\mathbb{V}_h^\ell \times \mathbb{V}_h^\ell$, throughout,

$$a_h(U, V) = a_h^\ell(U^\ell, V^\ell), \quad \forall \, U, V \in \mathbb{V}_h.$$

By applying the integral expressions (3.10), (3.6) and (3.4), then the expression of a_h^ℓ is given as follows for any $U^\ell, V^\ell \in \mathbb{V}_h^\ell$,

$$a_h^\ell(U^\ell, V^\ell) = \int_\Omega \mathcal{G}_h^{(r)}(\nabla U^\ell) \cdot \mathcal{G}_h^{(r)}(\nabla V^\ell) \frac{\mathrm{d}x}{J_h^\ell} + \beta \int_\Gamma A_h^\ell \nabla_\Gamma u_h^\ell \cdot \nabla_\Gamma v_h^\ell \, \mathrm{d}s + \alpha \int_\Gamma U^\ell V^\ell \frac{\mathrm{d}s}{J_b^\ell},$$

where J_h (resp. J_b) is the Jacobian of the lift transformation $G_h^{(r)}$ given in (3.1) (resp. the orthogonal projection b given in Proposition 2.0.1), A_h^ℓ is the lift of the matrix A_h given in (3.7) and $\mathcal{G}_h^{(r)}$ is defined in (3.9).

In a similar way, using (3.8), we define the expression of m_h^ℓ, defined on $\mathbb{V}_h^\ell \times \mathbb{V}_h^\ell$, throughout $m_h(U, V) = m_h^\ell(U^\ell, V^\ell)$ for $U, V \in \mathbb{V}_h$, as follows,

$$m_h^\ell(U^\ell, V^\ell) = \int_\Omega UV \frac{\mathrm{d}x}{J_h^\ell} = m_h(U, V).$$

Thus, we define the lifted formulation of Problem (6.3) given by,

$$\begin{cases} \text{find } (\Lambda, U^\ell) \in \mathbb{R} \times \mathbb{V}_h^\ell, \text{ such that,} \\ a_h^\ell(U^\ell, V) = \Lambda\ m_h^\ell(U^\ell, V),\ \forall\, V \in \mathbb{V}_h^\ell. \end{cases} \tag{6.4}$$

The lifted problem (6.4) shares the same eigenvalues as the discrete problem (6.3), denoted $\{\Lambda_j\}_{j=1}^{\dim(\mathbb{V}_h)}$, which are associated to the lift of the eigenfunctions of the discrete formulation (6.2), denoted $\{U_j^\ell\}_{j=1}^{\dim(\mathbb{V}_h)}$.

6.3 Error analysis

First of all, we recall that the exact eigenvalues are ordered increasingly with their multiplicities. Let $i \in \mathbb{N}^*$. We aim to estimate the error produced when approximating the eigenvalue λ_i of multiplicity N and its corresponding eigenfunctions, $\{u_j\}_{j\in \mathrm{J}}$ where $\mathrm{J} = \{i, ..., i+N-1\}$, using a $\mathbb{P}^k$ finite element method on a curved mesh Ω_h with order $r \geq 1$. These estimations are given in the following theorem, which is proved in the following sub-sections. To this end, we note that each eigenvalue Λ_j is associated to an eigenspace $\mathbb{E}_{\Lambda_j}^\ell$ in $\mathbb{V}_h^\ell$, which is the set of all the discrete eigenfunctions associated to Λ_j. Let $\mathbb{F}_h^\ell := \oplus_{j\in \mathrm{J}} \mathbb{E}_{\Lambda_j}^\ell$ be the space containing all the eigenspaces associated to $\{\Lambda_j\}_{j\in \mathrm{J}}$.

Throughout this section, c refers to a positive constant independent of the mesh step h and c_{λ_i} refers to a positive constant depending on the eigenvalue λ_i and independent of h. Keeping in mind that the domain Ω, is assumed to have a smooth boundary Γ (at least $\mathcal{C}^{k+1}$ regular) such that the exact eigenfunctions of Problem (6.1) are in $\mathrm{H}^{k+1}(\Omega, \Gamma)$.

Theorem 6.3.1. *Let λ_i be an eigenvalue of multiplicity N with its corresponding eigenfunctions, $\{u_p\}_{p\in \mathrm{J}}$ where $\mathrm{J} = \{i, ..., i+N-1\}$, arising in Problem (6.2). Then, for a sufficiently small mesh size $h > 0$ and for any $j \in \mathrm{J}$, there exists $c_{\lambda_i} > 0$,*

$$|\lambda_j - \Lambda_j| \leq c_{\lambda_i}(h^{2k} + h^{r+1}). \tag{6.5}$$

Additionally, there exists $c_{\lambda_i} > 0$ for any $j \in \mathrm{J}$ such that,

$$\inf_{U\in\mathbb{F}_h^\ell} \|u_j - U\ \|_{\mathrm{L}^2(\Omega)} \leq c_{\lambda_i}(h^{k+1} + h^{r+1/2}), \tag{6.6}$$

$$\inf_{U\in\mathbb{F}_h^\ell} \|u_j - U\|_{\mathrm{H}^1(\Omega,\Gamma)} \leq c_{\lambda_i}(h^k + h^{r+1/2}), \tag{6.7}$$

where $\mathbb{F}_h^\ell$ is the space containing all the eigenspaces associated to $\{\Lambda_j\}_{j\in\mathrm{J}}$.

Remark 6.3.2. *In a similar manner, there exists $c_{\lambda_i} > 0$ such that,*

$$\inf_{u\in\mathbb{E}_{\lambda_i}} \|U - u\|_{\mathrm{L}^2(\Omega)} \leq c_{\lambda_i}(h^{k+1} + h^{r+1/2}), \quad \inf_{u\in\mathbb{E}_{\lambda_i}} \|U - u\|_{\mathrm{H}^1(\Omega,\Gamma)} \leq c_{\lambda_i}(h^k + h^{r+1/2}),$$

where $U \in \mathbb{V}_h^\ell$ is a discrete eigenfunction associated to Λ_j and $\mathbb{E}_{\lambda_i}$ is the eigenspace of λ_i. These estimations, which are analogous to those presented in Theorem 6.3.1, are a consequence of Lemma 6.3.16 in Section 6.3.4.

In order to prove this theorem, we will proceed in several steps. In a nutshell, the main steps of the proof are to first estimate the so-called geometric error, second calculate a preliminary eigenvalue estimation, third estimate the eigenfunction error, and finally combine the last two steps to improve the eigenvalue error.

6.3.1 Geometric error

To estimate the geometric error produced while approximating a domain by a mesh of order $r \geq 1$, we bound the difference between the two bilinear forms a and a_h^ℓ (resp. m and m_h^ℓ).

Proposition 6.3.3. *There exists $c > 0$ such that the following geometric error estimations hold for all $v, w \in \mathbb{V}_h^\ell$,*

$$|(a - a_h^\ell)(v, w)| \leq c(h^r \|\nabla v\|_{\mathrm{L}^2(B_h^\ell)} \|\nabla w\|_{\mathrm{L}^2(B_h^\ell)} + h^{r+1} \|v\|_{\mathrm{H}^1(\Gamma)} \|w\|_{\mathrm{H}^1(\Gamma)}), \tag{6.8}$$

$$|(m - m_h^\ell)(v, w)| \leq c h^{r+1} \|v\|_{\mathrm{H}^1(\Omega)} \|w\|_{\mathrm{H}^1(\Omega)}. \tag{6.9}$$

Proof. Taking $\kappa = 0$ in Proposition 5.3.2, we obtain Inequality (6.8). To prove (6.9), consider $v, w \in \mathbb{V}_h^\ell$. We recall that $\frac{1}{J_h^\ell} - 1 = 0$ in $\Omega \backslash B_h^\ell$ where B_h^ℓ is the union of all the non-internal elements of the exact mesh $\mathcal{T}_h^{(e)}$, as mentioned in (3.13). This implies that we have,

$$|(m - m_h^\ell)(v, w)| = \left| \int_\Omega vw \,(1 - \frac{1}{J_h^\ell}) \mathrm{d}x \right| = \left| \int_{B_h^\ell} vw \,(1 - \frac{1}{J_h^\ell}) \mathrm{d}x \right|.$$

Applying the estimate of $\frac{1}{J_h^\ell} - 1$ in (3.12), we get,

$$|(m - m_h^\ell)(v,w)| \;\leq\; \left\|1 - \frac{1}{J_h^\ell}\right\|_{\mathrm{L}^\infty(B_h^\ell)} \|v\|_{\mathrm{L}^2(B_h^\ell)} \|w\|_{\mathrm{L}^2(B_h^\ell)} \;\leq\; ch^r \|v\|_{\mathrm{L}^2(B_h^\ell)} \|w\|_{\mathrm{L}^2(B_h^\ell)}.$$

Since $v, w \in \mathbb{V}_h^\ell \subset \mathrm{H}^1(\Omega,\Gamma)$, we apply (3.14) on the L^2 norms over B_h^ℓ as follows,

$$|(m - m_h^\ell)(v,w)| \leq ch^r \left(h^{1/2}\|v\|_{\mathrm{H}^1(\Omega)}\right)\left(h^{1/2}\|w\|_{\mathrm{H}^1(\Omega)}\right) \leq ch^{r+1}\|v\|_{\mathrm{H}^1(\Omega)}\|w\|_{\mathrm{H}^1(\Omega)}.$$

□

Corollary 6.3.4. *Considering a sufficiently small $h > 0$, there exists $c > 0$ mesh independent such that,*

$$\|.\|_{a_h^\ell} \leq (1 + ch^r)\|.\|_a, \qquad \|.\|_a \leq (1 + ch^r)\|.\|_{a_h^\ell},$$

$$\|.\|_{m_h^\ell} \leq (1 + ch^r)\|.\|_m, \qquad \|.\|_m \leq (1 + ch^r)\|.\|_{m_h^\ell},$$

where the norms $\|u\|_a, \|u\|_m, \|u\|_{a_h^\ell}, \|u\|_{m_h^\ell}$ are associated to the bilinear forms a, a_h^ℓ, m and m_h^ℓ, respectively. Consequently, the norms $\|.\|_{a_h^\ell}$ and $\|.\|_a$ (resp. $\|.\|_{m_h^\ell}$ and $\|.\|_m$) are equivalent.

Proof. This proof is an adaptation of the proof of [15, Corollary 2.3], which is detailed in the following for volume norms for readers convenience. Let $u \in \mathrm{H}^1(\Omega,\Gamma)$, one has,

$$\|u\|_{a_h^\ell}^2 - \|u\|_a^2 = a_h^\ell(u,u) - a(u,u) = \Big(a_h^\ell - a\Big)(u,u).$$

Then, we deduce that,

$$\|u\|_{a_h^\ell}^2 \leq \|u\|_a^2 + |\Big(a_h^\ell - a\Big)(u,u)| \leq (1 + ch^r)\|u\|_a^2,$$

where we used the geometric error estimation (6.8). Taking its square root, it follows that,

$$\|u\|_{a_h^\ell} \leq \sqrt{(1 + ch^r)}\|u\|_a \leq (1 + ch^r)\|u\|_a,$$

since for any $x \geq 0$, $1 + x \leq (1 + \frac{1}{2}x)^2$. In a similar manner, the rest of the inequalities can be proved, by using (6.8) and (6.9). □

6.3.2 Preliminary eigenvalue estimate

A preliminary eigenvalue error estimation is needed before proceeding with the error estimation. It has to be noted that the proof is based on a combination between the ideas established in [15, Th. 3.3] and in [45, Chapter 3.3], in the present setting of a spectral Ventcel problem on curved meshes.

Proposition 6.3.5. *Let λ_i be an exact eigenvalue of multiplicity N of Problem* (6.2)*, such that $\lambda_j = \lambda_i$, for any $j \in \mathrm{J} = \{i, ..., i+N-1\}$. Then, for any $j \in \mathrm{J}$, there exists $c_{\lambda_i} > 0$ such that,*

$$|\lambda_j - \Lambda_j| \leq c_{\lambda_i}(h^{2k} + h^r), \tag{6.10}$$

where Λ_j is an eigenvalue relatively to the discrete problem (6.3)*.*

Proof. Let $j \in \mathrm{J}$. To estimate the error $|\lambda_j - \Lambda_j|$, we introduce the following intermediate formulation,

$$\begin{cases} \text{find } (\tilde{\lambda}, \tilde{U}) \in \mathbb{R}^+ \times \mathbb{V}_h^\ell, \text{ such that,} \\ a(\tilde{U}, v) = \tilde{\lambda} m(\tilde{U}, v), \, \forall \, v \in \mathbb{V}_h^\ell. \end{cases} \tag{6.11}$$

Problem (6.11) has a finite number of eigenvalues, denote $\tilde{\Lambda}_p$, for $p = 1, ..., \dim(\mathbb{V}_h^\ell)$. Then for $j \in \mathrm{J}$, we separate the eigenvalue error as follows,

$$|\lambda_j - \Lambda_j| \leq |\lambda_j - \tilde{\Lambda}_j| + |\tilde{\Lambda}_j - \Lambda_j|,$$

and estimate each term separately.

For the estimation of $|\lambda_j - \tilde{\Lambda}_j|$, note that the spectral problem (6.11) is in a conforming, coercive and consistent setting. Indeed, the variationnal formulation is defined using the same bilinear forms a and m as in the initial formulation (6.2), with the approximation space $\mathbb{V}_h^\ell \subset \mathrm{H}^1(\Omega, \Gamma)$. Thus, we refer to the detailed explanation in [45, Chapter 3.3] to obtain the following classical estimation,

$$|\lambda_j - \tilde{\Lambda}_j| \leq c_{\lambda_i} h^{2k}. \tag{6.12}$$

From Inequality (6.12), we notice that $0 < \tilde{\Lambda}_j \leq c_{\lambda_i}$.

To estimate $|\tilde{\Lambda}_j - \Lambda_j|$, we proceed in a similar manner as in [15, Lemma 3.1]. Note that, by [45, Proposition 3.63], the discrete eigenvalues can be written as follows,

$$\Lambda_j = \min_{E \in V_j} \max_{v \in E} R_{a_h^\ell}(v) \quad \text{and} \quad \tilde{\Lambda}_j = \min_{E \in V_j} \max_{v \in E} R_a(v), \tag{6.13}$$

where the associated Rayleigh quotients are written as follows,

$$R_{a_h^\ell}(v) = \frac{a_h^\ell(v,v)}{m_h^\ell(v,v)} \quad \text{and} \quad R_a(v) = \frac{a(v,v)}{m(v,v)},$$

where V_j is the set of all sub-spaces of $\mathbb{V}_h^\ell$ of dimension j.

Consider $E \in V_j$. By definition of the Rayleigh quotient and using the norm equivalence in Corollary 6.3.4, we can deduce for any $v \in E$,

$$R_{a_h^\ell}(v) = \frac{a_h^\ell(v,v)}{m_h^\ell(v,v)} \leq \frac{(1+ch^r)^2 a(v,v)}{\frac{m(v,v)}{(1+ch^r)^2}} = (1+ch^r)^4 R_a(v).$$

Using (6.13), it follows that,

$$\Lambda_j \leq \min_{E \in V_j} \max_{v \in E} (1+ch^r)^4 R_a(v) = (1+ch^r)^4 \tilde{\Lambda}_j.$$

Then, $\Lambda_j \leq \tilde{\Lambda}_j + ch^r \tilde{\Lambda}_j$, and we have, $\Lambda_j - \tilde{\Lambda}_j \leq ch^r \tilde{\Lambda}_j \leq c_{\lambda_i} h^r$. In a similar manner, we can prove that $\tilde{\Lambda}_j - \Lambda_j \leq c_{\lambda_i} h^r$. To conclude, we combine these two inequalities as follows,

$$|\Lambda_j - \tilde{\Lambda}_j| \leq c_{\lambda_i} h^r. \tag{6.14}$$

To conclude, we combine (6.14) and (6.12) to arrive at (6.10). □

Remark 6.3.6. *As a result of the estimation* (6.10)*, the eigenvalues* $\{\lambda_j\}_{j \in \mathrm{J}}$ *are only approximated by the set of discrete eigenvalues* $\{\Lambda_j\}_{j \in \mathrm{J}}$*. Consequently, for a sufficiently small mesh step* h*, the following quantity, which appears in the eigenfunction estimations, is finite,*

$$\mu_J = \max_{j \in \mathrm{J}} \max_{p \notin \mathrm{J}} \left| \frac{\lambda_j}{\Lambda_p - \lambda_j} \right| < \infty.$$

Additionally, the set of eigenvalues $\{\Lambda_j\}_{j \in \mathrm{J}}$ *is separated from the rest of the continuous spectrum, i.e.,*

$$\lambda_{i-1} < \Lambda_i \quad \textit{and} \quad \Lambda_{i+N-1} < \lambda_{i+N}.$$

Furthermore, this set of discrete eigenvalues $\{\Lambda_j\}_{j \in \mathrm{J}}$ *can be bounded independently from* h*. Indeed, there exists* $c_{\lambda_i} > 0$*, such that,* $|\Lambda_j| \leq c_{\lambda_i}$*, for all* $j \in \mathrm{J}$*.*

We refer to [22, page 6], [48, Section 2.3], [50, page 3], [63, Section 3.2] and [15, Remark 3.4] for more details on this remark.

6.3.3 Eigenfunction error estimations

In this section, is presented the proof of the estimations (6.6) and (6.7) of Theorem 6.3.1. To begin with, we recall that $\mathbb{F}_h^\ell = \oplus_{j\in \mathrm{J}} \mathbb{E}_{\Lambda_j}^\ell = \oplus_{j\in \mathrm{J}} \mathrm{span}\{U_j^\ell\}$. We define the following projections, which are a useful tool in the eigenfunction error estimates (see [45, Section 1.6.3] and [44, §3.3]).

Definition 6.3.7. *We define the following projections.*

— *Let $\Pi_h : \mathrm{H}^1(\Omega,\Gamma) \to \mathbb{V}_h^\ell$ be the Ritz projection, such that for all $v \in \mathrm{H}^1(\Omega,\Gamma)$, there exists a unique finite element function $\Pi_h(v) \in \mathbb{V}_h^\ell$ that satisfies,*

$$a_h^\ell(\Pi_h(v), w) = a_h^\ell(v, w), \quad \forall\ w \in \mathbb{V}_h^\ell.$$

— *Let $\mathcal{P}_{a_h^\ell} : \mathrm{H}^1(\Omega,\Gamma) \to \mathbb{F}_h^\ell$ be the orthogonal projection with respect to a_h^ℓ onto $\mathbb{F}_h^\ell$, such that for all $v \in \mathrm{H}^1(\Omega,\Gamma)$,*

$$a_h^\ell(\mathcal{P}_{a_h^\ell}(v), w) = a_h^\ell(v, w), \quad \forall\ w \in \mathbb{F}_h^\ell.$$

— *Let $\mathcal{P}_{m_h^\ell} : \mathrm{H}^1(\Omega,\Gamma) \to \mathbb{F}_h^\ell$ be the orthogonal projection with respect to m_h^ℓ onto $\mathbb{F}_h^\ell$, such that for all $v \in \mathrm{H}^1(\Omega,\Gamma)$,*

$$m_h^\ell(\mathcal{P}_{m_h^\ell}(v), w) = m_h^\ell(v, w), \quad \forall\ w \in \mathbb{F}_h^\ell.$$

Remark 6.3.8. *Note that the previous orthogonal projections satisfy the following relation (see [15, Section 2.4] and [48, Lemma 2.2]):*

$$\mathcal{P}_{a_h^\ell} = \mathcal{P}_{m_h^\ell} \circ \Pi_h.$$

To prove this equality, we rely on the definition of orthogonal projections provided in Definition 6.3.7 and on the definition of $\mathbb{F}_h^\ell = \oplus_{j\in \mathrm{J}} \mathrm{span}\{U_j^\ell\}$, where the eigenfunctions U_j^ℓ are orthonormal with respect to m_h^ℓ.

Main proof idea. The key idea, in the proof of the estimations (6.6) and (6.7), is to separate the error in two terms for both norms using this projection as follows,

$$\inf_{U\in\mathbb{F}_h^\ell} \|u_j - U\ \| \leq \|u_j - \Pi_h u_j\ \| + \|\Pi_h u_j - \mathcal{P}_{a_h^\ell} u_j\ \|.$$

It is important to note that the Ritz projection Π_h will play a similar role to that of the interpolation operator $\mathcal{I}^\ell$ in the proofs presented in Chapter 5.

The first term will be bounded using a classical interpolation result (see [45, Section 1.6.3]). If $u_j \in \mathrm{H}^{k+1}(\Omega, \Gamma)$, by definition of the Ritz projection Π_h, there exists $c > 0$ such that,

$$\|u_j - \Pi_h u_j\|_{a_h^\ell} = \inf_{v \in \mathbb{V}_h^\ell} \|u_j - v\|_{a_h^\ell} \leq c h^k \|u_j\|_{\mathrm{H}^{k+1}(\Omega,\Gamma)}. \tag{6.15}$$

Using an Aubin-Nitsche argument as proved in Section 6.3.5, there exists $c > 0$ such that,

$$\|u_j - \Pi_h u_j\|_{m_h^\ell} \leq c h^{k+1}. \tag{6.16}$$

We also point out that no geometric error is present in (6.15) and (6.16). A similar estimation of this error is presented in [44, lem. 3.8].

As for the second term, we recall that $\{U_p^\ell\}_{p=1}^{\dim(\mathbb{V}_h)}$ forms an orthonormal basis of $\mathbb{V}_h^\ell$ with respect to m_h^ℓ. The lifted space finite element space can be decomposed as follows $\mathbb{V}_h^\ell := \mathbb{F}_h^\ell \oplus \mathbb{S}_h^\ell$, where $\mathbb{F}_h^\ell := \oplus_{j \in \mathrm{J}} \mathrm{span} U_j^\ell$ and $\mathbb{S}_h^\ell := \oplus_{p \notin \mathrm{J}} \mathrm{span} U_p^\ell$ are orthogonal spaces with respect to m_h^ℓ. We denote,

$$W := \Pi_h u_j - \mathcal{P}_{a_h^\ell} u_j = \Pi_h u_j - \mathcal{P}_{m_h^\ell} \circ \Pi_h u_j. \tag{6.17}$$

Since $\mathcal{P}_{m_h^\ell}$ is the orthogonal projection over $\mathbb{F}_h^\ell$ with respect to m_h^ℓ, then we have,

$$W \in \mathbb{S}_h^\ell, \quad m_h^\ell(W, U_j^\ell) = 0, \quad \forall\, j \in \mathrm{J}.$$

Consequently, $W = \sum_{p \notin \mathrm{J}} \beta_p U_p^\ell$, where we denote the coefficients $\beta_p := m_h^\ell(W, U_p^\ell)$, for all $p \notin \mathrm{J}$. Then the m_h^ℓ norm of W is given as follows,

$$\|W\|_{m_h^\ell}^2 = \sum_{p \notin \mathrm{J}} \beta_p^2, \tag{6.18}$$

since $\{U_p^\ell\}_{p \notin \mathrm{J}}$ forms an orthonormal basis of $\mathbb{S}_h^\ell$ for the product m_h^ℓ.

In the following propositions the a_h^ℓ and m_h^ℓ norms of W will be evaluated in order

to bound the error afterwards. We introduce the following notation,

$$Z := \sum_{p \notin \mathrm{J}} \frac{\lambda_i}{\Lambda_p - \lambda_i} \beta_p U_p^\ell, \tag{6.19}$$

where Λ_p is a discrete eigenvalue with its associated eigenfunction U_p^ℓ, and λ_i is the exact eigenvalue.

Proposition 6.3.9. *Let $j \in \mathrm{J}$ and u_j be an exact eigenfunction associated with λ_i. The norms of W, given in* (6.17)*, can be expressed as follows,*

$$\|W\|^2_{m_h^\ell} = m_h^\ell(u_j - \Pi_h u_j, Z) + (m - m_h^\ell)(u_j, Z) + \frac{1}{\lambda_i}(a_h^\ell - a)(u_j, Z), \tag{6.20}$$

$$\|W\|^2_{a_h^\ell} = \lambda_i m_h^\ell(u_j - \Pi_h u_j, W) + \lambda_i \|W\|^2_{m_h^\ell} + \lambda_i (m - m_h^\ell)(u_j, W) + (a_h^\ell - a)(u_j, W). \tag{6.21}$$

Proof. This proof is inspired from [15, Lemma 4.1], but for sake of completeness we detail it. The main difference is that in our case, we do not consider a surface problem as in [15] and the eigenfunctions $\{u_j\}_{j \in \mathrm{J}}$ are on Ω.

By Equation (6.18), the m_h^ℓ norm of W is written as follows,

$$\|W\|^2_{m_h^\ell} = \sum_{p \notin \mathrm{J}} \beta_p^2 = \sum_{p \notin \mathrm{J}} \beta_p m_h^\ell(W, U_p^\ell). \tag{6.22}$$

To prove Inequality (6.20), we try to estimate $m_h^\ell(W, U_p^\ell)$, for $p \notin \mathrm{J}$. By Remark 6.3.8, we have $\mathcal{P}_{a_h^\ell} = \mathcal{P}_{m_h^\ell} \circ \Pi_h$, and we get for $p \notin \mathrm{J}$,

$$m_h^\ell(\mathcal{P}_{a_h^\ell} v, U_p^\ell) = m_h^\ell(\mathcal{P}_{m_h^\ell}(\Pi_h v), U_p^\ell) = 0, \qquad \forall\, v \in \mathrm{H}^1(\Omega, \Gamma). \tag{6.23}$$

Using (6.23), we get for $p \notin \mathrm{J}$,

$$m_h^\ell(W, U_p^\ell) = m_h^\ell(\Pi_h u_j - \mathcal{P}_{a_h^\ell} u_j, U_p^\ell) = m_h^\ell(\Pi_h(u_j), U_p^\ell).$$

The next step is to estimate $m_h^\ell\Big(\Pi_h u_j, U_p^\ell\Big)$. We denote Λ_p a discrete eigenvalue associated to $U_p^\ell \in \mathbb{S}_h^\ell$ such that,

$$\Lambda_p m_h^\ell(V, U_p^\ell) = a_h^\ell(V, U_p^\ell), \quad \forall\, V \in \mathbb{V}_h^\ell.$$

Taking in the latter equation $V = \Pi_h u_j \in \mathbb{V}_h^\ell$, we get by using the definition of Π_h,

$$\Lambda_p m_h^\ell(\Pi_h u_j, U_p^\ell) = a_h^\ell(\Pi_h u_j, U_p^\ell) = a_h^\ell(u_j, U_p^\ell) = a(u_j, U_p^\ell) + (a_h^\ell - a)(u_j, U_p^\ell).$$

Since u_j is an exact eigenfunction associated to λ_i of Problem (6.2), we get,

$$\begin{aligned}\Lambda_p m_h^\ell(\Pi_h u_j, U_p^\ell) &= \lambda_i m(u_j, U_p^\ell) + (a_h^\ell - a)(u_j, U_p^\ell) \\ &= \lambda_i m_h^\ell(u_j, U_p^\ell) + \lambda_i(m - m_h^\ell)(u_j, U_p^\ell) + (a_h^\ell - a)(u_j, U_p^\ell),\end{aligned}$$

where we added and subtracted $\lambda_i m_h^\ell(u_j, U_p^\ell)$.

Subtracting $\lambda_i m_h^\ell(\Pi_h u_j, U_p^\ell)$ on both sides of the equation, we get,

$$(\Lambda_p - \lambda_i) m_h^\ell(\Pi_h u_j, U_p^\ell) = \lambda_i m_h^\ell(u_j - \Pi_h u_j, U_p^\ell) + \lambda_i(m - m_h^\ell)(u_j, U_p^\ell) + (a_h^\ell - a)(u_j, U_p^\ell).$$

For any $p \notin \mathrm{J}$, $\Lambda_p - \lambda_i \neq 0$, then we have,

$$\begin{aligned}m_h^\ell(\Pi_h u_j, U_p^\ell) &= \frac{1}{\Lambda_p - \lambda_i}\{\lambda_i m_h^\ell(u_j - \Pi_h u_j, U_p^\ell) + \lambda_i(m - m_h^\ell)(u_j, U_p^\ell) + (a_h^\ell - a)(u_j, U_p^\ell)\} \\ &= m_h^\ell(u_j - \Pi_h u_j, \frac{\lambda_i}{\Lambda_p - \lambda_i} U_p^\ell) + (m - m_h^\ell)(u_j, \frac{\lambda_i}{\Lambda_p - \lambda_i} U_p^\ell) + \frac{1}{\lambda_i}(a_h^\ell - a)(u_j, \frac{\lambda_i}{\Lambda_p - \lambda_i} U_p^\ell).\end{aligned}$$

To arrive to (6.20), we replace the latter expression in (6.22) as follows,

$$\begin{aligned}\|W\|_{m_h^\ell}^2 = \sum_{p \in \{1, \ldots dim(\mathbb{V}_h)\} \setminus \mathrm{J}} \beta_p \Big(& m_h^\ell(u_j - \Pi_h u_j, \frac{\lambda_i}{\Lambda_p - \lambda_i} U_p^\ell) \\ & + (m - m_h^\ell)(u_j, \frac{\lambda_i}{\Lambda_p - \lambda_i} U_p^\ell) + \frac{1}{\lambda_i}(a_h^\ell - a)(u_j, \frac{\lambda_i}{\Lambda_p - \lambda_i} U_p^\ell) \Big).\end{aligned}$$

The proof of (6.21) is a tad similar to the latter one. Keeping in mind that $W = (\mathrm{I}_d - \mathcal{P}_{m_h^\ell})\Pi_h u_j$, its a_h^ℓ-norm is written as follows,

$$\begin{aligned}\|W\|_{a_h^\ell}^2 = a_h^\ell(W, W) &= a_h^\ell((\mathrm{I}_d - \mathcal{P}_{m_h^\ell})\Pi_h u_j, (\mathrm{I}_d - \mathcal{P}_{m_h^\ell})\Pi_h u_j) \\ &= a_h^\ell(\Pi_h u_j, (\mathrm{I}_d - \mathcal{P}_{m_h^\ell})\Pi_h u_j) - a_h^\ell(\mathcal{P}_{m_h^\ell}\Pi_h u_j, (\mathrm{I}_d - \mathcal{P}_{m_h^\ell})\Pi_h u_j).\end{aligned}$$

Note that, for any $V \in \mathbb{F}_h^\ell$, we have,

$$a_h^\ell((\mathrm{I}_d - \mathcal{P}_{m_h^\ell})\Pi_h u_j, V) = a_h^\ell(\Pi_h u_j, V) - a_h^\ell(\mathcal{P}_{m_h^\ell} \circ \Pi_h u_j, V) = a_h^\ell(u_j, V) - a_h^\ell(\mathcal{P}_{a_h^\ell} u_j, V) = 0,$$

where we used the definitions of the orthogonal projections Π_h and $\mathcal{P}_{a_h^\ell}$. Thus, taking $V = \mathcal{P}_{m_h^\ell}\Pi_h u_j \in \mathbb{F}_h^\ell$, $a_h^\ell(\mathcal{P}_{m_h^\ell}\Pi_h u_j, (\mathrm{I}_d - \mathcal{P}_{m_h^\ell})\Pi_h u_j) = 0$. Then, the latter equation becomes,

$$\|W\|_{a_h^\ell}^2 = a_h^\ell(\Pi_h u_j, (\mathrm{I}_d - \mathcal{P}_{m_h^\ell})\Pi_h u_j) = a_h^\ell(u_j, (\mathrm{I}_d - \mathcal{P}_{m_h^\ell})\Pi_h u_j) = a_h^\ell(u_j, W),$$

where we used the definition of the orthogonal projection Π_h with respect to a_h^ℓ, given in Definition 6.3.7. Adding and subtracting $a(u_j, W)$, we get,

$$\|W\|_{a_h^\ell}^2 = a_h^\ell(u_j, W) = a(u_j, W) + (a_h^\ell(u_j, W) - a(u_j, W)) = \lambda_i m(u_j, W) + (a_h^\ell - a)(u_j, W)).$$

Since u_j is an exact eigenfunction associated to λ_i, the latter equation holds. Adding and subtracting $\lambda_i m_h^\ell(u_j, W)$, we have,

$$\|W\|_{a_h^\ell}^2 = \lambda_i m_h^\ell(u_j, W) + \lambda_i(m - m_h^\ell)(u_j, W) + (a_h^\ell - a)(u_j, W)). \tag{6.24}$$

Notice that $W = \sum_{p\notin \mathrm{J}} \beta_p U_p^\ell$, then by applying (6.23), we have $m_h^\ell(\mathcal{P}_{a_h^\ell} u_j, W) = 0$. Then, we notice that,

$$\begin{aligned}
&\lambda_i m_h^\ell(u_j, W) = \lambda_i m_h^\ell(u_j, W) - \lambda_i m_h^\ell(\mathcal{P}_{a_h^\ell} u_j, W) \\
&= \lambda_i m_h^\ell(u_j - \Pi_h u_j, W) + \lambda_i m_h^\ell(\Pi_h u_j - \mathcal{P}_{a_h^\ell} u_j, W) = \lambda_i m_h^\ell(u_j - \Pi_h u_j, W) + \lambda_i m_h^\ell(W, W),
\end{aligned}$$

where we added and subtracted $\lambda_i m_h^\ell(\Pi_h u_j, W)$. Thus after replacing the latter equation in (6.24), we get exactly (6.21),

$$\|W\|_{a_h^\ell}^2 = \lambda_i m_h^\ell(u_j - \Pi_h u_j, W) + \lambda_i \|W\|_{m_h^\ell}^2 + \lambda_i(m - m_h^\ell)(u_j, W) + (a_h^\ell - a)(u_j, W).$$

□

The following proposition is one of the main novelties of this work. We mention [15, 48, 22] that deal with different problems but in which similar ideas are presented.

Proposition 6.3.10. *Under the assumptions of Proposition 6.3.9, there exists* $c_{\lambda_i} > 0$ *such that,*

$$\|W\|_{m_h^\ell} \leq c_{\lambda_i}\|u_j - \Pi_h u_j\|_{m_h^\ell} + c_{\lambda_i} h^{r+1/2}\|u_j\|_{\mathrm{H}^2(\Omega,\Gamma)}, \tag{6.25}$$

$$\|W\|_{a_h^\ell} \leq c_{\lambda_i}\|u_j - \Pi_h u_j\|_{m_h^\ell} + c_{\lambda_i} h^{r+1/2}\|u_j\|_{\mathrm{H}^2(\Omega,\Gamma)}, \tag{6.26}$$

where the expression of W is given in (6.17).

Proof. This proof is decomposed into three steps.

1. Using the geometric error estimates (6.8) and (6.9), the m_h^ℓ-norm of W, given by (6.20), can be estimated as follows,

$$\begin{aligned}\|W\|^2_{m_h^\ell} &= m_h^\ell(u_j - \Pi_h u_j, Z) + \left[(m - m_h^\ell) + \frac{1}{\lambda_i}(a_h^\ell - a)\right](u_j, Z)\\ &\leq c\|u_j - \Pi_h u_j\|_{m_h^\ell}\|Z\|_{m_h^\ell} + ch^{r+1}\|u_j\|_{\mathrm{H}^1(\Omega)}\|Z\|_{\mathrm{H}^1(\Omega)}\\ &\quad + \frac{c}{\lambda_i}\left(h^r\|\nabla u_j\|_{\mathrm{L}^2(B_h^\ell)}\|\nabla Z\|_{\mathrm{L}^2(B_h^\ell)} + h^{r+1}\|u_j\|_{\mathrm{H}^1(\Gamma)}\|Z\|_{\mathrm{H}^1(\Gamma)}\right),\end{aligned}$$

where the expression of Z is given in (6.19). Keeping in mind that the discrete eigenfunctions are m_h^ℓ-orthogonal, by Remark 6.3.6 of μ_J, we have,

$$\|Z\|^2_{m_h^\ell} = \sum_{p\notin \mathrm{J}} \Big(\frac{\lambda_i}{\Lambda_p - \lambda_i}\Big)^2 \beta_p^2 \|U_p^\ell\|^2_{m_h^\ell} \leq \mu_J^2 \|W\|^2_{m_h^\ell}. \tag{6.27}$$

Since U_p^ℓ is a discrete eigenfunction associated to Λ_p, then for any $q \neq p$, we have $a_h^\ell(U_p^\ell, U_q^\ell) = \Lambda_p m_h^\ell(U_p^\ell, U_q^\ell)$. This implies that, that the discrete eigenfunctions $\{U_p^\ell\}_{p\notin \mathrm{J}}$ are a_h^ℓ-orthogonal, and that the following inequality holds,

$$\|Z\|^2_{a_h^\ell} \leq \mu_J^2 \|W\|^2_{a_h^\ell}.$$

As a consequence, one can deduce the following,

$$\|\nabla Z\|_{\mathrm{L}^2(B_h^\ell)} \leq \mu_J \|W\|_{a_h^\ell} \quad \text{and} \quad \|Z\|_{\mathrm{H}^1(\Gamma)} \leq \mu_J \|W\|_{a_h^\ell}. \tag{6.28}$$

Additionally, we get,

$$\|Z\|_{\mathrm{H}^1(\Omega)} \leq \|Z\|_{a_h^\ell} + \|Z\|_{m_h^\ell} \leq \mu_J \|W\|_{a_h^\ell} + \mu_J \|W\|_{m_h^\ell}.$$

Using the latter inequality alongside (6.27) and (6.28), we get,

$$\begin{aligned}\|W\|^2_{m_h^\ell} \leq c\mu_J \|u_j - \Pi_h u_j\|_{m_h^\ell}\|W\|_{m_h^\ell} + ch^{r+1}\mu_J\|u_j\|_{\mathrm{H}^1(\Omega)}(\|W\|_{a_h^\ell} + \|W\|_{m_h^\ell})\\ + \frac{c}{\lambda_i}\left(h^r\|\nabla u_j\|_{\mathrm{L}^2(B_h^\ell)} + h^{r+1}\|u_j\|_{\mathrm{H}^1(\Gamma)}\right)\mu_J\|W\|_{a_h^\ell}.\end{aligned}$$

Since the exact eigenfunctions u_j belongs to $\mathrm{H}^2(\Omega,\Gamma)$, by applying Inequality (3.14), we obtain,

$$\begin{aligned}\|W\|^2_{m_h^\ell} &\leq c\mu_J\|u_j-\Pi_h u_j\|_{m_h^\ell}\|W\|_{m_h^\ell}+ch^{r+1}\mu_J\|u_j\|_{\mathrm{H}^1(\Omega)}\|W\|_{m_h^\ell}\\ &\quad +c(1+\frac{1}{\lambda_i})\mu_J h^{r+1}\|u_j\|_{\mathrm{H}^1(\Omega,\Gamma)}\|W\|_{a_h^\ell}+c\mu_J\frac{1}{\lambda_i}h^{r+1/2}\|u_j\|_{\mathrm{H}^2(\Omega,\Gamma)}\|W\|_{a_h^\ell}\\ &\leq c\mu_J\|u_j-\Pi_h u_j\|_{m_h^\ell}\|W\|_{m_h^\ell}+ch^{r+1}\mu_J\|u_j\|_{\mathrm{H}^1(\Omega)}\|W\|_{m_h^\ell}\\ &\quad +c\mu_J h^{r+1}\|u_j\|_{\mathrm{H}^1(\Omega,\Gamma)}\|W\|_{a_h^\ell}+c\mu_J\frac{1}{\lambda_i}h^{r+1/2}\|u_j\|_{\mathrm{H}^2(\Omega,\Gamma)}\|W\|_{a_h^\ell}.\end{aligned}$$

Young's inequality, which states that, for all $\epsilon>0$, $ab\leq\frac{a^2}{\epsilon^2}+\epsilon^2b^2$, is applied in the following inequality multiple times as follows, for $\epsilon_1,\ \epsilon_2\ >\ 0$,

$$\begin{aligned}\|W\|^2_{m_h^\ell}&\leq 4c\mu_J^2\|u_j-\Pi_h u_j\|^2_{m_h^\ell}+\frac{1}{4}\|W\|^2_{m_h^\ell}+4ch^{2r+2}\mu_J^2\|u_j\|^2_{\mathrm{H}^1(\Omega)}+\frac{1}{4}\|W\|^2_{m_h^\ell}\\ &\quad+\frac{c}{\epsilon_1^2}\mu_J^2h^{2r+2}\|u_j\|^2_{\mathrm{H}^1(\Omega,\Gamma)}+\epsilon_1^2\|W\|^2_{a_h^\ell}+\frac{c}{\epsilon_2^2}\mu_J^2h^{2r+1}\|u_j\|^2_{\mathrm{H}^2(\Omega,\Gamma)}+\epsilon_2^2\frac{1}{\lambda_i^2}\|W\|^2_{a_h^\ell}.\end{aligned}$$

Then, we have,

$$\begin{aligned}\|W\|^2_{m_h^\ell}&\leq c\mu_J^2\|u_j-\Pi_h u_j\|^2_{m_h^\ell}+\frac{1}{2}\|W\|^2_{m_h^\ell}+c\Big(\frac{1}{\epsilon_1^2}+\frac{1}{\epsilon_2^2}\Big)h^{2r+1}\mu_J^2\|u_j\|^2_{\mathrm{H}^2(\Omega,\Gamma)}\\ &\quad+(\epsilon_1^2+\frac{\epsilon_2^2}{\lambda_i^2})\|W\|^2_{a_h^\ell}.\end{aligned}$$

Thus, we arrive at,

$$\|W\|^2_{m_h^\ell}\leq c\mu_J^2\|u_j-\Pi_h u_j\|^2_{m_h^\ell}+c\mu_J^2h^{2r+1}\|u_j\|^2_{\mathrm{H}^2(\Omega,\Gamma)}+(\epsilon_1^2+\frac{\epsilon_2^2}{\lambda_i^2})\|W\|^2_{a_h^\ell}.\quad(6.29)$$

It remains to bound $\|W\|^2_{a_h^\ell}$.

2. To estimate the a_h^ℓ-norm of W, we first recall (6.21) and we use the geometric error estimates (6.8) and (6.9) as follows,

$$\begin{aligned}\|W\|^2_{a_h^\ell}&\leq c\lambda_i\|u_j-\Pi_h u_j\|_{m_h^\ell}\|W\|_{m_h^\ell}+\lambda_i\|W\|^2_{m_h^\ell}+c\lambda_ih^{r+1}\|u_j\|_{\mathrm{H}^1(\Omega)}\|W\|_{\mathrm{H}^1(\Omega)}\\ &\quad+ch^r\|\nabla u_j\|_{\mathrm{L}^2(B_h^\ell)}\|\nabla W\|_{\mathrm{L}^2(B_h^\ell)}+ch^{r+1}\|u_j\|_{\mathrm{H}^1(\Gamma)}\|W\|_{\mathrm{H}^1(\Gamma)}.\end{aligned}$$

Since u_j belongs to $\mathrm{H}^2(\Omega,\Gamma)$, Inequality (3.14) is applied as follows,

$$\begin{aligned}\|W\|^2_{a_h^\ell} &\leq c\lambda_i\|u_j-\Pi_h u_j\|_{m_h^\ell}\|W\|_{m_h^\ell}+c\lambda_i h^{r+1}\|u_j\|_{\mathrm{H}^1(\Omega)}(\|W\|_{m_h^\ell}+\|W\|_{a_h^\ell})\\ &\quad +ch^{r+1/2}\|u_j\|_{\mathrm{H}^2(\Omega,\Gamma)}\|W\|_{a_h^\ell}+ch^{r+1}\|u_j\|_{\mathrm{H}^1(\Gamma)}\|W\|_{a_h^\ell}+\lambda_i\|W\|^2_{m_h^\ell}\\ &\leq c\lambda_i\|u_j-\Pi_h u_j\|_{m_h^\ell}\|W\|_{m_h^\ell}+\lambda_i\|W\|^2_{m_h^\ell}+c\lambda_i h^{r+1}\|u_j\|_{\mathrm{H}^1(\Omega)}\|W\|_{m_h^\ell}\\ &\quad +c(1+\lambda_i)h^{r+1/2}\|u_j\|_{\mathrm{H}^2(\Omega,\Gamma)}\|W\|_{a_h^\ell}.\end{aligned}$$

Young's inequality is applied as follows,

$$\begin{aligned}\|W\|^2_{a_h^\ell}\leq 4c\lambda_i\|u_j-\Pi_h u_j\|^2_{m_h^\ell}+\frac{1}{4}\lambda_i\|W\|^2_{m_h^\ell}+\lambda_i\|W\|^2_{m_h^\ell}+4c\lambda_i^2h^{2r+2}\|u_j\|^2_{\mathrm{H}^1(\Omega)}\\ +\frac{1}{4}\|W\|^2_{m_h^\ell}+4c(1+\lambda_i)^2h^{2r+1}\|u_j\|^2_{\mathrm{H}^2(\Omega)}+\frac{1}{4}\|W\|^2_{a_h^\ell}.\end{aligned}$$

Then, we deduce,

$$\|W\|^2_{a_h^\ell}\leq c\lambda_i\|u_j-\Pi_h u_j\|^2_{m_h^\ell}+c(1+\lambda_i)\|W\|^2_{m_h^\ell}+ch^{2r+1}(\lambda_i^2+(1+\lambda_i)^2)\|u_j\|^2_{\mathrm{H}^2(\Omega,\Gamma)}. \tag{6.30}$$

Using the estimation (6.30) in Inequality (6.29), we get,

$$\begin{aligned}\|W\|^2_{m_h^\ell}&\leq c\mu_J^2\|u_j-\Pi_h u_j\|^2_{m_h^\ell}+c\mu_J^2h^{2r+1}\|u_j\|^2_{\mathrm{H}^2(\Omega,\Gamma)}+(\epsilon_1^2+\frac{\epsilon_2^2}{\lambda_i^2})\|W\|^2_{a_h^\ell}\\ &\leq c\mu_J^2\|u_j-\Pi_h u_j\|^2_{m_h^\ell}+c\mu_J^2h^{2r+1}\|u_j\|^2_{\mathrm{H}^2(\Omega,\Gamma)}+c(\epsilon_1^2+\frac{\epsilon_2^2}{\lambda_i^2})\lambda_i\|u_j-\Pi_h u_j\|^2_{m_h^\ell}\\ &\quad +c(\epsilon_1^2+\frac{\epsilon_2^2}{\lambda_i^2})(1+\lambda_i)\|W\|^2_{m_h^\ell}+ch^{2r+1}(\epsilon_1^2+\frac{\epsilon_2^2}{\lambda_i^2})(\lambda_i^2+(1+\lambda_i)^2)\|u_j\|^2_{\mathrm{H}^2(\Omega,\Gamma)}\\ &\leq c\mu_J^2\|u_j-\Pi_h u_j\|^2_{m_h^\ell}+c\mu_J^2h^{2r+1}\|u_j\|^2_{\mathrm{H}^2(\Omega,\Gamma)}+c(\lambda_i+\frac{1}{\lambda_i})\|u_j-\Pi_h u_j\|^2_{m_h^\ell}\\ &\quad +c(\epsilon_1^2+\frac{\epsilon_2^2}{\lambda_i^2})(1+\lambda_i)\|W\|^2_{m_h^\ell}+ch^{2r+1}(1+\frac{1}{\lambda_i^2})(\lambda_i^2+(1+\lambda_i)^2)\|u_j\|^2_{\mathrm{H}^2(\Omega,\Gamma)}.\end{aligned}$$

Taking $\epsilon_1=\frac{1}{2}\sqrt{(\frac{1}{c(1+\lambda_i)})}$ and $\epsilon_2=\frac{\lambda_i}{2}\sqrt{(\frac{1}{c(1+\lambda_i)})}$, these quantities will satisfy the following inequality,

$$1-(\epsilon_1^2+\frac{\epsilon_2^2}{\lambda_i^2})(1+\lambda_i)>0.$$

Then we have,

$$\|W\|^2_{m_h^\ell} \leq c_{\lambda_i}\|u_j - \Pi_h u_j\|^2_{m_h^\ell} + c'_{\lambda_i} h^{2r+1}\|u_j\|^2_{\mathrm{H}^2(\Omega,\Gamma)},$$

where $c_{\lambda_i} = c(\mu_J^2 + \lambda_i + \frac{1}{\lambda_i})$ and $c'_{\lambda_i} = c(\mu_J^2 + (1+\frac{1}{\lambda_i^2})(\lambda_i^2 + (1+\lambda_i)^2))$. To arrive to Inequality (6.25), we take the square root of the latter inequality.

3. Lastly we also need to estimate the a_h^ℓ norm of W. We use the estimations (6.30) and (6.25) as follows,

$$\begin{aligned}
\|W\|^2_{a_h^\ell} &\leq c\lambda_i\|u_j - \Pi_h u_j\|^2_{m_h^\ell} + c(1+\lambda_i)\|W\|^2_{m_h^\ell} \\
&\qquad + ch^{2r+1}(\lambda_i^2 + (1+\lambda_i)^2)\|u_j\|^2_{\mathrm{H}^2(\Omega,\Gamma)} \\
&\leq c\lambda_i\|u_j - \Pi_h u_j\|^2_{m_h^\ell} + c(\lambda_i^2 + (1+\lambda_i)^2)h^{2r+1}\|u_j\|^2_{\mathrm{H}^2(\Omega)} \\
&\qquad + c(\lambda_i+1)\Big(c_{\lambda_i}\|u_j - \Pi_h u_j\|^2_{m_h^\ell} + c'_{\lambda_i} h^{2r+1}\|u_j\|^2_{\mathrm{H}^2(\Omega,\Gamma)}\Big).
\end{aligned}$$

Consequently we arrive at the desired result by taking its square root,

$$\|W\|_{a_h^\ell} \leq C_{\lambda_i}\|u_j - \Pi_h u_j\|_{m_h^\ell} + C'_{\lambda_i} h^{r+1/2}\|u_j\|_{\mathrm{H}^2(\Omega,\Gamma)},$$

where $C_{\lambda_i} = \sqrt{c\Big(\lambda_i + (\lambda_i+1)c_{\lambda_i}\Big)}$ and $C'_{\lambda_i} = \sqrt{c\Big(\lambda_i^2 + (1+\lambda_i)^2 + (\lambda_i+1)c'_{\lambda_i}\Big)}$.

□

Remark 6.3.11. *In this work, the function $W = \Pi_h u_j - \mathcal{P}_{a_h^\ell} u_j$ being a linear combination of lifted discrete eigenfunctions is in the lifted finite element space $\mathbb{V}_h^\ell$, which is a subspace of $\mathrm{H}^1(\Omega,\Gamma)$, therefore W is not necessarily in $\mathrm{H}^2(\Omega)$. However if, by considering other finite element method like Hermite, W belongs to $\mathrm{H}^2(\Omega,\Gamma)$, then Inequality (6.25) may be improved as follows,*

$$\|W\|^2_{m_h^\ell} \leq c_{\lambda_i}\|u_j - \Pi_h u_j\|^2_{m_h^\ell} + c_{\lambda_i} h^{2r+2}\|u_j\|^2_{\mathrm{H}^2(\Omega,\Gamma)}.$$

This may lead to a higher geometric error rate in the final error estimation for the L^2 norm. However, notice that this conjecture should be checked carefully.

The last step would be to combine all the previous results to estimate the eigenfunctions.

Proof of Theorem 6.3.1: the estimates (6.6) ***and*** (6.7)**.** To prove (6.7), we start by adding and subtracting $\Pi_h u_j$ as follows,

$$\|u_j - \mathcal{P}_{a_h^\ell} u_j\|_{a_h^\ell} \leq \|u_j - \Pi_h u_j\|_{a_h^\ell} + \|\Pi_h u_j - \mathcal{P}_{a_h^\ell} u_j\|_{a_h^\ell} = \|u_j - \Pi_h u_j\|_{a_h^\ell} + \|W\|_{a_h^\ell}.$$

The latter inequality is obtained by definition of $W = \Pi_h u_j - \mathcal{P}_{a_h^\ell} u_j$. Applying respectively (6.26), (6.16) and (6.15), we get,

$$\begin{aligned}\|u_j - \mathcal{P}_{a_h^\ell} u_j\|_{a_h^\ell} &\leq c\|u_j - \Pi_h u_j\|_{a_h^\ell} + C_{\lambda_i}\|u_j - \Pi_h u_j\|_{m_h^\ell} + C'_{\lambda_i} h^{r+1/2}\|u_j\|_{\mathrm{H}^2(\Omega,\Gamma)} \\ &\leq c_{\lambda_i}(h^k + h^{r+1/2}).\end{aligned}$$

By the norm equivalence between $\|\cdot\|_{a_h^\ell}$ and $\|\cdot\|_{\mathrm{H}^1(\Omega,\Gamma)}$ (see Inequalities (3.16) and (3.15)), the latter inequality leads to (6.7).

Since $\mathcal{P}_{m_h^\ell}$ is the orthogonal projection with respect to m_h^ℓ onto $\mathbb{F}_h^\ell$, then $\mathcal{P}_{m_h^\ell} u_j$ is the closest point to u_j with respect to the m_h^ℓ-norm. Since $\mathcal{P}_{a_h^\ell} = \mathcal{P}_{m_h^\ell} \circ \Pi_h$ as mentioned in Remark 6.3.8, we have,

$$\|u_j - \mathcal{P}_{m_h^\ell} u_j\|_{m_h^\ell} \leq \|u_j - \mathcal{P}_{a_h^\ell} u_j\|_{m_h^\ell} \leq \|u_j - \Pi_h u_j\|_{m_h^\ell} + \|\Pi_h u_j - \mathcal{P}_{a_h^\ell} u_j\|_{m_h^\ell}.$$

We apply (6.25) and (6.16) respectively to conclude,

$$\|u_j - \mathcal{P}_{m_h^\ell} u_j\|_{m_h^\ell} \leq c_{\lambda_i}\|u_j - \Pi_h u_j\|_{m_h^\ell} + c'_{\lambda_i} h^{r+1/2}\|u_j\|_{\mathrm{H}^2(\Omega,\Gamma)} \leq c_{\lambda_i}(h^{k+1} + h^{r+1/2}).$$

By the norm equivalence between $\|\cdot\|_{m_h^\ell}$ and $\|\cdot\|_{\mathrm{L}^2(\Omega)}$ (see Inequalities (3.16)), the latter inequality leads to (6.6). □

6.3.4 Eigenvalue error estimate

We recall that λ_i is an exact eigenvalue of finite multiplicity N of Problem (6.2), such that $\lambda_j = \lambda_i$, for any $j \in \mathrm{J} = \{i, ..., i + N - 1\}$. In order to improve the preliminary eigenvalue error estimation (6.10), we introduce $\mathcal{P}_m : \mathbb{V}_h^\ell \to \mathbb{E}_{\lambda_i}$ the orthogonal projection with respect to m onto the space $\mathbb{E}_{\lambda_i}$, such that for all $v \in \mathbb{V}_h^\ell$,

$$m(\mathcal{P}_m v, t) = m(v, t), \quad \forall\, t \in \mathbb{E}_{\lambda_i}.$$

The following lemma is inspired by [9, Lemma 2.3] and [10, Lemma 3.1]. However

the main difference here is that we need to take into consideration the geometric error (see [15, Lemma 6.1] and [11, Lemma 5.1]).

Lemma 6.3.12 (Eigenvalue bound)**.** *Let U_j^ℓ be a discrete eigenfuntion in $\mathbb{F}_h^\ell$ associated to Λ_j such that $\|U_j^\ell\|_m = 1$. Thus, the following inequality holds,*

$$|\lambda_j - \Lambda_j| \leq \|\mathcal{P}_m U_j^\ell - U_j^\ell\|_a^2 + \lambda_j \|\mathcal{P}_m U_j^\ell - U_j^\ell\|_m^2 + |a_h^\ell - a|(U_j^\ell, U_j^\ell) + \Lambda_j |m_h^\ell - m|(U_j^\ell, U_j^\ell). \tag{6.31}$$

Proof. First of all, we need to notice that $\mathcal{P}_m U_j^\ell$ is in $\mathbb{E}_{\lambda_i}$, thus,

$$a(\mathcal{P}_m U_j^\ell, v) = \lambda_j m(\mathcal{P}_m U_j^\ell, v), \quad \forall\ v \in \mathrm{H}^1(\Omega, \Gamma). \tag{6.32}$$

Taking $v = U_j^\ell \in \mathrm{H}^1(\Omega, \Gamma)$ in (6.32), we have,

$$a(\mathcal{P}_m U_j^\ell, U_j^\ell) = \lambda_j m(\mathcal{P}_m U_j^\ell, U_j^\ell).$$

Afterwards, taking $v = \mathcal{P}_m U_j^\ell \in \mathrm{H}^1(\Omega, \Gamma)$ in (6.32), we get,

$$\|\mathcal{P}_m U_j^\ell\|_a^2 = \lambda_j \|\mathcal{P}_m U_j^\ell\|_m^2.$$

Applying the latter two equations in the following estimation, we get,

$$\begin{aligned}
&\|\mathcal{P}_m U_j^\ell - U_j^\ell\|_a^2 - \lambda_j \|\mathcal{P}_m U_j^\ell - U_j^\ell\|_m^2 \\
&= \|\mathcal{P}_m U_j^\ell\|_a^2 + \|U_j^\ell\|_a^2 - 2a(U_j^\ell, \mathcal{P}_m U_j^\ell) - \lambda_j \|U_j^\ell\|_m^2 - \lambda_j \|\mathcal{P}_m U_j^\ell\|_m^2 + 2\lambda_j m(U_j^\ell, \mathcal{P}_m U_j^\ell) \\
&= \|U_j^\ell\|_a^2 - \lambda_j \|U_j^\ell\|_m^2.
\end{aligned}$$

Since $\|U_j^\ell\|_m = 1$, we have,

$$-\lambda_j = \|\mathcal{P}_m U_j^\ell - U_j^\ell\|_a^2 - \lambda_j \|\mathcal{P}_m U_j^\ell - U_j^\ell\|_m^2 - \|U_j^\ell\|_a^2.$$

Keeping in mind that $a_h^\ell(U_j^\ell, U_j^\ell) = \Lambda_j\ m_h^\ell(U_j^\ell, U_j^\ell)$, we get by adding and subtracting $a_h^\ell(U_j^\ell, U_j^\ell)$,

$$\begin{aligned}
-\lambda_j &= \|\mathcal{P}_m U_j^\ell - U_j^\ell\|_a^2 - \lambda_j \|\mathcal{P}_m U_j^\ell - U_j^\ell\|_m^2 - a(U_j^\ell, U_j^\ell) + a_h^\ell(U_j^\ell, U_j^\ell) - \Lambda_j\ m_h^\ell(U_j^\ell, U_j^\ell) \\
&= \|\mathcal{P}_m U_j^\ell - U_j^\ell\|_a^2 - \lambda_j \|\mathcal{P}_m U_j^\ell - U_j^\ell\|_m^2 + (a_h^\ell - a)(U_j^\ell, U_j^\ell) - \Lambda_j\ m_h^\ell(U_j^\ell, U_j^\ell).
\end{aligned}$$

Since $m(U_j^\ell, U_j^\ell) = 1$, then by adding $\Lambda_j m(U_j^\ell, U_j^\ell)$ to each side of this equation, we have,

$$\Lambda_j - \lambda_j = \|\mathcal{P}_m U_j^\ell - U_j^\ell\|_a^2 - \lambda_j \|\mathcal{P}_m U_j^\ell - U_j^\ell\|_m^2 + (a_h^\ell - a)(U_j^\ell, U_j^\ell) + \Lambda_j (m - m_h^\ell)(U_j^\ell, U_j^\ell).$$

By taking the absolute value of the latter equation and bounding it, we get Inequality (6.31). □

The proofs of the following lemma and corollary are inspired to the proofs of [15, Lemma 4.4 - Proposition 4.5], which were given for a surface problem. For readers convenience, we will detail these proofs, and we recall that there exists $c_{\lambda_i} > 0$, such that $0 < \Lambda_j \leq c_{\lambda_i}$, for all $j \in \mathrm{J}$.

Lemma 6.3.13. *Following the assumption in Lemma 6.3.12, there exists $c_{\lambda_i} > 0$ such that,*

$$\|\mathcal{P}_{m_h^\ell} v\|_{a_h^\ell} \leq c_{\lambda_i} \|v\|_{m_h^\ell}, \quad \forall\, v \in \mathrm{H}^1(\Omega, \Gamma), \tag{6.33}$$

where $\mathcal{P}_{m_h^\ell}$ is the orthogonal projection with respect to m_h^ℓ onto $\mathbb{F}_h^\ell$, given in Definition 6.3.7.

Proof. Notice that $\mathcal{P}_{m_h^\ell} v \in \mathbb{F}_h^\ell = \bigoplus_{j \in \mathrm{J}} \mathbb{E}_{\Lambda_j}^\ell$, then there exists constants $\beta_j \in \mathbb{R}$ for $j \in \mathrm{J}$ such that $\mathcal{P}_{m_h^\ell} v = \sum_{j \in \mathrm{J}} \beta_j U_j^\ell$. One can estimate its norm as follows,

$$\begin{aligned}\|\mathcal{P}_{m_h^\ell} v\|_{a_h^\ell}^2 = a_h^\ell(\mathcal{P}_{m_h^\ell} v, \mathcal{P}_{m_h^\ell} v) &= a_h^\ell\Big(\sum_{j \in \mathrm{J}} \beta_j U_j^\ell, \mathcal{P}_{m_h^\ell} v\Big) \\ &= \sum_{j \in \mathrm{J}} \beta_j a_h^\ell(U_j^\ell, \mathcal{P}_{m_h^\ell} v) = \sum_{j \in \mathrm{J}} \beta_j \Lambda_j m_h^\ell(U_j^\ell, \mathcal{P}_{m_h^\ell} v).\end{aligned}$$

Since $0 < \Lambda_j \leq c_{\lambda_i}$, for all $j \in \mathrm{J}$, we have,

$$\|\mathcal{P}_{m_h^\ell} v\|_{a_h^\ell}^2 \leq c_{\lambda_i} \sum_{j \in \mathrm{J}} \beta_j m_h^\ell(U_j^\ell, \mathcal{P}_{m_h^\ell} v) = c_{\lambda_i} m_h^\ell(\mathcal{P}_{m_h^\ell} v, \mathcal{P}_{m_h^\ell} v) = c_{\lambda_i} \|\mathcal{P}_{m_h^\ell} v\|_{m_h^\ell}^2.$$

Finally, by definition of the orthogonal projection $\mathcal{P}_{m_h^\ell}$, we conclude the proof as follows,

$$\|\mathcal{P}_{m_h^\ell} v\|_{a_h^\ell}^2 \leq c_{\lambda_i} \|v\|_{m_h^\ell}^2.$$

□

Corollary 6.3.14. *Following the assumptions of Lemma 6.3.13, this inequality holds for any exact eigenfunction u_j associated to λ_i, there exists $c_{\lambda_i} > 0$ such that,*

$$\|u_j - \mathcal{P}_{m_h^\ell} u_j\|_{a_h^\ell} \leq \|u_j - \mathcal{P}_{a_h^\ell} u_j\|_{a_h^\ell} + c_{\lambda_i} \|u_j - \Pi_h u_j\|_{m_h^\ell}, \tag{6.34}$$

where Π_h is the orthogonal projection with respect to a_h^ℓ onto $\mathbb{V}_h^\ell$ and $\mathcal{P}_{a_h^\ell}$ is the orthogonal projection with respect to a_h^ℓ onto $\mathbb{F}_h^\ell$, given in Definition 6.3.7.

Proof. By adding and subtracting $\mathcal{P}_{a_h^\ell} u_j$, we have,

$$\|u_j - \mathcal{P}_{m_h^\ell} u_j\|_{a_h^\ell} \leq \|u_j - \mathcal{P}_{a_h^\ell} u_j\|_{a_h^\ell} + \|\mathcal{P}_{a_h^\ell} u_j - \mathcal{P}_{m_h^\ell} u_j\|_{a_h^\ell}.$$

Since $\mathcal{P}_{a_h^\ell} = \mathcal{P}_{m_h^\ell} \circ \Pi_h$, we get,

$$\begin{aligned} \|u_j - \mathcal{P}_{m_h^\ell} u_j\|_{a_h^\ell} &\leq \|u_j - \mathcal{P}_{a_h^\ell} u_j\|_{a_h^\ell} + \|\mathcal{P}_{m_h^\ell} \circ \Pi_h u_j - \mathcal{P}_{m_h^\ell} u_j\|_{a_h^\ell} \\ &= \|u_j - \mathcal{P}_{a_h^\ell} u_j\|_{a_h^\ell} + \|\mathcal{P}_{m_h^\ell} (\Pi_h u_j - u_j)\|_{a_h^\ell}. \end{aligned}$$

To sum up, we apply (6.33) to arrive at (6.34). □

The error between a discrete eigenfunction and its projection onto the space spanned by the exact eigenfunctions is estimated in the following lemmas using $\mathcal{P}_m$ the orthogonal projection with respect to m onto the space $\mathbb{E}_{\lambda_i}$.

By [48, Lemma 5.1], for a sufficiently small h, $\{\mathcal{P}_{m_h^\ell} u_p, p \in \mathrm{J}\}$ forms a basis for $\mathbb{F}_h^\ell$. Since $U_j^\ell \in \mathbb{F}_h^\ell = \mathrm{span}\{\mathcal{P}_{m_h^\ell} u_p, p \in \mathrm{J}\}$, it can be written as follows,

$$U_j^\ell = \sum_{p \in \mathrm{J}} \alpha_p \mathcal{P}_{m_h^\ell} u_p. \tag{6.35}$$

Indeed, this can be traced back to the lower semicontinuity of the rank application and the fact that $\mathcal{P}_{m_h^\ell} u_p$ tends to u_p as h tends to 0, for all $p \in \mathrm{J}$.

Lemma 6.3.15. *Let U_j be a discrete eigenfunction associated to Λ_j, such that $\|U_j^\ell\|_m = 1$. Then, we have,*

$$\mathcal{P}_m U_j^\ell - U_j^\ell = \sum_{p \in \mathrm{J}} \alpha_p \left[\sum_{t \in \mathrm{J}} m(\mathcal{P}_{m_h^\ell} u_p - u_p, u_t) u_t + (u_p - \mathcal{P}_{m_h^\ell} u_p) \right], \tag{6.36}$$

where $\{u_p\}_{p \in \mathrm{J}}$ denotes an orthonormal basis of $\mathbb{E}_{\lambda_i}$ with respect to m (thus made of exact eigenfunctions associated to λ_i).

Proof. We extend the proof presented in [15, Lemma 6.3] to a volume problem using volume norms. We need to keep in mind that $\mathcal{P}_m$ is the orthogonal projection with respect to m on $\mathbb{E}_{\lambda_i}$. This implies that $\mathcal{P}_m U_j^\ell$ can be written as follows,

$$\mathcal{P}_m U_j^\ell = \sum_{t\in \mathrm{J}} m(U_j^\ell, u_t) u_t \in \mathbb{E}_{\lambda_i}. \tag{6.37}$$

Subtracting Equation (6.35) from the latter equation (6.37), we get,

$$\mathcal{P}_m U_j^\ell - U_j^\ell = \sum_{t\in \mathrm{J}} m(\sum_{p\in \mathrm{J}} \alpha_p \mathcal{P}_{m_h^\ell} u_p, u_t) u_t - \sum_{p\in \mathrm{J}} \alpha_p \mathcal{P}_{m_h^\ell} u_p. \tag{6.38}$$

Since $m(u_p, u_t) = \delta_{pt}$ for all $p, t \in \mathrm{J}$, we have,

$$-\sum_{p\in \mathrm{J}} \alpha_p m(u_p, u_p) u_p + \sum_{p\in \mathrm{J}} \alpha_p u_p = 0.$$

Inserting this in (6.38), we get,

$$\begin{aligned}
\mathcal{P}_m U_j^\ell - U_j^\ell &= \sum_{t\in \mathrm{J}} m(\sum_{p\in \mathrm{J}} \alpha_p \mathcal{P}_{m_h^\ell} u_p, u_t) u_t - \sum_{p\in \mathrm{J}} \alpha_p m(u_p, u_p) u_p + \sum_{p\in \mathrm{J}} \alpha_p (u_p - \mathcal{P}_{m_h^\ell} u_p) \\
&= \sum_{t\in \mathrm{J}} \sum_{p\in \mathrm{J}} \alpha_p m(\mathcal{P}_{m_h^\ell} u_p - u_p, u_t) u_t + \sum_{p\in \mathrm{J}} \alpha_p (u_p - \mathcal{P}_{m_h^\ell} u_p) \\
&= \sum_{p\in \mathrm{J}} \alpha_p \left[\sum_{t\in \mathrm{J}} m(\mathcal{P}_{m_h^\ell} u_p - u_p, u_t) u_t + (u_p - \mathcal{P}_{m_h^\ell} u_p) \right].
\end{aligned}$$

□

Lemma 6.3.16. *Let U_j be an eigenfunction associated to Λ_j such that $\|U_j^\ell\|_m = 1$. Then, for a sufficiently small mesh size h, there exists $c_{\lambda_i} > 0$ such that,*

$$\|U_j^\ell - \mathcal{P}_m U_j^\ell\|_a \leq c_{\lambda_i} \max_{p\in \mathrm{J}} \|u_p - \mathcal{P}_{m_h^\ell} u_p\|_a, \tag{6.39}$$

$$\|U_j^\ell - \mathcal{P}_m U_j^\ell\|_m \leq c_{\lambda_i} \max_{p\in \mathrm{J}} \|u_p - \mathcal{P}_{m_h^\ell} u_p\|_m, \tag{6.40}$$

$$\|U_j^\ell - \mathcal{P}_m U_j^\ell\|_a \leq c_{\lambda_i} (h^k + h^{r+1/2}), \tag{6.41}$$

$$\|U_j^\ell - \mathcal{P}_m U_j^\ell\|_m \leq c_{\lambda_i} (h^{k+1} + h^{r+1/2}), \tag{6.42}$$

where $\mathcal{P}_{m_h^\ell}$ is the orthogonal projection over $\mathbb{F}_h^\ell$ with respect to m_h^ℓ, given in Definition 6.3.7.

Proof. Taking the norm with respect to the bilinear form a of (6.36), we bound it as follows,

$$\|\mathcal{P}_m U_j^\ell - U_j^\ell\|_a \leq \sum_{p\in \mathrm{J}} |\alpha_p| \left[\sum_{t\in \mathrm{J}} |m(\mathcal{P}_{m_h^\ell} u_p - u_p, u_t)| \|u_t\|_a + \|u_p - \mathcal{P}_{m_h^\ell} u_p\|_a \right].$$

By applying Cauchy-Schwarz, we have,

$$\|\mathcal{P}_m U_j^\ell - U_j^\ell\|_a \leq (\sum_{p\in \mathrm{J}} |\alpha_p|^2)^{\frac{1}{2}} \left(\sum_{p\in \mathrm{J}} \left[\sum_{t\in \mathrm{J}} |m(\mathcal{P}_{m_h^\ell} u_p - u_p, u_t)| \|u_t\|_a + \|u_p - \mathcal{P}_{m_h^\ell} u_p\|_a \right]^2 \right)^{\frac{1}{2}}.$$

By Lemma 5.1 of [48] the coefficients $(\alpha_p)_{p\in \mathrm{J}}$ satisfy, $\sum_{p\in \mathrm{J}} |\alpha_p|^2 \leq C(N)$, where $C(N)$ is a constant dependent on the multiplicity N of λ_i. Keeping in mind that, for all $t \in \mathrm{J}$, u_t satisfies that, $a(u_t, v) = \lambda_i m(u_t, v)$, for any $v \in \mathrm{H}^1(\Omega, \Gamma)$, we have,

$$\begin{aligned}
\|\mathcal{P}_m U_j^\ell - U_j^\ell\|_a &\leq (C(N))^{\frac{1}{2}} \left(\sum_{p\in \mathrm{J}} \left[\sum_{t\in \mathrm{J}} \frac{1}{\lambda_i} |a(\mathcal{P}_{m_h^\ell} u_p - u_p, u_t)| \|u_t\|_a + \|u_p - \mathcal{P}_{m_h^\ell} u_p\|_a \right]^2 \right)^{\frac{1}{2}} \\
&\leq c_{\lambda_i} \left(\sum_{p\in \mathrm{J}} \left[\sum_{t\in \mathrm{J}} \frac{1}{\lambda_i} \|\mathcal{P}_{m_h^\ell} u_p - u_p\|_a \|u_t\|_a \|u_t\|_a + \|u_p - \mathcal{P}_{m_h^\ell} u_p\|_a \right]^2 \right)^{\frac{1}{2}} \\
&\leq c_{\lambda_i} \left(\sum_{p\in \mathrm{J}} \left[\sum_{t\in \mathrm{J}} \|\mathcal{P}_{m_h^\ell} u_p - u_p\|_a \frac{1}{\lambda_i} \|u_t\|_a^2 + \|u_p - \mathcal{P}_{m_h^\ell} u_p\|_a \right]^2 \right)^{\frac{1}{2}}.
\end{aligned}$$

Noticing that $\frac{1}{\lambda_i}\|u_t\|_a^2 = \|u_t\|_m^2 = 1$ for all $t \in \mathrm{J}$, we have,

$$\|\mathcal{P}_m U_j^\ell - U_j^\ell\|_a \leq c_{\lambda_i} \left(\sum_{p\in \mathrm{J}} \left[\sum_{t\in \mathrm{J}} 2\|\mathcal{P}_{m_h^\ell} u_p - u_p\|_a \right]^2 \right)^{\frac{1}{2}}.$$

Then, we arrive at Inequality (6.39) given by,

$$\|\mathcal{P}_m U_j^\ell - U_j^\ell\|_a \leq c_{\lambda_i} \max_{p\in \mathrm{J}} \|u_p - \mathcal{P}_{m_h^\ell} u_p\|_a.$$

To prove (6.41), we need to keep in mind that the norms with respect to the bilinear forms a and a_h^ℓ are equivalent and we use (6.34) as follows,

$$\|u_p - \mathcal{P}_{m_h^\ell} u_p\|_a \leq c\|u_p - \mathcal{P}_{m_h^\ell} u_p\|_{a_h^\ell} \leq c\|u_p - \mathcal{P}_{a_h^\ell} u_p\|_{a_h^\ell} + c_{\lambda_i}\|u_p - \Pi_h u_p\|_{m_h^\ell}.$$

By applying again the norm equivalence and using the error estimations (6.7) and (6.16), we have,

$$\|u_p - \mathcal{P}_{m_h^\ell} u_p\|_a \leq c_{\lambda_i}(h^k + h^{r+1/2}).$$

Combining the latter inequality with (6.39), we obtain (6.41).

Passing to the proof of Inequality (6.40), we consider the norm with respect to m of (6.36) as follows,

$$\|\mathcal{P}_m U_j^\ell - U_j^\ell\|_m \leq \sum_{p\in \mathrm{J}} |\alpha_p| \left[\sum_{t\in \mathrm{J}} |m(\mathcal{P}_{m_h^\ell} u_p - u_p, u_t)| \|u_t\|_m + \|u_p - \mathcal{P}_{m_h^\ell} u_p\|_m \right]$$

Using Cauchy-Schwarz, we proceed in a similar manner as for the previous inequality,

$$\begin{aligned}
\|\mathcal{P}_m U_j^\ell - U_j^\ell\|_m &\leq (\sum_{p\in \mathrm{J}} |\alpha_p|^2)^{\frac{1}{2}} \left(\sum_{p\in \mathrm{J}} \left[\sum_{t\in \mathrm{J}} |m(\mathcal{P}_{m_h^\ell} u_p - u_p, u_t)| \|u_t\|_m + \|u_p - \mathcal{P}_{m_h^\ell} u_p\|_m \right]^2 \right)^{\frac{1}{2}} \\
&\leq (C(N))^{\frac{1}{2}} \left(\sum_{p\in \mathrm{J}} \left[\sum_{t\in \mathrm{J}} \|\mathcal{P}_{m_h^\ell} u_p - u_p\|_m \|u_t\|_m \|u_t\|_m + \|u_p - \mathcal{P}_{m_h^\ell} u_p\|_m \right]^2 \right)^{\frac{1}{2}} \\
&\leq c_{\lambda_i} \left(\sum_{p\in \mathrm{J}} \left[\sum_{t\in \mathrm{J}} 2\|\mathcal{P}_{m_h^\ell} u_p - u_p\|_m \right]^2 \right)^{\frac{1}{2}},
\end{aligned}$$

where we used $\|u_t\|_m^2 = 1$. Consequently, we obtain Inequality (6.40). Lastly, using the error estimation (6.6), we obtain (6.42). □

Proof of Theorem 6.3.1: the eigenvalue estimation (6.5)**.** Firstly we recall Inequality (6.31),

$$|\lambda_j - \Lambda_j| \leq \|\mathcal{P}_m U_j^\ell - U_j^\ell\|_a^2 + \lambda_j \|\mathcal{P}_m U_j^\ell - U_j^\ell\|_m^2 + |a_h^\ell - a|(U_j^\ell, U_j^\ell) + \Lambda_j |m_h^\ell - m|(U_j^\ell, U_j^\ell).$$

Secondly, we apply inequalities (6.41), (6.42) and (6.9) to arrive at,

$$\begin{aligned}
|\lambda_j - \Lambda_j| &\leq c_{\lambda_i}(h^{2k} + h^{2r+1}) + \lambda_j c_{\lambda_i}(h^{2k+2} + h^{2r+1}) + |a_h^\ell - a|(U_j^\ell, U_j^\ell) + c\Lambda_j h^{r+1} \|U_j^\ell\|_{\mathrm{H}^1(\Omega,\Gamma)}^2 \\
&\leq c_{\lambda_i}(h^{2k} + h^{2r+1}) + |a_h^\ell - a|(U_j^\ell, U_j^\ell) + c\Lambda_j h^{r+1} \|U_j^\ell\|_{\mathrm{H}^1(\Omega,\Gamma)}^2.
\end{aligned}$$

The remaining term can be estimated as such by using (6.8),

$$|a_h^\ell - a|(U_j^\ell, U_j^\ell) \leq ch^r \|\nabla U_j^\ell\|_{\mathrm{L}^2(B_h^\ell)}^2 + ch^{r+1} \|U_j^\ell\|_{\mathrm{H}^1(\Gamma)}^2$$

By adding and subtraction $\mathcal{P}_m U_j^\ell$ as follow, and then applying (6.41), we get,

$$\begin{aligned}
|a_h^\ell - a|(U_j^\ell, U_j^\ell) &\leq ch^r \|\nabla(\mathcal{P}_m U_j^\ell - U_j^\ell)\|^2_{\mathrm{L}^2(B_h^\ell)} + ch^r \|\nabla(\mathcal{P}_m U_j^\ell)\|^2_{\mathrm{L}^2(B_h^\ell)} + ch^{r+1}\|U_j^\ell\|^2_{\mathrm{H}^1(\Gamma)} \\
&\leq c_{\lambda_i} h^r (h^{2k} + h^{2r+1}) + ch^r \|\nabla(\mathcal{P}_m U_j^\ell)\|^2_{\mathrm{L}^2(B_h^\ell)} + ch^{r+1}\|U_j^\ell\|^2_{\mathrm{H}^1(\Gamma)} \\
&\leq c_{\lambda_i} (h^{2k+r} + h^{3r+1}) + ch^r \|\nabla(\mathcal{P}_m U_j^\ell)\|^2_{\mathrm{L}^2(B_h^\ell)} + ch^{r+1}\|U_j^\ell\|^2_{\mathrm{H}^1(\Gamma)}.
\end{aligned}$$

Since we have $\mathcal{P}_m U_j^\ell \in \mathbb{E}_{\lambda_i}$ a linear combination of exacts eigenvalues, then $\mathcal{P}_m U_j^\ell \in \mathrm{H}^2(\Omega, \Gamma)$ and Inequality (3.14) can be applied to it as follows,

$$\begin{aligned}
|a_h^\ell - a|(U_j^\ell, U_j^\ell) &\leq c_{\lambda_i}(h^{2k+r} + h^{3r+1}) + ch^r \Big(h^{1/2}\|\mathcal{P}_m U_j^\ell\|_{\mathrm{H}^2(\Omega)}\Big)^2 + ch^{r+1}\|U_j^\ell\|^2_{\mathrm{H}^1(\Gamma)} \\
&\leq c_{\lambda_i}(h^{2k+r} + h^{3r+1}) + ch^{r+1}\|\mathcal{P}_m U_j^\ell\|^2_{\mathrm{H}^2(\Omega)} + ch^{r+1}\|U_j^\ell\|^2_{\mathrm{H}^1(\Gamma)} \\
&\leq c_{\lambda_i} h^{r+1}(\|\mathcal{P}_m U_j^\ell\|^2_{\mathrm{H}^2(\Omega)} + \|U_j^\ell\|^2_{\mathrm{H}^1(\Gamma)}),
\end{aligned}$$

where $\|\mathcal{P}_m U_j^\ell\|^2_{\mathrm{H}^2(\Omega)} + \|U_j^\ell\|^2_{\mathrm{H}^1(\Gamma)}$ is uniformly bounded with respect to h and r. Since the exact eigenfunctions are sufficiently regular and we supposed that $\|U_j^\ell\|_{\mathrm{L}^2(\Omega)} = \|u_t\|_{\mathrm{L}^2(\Omega)} = 1$, by (6.37), $\|\mathcal{P}_m U_j^\ell\|_{\mathrm{H}^2(\Omega)}$ is bounded independently of h. By Inequality (6.41), $\mathrm{dist}(U_j^\ell, \mathbb{E}_{\lambda_i}) \to 0$ where $\mathbb{E}_{\lambda_i}$ is of finite dimension, we can bound $\|U_j^\ell\|_{\mathrm{H}^1(\Gamma)}$ independently of h. Finally, replacing this inequality in the eigenvalue estimation, we get the desired result (6.5).

□

6.3.5 Proof of Inequality (6.16)

Keeping in mind the definition of $\Pi_h : \mathrm{H}^1(\Omega, \Gamma) \to \mathbb{V}_h$ as the Ritz projection in Definition 6.3.7, we want to prove Inequality (6.16), given by,

$$\|u - \Pi_h u\|_{m_h^\ell} \leq ch^{k+1}.$$

To prove this estimate, firstly, we need to recall that the lifted $\mathbb{P}^k$-Lagrangian finite element space is given in (4.2) by, $\mathbb{V}_h^\ell := \{v_h^\ell,\ v_h \in \mathbb{V}_h\}$. Its lifted finite element interpolation operator $\mathcal{I}^\ell$ defined in (4.3).

Secondly, we define the functional F_h on $\mathrm{H}^1(\Omega, \Gamma)$ as follow,

$$\begin{aligned}
F_h : \ \mathrm{H}^1(\Omega, \Gamma) &\longrightarrow \mathbb{R} \\
v &\longmapsto F_h(v) = (a - a_h^\ell)(u - \Pi_h u, v),
\end{aligned}$$

where a is the continuous bilinear form defined on $\mathrm{H}^1(\Omega,\Gamma)\times\mathrm{H}^1(\Omega,\Gamma)$ and a_h^ℓ is the lift of the discrete bilinear form defined on $\mathbb{V}_h^\ell\times\mathbb{V}_h^\ell$. Notice that for $v\in\mathbb{V}_h^\ell$, $F_h(v)=a(u-\Pi_h u,v)$, by Definition 6.3.7 of the projection Π_h.

In order to prove Inequality (6.16), we proceed by bounding F_h as follows in Lemma 6.3.17, with the help of the interpolation inequality defined in Proposition 4.1.1.

Lemma 6.3.17. *There exists $c>0$ such that,*

$$|F_h(v)|\leq ch^{k+r}\|v\|_{\mathrm{H}^1(\Omega,\Gamma)}\quad\forall\, v\in\mathrm{H}^1(\Omega,\Gamma). \tag{6.43}$$

Proof. Denote $e:=u-\Pi_h u$. Let $v\in\mathrm{H}^1(\Omega,\Gamma)$, using Inequality (6.8) we have,

$$\begin{aligned}|F_h(v)|=|a-a_h^\ell|(e,v)&\leq ch^r\|e\|_{\mathrm{H}^1(\Omega,\Gamma)}\|v\|_{\mathrm{H}^1(\Omega,\Gamma)}+ch^{r+1}\|e\|_{\mathrm{H}^1(\Omega,\Gamma)}\|v\|_{\mathrm{H}^1(\Omega,\Gamma)}\\&\leq ch^r(\|e\|_{\mathrm{H}^1(\Omega,\Gamma)}+ch\|e\|_{\mathrm{H}^1(\Omega,\Gamma)})\|v\|_{\mathrm{H}^1(\Omega,\Gamma)}.\end{aligned}$$

Then applying the H^1 error inequality (6.15), we get,

$$|F_h(v)|\leq ch^r(h^k+h^{k+1})\|v\|_{\mathrm{H}^1(\Omega,\Gamma)}\leq ch^{k+r}\|v\|_{\mathrm{H}^1(\Omega,\Gamma)}.$$

□

Proof of Inequality (6.16)**.** To begin with, we use an Aubin-Nitche argument. Let $e:=u-\Pi_h u\in\mathrm{H}^1(\Omega)$. Then there exists a unique solution $z_e\in\mathrm{H}^2(\Omega,\Gamma)$ solution of the weak formulation (6.2) with source terms satisfying,

$$\|z_e\|_{\mathrm{H}^2(\Omega,\Gamma)}\leq c\|e\|_{\mathrm{L}^2(\Omega)}. \tag{6.44}$$

We have, using the continuity of the bilinear form a,

$$\begin{aligned}\|u-\Pi_h u\|^2_{\mathrm{L}^2(\Omega)}=\|e\|^2_{\mathrm{L}^2(\Omega)}=a(e,z_e)&=a(e,z_e-\mathcal{I}^\ell z_e)+a(e,\mathcal{I}^\ell z_e)\\&\leq c_{cont}\|e\|_{\mathrm{H}^1(\Omega,\Gamma)}\|z_e-\mathcal{I}^\ell z_e\|_{\mathrm{H}^1(\Omega,\Gamma)}+|F_h(\mathcal{I}^\ell z_e)|.\end{aligned}$$

We apply Inequality (6.15) with the interpolation inequality in Proposition 4.1.1 for $z_e\in\mathrm{H}^2(\Omega,\Gamma)$ for the first term; as for the second term we use Inequality (6.43) since

$\mathcal{I}^\ell z_e \in \mathbb{V}_h^\ell$, as follows,

$$\|u - \Pi_h u\|^2_{\mathrm{L}^2(\Omega)} \leq c(h^k)h\|z_e\|_{\mathrm{H}^2(\Omega,\Gamma)} + ch^{k+r}\|z_e\|_{\mathrm{H}^1(\Omega,\Gamma)} \leq ch^{k+1}\|z_e\|_{\mathrm{H}^2(\Omega,\Gamma)}.$$

By applying (6.44) and dividing by $\|u - \Pi_h u\|_{\mathrm{L}^2(\Omega)}$, we obtain,

$$\|u - \Pi_h u\|_{\mathrm{L}^2(\Omega)} \leq ch^{k+1}.$$

By the equivalence between the norms the norms $\|\cdot\|_m = \|\cdot\|_{\mathrm{L}^2(\Omega)}$ and $\|\cdot\|_{m_h^\ell}$ in Corollary 6.3.4, we obtain (6.16).

□

6.4 Adaptation to another spectral Ventcel problem

For the sake of completeness, we note that instead of studying the Problem (6.1), we could also estimate the errors of the following spectral Ventcel problem,

$$\begin{cases} \Delta u = 0 & \text{in } \Omega, \\ -\beta\Delta_\Gamma u + \partial_{\mathrm{n}} u + \alpha u = \lambda u & \text{on } \Gamma, \end{cases} \tag{6.45}$$

where $\alpha, \beta > 0$ are some given constants.

The variational formulation of this problem is thus given by,

$$\begin{cases} \text{find } (\lambda, u) \in \mathbb{R} \times \mathrm{H}^1(\Omega,\Gamma), \quad \text{such that,} \\ a(u,v) = \lambda\, m_s(u,v), \quad \forall\ v \in \mathrm{H}^1(\Omega,\Gamma), \end{cases} \tag{6.46}$$

where a is the bilinear form, defined on $\mathrm{H}^1(\Omega,\Gamma) \times \mathrm{H}^1(\Omega,\Gamma)$, given by,

$$a(u,v) := \int_\Omega \nabla u \cdot \nabla v \,\mathrm{d}x + \beta \int_\Gamma \nabla_\Gamma u \cdot \nabla_\Gamma v \,\mathrm{d}s + \alpha \int_\Gamma uv \,\mathrm{d}s,$$

and m_s is the bilinear form, defined on $\mathrm{H}^1(\Omega,\Gamma) \times \mathrm{H}^1(\Omega,\Gamma)$, given by,

$$m_s(u,v) := \int_\Gamma uv \,\mathrm{d}x.$$

Note that the weak formulations (6.46) and (6.2) share the same left hand side

bilinear form a. The main difference in this case is the right hand side, where instead of have the $\mathrm{L}^2(\Omega)$ scalar product, denoted m, as in (6.2), we have the $\mathrm{L}^2(\Gamma)$ scalar product, denoted m_s in (6.46).

In this case, there exists an infinite number of eigenvalues with finite multiplicities to Problem (6.46), which form an increasing sequence $(\lambda_n)_{n\geq 1} \subset \mathbb{R}_+^*$ of positive real numbers, tending to infinity. Their associated eigenfunctions form an orthonormal Hilbert basis of $\mathrm{L}^2(\Gamma)$, denoted $(u_n)_{n\geq 1}$ satisfying,

$$u_n \in \mathrm{H}^1(\Omega,\Gamma), \text{ and } a(u_n,v) = \lambda_n m_s(u_n,v), \quad \forall\, v \ \in \ \mathrm{H}^1(\Omega,\Gamma).$$

Discrete formulation. The approximation problem of (6.46) is given by,

$$\begin{cases} \text{find } (\Lambda, U) \in \mathbb{R}\times\mathbb{V}_h, \text{ such that,} \\ a_h(U,V) = \Lambda\, m_{s,h}(U,V),\ \forall\, V \in \mathbb{V}_h, \end{cases} \tag{6.47}$$

where a_h is the same bilinear form, defined for the discrete problem (6.3) on $\mathbb{V}_h \times \mathbb{V}_h$ and $m_{s,h}$ is the following bilinear form, defined on $\mathbb{V}_h \times \mathbb{V}_h$, for any $U, V \in \mathbb{V}_h$,

$$m_{s,h}(U,V) := \int_{\Gamma_h} UV \mathrm{d}s.$$

The discrete problem (6.47) admits an increasing finite sequence of positive discrete eigenvalues $\Lambda_j \in \mathbb{R}_+^*$. There exists a basis of $\mathbb{V}_h$ made of discrete eigenfunctions $\{U_j\}_{j=1}^{\dim(\mathbb{V}_h)}$, which are $m_{s,h}$-orthogonal.

Lifted discrete formulation. Using the integral expression (3.4), we define the lifted bilinear form $m_{s,h}^\ell$ on $\mathbb{V}_h^\ell \times \mathbb{V}_h^\ell$, throughout $m_{s,h}(U,V) = m_{s,h}^\ell(U^\ell, V^\ell)$ for $U, V \in \mathbb{V}_h$, as follows,

$$m_{s,h}^\ell(U^\ell, V^\ell) := \int_\Gamma UV \frac{\mathrm{d}s}{J_b^\ell},$$

where J_b^ℓ is the lift of the jacobian J_b of the orthogonal projection b given in Proposition 2.0.1.

Hence, we define the lifted formulation of Problem (6.47) by,

$$\begin{cases} \text{find } (\Lambda, U^\ell) \in \mathbb{R}\times\mathbb{V}_h^\ell, \text{ such that,} \\ a_h^\ell(U^\ell, V) = \Lambda\ m_{s,h}^\ell(U^\ell, V),\ \forall\, V \in \mathbb{V}_h^\ell, \end{cases} \tag{6.48}$$

where a_h^ℓ is the same bilinear form as in the lifted discrete formulation (6.4).

The lifted problem (6.48) shares the same eigenvalues as the discrete problem (6.47), denoted $\{\Lambda_j\}_{j=1}^{\dim(\mathbb{V}_h)}$, which are associated to the lift of the eigenfunctions of the discrete formulation (6.46), denoted $\{U_j^\ell\}_{j=1}^{\dim(\mathbb{V}_h)}$.

Error estimations. To begin with, we assume that the exact eigenvalues are ordered increasingly with their multiplicities and counted with their multiplicities. Similarly to the previous case, one can estimate the eigenvalue and eigenfunction errors relative to this problem, as stated in the following theorem.

Theorem 6.4.1. *Let $i \in \mathbb{N}^*$. Let λ_i be an eigenvalue of multiplicity N with its corresponding eigenfunctions, $\{u_j\}_{j\in \mathrm{J}}$, where $\mathrm{J} = \{i, ..., i+N-1\}$, relatively to Problem* (6.45)*. Then, there exists a mesh independent constant $c_{\lambda_i} > 0$, such that, for any $j \in \mathrm{J}$,*

$$|\lambda_j - \Lambda_j| \leq c_{\lambda_i}(h^{2k} + h^{r+1}), \tag{6.49}$$

$$\inf_{U\in\mathbb{F}_h^\ell} \|u_j - U\|_{\mathrm{L}^2(\Gamma)} \leq c_{\lambda_i}(h^{k+1} + h^{r+1/2}), \tag{6.50}$$

$$\inf_{U\in\mathbb{F}_h^\ell} \|u_j - U\|_{\mathrm{H}^1(\Omega,\Gamma)} \leq c_{\lambda_i}(h^{k} + h^{r+1/2}), \tag{6.51}$$

where Λ_j is the eigenvalue of Problem (6.47) *of rank $j \in \mathrm{J}$, $\mathbb{F}_h$ is the space generated by the discrete eigenfunctions associated to $\{\Lambda_j\}_{j\in\mathrm{J}}$, and $\mathbb{F}_h^\ell$ is the lift of $\mathbb{F}_h$ made of functions defined on the physical domain Ω.*

Remark 6.4.2. *It is important to notice that the inequalities in Theorem 6.4.1 are analogous to the results in Theorem 6.3.1, which studied a different spectral problem. Indeed, we have similar convergence rates in both cases. The main difference in the estimations is that we estimate the $\mathrm{L}^2(\Gamma)$ norm of the eigenfunction error in* (6.50) *instead of estimating its $\mathrm{L}^2(\Omega)$ norm.*

6.4.1 Proof of Theorem 6.4.1

Step 1: the geometric error estimation. Since Problem (6.46) share the same bilinear form a as the one in the previous studied problem (6.2), Inequality (6.8) still holds. It remains to bound the difference between m_s and $m_{s,h}^\ell$ with respect to the mesh size h and the mesh order r.

Proposition 6.4.3. *For a sufficiently small h, there exists $c > 0$ such that the following geometric error estimations hold for all $v, w \in \mathbb{V}_h^\ell$,*

$$|(m_s - m_{s,h}^\ell)(v, w)| \leq ch^{r+1}\|v\|_{\mathrm{H}^1(\Gamma)}\|w\|_{\mathrm{H}^1(\Gamma)}. \tag{6.52}$$

Proof. Let $v, w \in \mathbb{V}_h^\ell$. The results can be easily obtained by applying the bound on $|1 - \frac{1}{J_b^\ell}|$ given in (3.11) as follows,

$$\begin{aligned}|(m_s - m_{s,h}^\ell)(v, w)| = \left|\int_\Gamma vw\,(1 - \frac{1}{J_b^\ell})\mathrm{d}s\right| &\leq \left\|1 - \frac{1}{J_b^\ell}\right\|_{\mathrm{L}^\infty(\Gamma)} \|v\|_{\mathrm{L}^2(\Gamma)}\|w\|_{\mathrm{L}^2(\Gamma)} \\ &\leq ch^{r+1}\|v\|_{\mathrm{L}^2(\Gamma)}\|w\|_{\mathrm{L}^2(\Gamma)}.\end{aligned}$$

□

Remark 6.4.4. *One might expect to improve Inequality* (6.52) *using a similar approach as in Chapter 5, where we used Inequality* (3.14) *that states that for any $v \in \mathrm{H}^1(\Omega)$, $\|v\|_{\mathrm{L}^2(B_h^\ell)} \leq ch^{1/2}\|v\|_{\mathrm{H}^1(\Omega)}$. Indeed, one hopes that the geometric error with respect to the m_s norm will be in $O(h^{r+2})$. Thus, this might impact the inequality for the eigenfunction error as follows,*

$$\inf_{U \in \mathbb{F}_h^\ell} \|u_j - U\ \|_{\mathrm{L}^2(\Gamma)} \leq c(h^k + h^{r+2}).$$

This inequality will be observed numerically, however until now we were not able to optimise the existing estimate of the $\mathrm{L}^2(\Gamma)$ eigenfunction error, from the theoretical point of view.

Step 2: the preliminary eigenvalue estimate. A preliminary eigenvalue error estimation is also needed before proceeding with the error estimation. Thus, we present the following proposition, which has the same proof as Proposition 6.3.5 but while considering m_s instead of m.

Proposition 6.4.5. *Let λ_i be an exact eigenvalue of multiplicity N of Problem* (6.46)*, such that $\lambda_j = \lambda_i$, for any $j \in \mathrm{J} = \{i, ..., i + N - 1\}$. Then, for any $j \in \mathrm{J}$, there exists $c_{\lambda_i} > 0$ such that,*

$$|\lambda_j - \Lambda_j| \leq c_{\lambda_i}(h^{2k} + h^r), \tag{6.53}$$

where Λ_j is an eigenvalue relatively to the discrete problem (6.47)*.*

Step 3: the eigenfunction error estimates. In order to estimate the eigenfunction error, we need to define $\mathcal{P}_{m^\ell_{s,h}} : \mathrm{H}^1(\Omega,\Gamma) \to \mathbb{F}^\ell_h$ the orthogonal projection with respect to $m^\ell_{s,h}$ onto $\mathbb{F}^\ell_h$, such that for all $v \in \mathrm{H}^1(\Omega,\Gamma)$,

$$m^\ell_{s,h}(\mathcal{P}_{m^\ell_{s,h}}(v), w) = m^\ell_{s,h}(v, w), \quad \forall\ w \in \mathbb{F}^\ell_h.$$

This projection will play the role $\mathcal{P}_{m^\ell_h}$. The key idea, in the proof of the $m^\ell_{s,h}$ error estimation, is to separate the error in two terms for both norms as follows,

$$\inf_{U\in\mathbb{F}^\ell_h} \|u_j - U\ \|_{m^\ell_{s,h}} \leq \|u_j - \Pi_h u_j\ \|_{m^\ell_{s,h}} + \|\Pi_h u_j - \mathcal{P}_{a^\ell_h} u_j\ \|_{m^\ell_{s,h}},$$

where in this context we have $\mathcal{P}_{a^\ell_h} = \mathcal{P}_{m^\ell_{s,h}} \circ \Pi_h$.

The first term will be bounded using a classical interpolation result and using an Aubin-Nitsche argument similarly as in Section 6.3.5. Let $u_j \in \mathrm{H}^{k+1}(\Omega,\Gamma)$ be an exact eigenfunction, then there exists $c > 0$ independent of h such that,

$$\|u_j - \Pi_h u_j\|_{m^\ell_{s,h}} \leq c h^{k+1}. \tag{6.54}$$

As for the second term, we proceed in a similar manner as in Section 6.3.3. Taking into consideration the projection $\mathcal{P}_{m^\ell_{s,h}}$ instead of $\mathcal{P}_{m^\ell_h}$ in Proposition 6.3.9 and in Proposition 6.3.10, similar results hold with the only change being the use of the $m^\ell_{s,h}$ norm instead of the m^ℓ_h norm. We thus obtain,

$$\|W\|_{m^\ell_{s,h}} \leq c_{\lambda_i}\|u_j - \Pi_h u_j\|_{m^\ell_{s,h}} + c_{\lambda_i} h^{r+1/2}\|u_j\|_{\mathrm{H}^2(\Omega,\Gamma)}, \tag{6.55}$$

Summing Inequality (6.55) and Inequality (6.54), we obtain the error estimate (6.50).

To prove the H^1 error estimation (6.51), we follow the same pattern and ideas presented in Section 6.3.3.

Step 4: the eigenvalue error estimate. In order to improve the preliminary eigenvalue error estimation (6.53), we introduce $\mathcal{P}_{m_s} : \mathbb{V}^\ell_h \to \mathbb{E}_{\lambda_i}$ the orthogonal projection with respect to m_s onto the space $\mathbb{E}_{\lambda_i}$, such that for all $v \in \mathbb{V}^\ell_h$,

$$m_s(\mathcal{P}_{m_s} v, t) = m_s(v, t), \quad \forall\ t \in \mathbb{E}_{\lambda_i}.$$

All the results of Section 6.3.4 still stand while using $\mathcal{P}_{m_s}$ instead of $\mathcal{P}_m$. Consequently, one can prove the eigenvalue error estimation (6.49).

6.5 Numerical experiments

In this section are presented numerical results aimed to illustrate the convergence estimates of Theorem 6.4.1. Hence, the Ventcel problem (6.45) is considered on various domains. Notice that one could implement and solve the spectral problem (6.1) to validate the results of Theorem 6.3.1, whose estimations are mostly analogous to Theorem 6.4.1. However, for the sake of simplicity we chose to work with Problem (6.45), since its eigenvalues and eigenfunctions are easily calculated analytically on the disk in 2D and on the ball in 3D: in this case the eigenfunctions are the harmonic polynomials. Whereas for Problem (6.1) the definition of the analytical solutions is not obvious as well as their numerical evaluation.

As in the previous chapters, we perform these simulations in the two dimensional and three dimensional cases. Here again, the discrete problem (6.47) is implemented and solved using the finite element library CUMIN [71]. Additionally, curved meshes of Ω of geometrical order $1 \leq r \leq 3$ have been generated using the curved meshes generator GMSH. We refer to Section 4.2 for more details.

The resolution of the spectral problem is done with the help of the library ARPACK [1], which is a numerical software library for solving large scale eigenvalue problems. The symmetric case (the iterative Lanczos algorithm) is used in shift invert mode with a shift value $\sigma = -1$ (in order to accurately compute the eigenvalues of smallest amplitude). For this method, linear systems $Ax = b$ have to be solved for a single matrix A and for numerous varying right hand sides: a linear system solver is required for the sparse CSR matrix A that is symmetric and positive definite.

In dimension 2, the direct solver MUMPS [2] is considered allowing fast computations. It is particularly well adapted in the present context where linear systems involving the same matrix A have to be solved many times. Cholesky LL^{T} decomposition of a single (positive definite) CSR sparse matrix is computed once at the beginning and afterwards used for numerous linear equation resolutions all along the spectral Lanczos

1. https://www.arpack.fr/
2. https://mumps-solver.org/index.php

algorithm. The tolerance for the Lanczos algorithm was set to a low value (1E−12): this allowed to compute quickly, while using MUMPS, the numerical errors up to error values of 1E−11, allowing us to study the convergence asymptotic regimes. More details on the computational efforts are given in the following paragraph devoted to the unit disk case.

In dimension 3, memory requirements imposed a lighter method: a conjugate gradient with Jacobi preconditioning has been used. The tolerances for the iterative algorithms (Lanczos and conjugate gradient) have been set to very low values (1E−14): this generally allowed to compute accurately the numerical errors up to error values of 1E−10, which was necessary in order to well capture the convergence asymptotic regimes. The 3D computations are the most demanding in terms of computational effort and time. Therefore, they deserved a specific attention, which is given in the paragraph dealing with the unit ball.

Convergence towards the eigenfunctions has only been studied on domains where the analytical solutions are known (the disk and the ball). On domains where the eigenfunctions are not analytically known, like the one in Figure 6.1, such a convergence study is much more complicated to handle. We would need to compute reference eigenfunctions on a refined reference grid and also to project the numerical solutions defined on coarser meshes. However, in the context of curved meshes, this would lead to non trivial difficulties, which is not considered in the present work.

6.5.1 The two dimensional case

In this section, are presented the 2D numerical experiments: firstly, the spectral Ventcel problem is considered on a not so typical non-symmetric and non convex smooth domain. In such case, we only tested out the eigenvalue error estimate, as it is detailed below. Secondly, we consider a typical 2D smooth domain where the exact solutions are known: the unit disk. On this domain, we proceed by testing the accuracy of all the inequalities in Theorem 6.4.1.

Eigenvalue estimate on a smooth domain. The Ventcel problem (6.45) is considered on a smooth domain defined as the interior of a Jordan curve, denoted γ. The curve γ has been set in such a way to have a smooth and connex domain, which moreover is non-convex with no symmetries.

Indeed, the domain Ω is the interior of the Jordan curve $\gamma : \theta \in [0, 2\pi] \to \gamma(\theta) \in \mathbb{R}^2$ satisfying $\gamma(0) = \gamma(2\pi)$. For any $\theta \in [0, 2\pi]$, the function gamma is given by,

$$\gamma(\theta) = (\kappa(\theta)\cos\theta, \kappa(\theta)\sin\theta),$$

where $\kappa(\theta) = 1 + \alpha\cos\theta + \beta\sin\theta + \frac{\beta}{2}\sin 3\theta$, with $\alpha = 0.3$ and $\beta = 0.4$. In Figure 6.1, are displayed linear and quadratic coarse meshes of the domain.

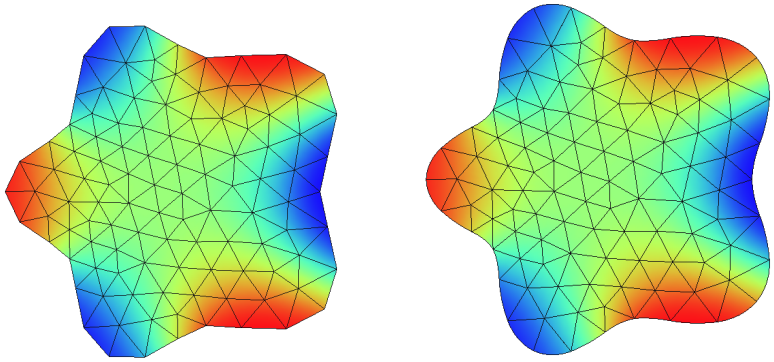

Figure 6.1 – Representation of the 6^{th} eigenfunction computed using $\mathbb{P}^3$ finite element on a (coarse) mesh of Ω: affine mesh (left) and quadratic mesh (right).

The mesh degree and the finite element order being fixed, the 10 first eigenvalues are computed on a series of successively refined meshes: each mesh counts $20 \times 2^{n-1}$ edges on the domain boundary, for $n = 1, \ldots, 5$. We do not know the exact eigenvalues of the Ventcel problem (6.45) on this domain. Thus, reference eigenvalues have been computed on a reference mesh of order $r = 3$ using a $\mathbb{P}^4$ finite element method. The reference mesh counts 20×2^5 boundary edges and is made of approximately 76 000 cubic triangles, the associated $\mathbb{P}^4$ finite element space has approximately 610 000 degrees of freedom. We mention that the computation time is very fast in the present case: total computations roughly last one minute on a simple laptop, which are made really efficient with the direct solver MUMPS here.

To calculate the eigenvalue error, we estimate the difference between the reference eigenvalues, denoted λ_j, and the computed eigenvalues denoted Λ_j. In Table 6.1, we present the convergence order of the error associated to the 6^{th} eigenvalue given by,

$$e_{\lambda_6} := |\lambda_6 - \Lambda_6|.$$

We mention that any other choice within the 10 eigenvalues that have been computed lead to the same convergence pattern. The convergence orders are evaluated from the error ratio between two successive meshes. The order estimations display very stable behaviour (no oscillation): we reported in Table 6.1 the convergence orders estimated between the two finest meshes.

	e_{λ_6}			
Mesh type	$\mathbb{P}^1$	$\mathbb{P}^2$	$\mathbb{P}^3$	$\mathbb{P}^4$
Affine (r=1)	1.96	2.00	2.00	2.00
Quadratic (r=2)	1.99	3.97	3.98	3.97
Cubic (r=3)	1.99	2.99	4.07	4.08

Table 6.1 – Convergence order of e_{λ_6} (Figures in red represent a loss in the convergence rate and figures in blue represent the super-convergence of the error).

As displayed in Table 6.1, the convergence rate of e_{λ_6} on an affine mesh ($r = 1$) are equal to $r + 1 = 2$ for any $\mathbb{P}^k$ finite element method used as expected by the theory.

For the quadratic case ($r = 2$), as expected from Section 4.4, the error presents a super-convergence: a saturation of the error occurs at order 4 when it was expected to stop at 3 for a $\mathbb{P}^k$ method with $k \geq 2$, following Inequality (6.49). It is interesting to notice that this super-convergence also occurs in the present example where a spectral problem is considered on a domain that is neither convex nor symmetric.

On the cubic meshes ($r = 3$), the convergence order of e_{λ_6} follows the expected estimate (6.49): indeed the convergence rate of the error is equal to 2 for a $\mathbb{P}^1$ method. Additionally, a saturation of the error rate is observed at order $r + 1 = 4$ for any $\mathbb{P}^3$ or $\mathbb{P}^4$ method. The only odd case is when using a $\mathbb{P}^2$ finite element method on a cubic mesh, where we obtained a convergence order of 3 whereas the theory predicts a convergence order of 4. This loss is observed in all the numerical experiments as it was thoroughly discussed in Section 4.5. In the case of an eigenvalue error, this default will be discussed in details in the following paragraph.

Error estimates on the unit disk. The Ventcel problem (6.45) is considered on the unit disk $\mathrm{D}(\mathrm{O}, 1) \subset \mathbb{R}^2$. In this case, the eigenfunctions are the harmonic polynomials. A convergence analysis is performed on the 6^{th} eigenvalue λ_6 of multiplicity 2 with corresponding eigenspace, denoted E_3, equal to the space of harmonic polynomials of degree 3.

To proceed, $\mathbb{P}^k$ finite element methods, of degrees $k = 1, \dots, 4$, are used for the error estimates on meshes of order $r = 1, \dots, 3$ (see Figure 6.2 for linear and quadratic meshes). The mesh order and the finite element degree being fixed, the 12 first eigenvalues are computed on a series of five successively refined meshes: each mesh counts $20 \times 2^{n-1}$ edges on the domain boundary, for $n = 1, \dots, 5$. On the most refined mesh using a $\mathbb{P}^4$ finite element method, we counted 20×2^5 boundary edges and approximately 75 500 triangles. The associated $\mathbb{P}^4$ finite element space has approximately 605 600 degrees of freedom. The computations are accomplished very quickly, the total computation time is less than four minutes on a regular computer.

We denote Λ_6 a numerical eigenvalue approximating λ_6 with U_6 as its associated computed eigenfunction. For each mesh order r and each finite element degree k, the following numerical errors are computed on a series of refined meshes:

$$e_{\mathrm{L}^2(\Omega)} := \inf\{\|U_6^\ell - u\|_{\mathrm{L}^2(\Omega)}, u \in \mathrm{E}_3\}, \quad e_{\mathrm{H}_0^1(\Omega)} := \inf\{\|\nabla(U_6^\ell - u)\|_{\mathrm{L}^2(\Omega)}, u \in \mathrm{E}_3\},$$

$$e_{\mathrm{L}^2(\Gamma)} := \inf\{\|U_6^\ell - u\|_{\mathrm{L}^2(\Gamma)}, u \in \mathrm{E}_3\}, \quad e_{\mathrm{H}_0^1(\Gamma)} := \inf\{\|\nabla_\Gamma(U_6^\ell - u)\|_{\mathrm{L}^2(\Omega)}, u \in \mathrm{E}_3\},$$

$$\text{and} \quad e_{\lambda_6} := |\lambda_6 - \Lambda_6|.$$

The $\mathrm{L}^2(\Omega)$ (resp. $\mathrm{L}^2(\Gamma)$) distance between U_6^ℓ and the eigenspace E_3, denoted $e_{\mathrm{L}^2(\Omega)}$ (resp. $e_{\mathrm{L}^2(\Gamma)}$), is computed using the $\mathrm{L}^2(\Omega)$ (resp. $\mathrm{L}^2(\Gamma)$) orthogonal projection of U_6^ℓ onto E_3. In a similar manner, the $\mathrm{L}^2(\Omega)$ distance between ∇U_6^ℓ and the space $\nabla \mathrm{E}_3 = \{\nabla u, u \in \mathrm{E}_3\}$, denoted $e_{\mathrm{H}_0^1(\Omega)}$, is also computed using the $\mathrm{L}^2(\Omega)$ orthogonal projection of ∇U_6^ℓ onto $\nabla \mathrm{E}_3$. Lastly, the $\mathrm{L}^2(\Gamma)$ distance between $\nabla_\Gamma U_6^\ell$ and the space $\nabla_\Gamma \mathrm{E}_3 = \{\nabla_\Gamma u, u \in \mathrm{E}_3\}$, denoted $e_{\mathrm{H}_0^1(\Gamma)}$, is also computed using the $\mathrm{L}^2(\Gamma)$ orthogonal projection of $\nabla_\Gamma U_6^\ell$ onto $\nabla_\Gamma \mathrm{E}_3$.

In Tables 6.2, 6.3 and 6.4, the convergence orders of $e_{\mathrm{L}^2(\Omega)}$, $e_{\mathrm{H}_0^1(\Omega)}$, $e_{\mathrm{L}^2(\Gamma)}$, $e_{\mathrm{H}_0^1(\Gamma)}$ and e_{λ_6} are reported. They are evaluated from the error ratio between two successive meshes that display very stable behaviour, detecting no oscillation. The displayed error rates are estimated between the two finest meshes.

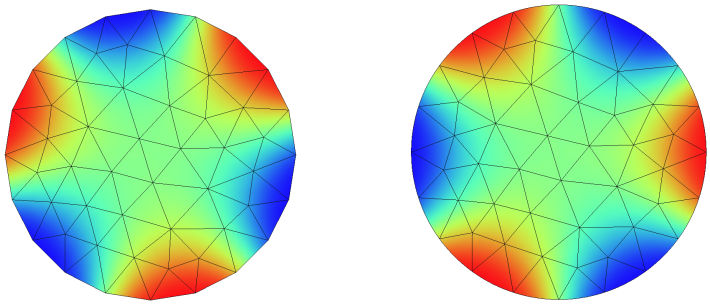

Figure 6.2 – Display of the eigenfunction U_6 associated to the computed eigenvalue Λ_6 using $\mathbb{P}^3$ method on an affine mesh (left) and a quadratic mesh (right).

	$e_{\mathrm{L}^2(\Omega)}$				$e_{\mathrm{H}^1_0(\Omega)}$			
	$\mathbb{P}^1$	$\mathbb{P}^2$	$\mathbb{P}^3$	$\mathbb{P}^4$	$\mathbb{P}^1$	$\mathbb{P}^2$	$\mathbb{P}^3$	$\mathbb{P}^4$
Affine mesh (r=1)	2.01	2.48	2.48	2.48	1.00	1.51	1.50	1.50
Quadratic mesh (r=2)	2.01	3.07	4.5	4.47	1.00	2.01	3.5	3.49
Cubic mesh (r=3)	2.01	2.47	3.48	4.49	0.99	1.49	2.48	3.49

Table 6.2 – Convergence order of the eigenfunctions errors in $\mathrm{L}^2(\Omega)$ and $\mathrm{H}^1_0(\Omega)$ norms (Figures in red represent a loss in the convergence rate and figures in blue represent the super-convergence of the error).

The $\mathrm{H}^1_0(\Omega)$ error convergence rate in Table 6.2 is equal to $\min\{k, r+1/2\}$, for the most part: on an affine mesh, the order of $e_{\mathrm{H}^1_0(\Omega)}$ is equal to 1.5, for all $\mathbb{P}^k$ method with $k \geq 2$, as expected.

On the quadratic mesh, similarly to the result in Table 6.1, the usual super-convergence of the error on the quadratic mesh is depicted: the error rate is equal to 3.5 instead of 2.5 for a $\mathbb{P}^4$ method, as if r is equal to 3 as discussed in Section 4.4. However, one needs to point out that, with a $\mathbb{P}^3$ method, the order is equal to 3.5 surpassing the expected value equal to $3 = \min\{k, r+1/2\}$. A possible explanation for this behavior is that the eigenspace E_3 associated to λ_6 is equal to the space of harmonic polynomials of degree 3 on the disk, as stated before. Moreover, the finite element approximation space $\mathbb{V}_h$ is also made of polynomials on most of the domain (all the elements that do not have an edge on the boundary, i.e. $\Omega \setminus B_h^\ell$ where $B_h^\ell = \{T^{(e)} \in \mathcal{T}_h^{(e)};\ T^{(e)} \text{ has at least two vertices on } \Gamma\}$). This large vicinity between E_3 and $\mathbb{V}_h$ may be a possible cause for the super-convergence observed here.

Lastly, on the cubic mesh, for a $\mathbb{P}^4$ method the rate of $e_{\mathrm{H}^1_0(\Omega)}$ is equal to 3.5, following Inequality (6.51). However, following Section 4.5, for a $\mathbb{P}^2$ and $\mathbb{P}^3$ method, a loss in

the order of convergence of $e_{\mathrm{H}_0^1(\Omega)}$ is depicted and highlighted in red. Instead of having a convergence rate equal to 2 (resp. 3) for a $\mathbb{P}^2$ (resp. $\mathbb{P}^3$) method we obtained 1.5 (resp. 2.49).

The $\mathrm{L}^2(\Omega)$ error convergence rates are displayed in Table 6.2, where a super-convergence is quickly noticed: in the affine case ($r = 1$), the convergence rate of $e_{\mathrm{L}^2(\Omega)}$ is equal to 2.5 instead of 1.5 for a $\mathbb{P}^k$ method with $k \geq 2$. As discussed in Section 4.4, a super-convergence of the error rate on the quadratic meshes is expected to be present, where similar convergence rates as in the cubic case with $r = 3$ are observed. However, the convergence order depicted in Table 6.2 is equal to 4.5 surpassing the expected order of 3.5 for a $\mathbb{P}^3$ and $\mathbb{P}^4$ method. In the cubic case, the convergence rate is equal to 4.5 instead of 3.5 for a $\mathbb{P}^4$ method. In light of this super-convergence on all curved meshes of order $r = 1, 2, 3$, the L^2 estimate can be formulated as follows:

$$e_{\mathrm{L}^2(\Omega)} \leq c_{\lambda_i}(h^{k+1} + h^{r+1}). \tag{6.56}$$

We obtained a similar error estimation in the L^2 norm for the Poisson-Ventcel problem with source terms in Chapter 5. However we have not been able to prove Estimate (6.56), which remains a conjecture. One has to point out that even with Estimate (6.56) a super-convergence is still observed in the following cases: on affine mesh with a $\mathbb{P}^k$ method with $k \geq 2$, the rate of $e_{\mathrm{L}^2(\Omega)}$ is equal to 2.5 instead of $2 = r + 1$. Additionally, on quadratic meshes with a $\mathbb{P}^3$ and $\mathbb{P}^4$ method, the order of $e_{\mathrm{L}^2(\Omega)}$ is equal to 4.5 instead of $4 = r + 1$. Similarly, on cubic meshes with a $\mathbb{P}^4$ method, the error order is equal to 4.5 instead of $4 = r + 1$. As stated in the case of the $\mathrm{H}_0^1(\Omega)$ error, the large similarity between the eigenspace E_3 associated to λ_6 and the finite element space $\mathbb{V}_h$ may be a possible cause for this super-convergence.

One needs to stress that similarly to the results in Table 6.1, a loss in the convergence rate is detected on a cubic mesh with a $\mathbb{P}^2$ method: The convergence rate of $e_{\mathrm{L}^2(\Omega)}$ is equal to 2.5 instead of 3.

Let us now discuss the results in Table 6.3 starting by $e_{\mathrm{H}_0^1(\Gamma)}$ that seems to be in $O(h^k + h^{r+1})$ as observed in Chapter 5 for the $\mathrm{H}_0^1(\Gamma)$ error. Indeed, in the affine case ($r = 1$), the convergence rate is always equal to $r+1$, for any $\mathbb{P}^k$ method with $k \geq 2$. The only exception being when using a $\mathbb{P}^1$ method, where the rate is equal to $k = 1$. The quadratic meshes behave as expected: a super-convergence of the error rate is clearly observed. Indeed, when comparing the last two lines in the table, where r is

	$e_{\mathrm{L}^2(\Gamma)}$				$e_{\mathrm{H}^1_0(\Gamma)}$			
	$\mathbb{P}^1$	$\mathbb{P}^2$	$\mathbb{P}^3$	$\mathbb{P}^4$	$\mathbb{P}^1$	$\mathbb{P}^2$	$\mathbb{P}^3$	$\mathbb{P}^4$
Affine (r=1)	2.00	2.99	3.01	2.99	0.99	1.99	2.00	2.00
Quadratic (r=2)	2.00	2.99	3.99	4.97	0.99	1.99	2.99	3.99
Cubic (r=3)	2.00	3.00	3.99	4.99	0.99	1.99	2.99	3.72

Table 6.3 – Convergence order of the eigenfunctions errors in $\mathrm{L}^2(\Gamma)$ and $\mathrm{H}^1_0(\Gamma)$ norms (Figures in blue represent the super-convergence of the error).

equal to 2 and 3 respectively: we notice that they have the same convergence rates for all $\mathbb{P}^k$ method. Moreover, analysing the cubic case, one can see that the error $e_{\mathrm{H}^1_0(\Gamma)}$ is in $O(h^k+h^{r+1})$ without any loss in the convergence order, as experienced in Section 4.5.

Now, we pass on to analysing the results of $e_{\mathrm{L}^2(\Gamma)}$: in the affine case, with a $\mathbb{P}^k$ method, with $k \geq 1$, the convergence rate is larger than $\min\{k+1, r+1/2\} = 1.5$: it seems that when $k = 1$, the convergence rate is equal to $2 = k+1$ and when $k \geq 2$, it is equal to $3 = r+2$. This behavior follows Remark 6.4.4, where we sensed that the $\mathrm{L}^2(\Gamma)$ error would be in $O(h^{k+1} + h^{r+2})$ and not just in $O(h^{k+1} + h^{r+1/2})$. This experiments confirms this conjecture even though we were not able to theoretically prove it yet. The quadratic and cubic meshes also follow the same pattern with a convergence rate equal to $\min\{k+1, r+2\}$, while taking into account the super-convergence of the error rate in the quadratic case.

Remark 6.5.1. *We have to mention that the overall results in Table 6.2 and in Table 6.3 validate the* $\mathrm{H}^1(\Omega,\Gamma)$ *error estimate* (6.51)*: even though we noticed that the convergence order of the surface errors and of the* $\mathrm{L}^2(\Omega)$ *error surpass the expected value equal to* $\min\{k, r+1/2\}$*, the rate of the overall* $\mathrm{H}^1(\Omega,\Gamma)$ *error correspond with the theory.*

	e_{λ_6}			
Mesh type	$\mathbb{P}^1$	$\mathbb{P}^2$	$\mathbb{P}^3$	$\mathbb{P}^4$
Affine (r=1)	2.00	2.00	2.00	2.00
Quadratic (r=2)	2.00	4.01	4.01	3.99
Cubic (r=3)	2.00	3.27	3.89	4.00

Table 6.4 – Convergence order of $e_{\lambda_6} = |\lambda_6 - \Lambda_6|$ (Figures in red represent a loss in the convergence rate and figures in blue represent the super-convergence of the error).

The convergence rates of e_{λ_6} observed in Table 6.4 are analogous to the results of Table 6.1: in the affine case, the convergence order is equal to 2 for all degrees of the

finite element method used. As anticipated, the quadratic mesh ($r = 2$) behaves as if r is taken equal to 3: the convergence rate of e_{λ_6} is equal to 4 instead of 3, for all $\mathbb{P}^k$ method with $k \geq 2$. A loss in the convergence rate is highlighted in red in Table 6.4 and in Table 6.1, in the cubic case ($r = 3$) for a $\mathbb{P}^2$ method. Indeed, in the same case, the H_0^1 order of convergence for the associated eigenfunction in Table 6.2 is equal to 1.5 instead of 2. This seems to imply an order of convergence of $2 \times 1.5 = 3$ instead of $2 \times 2 = 4$ for the eigenvalues. Thus, the total convergence rate of e_{λ_6} seems to saturate with the finite element error rate equal to 3.

6.5.2 A 3D case: error estimates on the unit ball

To conclude these numerical experiments, the system (6.45) is now considered on the unit ball $\mathrm{B}(\mathrm{O}, 1) \subset \mathbb{R}^3$. The ball is discretized using meshes of order $r = 1, \ldots, 3$, which are depicted in Figure 6.3 for affine and quadratic meshes. A convergence analysis is performed on the 10^{th} eigenvalue λ_{10} of multiplicity 7. Since on the unit ball, the eigenfunctions are the harmonic polynomial, the corresponding eigenspace E_3 to λ_{10} is equal to the space of harmonic polynomials of degree 3.

For each mesh order r and finite element degree k, we compute the 12 first eigenvalues on a series of five successively refined meshes: it has been necessary to consider these five meshes in order to obtain a reliable estimation of the convergence rates (considering a 6^{th} mesh however would have been unaffordable in terms of computational efforts). Each mesh counts $20 \times 2^{n-1}$ edges on the equator circle, for $n = 1, \ldots, 5$. The most refined mesh has approximately $2,4 \times 10^6$ tetrahedra and the associated $\mathbb{P}^3$ finite element method counts 11×10^6 degrees of freedom. Consequently the matricial system of the spectral problem, which needs to be solved, has a size 11×10^6 with a rather large stencil. As a result, in the 3D case, the computations are much more demanding, both in terms of CPU time and of memory consumption. The use of MUMPS, as we did in the 2D case, is no longer an option due to memory limitation. The inversion of the linear system is done using the conjugate gradient method with a Jacobi preconditioner. With this strategy, 8 iterations of ARPACK were in general required to reach convergence (with a tolerance threshold of $1\mathrm{E}-14$ as stated in this section's introduction): each iteration of ARPACK required roughly 130 linear system inversions, each of which involving 2 000 iterations of the preconditioned CG algorithm. To handle these

computations, we resorted to the UPPA research computer cluster PYRENE [3]. Using shared memory parallelism on a single CPU with 32 cores and 2 000 Mb of memory, each case required between 10 to 30 hours of computations.

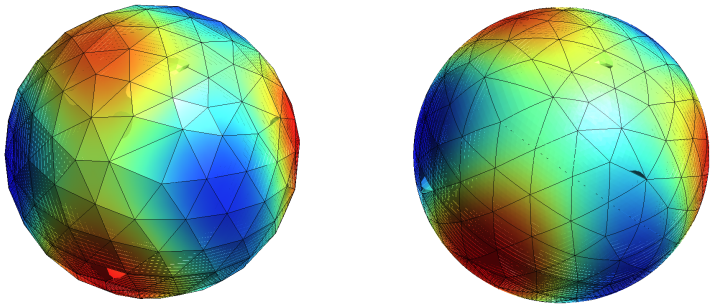

Figure 6.3 – Display of the eigenfunction associated with the eigenvalue Λ_{10} using $\mathbb{P}^2$ finite element on an affine mesh (left) and a quadratic mesh (right).

Denote Λ_{10} a numerical eigenvalue approximating λ_{10} with U_{10} as its associated computed eigenfunction. In each case, the following numerical errors are computed on a series of refined meshes,

$$e_{\mathrm{L}^2(\Omega)} := \inf\{\|U_{10}^\ell - u\|_{\mathrm{L}^2(\Omega)}, u \in \mathrm{E}_3\}, \quad e_{\mathrm{H}_0^1(\Omega)} := \inf\{\|\nabla(U_{10}^\ell - u)\|_{\mathrm{L}^2(\Omega)}, u \in \mathrm{E}_3\},$$

$$e_{\mathrm{L}^2(\Gamma)} := \inf\{\|U_{10}^\ell - u\|_{\mathrm{L}^2(\Gamma)}, u \in \mathrm{E}_3\}, \quad e_{\mathrm{H}_0^1(\Gamma)} := \inf\{\|\nabla_\Gamma(U_{10}^\ell - u)\|_{\mathrm{L}^2(\Gamma)}, u \in \mathrm{E}_3\},$$

$$\text{and} \quad e_{\lambda_{10}} := |\lambda_{10} - \Lambda_{10}|.$$

Similarly to the disk case, orthogonal projections onto E_3 are used in order to compute the L^2 (resp. H_0^1) distances between U_{10}^ℓ and the eigenspace E_3, denoted $e_{\mathrm{L}^2(\Omega)}$ and $e_{\mathrm{L}^2(\Gamma)}$ (resp. $e_{\mathrm{H}_0^1(\Omega)}$ and $e_{\mathrm{H}_0^1(\Gamma)}$).

3. PYRENE Mesocentre de Calcul Intensif Aquitain, https://git.univ-pau.fr/num-as/pyrene-cluster

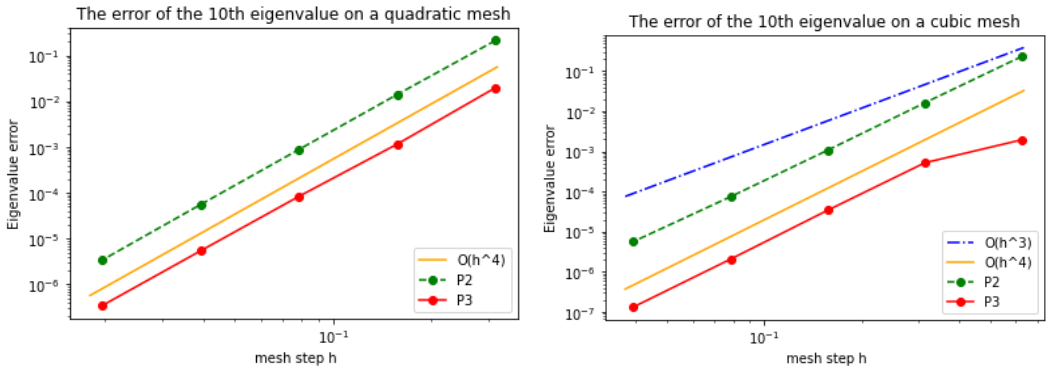

Figure 6.4 – Display of the convergence rate of $e_{\lambda_{10}} = |\lambda_{10} - \Lambda_{10}|$ using $\mathbb{P}^2$ and $\mathbb{P}^3$ finite element on a quadratic mesh (left) and a cubic mesh (right).

In Figure 6.4, is displayed a log–log graph of the error $e_{\lambda_{10}}$ with respect to the mesh step, on a quadratic mesh (right) and a cubic mesh (left). In the quadratic case, as in the two dimensional experiments, the error is in $O(h^4)$ whereas $O(h^3)$ was expected from the theory. The usual super-convergence phenomena of quadratic meshes is present as in the 2D case: it is very interesting to underline this behaviour of the quadratic meshes, which brought a $O(h^4)$ geometric error also in three dimensions. In the cubic case, when using a $\mathbb{P}^2$ method, the convergence rate of $e_{\lambda_{10}}$ starts around 4 tending to 3, in hopes of following the loss in the convergence rate observed in the 2D case. Note that for the 10^{th} eigenvalue, its asymptotic regime is quite harder to capture than the first ones. For an eigenvalue λ_j with lower rank $j < 10$, the convergence rate goes faster to 3, strengthening the hypothesis of a convergence loss in this case. Finally, when using a $\mathbb{P}^3$ method on a cubic mesh the error $e_{\lambda_{10}}$ seems to be in $O(h^4)$, following Inequality (6.49).

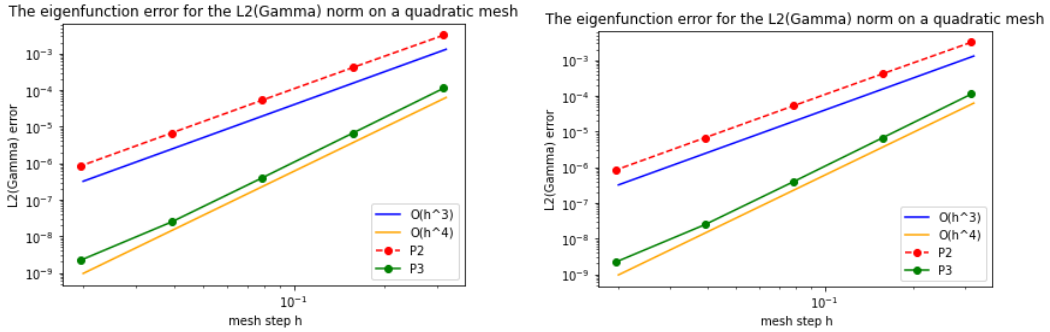

Figure 6.5 – Display of the convergence rate of $e_{\mathrm{L}^2(\Gamma)}$ using $\mathbb{P}^2$ and $\mathbb{P}^3$ finite element on a quadratic mesh (left) and a cubic mesh (right).

In Figure 6.5, is displayed a log–log graph of the $\mathrm{L}^2(\Gamma)$ error $e_{\mathrm{L}^2(\Gamma)}$ with respect to the mesh step, on a quadratic mesh (right) and a cubic mesh (left). We need to keep in mind Remark 6.4.4, where we stated without any theoretical proof that,

$$e_{\mathrm{L}^2(\Gamma)} \leq c(h^{k+1} + h^{r+2}). \tag{6.57}$$

Following the 2D results in Table 6.3, on the quadratic mesh, for a $\mathbb{P}^2$ (resp. $\mathbb{P}^3$) method, the order of $e_{\mathrm{L}^2(\Gamma)}$ is equal to 3 (resp. 4). While taking into account the super-convergence of the error rate on quadratic meshes, this implies that Inequality (6.57) is satisfied. In the cubic case with a $\mathbb{P}^2$ (resp. $\mathbb{P}^3$) method, the graph of $e_{\mathrm{L}^2(\Gamma)}$ has a slope to 3 (resp. 4), also satisfying Inequality (6.57).

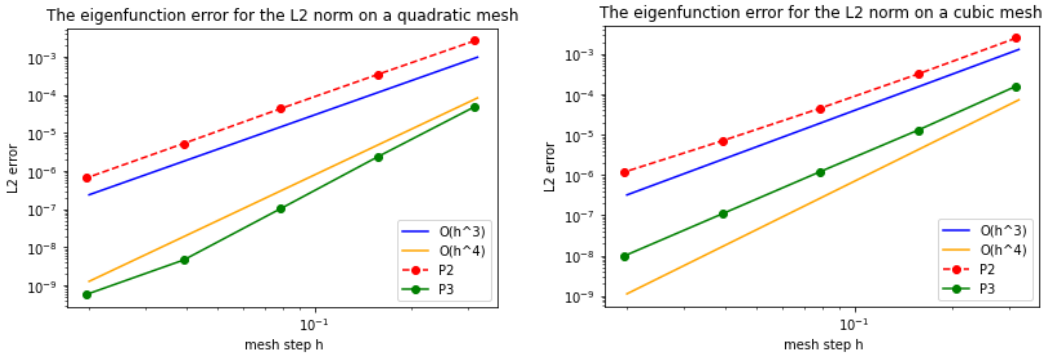

Figure 6.6 – Display of the convergence rate of $e_{\mathrm{L}^2(\Omega)}$ using $\mathbb{P}^2$ and $\mathbb{P}^3$ finite element on a quadratic mesh (left) and a cubic mesh (right).

In Figure 6.6, is displayed a log–log graph of the L^2 error $e_{\mathrm{L}^2(\Omega)}$ with respect to the mesh step, on a quadratic mesh (right) and a cubic mesh (left). On the quadratic mesh, for a $\mathbb{P}^2$ method, the order of $e_{\mathrm{L}^2(\Omega)}$ is equal to 3, as expected. However, for a method of degree $k = 3$, the error order seems to be slightly more than 4 for the first 4 meshes. Though the convergence rate decreases on the last point, this seems to confirm that the expected super-convergence for quadratic meshes also holds on the eigenfunctions in 3D. In the cubic case with a $\mathbb{P}^2$ (resp. $\mathbb{P}^3$) method, the graph of $e_{\mathrm{L}^2(\Omega)}$ seems to have a slope approximately equal to 2.5 (resp. 3.5). The same loss in convergence as in the 2D case is observed, see Table 6.2: this convergence default of $-1/2$ has been formerly discussed in Section 4.5.

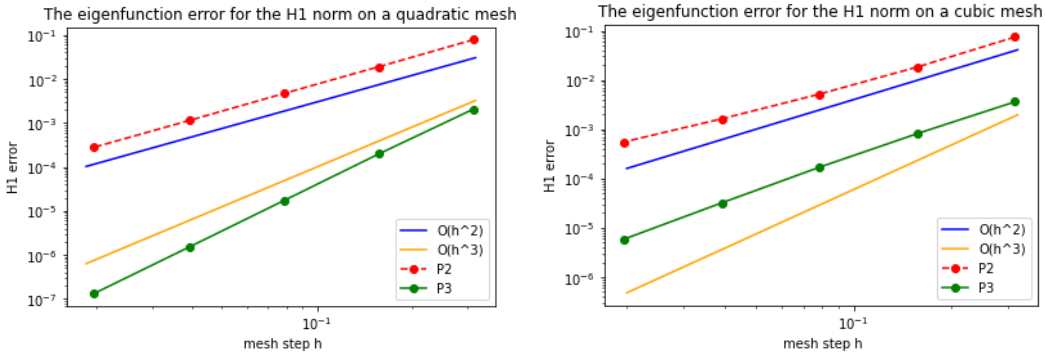

Figure 6.7 – Display of the convergence rate of $e_{\mathrm{H}_0^1(\Omega)}$ using $\mathbb{P}^2$ and $\mathbb{P}^3$ finite element on a quadratic mesh (left) and a cubic mesh (right).

Concerning the $\mathrm{H}_0^1(\Omega)$ error, the results obtained in Figure 6.7 agree with the rates obtained on the disk. The convergence order is equal to 2 on the quadratic mesh with a finite element degree $k = 2$. With a $\mathbb{P}^3$ method, the graph of $e_{\mathrm{H}_0^1(\Omega)}$ seems to have a sloop around 3.5 higher than the awaited value of 3. As for the cubic mesh, the loss in the convergence rate of $e_{\mathrm{H}_0^1(\Omega)}$ was already observed and discussed in the case of the disk: for a $\mathbb{P}^2$ (resp. $\mathbb{P}^3$) method, one can assess that the order of $e_{\mathrm{H}_0^1(\Omega)}$ is slightly less than 2 (resp. 3), similarly to Table 6.2.

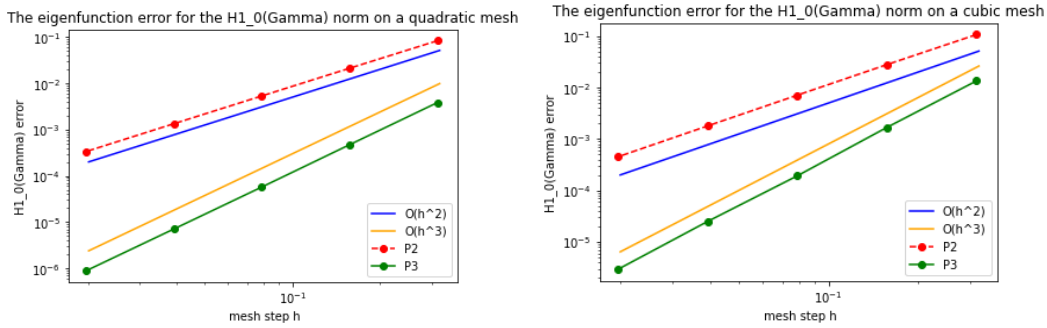

Figure 6.8 – Display of the convergence rate of $e_{\mathrm{H}_0^1(\Gamma)}$ using $\mathbb{P}^2$ and $\mathbb{P}^3$ finite element on a quadratic mesh (left) and a cubic mesh (right).

Lastly, the $\mathrm{H}_0^1(\Gamma)$ error, the results obtained in Figure 6.8 agree with the rates obtained on the disk. The convergence order is equal to 2 on the quadratic mesh with a finite element degree $k = 2$. With a $\mathbb{P}^3$ method, the graph of $e_{\mathrm{H}_0^1(\Gamma)}$ has a sloop equal to 3. As for the cubic mesh, no loss in the convergence rate of $e_{\mathrm{H}_0^1(\Gamma)}$ was observed and similar results are obtained as in Table 6.3: for a $\mathbb{P}^2$ (resp. $\mathbb{P}^3$) method, one can assess that the order of $e_{\mathrm{H}_0^1(\Omega)}$ is slightly less than 2 (resp. 3).

Remark 6.5.2. *Combining the results obtained in Figures 6.6, 6.5, 6.7 and 6.8, we notice that the* $\mathrm{H}^1(\Omega, \Gamma)$ *error estimation* (6.51) *is satisfied.*

Chapter 7

The linear elasticity problem with Ventcel boundary conditions

In this chapter, the a priori error estimates of the linear elasticity problem with Ventcel boundary conditions (1.18), on curved meshes is established using the Lagrangian finite element method.

7.1 The continuous problem and main novelties

The linear elasticity problem with Ventcel boundary conditions. We recall that Ω is a nonempty bounded connected domain in $\mathbb{R}^d$, $d = 2, 3$, with a smooth boundary $\Gamma = \partial\Omega$ and we also recall that $\alpha, \beta > 0$ are some given constants, with $\boldsymbol{f} \in \mathbf{L}^2(\Omega)$, $\boldsymbol{g} \in \mathbf{L}^2(\Gamma)$ as source terms.

Following the notations in Section 1.2, we recall the following elasticity problem with Ventcel boundary conditions defined in (1.18) as follows,

$$\begin{cases} -\mathrm{div}(\mathbf{A}_\Omega e(\boldsymbol{u})) = \boldsymbol{f} & \text{in } \Omega, \\ -\beta \mathrm{div}_\Gamma(\mathbf{A}_\Gamma e_\Gamma(\boldsymbol{u})) + \mathbf{A}_\Omega e(\boldsymbol{u})\mathbf{n} + \alpha \boldsymbol{u} = \boldsymbol{g} & \text{on } \Gamma. \end{cases} \tag{7.1}$$

For the sake of completeness, we recall the definition of the following space,

$$\mathbf{V}_\Gamma = \{\boldsymbol{v} \in \mathbf{L}^2(\Gamma),\, e_\Gamma(\boldsymbol{v}) \in [\mathrm{L}^2(\Gamma)]^{d\times d}\},$$

endowed with the norm, $\|\boldsymbol{v}\|^2_{\mathbf{V}_\Gamma} = \|\boldsymbol{v}\|^2_{\mathbf{L}^2(\Gamma)} + \|e_\Gamma(\boldsymbol{v})\|^2_{[\mathrm{L}^2(\Gamma)]^{d\times d}}$. Throughout this chapter, we rely on the following space,

$$\mathbf{H}_{(\Omega,\Gamma)} = \{\boldsymbol{v} \in \mathbf{H}^1(\Omega);\, \boldsymbol{v}_{|\Gamma} \in \mathbf{V}_\Gamma\},$$

endowed with the norm, $\|\boldsymbol{v}\|^2_{\mathbf{H}_{(\Omega,\Gamma)}} = \|\boldsymbol{v}\|^2_{\mathbf{H}^1(\Omega)} + \|\boldsymbol{v}\|^2_{\mathbf{V}_\Gamma}$. It is also recalled that $\mathbf{H}_{(\Omega,\Gamma)}$

is equal to the space $\mathbf{H}^1(\Omega,\Gamma)$ with equivalent norms satisfying (1.15).

We recall the following variational formulation of Problem (7.1),

$$\begin{cases} \text{find } \boldsymbol{u} \in \mathbf{H}_{(\Omega,\Gamma)}, \quad \text{such that,} \\ a(\boldsymbol{u},\boldsymbol{v}) = l(\boldsymbol{v}),\ \forall\ \boldsymbol{v} \in \mathbf{H}_{(\Omega,\Gamma)}, \end{cases} \tag{7.2}$$

where the bilinear form a, defined on $\mathbf{H}_{(\Omega,\Gamma)} \times \mathbf{H}_{(\Omega,\Gamma)}$, given by,

$$a(\boldsymbol{u},\boldsymbol{v}) = \int_\Omega \mathbf{A}_\Omega(e(\boldsymbol{u})) : \nabla \boldsymbol{v}\, \mathrm{d}x + \beta \int_\Gamma \mathbf{A}_\Gamma(e_\Gamma(\boldsymbol{u})) : \nabla_\Gamma \boldsymbol{v}\, \mathrm{d}s + \alpha \int_\Gamma \boldsymbol{u}\cdot\boldsymbol{v}\, \mathrm{d}s,$$

and the linear form l, defined on $\mathbf{H}_{(\Omega,\Gamma)}$, is given by,

$$l(\boldsymbol{v}) = \int_\Omega \boldsymbol{f}\cdot\boldsymbol{v}\, \mathrm{d}x + \int_\Gamma \boldsymbol{g}\cdot\boldsymbol{v}\, \mathrm{d}s. \tag{7.3}$$

We need to keep in mind that by Theorem 1.2.3, Problem (7.2) admits a unique solution $\boldsymbol{u} \in \mathbf{H}_{(\Omega,\Gamma)}$, satisfying the following inequality,

$$\|\boldsymbol{u}\|_{\mathbf{H}_{(\Omega,\Gamma)}} \leq c(\|\boldsymbol{f}\|_{\mathbf{L}^2(\Omega)} + \|\boldsymbol{g}\|_{\mathbf{L}^2(\Gamma)}).$$

Remark 7.1.1. *Throughout this chapter, the Lamé coefficients $\mu_\Omega > 0$ and $\lambda_\Omega > 0$ (resp. $\mu_\Gamma > 0$ and $\lambda_\Gamma > 0$), are supposed constant at each point x of Ω (resp. Γ). We have to mention that all the Lamé coefficients can be assumed to be variable if we suppose that they are bounded and superior to a constant $\epsilon > 0$. In this case, an additional technical difficulty arises: the Lamé coefficient associated to the discrete formulation of the problem need to be lifted from Ω_h (resp. Γ_h) onto Ω (resp. Γ). This is not a trivial difficulty to deal with even though one may expect to obtain similar results as those presented in this chapter.*

The domain Ω is discretized using curved meshes of geometrical order $r \geq 1$, denoted $\mathcal{T}_h^{(r)}$. The mesh domain is denoted by Ω_h and its boundary is denoted by Γ_h. The main objective of this work is to establish a priori error estimations related to the linear elasticity problem (7.1) using the $\mathbb{P}^k$ finite element method. A discrete formulation is defined in Section 4.1.2, having a unique solution, denoted $\boldsymbol{u}_h$ defined on the mesh domain Ω_h. In order to proceed with the error estimation, the lift operator introduced in Chapter 3 is used thorough the error analysis of the problem.

Main novelties. The main result of this chapter reads: let $\boldsymbol{u}$ be the solution of (7.1) and $\boldsymbol{u}_h$ the solution of the discrete problem with $\boldsymbol{u}_h^\ell$ as its lift. For a sufficiently small mesh size $h > 0$, there exists a constant $c > 0$ independent of h, such that the following inequalities stand,

$$\|\boldsymbol{u} - \boldsymbol{u}_h^\ell\|_{\mathbf{H}_{(\Omega,\Gamma)}} \leq c(h^k + h^r) \quad \text{and} \quad \|\boldsymbol{u} - \boldsymbol{u}_h^\ell\|_{\mathbf{L}^2(\Omega,\Gamma)} \leq c(h^{k+1} + h^r).$$

The scheme of the proof is inspired by the error estimates proof in the scalar case presented in Chapter 5. However, in this case, technical difficulties, arising from the consideration of a linear elasticity module, are quickly noticed, since we are dealing with vector-valued functions. Additionally, elasticity related terms have to be dealt with throughout the proofs in order to establish the error estimates with respect to the required parameters.

7.2 The finite element approximation

The discrete formulation. Let $\boldsymbol{V}_h$ denote the $\mathbb{P}^k$-Lagrangian finite element vector space given in (4.5) with $k \geq 1$. We define the discrete linear form l_h on $\boldsymbol{V}_h$, given as follows for $\boldsymbol{v}_h \in \boldsymbol{V}_h$,

$$l_h(\boldsymbol{v}_h) := \int_{\Omega_h} (\boldsymbol{f}^{-\ell} J_h) \cdot \boldsymbol{v}_h \, \mathrm{d}x + \int_{\Gamma_h} (\boldsymbol{g}^{-\ell} J_b) \cdot \boldsymbol{v}_h \, \mathrm{d}s, \tag{7.4}$$

where J_h (resp. J_b) is the Jacobian of the lift transformation $G_h^{(r)}$ defined in (3.1) (resp. the orthogonal projection b onto Γ defined in Proposition 2.0.1) and $\boldsymbol{f}^{-\ell}$ (resp. $\boldsymbol{g}^{-\ell}$) is the inverse lift of $\boldsymbol{f}$ (resp. $\boldsymbol{g}$).

The approximation problem is given by,

$$\begin{cases} \text{find } \boldsymbol{u}_h \in \boldsymbol{V}_h, \quad \text{such that,} \\ a_h(\boldsymbol{u}_h, \boldsymbol{v}_h) = l_h(\boldsymbol{v}_h), \, \forall \, \boldsymbol{v}_h \in \boldsymbol{V}_h, \end{cases} \tag{7.5}$$

where a_h is the following bilinear form, defined on $\boldsymbol{V}_h \times \boldsymbol{V}_h$, for $\boldsymbol{u}_h, \boldsymbol{v}_h \in \boldsymbol{V}_h$,

$$a_h(\boldsymbol{u}_h, \boldsymbol{v}_h) := \int_{\Omega_h} \mathbf{A}_\Omega(e(\boldsymbol{u}_h)) : \nabla \boldsymbol{v}_h \, \mathrm{d}x \, \mathrm{d}x + \beta \int_{\Gamma_h} \mathbf{A}_{\Gamma_h}(e_{\Gamma_h}(\boldsymbol{u})) : \nabla_{\Gamma_h} \boldsymbol{v}_h \, \mathrm{d}s + \alpha \int_{\Gamma_h} \boldsymbol{u}_h \cdot \boldsymbol{v}_h \, \mathrm{d}s,$$

where the discrete tensor $\mathbf{A}_{\Gamma_h}$ is defined for any symmetric matrix ξ, by $\mathbf{A}_{\Gamma_h}\xi = 2\mu_\Gamma\xi + \lambda_\Gamma \mathrm{Tr}(\xi)\mathrm{P}_h$ and $\mathrm{P}_h(x) = \mathrm{I}_d - (\mathbf{n}_h \otimes \mathbf{n}_h)(x)$ is the orthogonal projection over the tangential space of Γ_h at a point $x \in \Gamma_h$.

Since a_h is bilinear symmetric positive definite on a finite dimensional space, then there exists a unique solution $\boldsymbol{u}_h \in \boldsymbol{V}_h$ to the discrete problem (7.5).

The lifted discrete formulation. To define the lifted discrete formulation, we rely on the lifted finite element vector space defined in (4.6) by, $\boldsymbol{V}_h^\ell := \{\boldsymbol{v}_h^\ell;\ \boldsymbol{v}_h \in \boldsymbol{V}_h\}$. To begin with, we need to point out that the lifted finite element space $\boldsymbol{V}_h^\ell$ is embedded in the Sobolev space $\mathbf{H}^1(\Omega, \Gamma)$. Thus, the equations (3.38), (3.32), (3.35) and (3.27), where integrals on Ω_h (resp. Γ_h) are expressed in terms of integrals on Ω (resp. Γ), can be applied for lifted finite element vector functions in the following. We refer to Section 3.2 for exhaustive details.

We define the lifted bilinear form a_h^ℓ, on $\boldsymbol{V}_h^\ell \times \boldsymbol{V}_h^\ell$, throughout,

$$a_h(\boldsymbol{u}_h, \boldsymbol{v}_h) = a_h^\ell(\boldsymbol{u}_h^\ell, \boldsymbol{v}_h^\ell), \quad \forall\, \boldsymbol{u}_h, \boldsymbol{v}_h \in \boldsymbol{V}_h.$$

By applying (3.38), (3.32) and (3.27), then the expression of a_h^ℓ is given as follows for all $\boldsymbol{u}_h^\ell, \boldsymbol{v}_h^\ell \in \boldsymbol{V}_h^\ell$,

$$\begin{aligned} a_h^\ell(\boldsymbol{u}_h^\ell, \boldsymbol{v}_h^\ell) = \mu_\Omega \int_\Omega (\nabla \boldsymbol{u}_h^\ell\, \mathcal{G}^\mathsf{T}) : (\nabla \boldsymbol{v}_h^\ell\, \mathcal{G}^\mathsf{T})\, \frac{1}{J_h^\ell}\, \mathrm{d}x + \mu_\Omega \int_\Omega (\nabla \boldsymbol{u}_h^\ell\, \mathcal{G}^\mathsf{T})^\mathsf{T} : (\nabla \boldsymbol{v}_h^\ell\, \mathcal{G}^\mathsf{T})\, \frac{1}{J_h^\ell}\, \mathrm{d}x \\ + \lambda_\Omega \int_\Omega \mathrm{Tr}(\nabla \boldsymbol{u}_h^\ell\, \mathcal{G}^\mathsf{T})\, \mathrm{Tr}(\nabla \boldsymbol{v}_h^\ell\, \mathcal{G}^\mathsf{T})\, \frac{1}{J_h^\ell}\, \mathrm{d}x + \beta \Big(\mu_\Gamma \int_\Gamma (\mathrm{P}_h^\ell \nabla_\Gamma \boldsymbol{u}_h^\ell\, A_h^\ell) : \nabla_\Gamma \boldsymbol{v}_h^\ell\, \mathrm{d}s \\ + \mu_\Gamma \int_\Gamma (\nabla_\Gamma \boldsymbol{u}_h^\ell\, \mathcal{D}_h^\ell)^\mathsf{T} : (\nabla_\Gamma \boldsymbol{v}_h^\ell\, \mathcal{D}_h^\ell)\, \frac{1}{J_b^\ell}\, \mathrm{d}s + \lambda_\Gamma \int_\Gamma \mathrm{Tr}(\nabla_\Gamma \boldsymbol{u}_h^\ell\, \mathcal{D}_h^\ell)\, \mathrm{Tr}(\nabla_\Gamma \boldsymbol{v}_h^\ell\, \mathcal{D}_h^\ell) \frac{1}{J_b^\ell} \mathrm{d}s \Big) \\ + \alpha \int_\Gamma \boldsymbol{u}_h^\ell \cdot \boldsymbol{v}_h^\ell\, \frac{1}{J_b^\ell}\, \mathrm{d}s. \end{aligned}$$

Using (3.35) and (3.27), we notice that the linear forms l and l_h given respectively in (7.3) and in (7.4) satisfy the following equation for all $\boldsymbol{u}_h^\ell, \boldsymbol{v}_h^\ell \in \boldsymbol{V}_h^\ell$,

$$l_h(\boldsymbol{v}_h) = \int_{\Omega_h} (\boldsymbol{f}^{-\ell} J_h) \cdot \boldsymbol{v}_h\, \mathrm{d}x + \int_{\Gamma_h} (\boldsymbol{g}_h^{-\ell} J_b) \cdot \boldsymbol{v}_h\, \mathrm{d}s = \int_\Omega \boldsymbol{f} \cdot \boldsymbol{v}_h^\ell\, \mathrm{d}x + \int_\Gamma \boldsymbol{g} \cdot \boldsymbol{v}_h^\ell\, \mathrm{d}s = l(\boldsymbol{v}_h^\ell).$$

Consequently, we define the lifted formulation of the discrete problem (7.5) by,

$$\begin{cases} \text{find } \boldsymbol{u}_h^\ell \in \boldsymbol{V}_h^\ell, \text{ such that,} \\ a_h^\ell(\boldsymbol{u}_h^\ell, \boldsymbol{v}_h^\ell) = l(\boldsymbol{v}_h^\ell),\ \forall\, \boldsymbol{v}_h^\ell \in \boldsymbol{V}_h^\ell. \end{cases}$$

This problem is well-posed and admits a unique solution $\boldsymbol{u}_h^\ell \in \boldsymbol{V}_h^\ell$, that is the lift of the unique solution u_h of the discrete problem (7.5).

Remark 7.2.1. *Keeping in mind that $\boldsymbol{u}$ is the solution of (7.2) and $\boldsymbol{u}_h^\ell$ is the lift of the solution of (7.5), we need to point out that, for any $\boldsymbol{v}_h^\ell \in \boldsymbol{V}_h^\ell \subset \mathbf{H}_{(\Omega,\Gamma)}$, the following equation stands,*

$$a(\boldsymbol{u}, \boldsymbol{v}_h^\ell) = l(\boldsymbol{v}_h^\ell) = l_h(\boldsymbol{v}_h) = a_h(\boldsymbol{u}_h, \boldsymbol{v}_h) = a_h^\ell(\boldsymbol{u}_h^\ell, \boldsymbol{v}_h^\ell). \tag{7.6}$$

7.3 Error analysis

Throughout this section, we consider that the mesh size h is sufficiently small and that c refers to a positive constant independent of h.

Remark 7.3.1. *In the following we assume that $\boldsymbol{u} \in \mathbf{H}^{k+1}(\Omega, \Gamma)$. Up to my knowledge, this regularity result does not exist in the literature. This is not the topic of the present work to prove this non trivial result. Hence, we assume such a regularity noticing that it seems reasonable by taking sufficiently smooth right hand side vector functions $\boldsymbol{f}$ and $\boldsymbol{g}$ on a smooth domain (see [62] for similar problem in the scalar case). We also assume that $\boldsymbol{u} \in \mathbf{H}^2(\Omega, \Gamma)$ satisfies the following classical energy inequality,*

$$\|\boldsymbol{u}\|_{\mathbf{H}^2(\Omega,\Gamma)} \leq c(\|\boldsymbol{f}\|_{\mathbf{L}^2(\Omega)} + \|\boldsymbol{g}\|_{\mathbf{L}^2(\Gamma)}). \tag{7.7}$$

We note that in the scalar case, in Chapter 5, such regularity is satisfied by the exact solution.

Our goal in this chapter is to prove an a priori error estimates, stated as follows.

Theorem 7.3.2. *Let $\boldsymbol{u} \in \mathbf{H}^1(\Omega, \Gamma)$ be the solution of the variational problem (7.2) and $\boldsymbol{u}_h \in \boldsymbol{V}_h$ be the solution of the finite element formulation (7.5). Following Remark 7.3.1, it is assumed that $\boldsymbol{u}$ belongs to $\mathbf{H}^{k+1}(\Omega, \Gamma)$ and that $\boldsymbol{u}$ also satisfies the energy inequality (7.7). Then for a sufficiently small h, there exists a mesh independent constant $c > 0$ such that,*

$$\|\boldsymbol{u} - \boldsymbol{u}_h^\ell\|_{\mathbf{H}_{(\Omega,\Gamma)}} \leq c(h^k + h^r) \quad \text{and} \quad \|\boldsymbol{u} - \boldsymbol{u}_h^\ell\|_{\mathbf{L}^2(\Omega,\Gamma)} \leq c(h^{k+1} + h^r), \tag{7.8}$$

where $\boldsymbol{u}_h^\ell \in \boldsymbol{V}_h^\ell$ *denotes the lift of* $\boldsymbol{u}_h$ *onto* Ω*, given in Definition 3.2.1.*

Here again, the errors in (7.8) are controlled by two main components: the finite element error, represented by the interpolation estimate in Proposition 4.1.3 and the geometrical error, which is the error produced while approximating a domain by a mesh of order r. Thus the first step towards proving Theorem 7.3.2 is to estimate the geometric error in Section 7.3.1. Then, we proceed by proving the $\mathbf{H}_{(\Omega,\Gamma)}$ error, where the interpolation inequality and the geometric error will be employed. Lastly, the proof of the $\mathbf{L}^2$ error relies on the same key ingredients (the geometric error estimation and the interpolation inequality) along side an Aubin-Nitsche type argument.

The upcoming proofs in this section are an adaptation of the proofs of the error estimations of the Poisson-Ventcel problem in Chapter 5 in the elasticity case where instead of having scalar functions we are dealing with vector fields. This change of settings produces many technical difficulties, mainly the new terms relative to the linear elasticity problem which are not trivial to deal with. Indeed, we are dealing with a more complex bilinear form a taking into account elasticity derived terms.

7.3.1 Geometric error estimation

To begin with, we state and prove the following proposition that is used to bound the geometric error.

Proposition 7.3.3. *There exist mesh independent constants* $c_1, c_2 > 0$ *such that the following inequalities hold,*

$$\|\mathrm{P}_h^\ell - \mathrm{P}\|_{\mathrm{L}^\infty(\Gamma)} \leq c_1 h^r, \tag{7.9}$$

$$\|\mathcal{D}_h^\ell - \mathrm{P}\|_{\mathrm{L}^\infty(\Gamma)} \leq c_2 h^r, \tag{7.10}$$

where $\mathcal{D}_h^\ell$ *is defined in* (3.31)*,* $\mathrm{P}(x)$ *is the orthogonal projection over the tangential space of* Γ *in point* $x \in \Gamma$ *and* P_h^ℓ *is the lift of the orthogonal projection over the tangential space of* Γ_h*.*

Proof. To prove inequality (7.9), we start by adding and subtracting $\mathbf{n}_h^\ell \otimes \mathbf{n}$ as follows,

$$\begin{aligned}\mathrm{P}_h^\ell - \mathrm{P} &= \mathrm{I}_d - \mathbf{n}_h^\ell \otimes \mathbf{n}_h^\ell - \mathrm{I}_d + \mathbf{n} \otimes \mathbf{n} \\ &= \mathbf{n} \otimes \mathbf{n} - \mathbf{n}_h^\ell \otimes \mathbf{n}_h^\ell \\ &= (\mathbf{n} - \mathbf{n}_h^\ell) \otimes \mathbf{n} + \mathbf{n}_h^\ell \otimes (\mathbf{n} - \mathbf{n}_h^\ell).\end{aligned}$$

Using Inequality (2.8) of [36], that states that $\|\mathbf{n}-\mathbf{n}_h^\ell\|_{\mathrm{L}^\infty(\Gamma)} \leq ch^r$, we get the expected inequality (7.9),

$$\|\mathrm{P}_h^\ell - \mathrm{P}\|_{\mathrm{L}^\infty(\Gamma)} \leq ch^r.$$

Next to prove (7.10), we recall the definition of $\mathcal{D}_h^\ell$ defined in (3.31) as follows,

$$\|\mathcal{D}_h^\ell - \mathrm{P}\|_{\mathrm{L}^\infty(\Gamma)} = \|\mathrm{P}(\mathrm{I}_d - \mathrm{d}^\ell \mathcal{H}^\ell)\mathrm{P}_h^\ell - \mathrm{P}\|_{\mathrm{L}^\infty(\Gamma)} = \|\mathrm{P}\mathrm{P}_h^\ell - \mathrm{d}^\ell \mathrm{P}\mathcal{H}^\ell \mathrm{P}_h^\ell - \mathrm{P}\|_{\mathrm{L}^\infty(\Gamma)}.$$

Thus, we have,

$$\|\mathcal{D}_h^\ell - \mathrm{P}\|_{\mathrm{L}^\infty(\Gamma)} \leq \|\mathrm{P}\mathrm{P}_h^\ell - \mathrm{P}\|_{\mathrm{L}^\infty(\Gamma)} + \|\mathrm{d}^\ell \mathrm{P}\mathcal{H}^\ell \mathrm{P}_h^\ell\|_{\mathrm{L}^\infty(\Gamma)}. \tag{7.11}$$

Then, we proceed to bound each term separately.

Since $\mathrm{P}^2 = \mathrm{P}$, the first one can be written as follows,

$$\|\mathrm{P}\mathrm{P}_h^\ell - \mathrm{P}\|_{\mathrm{L}^\infty(\Gamma)} = \|\mathrm{P}(\mathrm{P}_h^\ell - \mathrm{P})\|_{\mathrm{L}^\infty(\Gamma)} \leq \|\mathrm{P}\|_{\mathrm{L}^\infty(\Gamma)} \|\mathrm{P}_h^\ell - \mathrm{P}\|_{\mathrm{L}^\infty(\Gamma)} = \|\mathrm{P}_h^\ell - \mathrm{P}\|_{\mathrm{L}^\infty(\Gamma)}.$$

Using Inequality (7.9), we get,

$$\|\mathrm{P}\mathrm{P}_h^\ell - \mathrm{P}\|_{\mathrm{L}^\infty(\Gamma)} \leq ch^r. \tag{7.12}$$

As for the second term, using Inequality (2.6) of [36] that implies that $\|\mathrm{d}^\ell\|_{\mathrm{L}^\infty(\Gamma)} \leq ch^{r+1}$, we get that,

$$\|\mathrm{d}^\ell \mathrm{P}\mathcal{H}^\ell \mathrm{P}_h^\ell\|_{\mathrm{L}^\infty(\Gamma)} \leq ch^{r+1}. \tag{7.13}$$

Lastly, summing up (7.12) and (7.13), we get Inequality (7.10).

□

The geometric error, represented by the difference between a and a_h^ℓ, is evaluated in the following proposition.

Proposition 7.3.4. *There exists a constant $c > 0$ independent of h, such that the following geometric error estimation holds for any $\boldsymbol{u}, \boldsymbol{v} \in \boldsymbol{V}_h^\ell$,*

$$|a(\boldsymbol{u},\boldsymbol{v}) - a_h^\ell(\boldsymbol{u},\boldsymbol{v})| \leq ch^r \|\nabla \boldsymbol{u}\|_{\mathbf{L}^2(B_h^\ell)} \|\nabla \boldsymbol{v}\|_{\mathbf{L}^2(B_h^\ell)} + ch^r \|\boldsymbol{u}\|_{\mathbf{H}^1(\Gamma)} \|\boldsymbol{v}\|_{\mathbf{H}^1(\Gamma)}. \tag{7.14}$$

Proof. Let $\boldsymbol{u}, \boldsymbol{v} \in \boldsymbol{V}_h^\ell$. We start by giving a detailed expression of the bilinear form a as follows by applying the expressions of $\mathbf{A}_\Omega(e(\boldsymbol{u})) : \nabla \boldsymbol{v}$ and $\mathbf{A}_\Gamma(e_\Gamma(\boldsymbol{u})) : \nabla_\Gamma \boldsymbol{v}$ given respectively in Equation (1.16) and in Equation (1.17),

$$\begin{aligned} a(\boldsymbol{u},\boldsymbol{v}) = \mu_\Omega \Big\{ \int_\Omega \nabla \boldsymbol{u} : \nabla \boldsymbol{v} \, \mathrm{d}x + \int_\Omega (\nabla \boldsymbol{u})^\intercal : \nabla \boldsymbol{v} \, \mathrm{d}x \Big\} + \lambda_\Omega \int_\Omega \mathrm{div}(\boldsymbol{u}) \, \mathrm{div}(\boldsymbol{v}) \, \mathrm{d}x \\ + \beta\mu_\Gamma \Big\{ \int_\Gamma \mathrm{P} \, \nabla_\Gamma \boldsymbol{u} : \nabla_\Gamma \boldsymbol{v} \, \mathrm{d}s + \int_\Gamma (\nabla_\Gamma \boldsymbol{u})^\intercal : \nabla_\Gamma \boldsymbol{v} \, \mathrm{d}s \Big\} + \beta\lambda_\Gamma \int_\Gamma \mathrm{div}_\Gamma(\boldsymbol{u}) \, \mathrm{div}_\Gamma(\boldsymbol{v}) \, \mathrm{d}s \\ + \alpha \int_\Gamma \boldsymbol{u} \cdot \boldsymbol{v} \, \mathrm{d}s. \end{aligned}$$

By the definitions of the bilinear forms a and a_h^ℓ, their difference can be written as follows,

$$\begin{aligned} |a(\boldsymbol{u},\boldsymbol{v}) - a_h^\ell(\boldsymbol{u},\boldsymbol{v})| \leq \mu_\Omega \left\{ a_1(\boldsymbol{u},\boldsymbol{v}) + a_2(\boldsymbol{u},\boldsymbol{v}) \right\} + \lambda_\Omega \, a_3(\boldsymbol{u},\boldsymbol{v}) \\ + \alpha \, a_4(\boldsymbol{u},\boldsymbol{v}) + \beta\mu_\Gamma \left\{ a_5(\boldsymbol{u},\boldsymbol{v}) + a_6(\boldsymbol{u},\boldsymbol{v}) \right\} + \beta\lambda_\Gamma \, a_7(\boldsymbol{u},\boldsymbol{v}), \end{aligned}$$

where the terms a_i, defined on $\boldsymbol{V}_h^\ell \times \boldsymbol{V}_h^\ell$, are respectively given by,

$$\begin{aligned} a_1(\boldsymbol{u},\boldsymbol{v}) &:= \left| \int_\Omega \nabla \boldsymbol{u} : \nabla \boldsymbol{v} \, \mathrm{d}x - \int_\Omega (\nabla \boldsymbol{u} \, \mathcal{G}^\intercal) : (\nabla \boldsymbol{v} \, \mathcal{G}^\intercal) \, \frac{1}{J_h^\ell} \, \mathrm{d}x \right|, \\ a_2(\boldsymbol{u},\boldsymbol{v}) &:= \left| \int_\Omega (\nabla \boldsymbol{u})^\intercal : \nabla \boldsymbol{v} \, \mathrm{d}x - \int_\Omega (\nabla \boldsymbol{u} \, \mathcal{G}^\intercal)^\intercal : (\nabla \boldsymbol{v} \, \mathcal{G}^\intercal) \, \frac{1}{J_h^\ell} \, \mathrm{d}x \right|, \\ a_3(\boldsymbol{u},\boldsymbol{v}) &:= \left| \int_\Omega \mathrm{Tr}(\nabla \boldsymbol{u}) \, \mathrm{Tr}(\nabla \boldsymbol{v}) \mathrm{d}x - \int_\Omega \mathrm{Tr}(\nabla \boldsymbol{u} \, \mathcal{G}^\intercal) \, \mathrm{Tr}(\nabla \boldsymbol{v} \, \mathcal{G}^\intercal) \, \frac{1}{J_h^\ell} \, \mathrm{d}x \right|, \\ a_4(\boldsymbol{u},\boldsymbol{v}) &:= \left| \int_\Gamma \boldsymbol{u} \cdot \boldsymbol{v} \, (1 - \frac{1}{J_b^\ell}) \, \mathrm{d}s \right|, \\ a_5(\boldsymbol{u},\boldsymbol{v}) &:= \left| \int_\Gamma \mathrm{P} \, \nabla_\Gamma \boldsymbol{u} : \nabla_\Gamma \boldsymbol{v} \, \mathrm{d}s - \int_\Gamma (\mathrm{P}_h^\ell \, \nabla_\Gamma \boldsymbol{u} A_h^\ell) : \nabla_\Gamma \boldsymbol{v} \, \mathrm{d}s \right|, \\ a_6(\boldsymbol{u},\boldsymbol{v}) &:= \left| \int_\Gamma (\nabla_\Gamma \boldsymbol{u})^\intercal : (\nabla_\Gamma \boldsymbol{v}) \, \mathrm{d}s - \int_\Gamma (\nabla_\Gamma \boldsymbol{u} \mathcal{D}_h^\ell)^\intercal : (\nabla_\Gamma \boldsymbol{v} \mathcal{D}_h^\ell) \frac{1}{J_b^\ell} \, \mathrm{d}s \right|, \end{aligned}$$

$$a_7(\boldsymbol{u},\boldsymbol{v}) := \left| \int_\Gamma \mathrm{Tr}(\nabla_\Gamma \boldsymbol{u})\,\mathrm{Tr}(\nabla_\Gamma \boldsymbol{v}) - \mathrm{Tr}(\nabla_\Gamma \boldsymbol{u}\mathcal{D}_h^\ell)\,\mathrm{Tr}(\nabla_\Gamma \boldsymbol{v}\mathcal{D}_h^\ell)\frac{1}{J_b^\ell}\,\mathrm{d}s \right|,$$

where $\mathcal{G}^\mathsf{T}$ and $\mathcal{D}_h^\ell$ are respectively defined in (3.36) and (3.31) and where A_h^ℓ is the lift of the matrix A_h defined in (3.7). The next step is to bound each a_i, for $i = 1,\ldots,7$, while using the inequalities in (3.12) and in (3.11) where we bound $\|\mathcal{G}^\mathsf{T} - \mathrm{I}_d\|$ and $|\frac{1}{J_h^\ell} - 1|$, $\|A_h^\ell - \mathrm{P}\|$ and $|\frac{1}{J_b^\ell} - 1|$ with respect to h and r. As stated before we will also use Inequalities (7.9) and (7.10).

First of all, we break down the first term as follows, $a_1(\boldsymbol{u},\boldsymbol{v}) \leq Q_1 + Q_2 + Q_3$, where,

$$\begin{aligned}
Q_1 &:= \left| \int_\Omega \left(\nabla \boldsymbol{u}\,(\mathcal{G}^\mathsf{T} - \mathrm{I}_d) \right) : (\nabla \boldsymbol{v}\,\mathcal{G}^\mathsf{T})\,\frac{1}{J_h^\ell}\,\mathrm{d}x \right|, \\
Q_2 &:= \left| \int_\Omega \nabla \boldsymbol{u} : \left(\nabla \boldsymbol{v}\,(\mathcal{G}^\mathsf{T} - \mathrm{I}_d) \right) \frac{1}{J_h^\ell}\,\mathrm{d}x \right|, \\
Q_3 &:= \left| \int_\Omega \nabla \boldsymbol{u} : \nabla \boldsymbol{v}\,(\frac{1}{J_h^\ell} - 1)\,\mathrm{d}x \right|.
\end{aligned}$$

We note that $\mathcal{G}^\mathsf{T} - \mathrm{I}_d = 0$, and $\frac{1}{J_h^\ell} - 1 = 0$ in $\Omega \backslash B_h^\ell$ where B_h^ℓ is the union of all the non-internal elements of the exact mesh $\mathcal{T}_h^{(e)}$, following (3.13). Taking advantage of these equations, we apply the inequalities in (3.12) to estimate each Q_j as follows,

$$\begin{aligned}
Q_1 &= \left| \int_{B_h^\ell} \left(\nabla \boldsymbol{u}\,(\mathcal{G}^\mathsf{T} - \mathrm{I}_d) \right) : (\nabla \boldsymbol{v}\,\mathcal{G}^\mathsf{T})\,\frac{1}{J_h^\ell}\,\mathrm{d}x \right| \leq ch^r \|\nabla \boldsymbol{u}\|_{\mathbf{L}^2(B_h^\ell)} \|\nabla \boldsymbol{v}\|_{\mathbf{L}^2(B_h^\ell)}, \\
Q_2 &= \left| \int_{B_h^\ell} \nabla \boldsymbol{u} : \left(\nabla \boldsymbol{v}\,(\mathcal{G}^\mathsf{T} - \mathrm{I}_d) \right) \frac{1}{J_h^\ell}\,\mathrm{d}x \right| \leq ch^r \|\nabla \boldsymbol{u}\|_{\mathbf{L}^2(B_h^\ell)} \|\nabla \boldsymbol{v}\|_{\mathbf{L}^2(B_h^\ell)}, \\
Q_3 &= \left| \int_{B_h^\ell} \nabla \boldsymbol{u} : \nabla \boldsymbol{v}\,(\frac{1}{J_h^\ell} - 1)\,\mathrm{d}x \right| \leq ch^r \|\nabla \boldsymbol{u}\|_{\mathbf{L}^2(B_h^\ell)} \|\nabla \boldsymbol{v}\|_{\mathbf{L}^2(B_h^\ell)}.
\end{aligned}$$

Summing up the latter terms, we get, $a_1(\boldsymbol{u},\boldsymbol{v}) \leq ch^r \|\nabla \boldsymbol{u}\|_{\mathbf{L}^2(B_h^\ell)} \|\nabla \boldsymbol{v}\|_{\mathbf{L}^2(B_h^\ell)}$.

In a similar manner, we break down a_2 as follows, $a_2(\boldsymbol{u},\boldsymbol{v}) \leq \widetilde{Q_1} + \widetilde{Q_2} + \widetilde{Q_3}$, where,

$$\widetilde{Q_1} := \left| \int_\Omega \left(\nabla \boldsymbol{u}\,(\mathcal{G}^\mathsf{T} - \mathrm{I}_d) \right)^\mathsf{T} : (\nabla \boldsymbol{v}\,\mathcal{G}^\mathsf{T})\,\frac{1}{J_h^\ell}\,\mathrm{d}x \right|,$$

$$\begin{aligned}\widetilde{Q_2} &:= \left|\int_\Omega (\nabla \boldsymbol{u})^\mathsf{T} : \left(\nabla \boldsymbol{v}\,(\mathcal{G}^\mathsf{T} - \mathrm{I}_d)\right)\frac{1}{J_h^\ell}\,\mathrm{d}x\right|,\\ \widetilde{Q_3} &:= \left|\int_\Omega (\nabla \boldsymbol{u})^\mathsf{T} : (\nabla \boldsymbol{v})\,(\frac{1}{J_h^\ell} - 1)\,\mathrm{d}x\right|.\end{aligned}$$

We apply respectively Equation (3.13) and Inequalities (3.12) to estimate each $\widetilde{Q_j}$ as follows,

$$\begin{aligned}\widetilde{Q_1} &= \left|\int_{B_h^\ell} \left(\nabla \boldsymbol{u}\,(\mathcal{G}^\mathsf{T} - \mathrm{I}_d)\right)^\mathsf{T} : (\nabla \boldsymbol{v}\,\mathcal{G}^\mathsf{T})\,\frac{1}{J_h^\ell}\,\mathrm{d}x\right| \leq ch^r \|\nabla \boldsymbol{u}\|_{\mathbf{L}^2(B_h^\ell)} \|\nabla \boldsymbol{v}\|_{\mathbf{L}^2(B_h^\ell)},\\ \widetilde{Q_2} &= \left|\int_{B_h^\ell} (\nabla \boldsymbol{u})^\mathsf{T} : \left(\nabla \boldsymbol{v}\,(\mathcal{G}^\mathsf{T} - \mathrm{I}_d)\right)\frac{1}{J_h^\ell}\,\mathrm{d}x\right| \leq ch^r \|\nabla \boldsymbol{u}\|_{\mathbf{L}^2(B_h^\ell)} \|\nabla \boldsymbol{v}\|_{\mathbf{L}^2(B_h^\ell)},\\ \widetilde{Q_3} &= \left|\int_{B_h^\ell} (\nabla \boldsymbol{u})^\mathsf{T} : (\nabla \boldsymbol{v})\,(\frac{1}{J_h^\ell} - 1)\,\mathrm{d}x\right| \leq ch^r \|\nabla \boldsymbol{u}\|_{\mathbf{L}^2(B_h^\ell)} \|\nabla \boldsymbol{v}\|_{\mathbf{L}^2(B_h^\ell)}.\end{aligned}$$

Summing up the latter terms, we get, $a_2(\boldsymbol{u}, \boldsymbol{v}) \leq ch^r \|\nabla \boldsymbol{u}\|_{\mathbf{L}^2(B_h^\ell)} \|\nabla \boldsymbol{v}\|_{\mathbf{L}^2(B_h^\ell)}$.

Similarly, we also decompose the term a_3 as follows, $a_3(\boldsymbol{u}, \boldsymbol{v}) \leq S_1 + S_2 + S_3$, where,

$$\begin{aligned}S_1 &:= \left|\int_\Omega \mathrm{Tr}\left(\nabla \boldsymbol{u}\,(\mathcal{G}^\mathsf{T} - \mathrm{I}_d)\right)\mathrm{Tr}(\nabla \boldsymbol{v}\,\mathcal{G}^\mathsf{T})\,\frac{1}{J_h^\ell}\,\mathrm{d}x\right|,\\ S_2 &:= \left|\int_\Omega \mathrm{Tr}(\nabla \boldsymbol{u})\,\mathrm{Tr}\left(\nabla \boldsymbol{v}\,(\mathcal{G}^\mathsf{T} - \mathrm{I}_d)\right)\frac{1}{J_h^\ell}\,\mathrm{d}x\right|,\\ S_3 &:= \left|\int_\Omega \mathrm{Tr}(\nabla \boldsymbol{u})\,\mathrm{Tr}(\nabla \boldsymbol{v})\left(\frac{1}{J_h^\ell} - 1\right)\mathrm{d}x\right|.\end{aligned}$$

Equation (3.13) alongside (3.12), which bounds $\|\mathcal{G}_h^{(r)} - \mathrm{I}_d\|$ and $|\frac{1}{J_h^\ell} - 1|$ are respectively applied to estimate each S_j as follows,

$$\begin{aligned}S_1 &= \left|\int_{B_h^\ell} \mathrm{Tr}\left(\nabla \boldsymbol{u}\,(\mathcal{G}^\mathsf{T} - \mathrm{I}_d)\right)\mathrm{Tr}(\nabla \boldsymbol{v}\,\mathcal{G}^\mathsf{T})\,\frac{1}{J_h^\ell}\,\mathrm{d}x\right| \leq ch^r \|\nabla \boldsymbol{u}\|_{\mathbf{L}^2(B_h^\ell)} \|\nabla \boldsymbol{v}\|_{\mathbf{L}^2(B_h^\ell)},\\ S_2 &= \left|\int_{B_h^\ell} \mathrm{Tr}(\nabla \boldsymbol{u})\,\mathrm{Tr}\left(\nabla \boldsymbol{v}\,(\mathcal{G}^\mathsf{T} - \mathrm{I}_d)\right)\frac{1}{J_h^\ell}\,\mathrm{d}x\right| \leq ch^r \|\nabla \boldsymbol{u}\|_{\mathbf{L}^2(B_h^\ell)} \|\nabla \boldsymbol{v}\|_{\mathbf{L}^2(B_h^\ell)},\end{aligned}$$

$$S_3 = \left|\int_{B_h^\ell} \mathrm{Tr}(\nabla \boldsymbol{u})\,\mathrm{Tr}(\nabla \boldsymbol{v})\left(\frac{1}{J_h^\ell} - 1\right)\mathrm{d}x\right| \leq ch^r \|\nabla \boldsymbol{u}\|_{\mathbf{L}^2(B_h^\ell)} \|\nabla \boldsymbol{v}\|_{\mathbf{L}^2(B_h^\ell)}.$$

Summing up the latter terms, we get, $a_3(\boldsymbol{u}, \boldsymbol{v}) \leq ch^r \|\nabla \boldsymbol{u}\|_{\mathbf{L}^2(B_h^\ell)} \|\nabla \boldsymbol{v}\|_{\mathbf{L}^2(B_h^\ell)}$.

Next, a_4 can be bounded simply by using (3.11), where we bound $|\frac{1}{J_b^\ell}-1|$ as follows,

$$a_4(\boldsymbol{u},\boldsymbol{v}) = \left|\int_\Gamma \boldsymbol{u}\cdot\boldsymbol{v}\left(1-\frac{1}{J_b^\ell}\right)\mathrm{d}s\right| \leq ch^{r+1}\|\boldsymbol{u}\|_{\mathbf{L}^2(\Gamma)}\|\boldsymbol{v}\|_{\mathbf{L}^2(\Gamma)}.$$

Next we estimate a_5 as follows,

$$a_5(\boldsymbol{u},\boldsymbol{v}) \leq \left|\int_\Gamma \left(\mathrm{P}_h^\ell\,\nabla_\Gamma\boldsymbol{u}\,(A_h^\ell-\mathrm{P})\right):\nabla_\Gamma\boldsymbol{v}\,\mathrm{d}s\right| + \left|\int_\Gamma(\mathrm{P}_h^\ell\,\nabla_\Gamma\boldsymbol{u}\,\mathrm{P}):\nabla_\Gamma\boldsymbol{v}\,\mathrm{d}s - \int_\Gamma \mathrm{P}\,\nabla_\Gamma\boldsymbol{u}:\nabla_\Gamma\boldsymbol{v}\,\mathrm{d}s\right|.$$

Notice that, by definition of the tangential gradient over Γ of a vector field we can write, $\nabla_\Gamma\boldsymbol{u}\,\mathrm{P}=\nabla_\Gamma\boldsymbol{u}$, where we recall that $\mathrm{P}(x)$ is the orthogonal projection over the tangential spaces of Γ at point $x\in\Gamma$. Applying (3.11) and (7.9), we get,

$$\begin{aligned} a_5(\boldsymbol{u},\boldsymbol{v}) &\leq \left|\int_\Gamma \left(\mathrm{P}_h^\ell\,\nabla_\Gamma\boldsymbol{u}\,(A_h^\ell-\mathrm{P})\right):\nabla_\Gamma\boldsymbol{v}\,\mathrm{d}s\right| + \left|\int_\Gamma \left((\mathrm{P}_h^\ell-\mathrm{P})\,\nabla_\Gamma\boldsymbol{u}\right):\nabla_\Gamma\boldsymbol{v}\,\mathrm{d}s\right| \\ &\leq c\left(\|A_h^\ell-\mathrm{P}\|_{\mathrm{L}^\infty(\Gamma)}+\|\mathrm{P}_h^\ell-\mathrm{P}\|_{\mathrm{L}^\infty(\Gamma)}\right)\|\nabla_\Gamma\boldsymbol{u}\|_{\mathbf{L}^2(\Gamma)}\|\nabla_\Gamma\boldsymbol{v}\|_{\mathbf{L}^2(\Gamma)} \\ &\leq ch^r\|\nabla_\Gamma\boldsymbol{u}\|_{\mathbf{L}^2(\Gamma)}\|\nabla_\Gamma\boldsymbol{v}\|_{\mathbf{L}^2(\Gamma)}. \end{aligned}$$

Next, to be able to bound the term a_6, one needs to notice that it can be decomposed into 3 terms, as follows $a_6(\boldsymbol{u},\boldsymbol{v})\leq R_1+R_2+R_3$, where,

$$\begin{aligned} R_1 &:= \left|\int_\Gamma\left(\nabla_\Gamma\boldsymbol{u}\,(\mathcal{D}_h^\ell-\mathrm{I}_d)\right)^\mathsf{T}:(\nabla_\Gamma\boldsymbol{v}\,\mathcal{D}_h^\ell)\,\frac{1}{J_b^\ell}\,\mathrm{d}s\right|, \\ R_2 &:= \left|\int_\Gamma(\nabla_\Gamma\boldsymbol{u})^\mathsf{T}:\left(\nabla_\Gamma\boldsymbol{v}\,(\mathcal{D}_h^\ell-\mathrm{I}_d)\right)\frac{1}{J_b^\ell}\,\mathrm{d}s\right|, \\ R_3 &:= \left|\int_\Gamma(\nabla_\Gamma\boldsymbol{u})^\mathsf{T}:(\nabla_\Gamma\boldsymbol{v})\left(\frac{1}{J_b^\ell}-1\right)\mathrm{d}s\right|. \end{aligned}$$

Therefore, with the help of Inequality (7.10) and using that $\nabla_\Gamma\boldsymbol{u}\,\mathrm{P}=\nabla_\Gamma\boldsymbol{u}$, one can estimate R_1 and R_2 as follows,

$$\begin{aligned} R_1 &= \left|\int_\Gamma\left(\nabla_\Gamma\boldsymbol{u}\,(\mathcal{D}_h^\ell-\mathrm{P})\right)^\mathsf{T}:(\nabla_\Gamma\boldsymbol{v}\,\mathcal{D}_h^\ell)\,\frac{1}{J_b^\ell}\,\mathrm{d}s\right| \leq ch^r\|\nabla_\Gamma\boldsymbol{u}\|_{\mathbf{L}^2(\Gamma)}\|\nabla_\Gamma\boldsymbol{v}\|_{\mathbf{L}^2(\Gamma)}, \\ R_2 &= \left|\int_\Gamma(\nabla_\Gamma\boldsymbol{u})^\mathsf{T}:\left(\nabla_\Gamma\boldsymbol{v}\,(\mathcal{D}_h^\ell-\mathrm{P})\right)\frac{1}{J_b^\ell}\,\mathrm{d}s\right| \leq ch^r\|\nabla_\Gamma\boldsymbol{u}\|_{\mathbf{L}^2(\Gamma)}\|\nabla_\Gamma\boldsymbol{v}\|_{\mathbf{L}^2(\Gamma)}. \end{aligned}$$

To estimate R_3, Inequality (3.11) is applied as follows,

$$R_3 = \left| \int_\Gamma (\nabla_\Gamma \boldsymbol{u})^\mathsf{T} : (\nabla_\Gamma \boldsymbol{v}) \left(\frac{1}{J_b^\ell} - 1 \right) \mathrm{d}s \right| \leq ch^{r+1} \|\nabla_\Gamma \boldsymbol{u}\|_{\mathbf{L}^2(\Gamma)} \|\nabla_\Gamma \boldsymbol{v}\|_{\mathbf{L}^2(\Gamma)}.$$

Summing up the latter terms, we get, $a_6(\boldsymbol{u}, \boldsymbol{v}) \leq ch^r \|\nabla_\Gamma \boldsymbol{u}\|_{\mathbf{L}^2(\Gamma)} \|\nabla_\Gamma \boldsymbol{v}\|_{\mathbf{L}^2(\Gamma)}$.

Lastly, to be able to bound the last term a_7, one needs to notice that it can be decomposed into 3 terms, as follows $a_7(\boldsymbol{u}, \boldsymbol{v}) \leq \widetilde{R_1} + \widetilde{R_2} + \widetilde{R_3}$, where,

$$\begin{aligned}
\widetilde{R_1} &:= \left| \int_\Gamma \mathrm{Tr}\Big(\nabla_\Gamma \boldsymbol{u} \left(\mathcal{D}_h^\ell - \mathrm{I}_d \right) \Big) \mathrm{Tr}\Big(\nabla_\Gamma \boldsymbol{v}\, \mathcal{D}_h^\ell \Big) \frac{1}{J_b^\ell} \, \mathrm{d}s \right|, \\
\widetilde{R_2} &:= \left| \int_\Gamma \mathrm{Tr}\Big(\nabla_\Gamma \boldsymbol{u} \Big) \mathrm{Tr}\Big(\nabla_\Gamma \boldsymbol{v} \left(\mathcal{D}_h^\ell - \mathrm{I}_d \right) \Big) \frac{1}{J_b^\ell} \, \mathrm{d}s \right|, \\
\widetilde{R_3} &:= \left| \int_\Gamma \mathrm{Tr}(\nabla_\Gamma \boldsymbol{u}) \, \mathrm{Tr}(\nabla_\Gamma \boldsymbol{v}) \left(\frac{1}{J_b^\ell} - 1 \right) \mathrm{d}s \right|.
\end{aligned}$$

In order to bound each $\widetilde{R_j}$, with the help of Inequality (7.10) and the fact that $\nabla_\Gamma \boldsymbol{u}\, \mathrm{P} = \nabla_\Gamma \boldsymbol{u}$, one can estimate $\widetilde{R_1}$ and $\widetilde{R_2}$ as follows,

$$\begin{aligned}
\widetilde{R_1} &= \left| \int_\Gamma \mathrm{Tr}\Big(\nabla_\Gamma \boldsymbol{u} \left(\mathcal{D}_h^\ell - \mathrm{P} \right) \Big) \mathrm{Tr}\Big(\nabla_\Gamma \boldsymbol{v}\, \mathcal{D}_h^\ell \Big) \frac{1}{J_b^\ell} \, \mathrm{d}s \right| \leq ch^r \|\nabla_\Gamma \boldsymbol{u}\|_{\mathbf{L}^2(\Gamma)} \|\nabla_\Gamma \boldsymbol{v}\|_{\mathbf{L}^2(\Gamma)}, \\
\widetilde{R_2} &= \left| \int_\Gamma \mathrm{Tr}(\nabla_\Gamma \boldsymbol{u}) \, \mathrm{Tr}\Big(\nabla_\Gamma \boldsymbol{v} \left(\mathcal{D}_h^\ell - \mathrm{P} \right) \Big) \frac{1}{J_b^\ell} \, \mathrm{d}s \right| \leq ch^r \|\nabla_\Gamma \boldsymbol{u}\|_{\mathbf{L}^2(\Gamma)} \|\nabla_\Gamma \boldsymbol{v}\|_{\mathbf{L}^2(\Gamma)}.
\end{aligned}$$

To estimate $\widetilde{R_3}$, Inequality (3.11) is applied as follows,

$$\widetilde{R_3} = \left| \int_\Gamma \mathrm{Tr}(\nabla_\Gamma \boldsymbol{u}) \, \mathrm{Tr}(\nabla_\Gamma \boldsymbol{v}) \left(\frac{1}{J_b^\ell} - 1 \right) \mathrm{d}s \right| \leq ch^{r+1} \|\nabla_\Gamma \boldsymbol{u}\|_{\mathbf{L}^2(\Gamma)} \|\nabla_\Gamma \boldsymbol{v}\|_{\mathbf{L}^2(\Gamma)}.$$

Summing up the latter terms, we get, $a_7(\boldsymbol{u}, \boldsymbol{v}) \leq ch^r \|\nabla_\Gamma \boldsymbol{u}\|_{\mathbf{L}^2(\Gamma)} \|\nabla_\Gamma \boldsymbol{v}\|_{\mathbf{L}^2(\Gamma)}$.

To conclude, Inequality (7.14) is easy to obtain when summing up a_i, for all $i = 1, \ldots, 7$, since $\alpha, \beta, \mu_\Omega, \mu_\Gamma, \lambda_\Omega, \lambda_\Gamma$ are mesh independent constants. □

Remark 7.3.5. *Keeping in mind that $\boldsymbol{u}$ and $\boldsymbol{u}_h$ are respectively the solutions of* (7.2) *and of* (7.5)*, we point out that, for a sufficiently small h, the lift of $\boldsymbol{u}_h$ denoted $\boldsymbol{u}_h^\ell$ satisfies the following inequality,*

$$\|\boldsymbol{u}_h^\ell\|_{\mathbf{H}_{(\Omega,\Gamma)}} \leq c \|\boldsymbol{u}\|_{\mathbf{H}_{(\Omega,\Gamma)}}, \tag{7.15}$$

where the constant $c > 0$ is independent of h.

Indeed, a relatively easy way to prove Inequality (7.15) *is by using the geometric error estimation* (7.14)*. To begin with, since the bilinear form a is coercive with respect to the $\mathbf{H}_{(\Omega,\Gamma)}$ norm (see [26]), we have,*

$$c_c\|\boldsymbol{u}_h^\ell\|^2_{\mathbf{H}_{(\Omega,\Gamma)}} \leq a(\boldsymbol{u}_h^\ell, \boldsymbol{u}_h^\ell) \leq a(\boldsymbol{u}_h^\ell, \boldsymbol{u}_h^\ell) - a(\boldsymbol{u}, \boldsymbol{u}_h^\ell) + a(\boldsymbol{u}, \boldsymbol{u}_h^\ell),$$

where c_c denotes the coercivity constant. Using Equality (7.6)*, we get,*

$$c_c\|\boldsymbol{u}_h^\ell\|^2_{\mathbf{H}_{(\Omega,\Gamma)}} \leq a(\boldsymbol{u}_h^\ell, \boldsymbol{u}_h^\ell) - a_h^\ell(\boldsymbol{u}_h^\ell, \boldsymbol{u}_h^\ell) + a(\boldsymbol{u}, \boldsymbol{u}_h^\ell) = (a - a_h^\ell)(\boldsymbol{u}_h^\ell, \boldsymbol{u}_h^\ell) + a(\boldsymbol{u}, \boldsymbol{u}_h^\ell).$$

Then we apply the geometric error estimation (7.14) *along with the continuity of a with respect to the $\mathbf{H}_{(\Omega,\Gamma)}$-norm as follows,*

$$\begin{aligned}\|\boldsymbol{u}_h^\ell\|^2_{\mathbf{H}_{(\Omega,\Gamma)}} &\leq ch^r\|\nabla\boldsymbol{u}_h^\ell\|^2_{\mathrm{L}^2(B_h^\ell)} + ch^r\|\boldsymbol{u}_h^\ell\|^2_{\mathbf{H}^1(\Gamma)} + c\|\boldsymbol{u}\|_{\mathbf{H}_{(\Omega,\Gamma)}}\|\boldsymbol{u}_h^\ell\|_{\mathbf{H}_{(\Omega,\Gamma)}} \\ &\leq ch^r\|\boldsymbol{u}_h^\ell\|^2_{\mathbf{H}_{(\Omega,\Gamma)}} + c\|\boldsymbol{u}\|_{\mathbf{H}_{(\Omega,\Gamma)}}\|\boldsymbol{u}_h^\ell\|_{\mathbf{H}_{(\Omega,\Gamma)}},\end{aligned}$$

where in the latter inequality, the equivalence between the $\mathbf{H}_{(\Omega,\Gamma)}$-norm and the $\mathbf{H}^1(\Omega,\Gamma)$-norm in Inequality (1.15) *is employed. Thus, we have,*

$$(1 - ch^r)\|\boldsymbol{u}_h^\ell\|^2_{\mathbf{H}_{(\Omega,\Gamma)}} \leq c\|\boldsymbol{u}\|_{\mathbf{H}_{(\Omega,\Gamma)}}\|\boldsymbol{u}_h^\ell\|_{\mathbf{H}_{(\Omega,\Gamma)}}.$$

For a sufficiently small h, we have $1 - ch^r \geq \epsilon$, for a given $\epsilon > 0$, which concludes the proof.

7.3.2 Proof of the $\mathbf{H}_{(\Omega,\Gamma)}$ error bound in Theorem 7.3.2

To begin with, we need to notice that the error $\|\boldsymbol{u} - \boldsymbol{u}_h^\ell\|_{\mathbf{H}_{(\Omega,\Gamma)}}$ can be separated as follows using the interpolation operator $\boldsymbol{I}^{\boldsymbol{\ell}}$,

$$\|\boldsymbol{u} - \boldsymbol{u}_h^\ell\|_{\mathbf{H}_{(\Omega,\Gamma)}} \leq \|\boldsymbol{u} - \boldsymbol{I}^{\boldsymbol{\ell}}\boldsymbol{u}\|_{\mathbf{H}_{(\Omega,\Gamma)}} + \|\boldsymbol{I}^{\boldsymbol{\ell}}\boldsymbol{u} - \boldsymbol{u}_h^\ell\|_{\mathbf{H}_{(\Omega,\Gamma)}}. \tag{7.16}$$

We proceed by bounding each term separately.

The first term can be bounded using the interpolation inequality given in Proposi-

tion 4.1.3 while using the norm equivalence in (1.15) as follows,

$$\|\boldsymbol{u} - \boldsymbol{I}^{\ell}\boldsymbol{u}\|_{\mathbf{H}_{(\Omega,\Gamma)}} \leq c\|\boldsymbol{u} - \boldsymbol{I}^{\ell}\boldsymbol{u}\|_{\mathbf{H}^1(\Omega,\Gamma)} \leq ch^k\|\boldsymbol{u}\|_{\mathbf{H}^{k+1}(\Omega,\Gamma)}. \tag{7.17}$$

Afterwards, we proceed by bounding the remaining term. Since the bilinear form a is coercive with respect to the norm of $\mathbf{H}_{(\Omega,\Gamma)}$, denoting c_c as the coercivity constant, we have,

$$\begin{aligned} c_c\|\boldsymbol{I}^{\ell}\boldsymbol{u} - \boldsymbol{u}_h^{\ell}\|^2_{\mathbf{H}_{(\Omega,\Gamma)}} &\leq a(\boldsymbol{I}^{\ell}\boldsymbol{u} - \boldsymbol{u}_h^{\ell}, \boldsymbol{I}^{\ell}\boldsymbol{u} - \boldsymbol{u}_h^{\ell}) = a(\boldsymbol{I}^{\ell}\boldsymbol{u}, \boldsymbol{I}^{\ell}\boldsymbol{u} - \boldsymbol{u}_h^{\ell}) - a(\boldsymbol{u}_h^{\ell}, \boldsymbol{I}^{\ell}\boldsymbol{u} - \boldsymbol{u}_h^{\ell}) \\ &= a(\boldsymbol{I}^{\ell}\boldsymbol{u} - \boldsymbol{u}, \boldsymbol{I}^{\ell}\boldsymbol{u} - \boldsymbol{u}_h^{\ell}) + a(\boldsymbol{u}, \boldsymbol{I}^{\ell}\boldsymbol{u} - \boldsymbol{u}_h^{\ell}) - a(\boldsymbol{u}_h^{\ell}, \boldsymbol{I}^{\ell}\boldsymbol{u} - \boldsymbol{u}_h^{\ell}), \end{aligned}$$

where in the latter equation, we added and subtracted $a(\boldsymbol{u}, \boldsymbol{I}^{\ell}\boldsymbol{u} - \boldsymbol{u}_h^{\ell})$. Afterwards, we apply Equation (7.6), for $\boldsymbol{v} = \boldsymbol{I}^{\ell}\boldsymbol{u} - \boldsymbol{u}_h^{\ell} \in \boldsymbol{V}_h^{\ell}$,

$$c_c\|\boldsymbol{I}^{\ell}\boldsymbol{u} - \boldsymbol{u}_h^{\ell}\|^2_{\mathbf{H}_{(\Omega,\Gamma)}} \leq |a(\boldsymbol{I}^{\ell}\boldsymbol{u} - \boldsymbol{u}, \boldsymbol{I}^{\ell}\boldsymbol{u} - \boldsymbol{u}_h^{\ell})| + \Big|a_h^{\ell} - a\Big|(\boldsymbol{u}_h^{\ell}, \boldsymbol{I}^{\ell}\boldsymbol{u} - \boldsymbol{u}_h^{\ell}).$$

Taking advantage of the continuity of a and the geometric estimate (7.14), we obtain,

$$\begin{aligned} &c_c\|\boldsymbol{I}^{\ell}\boldsymbol{u} - \boldsymbol{u}_h^{\ell}\|^2_{\mathbf{H}_{(\Omega,\Gamma)}} \\ &\quad\leq c\Big(h^r\|\nabla\boldsymbol{u}_h^{\ell}\|_{\mathbf{L}^2(B_h^{\ell})}\|\nabla(\boldsymbol{I}^{\ell}\boldsymbol{u} - \boldsymbol{u}_h^{\ell})\|_{\mathbf{L}^2(B_h^{\ell})} + h^r\|\boldsymbol{u}_h^{\ell}\|_{\mathbf{H}^1(\Gamma)}\|\boldsymbol{I}^{\ell}\boldsymbol{u} - \boldsymbol{u}_h^{\ell}\|_{\mathbf{H}^1(\Gamma)}\Big) \\ &\qquad\quad + c_{cont}\|\boldsymbol{I}^{\ell}\boldsymbol{u} - \boldsymbol{u}\|_{\mathbf{H}_{(\Omega,\Gamma)}}\|\boldsymbol{I}^{\ell}\boldsymbol{u} - \boldsymbol{u}_h^{\ell}\|_{\mathbf{H}_{(\Omega,\Gamma)}} \\ &\quad\leq c\Big(h^r\|\nabla\boldsymbol{u}_h^{\ell}\|_{\mathbf{L}^2(B_h^{\ell})} + h^r\|\boldsymbol{u}_h^{\ell}\|_{\mathbf{H}^1(\Gamma)} + \|\boldsymbol{I}^{\ell}\boldsymbol{u} - \boldsymbol{u}\|_{\mathbf{H}_{(\Omega,\Gamma)}}\Big)\|\boldsymbol{I}^{\ell}\boldsymbol{u} - \boldsymbol{u}_h^{\ell}\|_{\mathbf{H}_{(\Omega,\Gamma)}}, \end{aligned}$$

where we used the norm equivalence in (1.15). Then, dividing by $\|\boldsymbol{I}^{\ell}\boldsymbol{u} - \boldsymbol{u}_h^{\ell}\|_{\mathbf{H}_{(\Omega,\Gamma)}}$, we have,

$$\|\boldsymbol{I}^{\ell}\boldsymbol{u} - \boldsymbol{u}_h^{\ell}\|_{\mathbf{H}_{(\Omega,\Gamma)}} \leq c\Big(h^r\|\nabla\boldsymbol{u}_h^{\ell}\|_{\mathbf{L}^2(B_h^{\ell})} + h^r\|\boldsymbol{u}_h^{\ell}\|_{\mathbf{H}^1(\Gamma)} + \|\boldsymbol{I}^{\ell}\boldsymbol{u} - \boldsymbol{u}\|_{\mathbf{H}_{(\Omega,\Gamma)}}\Big). \tag{7.18}$$

To conclude, we replace Inequality (7.18) in the error estimation (7.16) as follows,

$$\|\boldsymbol{u} - \boldsymbol{u}_h^{\ell}\|_{\mathbf{H}_{(\Omega,\Gamma)}} \leq c\Big(h^r\|\nabla\boldsymbol{u}_h^{\ell}\|_{\mathbf{L}^2(B_h^{\ell})} + h^r\|\boldsymbol{u}_h^{\ell}\|_{\mathbf{H}^1(\Gamma)} + \|\boldsymbol{u} - \boldsymbol{I}^{\ell}\boldsymbol{u}\|_{\mathbf{H}_{(\Omega,\Gamma)}}\Big).$$

Lastly, applying (7.17) and (1.15), we arrive at,

$$\|\boldsymbol{u} - \boldsymbol{u}_h^{\ell}\|_{\mathbf{H}_{(\Omega,\Gamma)}} \leq c\left(h^r\|\boldsymbol{u}_h^{\ell}\|_{\mathbf{H}_{(\Omega,\Gamma)}} + h^k\|\boldsymbol{u}\|_{\mathbf{H}^{k+1}(\Omega,\Gamma)}\right).$$

This provides the desired result using Inequality (7.15).

7.3.3 Proof of the L^2 error bound in Theorem 7.3.2

To estimate the $\mathbf{L}^2$ norm of the error, we define the functional F_h by,

$$\begin{aligned} F_h : \ \mathbf{H}_{(\Omega,\Gamma)} &\longrightarrow \mathbb{R} \\ \boldsymbol{v} &\longmapsto F_h(\boldsymbol{v}) = a(\boldsymbol{u} - \boldsymbol{u}_h^\ell, \boldsymbol{v}). \end{aligned}$$

We begin by bounding $|F_h(\boldsymbol{v})|$ for any $\boldsymbol{v} \in \mathbf{H}^2(\Omega, \Gamma)$ in Lemma 7.3.6. Afterwards an Aubin-Nitsche argument is applied in order to prove the $\mathbf{L}^2$ error estimation (7.8), while following the same strategy used in the scalar case in Chapter 5.

Lemma 7.3.6. *For a sufficiently small h, there exists a mesh independent constant $c > 0$ such that the following inequality holds for any $\boldsymbol{v} \in \mathbf{H}^2(\Omega, \Gamma)$,*

$$|F_h(\boldsymbol{v})| \leq c(h^{k+1} + h^r)\|\boldsymbol{v}\|_{\mathbf{H}^2(\Omega,\Gamma)}. \tag{7.19}$$

We start by summarizing the essential ingredients to prove this lemma. The interpolation inequality in Proposition 4.1.3 implies that,

$$\|\boldsymbol{I}^\ell \boldsymbol{v} - \boldsymbol{v}\|_{\mathbf{H}^1(\Omega,\Gamma)} \leq ch\|\boldsymbol{v}\|_{\mathbf{H}^2(\Omega,\Gamma)}, \quad \forall\, \boldsymbol{v} \in \mathbf{H}^2(\Omega, \Gamma). \tag{7.20}$$

Moreover, applying Equality (7.6) for $\boldsymbol{I}^\ell \boldsymbol{v} \in \boldsymbol{V}_h^\ell$, we have,

$$a(\boldsymbol{u}, \boldsymbol{I}^\ell \boldsymbol{v}) = l(\boldsymbol{I}^\ell \boldsymbol{v}) = a_h^\ell(\boldsymbol{u}_h^\ell, \boldsymbol{I}^\ell \boldsymbol{v}). \tag{7.21}$$

Proof of Lemma 7.3.6. Consider $\boldsymbol{v} \in \mathbf{H}^2(\Omega, \Gamma)$. To begin with, we decompose $|F_h(\boldsymbol{v})|$ in two terms as follows,

$$\begin{aligned} |F_h(\boldsymbol{v})| = |a(\boldsymbol{u} - \boldsymbol{u}_h^\ell, \boldsymbol{v})| &= |a(\boldsymbol{u} - \boldsymbol{u}_h^\ell, \boldsymbol{v}) + a(\boldsymbol{u} - \boldsymbol{u}_h^\ell, \boldsymbol{I}^\ell \boldsymbol{v}) - a(\boldsymbol{u} - \boldsymbol{u}_h^\ell, \boldsymbol{I}^\ell \boldsymbol{v})| \\ &\leq |a(\boldsymbol{u} - \boldsymbol{u}_h^\ell, \boldsymbol{v} - \boldsymbol{I}^\ell \boldsymbol{v})| + |a(\boldsymbol{u} - \boldsymbol{u}_h^\ell, \boldsymbol{I}^\ell \boldsymbol{v})| =: F_1 + F_2. \end{aligned}$$

Firstly, to bound F_1, we take advantage of the continuity of the bilinear form a with

respect to the norm $\|\cdot\|_{\mathbf{H}_{(\Omega,\Gamma)}}$ and apply the $\mathbf{H}_{(\Omega,\Gamma)}$ error estimation (7.8) as follows,

$$F_1 \leq c_{cont}\,\|\boldsymbol{u}-\boldsymbol{u}_h^\ell\|_{\mathbf{H}_{(\Omega,\Gamma)}}\|\boldsymbol{v}-\boldsymbol{I}^{\boldsymbol{\ell}}\boldsymbol{v}\|_{\mathbf{H}_{(\Omega,\Gamma)}} \leq c(h^k+h^r)\,h\|\boldsymbol{v}\|_{\mathbf{H}^2(\Omega,\Gamma)} \\ \leq c(h^{k+1}+h^{r+1})\,\|\boldsymbol{v}\|_{\mathbf{H}^2(\Omega,\Gamma)},$$

where we used the norm equivalence in Inequality (1.15) alongside Inequality (7.20).

Secondly, to estimate F_2, we notice that Equality (7.21) is applied with the geometric error estimation (7.14) as follows,

$$F_2 = |a(\boldsymbol{u},\boldsymbol{I}^{\boldsymbol{\ell}}\boldsymbol{v})-a(\boldsymbol{u}_h^\ell,\boldsymbol{I}^{\boldsymbol{\ell}}\boldsymbol{v})| = |a_h^\ell(\boldsymbol{u}_h^\ell,\boldsymbol{I}^{\boldsymbol{\ell}}\boldsymbol{v})-a(\boldsymbol{u}_h^\ell,\boldsymbol{I}^{\boldsymbol{\ell}}\boldsymbol{v})| = |(a_h^\ell-a)(\boldsymbol{u}_h^\ell,\boldsymbol{I}^{\boldsymbol{\ell}}\boldsymbol{v})| \\ \leq ch^r\|\nabla\boldsymbol{u}_h^\ell\|_{\mathbf{L}^2(B_h^\ell)}\|\nabla(\boldsymbol{I}^{\boldsymbol{\ell}}\boldsymbol{v})\|_{\mathbf{L}^2(B_h^\ell)} + ch^r\|\boldsymbol{u}_h^\ell\|_{\mathbf{H}^1(\Gamma)}\|\boldsymbol{I}^{\boldsymbol{\ell}}\boldsymbol{v}\|_{\mathbf{H}^1(\Gamma)}.$$

Moreover, using Inequality (4.7), which states that $\|\boldsymbol{I}^{\boldsymbol{\ell}}\boldsymbol{v}\|_{\mathbf{H}^1(\Omega,\Gamma)} \leq c\|\boldsymbol{v}\|_{\mathbf{H}^2(\Omega,\Gamma)}$, and by applying the norm equivalence (1.15), we get,

$$F_2 \leq ch^r\|\boldsymbol{u}_h^\ell\|_{\mathbf{H}_{(\Omega,\Gamma)}}\|\boldsymbol{v}\|_{\mathbf{H}^2(\Omega,\Gamma)} \leq ch^r\|\boldsymbol{u}\|_{\mathbf{H}_{(\Omega,\Gamma)}}\|\boldsymbol{v}\|_{\mathbf{H}^2(\Omega,\Gamma)},$$

where we also used Inequality (7.15).

We conclude the proof by summing the estimates of F_1 and F_2. □

Proof of the $\mathbf{L}^2$ ***estimate*** (7.8)**.** Defining $\mathbf{e} := \boldsymbol{u}-\boldsymbol{u}_h^\ell \in \mathbf{H}_{(\Omega,\Gamma)}$, we aim to estimate the $\mathbf{L}^2$ error norm: $\|\mathbf{e}\|^2_{\mathbf{L}^2(\Omega,\Gamma)} = \|\boldsymbol{u}-\boldsymbol{u}_h^\ell\|^2_{\mathbf{L}^2(\Omega)} + \|\boldsymbol{u}-\boldsymbol{u}_h^\ell\|^2_{\mathbf{L}^2(\Gamma)}$. In order to do that, an Aubin–Nitsche duality argument is used. We apply Theorem 1.2.3 for $\boldsymbol{f}=\mathbf{e}$ and $\boldsymbol{g}=\mathbf{e}_{|\Gamma}$ as follows: there exists a unique solution $\mathbf{z_e} \in \mathbf{H}_{(\Omega,\Gamma)}$ to Problem (7.2). By the regularity assumptions considered, $\mathbf{z_e}$ satisfies Inequality (7.7) as follows,

$$\|\mathbf{z_e}\|_{\mathbf{H}^2(\Omega,\Gamma)} \leq c\|\mathbf{e}\|_{\mathbf{L}^2(\Omega,\Gamma)}. \tag{7.22}$$

Notice that,

$$\|\mathbf{e}\|^2_{\mathbf{L}^2(\Omega,\Gamma)} = a(\mathbf{e},\mathbf{z_e}) = |F_h(\mathbf{z_e})|.$$

Applying Inequality (7.19) and Inequality (7.22), we have,

$$\|\mathbf{e}\|^2_{\mathbf{L}^2(\Omega,\Gamma)} \leq c(h^{k+1}+h^r)\|\mathbf{z_e}\|_{\mathbf{H}^2(\Omega,\Gamma)} \leq c(h^{k+1}+h^r)\|\mathbf{e}\|_{\mathbf{L}^2(\Omega,\Gamma)},$$

which concludes the proof.

□

7.4 Supplementary theoretical observations

Throughout this chapter, in the error estimates (7.8), we obtain convergence rates for the $\mathbf{H}_{(\Omega,\Gamma)}$ norm (resp. $\mathbf{L}^2$ norm) of the error equal to $\min\{k, r\}$ (resp. $\min\{k+1, r\}$). In Chapter 5, we have studied the analogous scalar problem and the convergence rates of the error that we have obtained in (5.5) are respectively equal to $\min\{k, r + 1/2\}$ and $\min\{k + 1, r + 1\}$ for the H^1 and L^2 errors in the scalar case. Thus a loss in the convergence rates of the geometric error is observed in the present vector case.

An intuition in order to improve the error estimates in (7.8) is to improve the estimates (7.9) and (7.10) as follows,

$$\|\mathcal{D}_h^\ell - \mathrm{P}\|_{\mathrm{L}^\infty(\Gamma)} \leq ch^{r+1}, \quad \text{and} \quad \|\mathrm{P}_h^\ell - \mathrm{P}\|_{\mathrm{L}^\infty(\Gamma)} \leq ch^{r+1}. \tag{7.23}$$

We underline that having these two inequalities instead of (7.9) and (7.10) is sufficient to obtain the following geometric error estimates (instead of (7.14)),

$$|a(\boldsymbol{u}, \boldsymbol{v}) - a_h^\ell(\boldsymbol{u}, \boldsymbol{v})| \leq ch^r \|\nabla \boldsymbol{u}\|_{\mathbf{L}^2(B_h^\ell)} \|\nabla \boldsymbol{v}\|_{\mathbf{L}^2(B_h^\ell)} + ch^{r+1} \|\boldsymbol{u}\|_{\mathbf{H}^1(\Gamma)} \|\boldsymbol{v}\|_{\mathbf{H}^1(\Gamma)}.$$

Consequently, following a similar error analysis pattern as in Chapter 5 while taking into account the elasticity related difficulties, the following error estimations could hold,

$$\|\boldsymbol{u} - \boldsymbol{u}_h^\ell\|_{\mathbf{H}_{(\Omega,\Gamma)}} \leq c(h^k + h^{r+1/2}) \quad \text{and} \quad \|\boldsymbol{u} - \boldsymbol{u}_h^\ell\|_{\mathbf{L}^2(\Omega,\Gamma)} \leq c(h^{k+1} + h^{r+1}). \tag{7.24}$$

However, obtaining the improved inequalities in (7.23) is not straightforward: it requires intricate estimates while dealing with the tensor product. We first noticed that if the left estimate in (7.23) holds so does the right one: to bound $\|\mathrm{P}_h^\ell - \mathrm{P}\|_{\mathrm{L}^\infty(\Gamma)}$, we started by estimating $\|\mathcal{D}_h^\ell - \mathrm{P}\|_{\mathrm{L}^\infty(\Gamma)}$. To begin with, we separate it into two terms,

$$\|\mathcal{D}_h^\ell - \mathrm{P}\|_{\mathrm{L}^\infty(\Gamma)} \leq \|\mathcal{D}_h^\ell \mathrm{P} - \mathrm{P}\|_{\mathrm{L}^\infty(\Gamma)} + \|\mathcal{D}_h^\ell (\mathbf{n} \otimes \mathbf{n})\|_{\mathrm{L}^\infty(\Gamma)}.$$

Then, we proceed to bound each term separately.

We are able to prove that the following inequality holds,

$$\|\mathcal{D}_h^\ell \mathrm{P} - \mathrm{P}\|_{\mathrm{L}^\infty(\Gamma)} \leq ch^{r+1},$$

while using Inequality (2.6) of [36] and Inequality (3.11).

The second term is quite complicated to bound due to all the tensor products that it puts forward. At best, we are only able to obtain the following inequality,

$$\|\mathcal{D}_h^\ell(\mathbf{n} \otimes \mathbf{n})\|_{\mathrm{L}^\infty(\Gamma)} \leq ch^r.$$

This inequality is not sufficient to obtain the desired results and needs to be further improved.

Notice that these improved error inequalities in (7.24) remain some speculations that we put forward following a comparison with the scalar case. However, the elasticity problem takes into account many more complex elements like the Hook tensors and the strain tensors in the volume and on the boundary. This makes the comparison between the results in Chapters 5 and 7 more difficult to support, but we are currently carrying out numerical experiments to estimate numerically the errors of the elasticity problem. After performing these simulations and analyzing the errors, we will be able to assess the optimality of the established error estimations presented in this chapter.

Remark 7.4.1. *It should be noted that obtaining the inequalities in* (7.23) *may not be possible in our case. Indeed these inequalities rely on the following estimation, which is proved in [36]:*

$$\|\mathbf{n} - \mathbf{n}_h^\ell\|_{\mathrm{L}^\infty(\Gamma)} \leq ch^r. \tag{7.25}$$

This bound forms the basis for two other estimates, as detailed in the proof of Proposition 7.3.3. Additionally, we computed $\|\mathbf{n} - \mathbf{n}_h^\ell\|_{\mathrm{L}^\infty(\Gamma)}$ *numerically and we observed that the estimate* (7.25) *is indeed optimal.*

Conclusion and perspectives

Accomplished work

This thesis is centered around the error analysis of partial differential equations with high-order boundary conditions: the Ventcel boundary conditions. In Chapter 1 are presented the three studied problems in this work: the Poisson-Ventcel problem, the spectral Ventcel problem and the linear elasticity problem with Ventcel boundary conditions.

These Ventcel boundary conditions, which contain the Laplace-Beltrami operator, are well defined if the boundary of the domain is assumed to be smooth. Hence, many difficulties arise from this regularity assumption since any mesh of the physical domain may not cover it exactly. Consequently a defect between the physical and the discrete domains emerges. To decrease this geometric error, curved meshes are employed and introduced in Chapter 2.

Another difficulty arises from this difference between the exact domain and the discrete domain. In order to compare between the exact solution of the continuous problems and the discrete finite element solutions, we define the lift operator in Chapter 3. Consequently, a function defined on the mesh domain can be lifted onto the physical one using this tool. Hence, we compute the difference between the exact solution and the lift of the discrete one, which are both defined on the same domain.

Afterwards in Chapter 4 is presented the Lagrangian finite element framework used to define the discrete problems. Additionally, we define the lifted finite element space with its associated lifted interpolation operator both in a scalar and vector case using the lift operator. The numerical setting is then presented putting forward the library CUMIN used all throughout this thesis. Preliminary computations intended to reproduce established results from the literature reveal two numerical behaviors:

— on quadratic meshes, the convergence rate of the error presents a super-convergence acting as if we are working on cubic meshes;

— on cubic meshes, a loss in the finite element interpolation convergence rate is observed.

These two phenomena are investigated in dedicated sections in Chapter 4 to better understand each one of them.

Chapters 5, 6 and 7 tackle the error analysis of each problem with Ventcel boundary conditions, while using curved meshes and the lift operator. As discussed in Chapter 5, we are able to assess the optimality of the theoretical error estimations obtained for the Poisson-Ventcel problem through the numerical simulations we present. In Chapter 6, the optimality of two theoretical estimates obtained, the H^1 eigenfunction error and the eigenvalue error, is highlighted through numerical computations. However, a sub-optimality is observed for the L^2 eigenfunction error and a conjecture is then formulated. Chapter 7 focuses on the establishment of theoretical error estimates for the linear elasticity problem, where we deal with the difficulties arising from the use of vector valued function and from the elasticity related terms.

To conclude, we briefly summarise the obtained results concerning the three studied problems in the following table:

Error analysis	Poisson-Ventcel	Spectral Ventcel	Linear elasticity with Ventcel
Theoretical	✓	✓	✓
Numerical	✓	✓	in progress

On going investigation

Error analysis. As explained in Section 7.4, we will attempt to improve the error estimates we obtained for the elasticity problem presented in Chapter 7. As indicated in the previous summary table, we started numerically estimating these errors. We are currently in the process of implementing the Ventcel boundary conditions within the context of linear elasticity equations in CUMIN to validate or guide further investigations into the estimates we have established.

As stated in the introduction of this work, an application objective is to optimize the spectral properties related to the elastic behavior of mechanical parts surrounded by specific thin layers. Hence, another intriguing problem not investigated in this thesis is the error analysis of the spectral linear elasticity problem with Ventcel boundary

conditions, defined as follows,

$$\begin{cases} -\mathrm{div}(\mathbf{A}_\Omega e(\boldsymbol{u})) = 0 & \text{in } \Omega, \\ -\beta \mathrm{div}_\Gamma(\mathbf{A}_\Gamma e_\Gamma(\boldsymbol{u})) + \mathbf{A}_\Omega e(\boldsymbol{u})\mathbf{n} + \alpha \boldsymbol{u} = \Lambda \boldsymbol{u} & \text{on } \Gamma. \end{cases} \tag{E1}$$

To estimate the errors of this problem, we intend to combine the techniques outlined in Chapter 6 on the spectral Ventcel problem in the scalar case and in Chapter 7, where we studied the linear elasticity problem with source terms.

We should also mention a more complex problem which consists of considering the time-dependant equations with Ventcel boundary conditions, incorporating the time variable as described in [64, 6, 67, 68].

Shape optimisation. Following the motivation behind this work, we aim to optimize the spectral properties of the elasticity problem with Ventcel boundary conditions (E1). A first step is to consider a shape optimisation problem for the spectral Ventcel problem in the scalar case on a nonempty bounded connected open domain Ω with a smooth boundary Γ given as follows,

$$\begin{cases} -\Delta u = 0 & \text{in } \Omega, \\ -\beta \Delta_\Gamma u + \partial_{\mathrm{n}} u = \lambda u & \text{on } \Gamma. \end{cases} \tag{E2}$$

In the following we denote λ_k the k^{th} eigenvalue associated to its corresponding normalized eigenfunction denoted by u_k.

Thus, we consider the shape optimisation problem under a fixed volume constraint C given as follows,

$$\max\{\lambda_k(\Omega), \Omega \subset \mathbb{R}^2 \text{ connected smooth}, |\Omega| = C\}. \tag{E3}$$

In order to numerically solve Problem (E3), we aim to perform a gradient method. Then we need to compute the shape gradient of the exact eigenvalue λ_k of Problem (E2). We refer to [3, 59, 74] for classical shape optimisation references. In [34, Theorem 1.4] is computed the shape gradient of the eigenvalue functional in an admissible perturbation direction V and it is given by,

$$\nabla \lambda_k(\Omega) \cdot V = \int_\Gamma V \cdot \mathbf{n}(|\nabla_\Gamma u_k|^2 - |\partial_{\mathrm{n}} u_k|^2 - \lambda_k \mathrm{H}|u_k|^2 + \beta(\mathrm{H}\mathrm{I}_d - 2\mathcal{H})\nabla_\Gamma u_k \cdot \nabla_\Gamma u_k)\mathrm{d}s, \tag{E4}$$

where,

— $\mathcal{H} = \mathrm{D}^2\mathrm{d}$ is the Hessian of the signed distance function d,

— H is the mean curvature on Γ,

— I_d is the identity matrix of size $d \times d$.

To begin with, we consider a two dimensional connected and star-shaped smooth domain denoted Ω. Then, a classical approach in order to tackle the shape optimisation problem (E3) through a gradient-based optimisation method is to consider the following parametrisation of the domain by polar coordinates:

$$(\rho(\theta), \theta) \in \mathbb{R}^+ \times [0, 2\pi[\ \rightarrow \ (\rho(\theta)\cos(2\pi\theta), \rho(\theta)\sin(2\pi\theta)) \in \mathbb{R}^2,$$

where the radial function $\rho : [0, 2\pi[\rightarrow \mathbb{R}^+$ is approximated by truncating its Fourier series to include $2n + 1$ coefficients:

$$\rho(\theta) = a_0 + \sum_{i=1}^{n} a_i \cos(i\theta) + b_i \sin(i\theta),$$

where $a_i, b_j \in \mathbb{R}$ for any $i = 0, \ldots, n$ and $j = 1, \ldots, n$ and where $n \in \mathbb{N}$. In Figure F1, is displayed an example of a parameterized domain with Fourier series. In this case, optimising the shape of Ω in the context of Problem (E3) amounts to optimising the Fourier coefficients a_i, b_j for $i = 0, \ldots, n$ and $j = 1, \ldots, n$. This kind of approach is well known and was used in [7, 70] for optimizing the eigenvalues of the Dirichlet Laplacian, in [2] in the case of the Steklov eigenvalues and also in [13] in the case of the Ventcel eigenvalues.

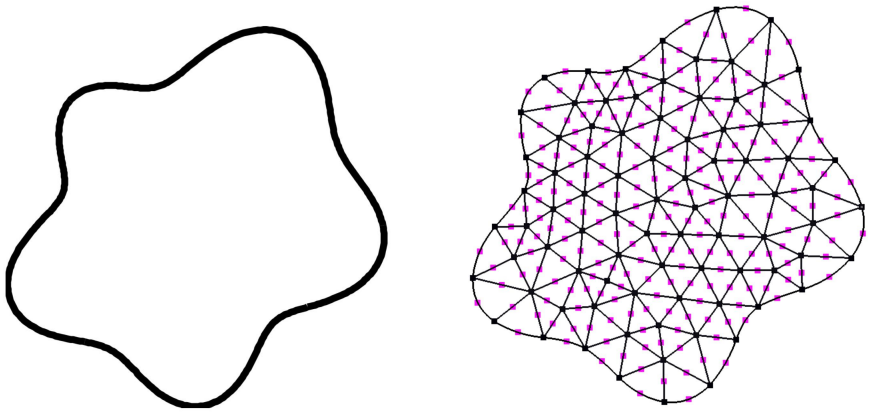

Figure F1 – Initial domain with Fourier coefficients equal to [1, 0.1, 0, 0, 0, 0.1, 0, 0.1, 0, 0, -0.1] (on the left) with its quadratic mesh domain (on the right).

In this setting, the shape derivative formula of $\lambda_k(\Omega)$ given in (E4) can be expressed component wise with respect to the Fourier coefficients as follows,

$$\frac{\partial \lambda_k}{\partial a_i} = \int_0^{2\pi} \Big(|\nabla_\Gamma u_k|^2 - |\partial_{\mathrm{n}} u_k|^2 - \lambda_k \mathrm{H} |u_k|^2 + \beta(\mathrm{HI}_d - 2\mathcal{H}) \nabla_\Gamma u_k \cdot \nabla_\Gamma u_k \Big) \rho(\theta) \cos(i\theta) \mathrm{d}\theta,$$

$$\frac{\partial \lambda_k}{\partial b_j} = \int_0^{2\pi} \Big(|\nabla_\Gamma u_k|^2 - |\partial_{\mathrm{n}} u_k|^2 - \lambda_k \mathrm{H} |u_k|^2 + \beta(\mathrm{HI}_d - 2\mathcal{H}) \nabla_\Gamma u_k \cdot \nabla_\Gamma u_k \Big) \rho(\theta) \sin(j\theta) \mathrm{d}\theta,$$

for all $i = 0, \dots, n$ and $j = 1, \dots, n$.

The perspectives concern the use of curved meshes in this shape optimisation context. As a first step, we start by considering the Steklov Problem (i.e. the case $\beta = 0$) replacing problem (E2) by,

$$\begin{cases} -\Delta u = 0 & \text{in } \Omega, \\ \partial_n u = \lambda u & \text{on } \Gamma, \end{cases} \tag{E5}$$

with the same eigenvalue maximization problem under volume constraint (E3). We consider the initial domain displayed in Figure F1, which is parameterized with Fourier coefficients such that its initial volume is equal to π.

The case of maximizing the Steklov eigenvalues under volume constraint has been recently studied in [13] where the author numerically obtained the optimal shapes maximising the five first non-zero eigenvalues of the Steklov Problem. These domains are displayed on the right hand side of Figure F2. In this context, we have first implement this shape optimisation process in Freefem++ (see [57]) obtaining similar results than in [13]. However, our objective is to use curved meshes to optimize the process: decreasing the computational time, while still conserving similar accuracy by working on higher order meshes. To accomplish this goal, I am currently implementing an optimisation module in CUMIN. We obtained first results concerning the optimisation problem (E3) for the Steklov problem, with the same initial domain than previously while using quadratic meshes. We display on the left hand side of Figure F2 the five final shapes obtained while respectively optimising the first five non-zero eigenvalues of the Steklov problem using CUMIN. We can then see a strong similarity in the optimal shapes obtained using curved meshes and the ones obtained by Bogosel in [13]. Furthermore, we highlight that the computational time is much less when using CUMIN with compared to Freefem++ that it is restricted to the use of affine meshes: when working with curved meshes we do not need as much discretization nodes with compared to the

affine case to approximate well the considered functional.

In the following table, we display the obtained maximized values of the first five non-zero eigenvalues of the optimisation Steklov problem (E3) using CUMIN on quadratic meshes having only 25 nodes on the boundary, with a total of 170 triangles. On the right of the table, are displayed the expected values in each case as presented in [13], where he used 300 discretization nodes.

	using CUMIN	expected values
λ_1	1.00	1.00
λ_2	1.64	1.64
λ_3	2.29	2.33
λ_4	2.94	2.97
λ_5	3.63	3.66

Table T1 – Final values of the first five non-zero eigenvalues of the optimisation Steklov problem (E3) using CUMIN and their expected values by Bogosel in [13].

We noticed an error when maximizing eigenvalues of rank $k \geq 3$, this might be due to the optimisation method. Since we considered a projected gradient algorithm, we will now explore other methods with adapted optimisation steps.

This acceleration in computation time will then make it possible to deal with problems having Ventcel boundary conditions (with $\beta \neq 0$), which takes more computational time due to the additional terms. We hope to finally be able to consider the vector case of linear elasticity equations, in 2D and 3D, in order to numerically optimise the associated eigenvalues.

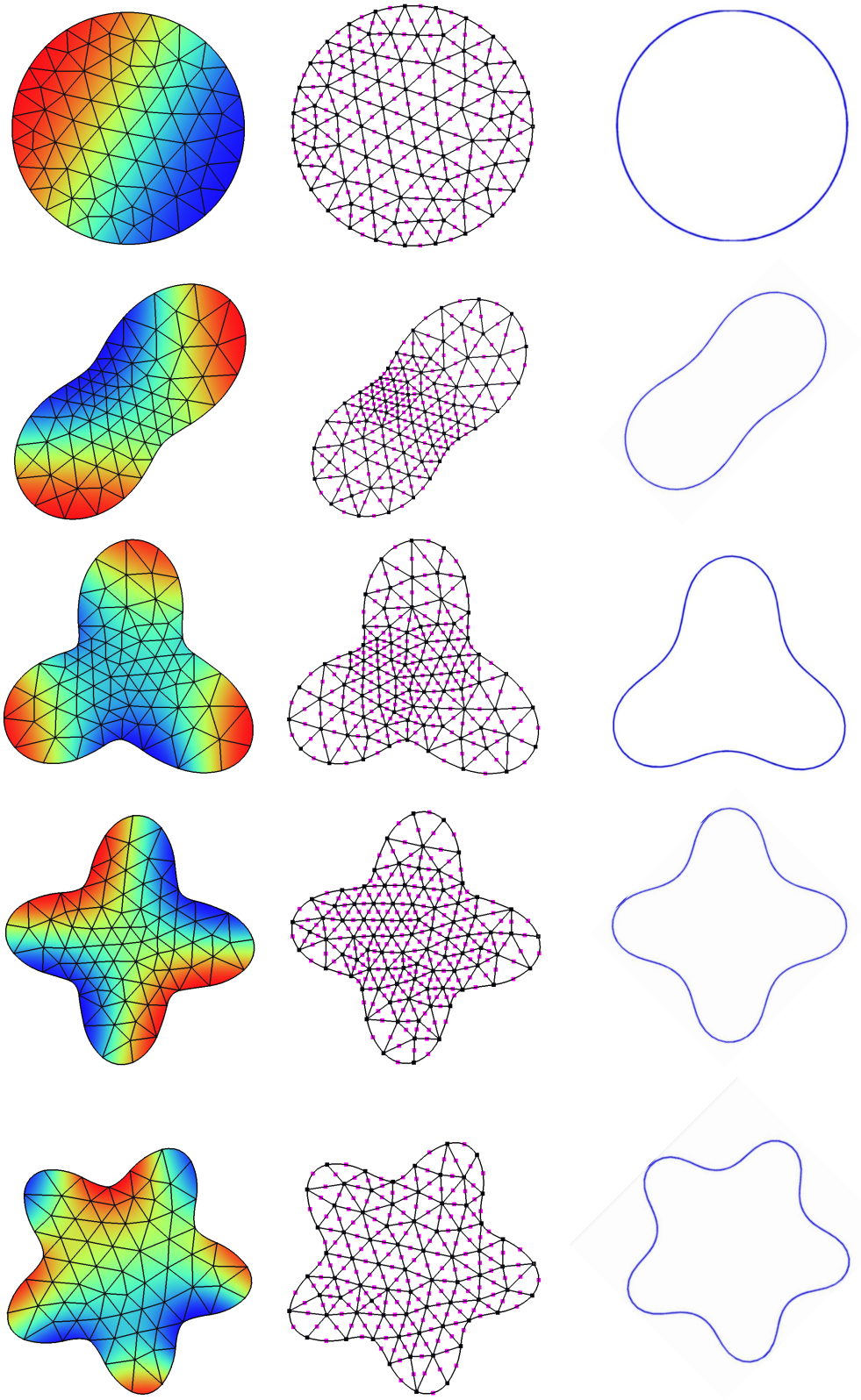

Figure F2 – Numerical maximizers for the first five non-zero Steklov eigenvalues under volume constraint: using CUMIN with quadratic meshes (on the left: the associated eigenfunctions; in the middle: the mesh of the optimal shapes) and the expected final shapes obtained in [13] (on the right).

BIBLIOGRAPHY

[1] M. Ainsworth and J. T. Oden. *A Posteriori Error Estimation in Finite Element Analysis*. John Wiley & Sons, 2000.

[2] E. Akhmetgaliyev, C.-Y. Kao, and B. Osting. Computational methods for extremal steklov problems. *SIAM Journal on Control and Optimization*, 55(2):1226–1240, 2017.

[3] G. Allaire. *Conception optimale de structures*. Springer Science & Business Media, 2007.

[4] G. Allaire. *Numerical analysis and optimization*. Numerical Mathematics and Scientific Computation. Oxford University Press, Oxford, 2007.

[5] A. B. Andreev and T. D. Todorov. Isoparametric finite-element approximation of a steklov eigenvalue problem. *IMA journal of numerical analysis*, 24(2):309–322, 2004.

[6] P. F. Antonietti, M. Grasselli, S. Stangalino, and M. Verani. Discontinuous galerkin approximation of linear parabolic problems with dynamic boundary conditions. *Journal of Scientific Computing*, 66:1260–1280, 2016.

[7] P. R. Antunes and P. Freitas. Numerical optimization of low eigenvalues of the dirichlet and neumann laplacians. *Journal of Optimization Theory and Applications*, 154:235–257, 2012.

[8] J. H. Argyris. Energy theorems and structural analysis: A generalized discourse with applications on energy principles of structural analysis including the effects of temperature and non-linear stress-strain relations. *Aircraft Eng. and Aerospace Tech.*, 1954.

[9] I. Babuska and J. E. Osborn. Estimates for the errors in eigenvalue and eigenvector approximation by Galerkin methods, with particular attention to the case of multiple eigenvalues. *SIAM J. Numer. Anal.*, 24(6):1249–1276, 1987.

[10] I. Babuska and J. E. Osborn. Finite element-Galerkin approximation of the eigenvalues and eigenvectors of selfadjoint problems. *Math. Comp.*, 52(186):275–297, 1989.

[11] U. Banerjee and J. E. Osborn. Estimation of the effect of numerical integration in finite element eigenvalue approximation. *Numer. Math.*, 56(8):735–762, 1990.

[12] C. Bernardi. Optimal finite-element interpolation on curved domains. *SIAM J. Numer. Anal.*, 26(5):1212–1240, 1989.

[13] B. Bogosel. The method of fundamental solutions applied to boundary eigenvalue problems. *J. Comput. Appl. Math.*, 306:265–285, 2016.

[14] A. Bonito, A. Demlow, and R. H. Nochetto. Finite element methods for the Laplace-Beltrami operator. In *Geometric partial differential equations. Part I*, volume 21 of *Handb. Numer. Anal.*, pages 1–103. 2019.

[15] A. Bonito, A. Demlow, and J. Owen. A priori error estimates for finite element approximations to eigenvalues and eigenfunctions of the Laplace-Beltrami operator. *SIAM J. Numer. Anal.*, 56(5):2963–2988, 2018.

[16] V. Bonnaillie-Noël, D. Brancherie, M. Dambrine, F. Hérau, S. Tordeux, and G. Vial. Multiscale expansion and numerical approximation for surface defects. In *CANUM 2010,* 40^{e} *Congrès National d'Analyse Numérique*, volume 33 of *ESAIM Proc.*, pages 22–35. EDP Sci., Les Ulis, 2011.

[17] V. Bonnaillie-Noël, M. Dambrine, F. Hérau, and G. Vial. On generalized ventcel's type boundary conditions for laplace operator in a bounded domain. *SIAM Journal on Mathematical Analysis*, 42(2):931–945, 2010.

[18] L. Bourgeois, N. Chaulet, and H. Haddar. On simultaneous identification of the shape and generalized impedance boundary condition in obstacle scattering. *SIAM J. Sci. Comput.*, 34(3):A1824–A1848, 2012.

[19] S. C. Brenner and L. R. Scott. *The mathematical theory of finite element methods*, volume 15 of *Texts in Applied Mathematics*. Springer-Verlag, New York, 1994.

[20] S. C. Brenner and L. R. Scott. The mathematical theory of finite element methods. 15:16,361, 2002.

[21] H. Brezis. *Functional Analysis, Sobolev Spaces and Partial Differential Equations*. Universitext. Springer, New York, 2010.

[22] C. Carstensen and J. Gedicke. An oscillation-free adaptive FEM for symmetric eigenvalue problems. *Numer. Math.*, 118(3):401–427, 2011.

[23] F. Caubet, J. Ghantous, and C. Pierre. Numerical study of a diffusion equation with ventcel boundary condition using curved meshes. *Monografías Matemáticas García de Galdeano*, 2023.

[24] F. Caubet, J. Ghantous, and C. Pierre. Finite element analysis of a spectral problem on curved meshes occurring in diffusion with high order boundary conditions. *(submitted)*, 2024.

[25] F. Caubet, J. Ghantous, and C. Pierre. A priori error estimates of a poisson equation with ventcel boundary conditions on curved meshes. *SIAM Journal on Numerical Analysis*, 62(4):1929–1955, 2024.

[26] F. Caubet, D. Kateb, and F. Le Louër. Shape sensitivity analysis for elastic structures with generalized impedance boundary conditions of the Wentzell type application to compliance minimization. *J. Elasticity*, 136(1):17–53, 2019.

[27] M. Cenanovic, P. Hansbo, and M. G. Larson. Cut finite element modeling of linear membranes. *Computer Methods in Applied Mechanics and Engineering*, 310:98–111, 2016.

[28] G. A. Chechkin, A. L. Piatnitski, and A. S. Shamaev. On generalized ventcel's type boundary conditions for laplace operator in a bounded domain. *Applicable Analysis*, 86(6):769–783, 2007.

[29] P. Ciarlet. *Mathematical Elasticity, Volume I: Three-Dimensional Elasticity*. Classics in applied mathematics. Society for Industrial and Applied Mathematics, 2022.

[30] P. Ciarlet and E. Luneville. *La méthode des éléments finis : de la théorie à la pratique . I . Concepts généraux*. ISTE Group, 2009.

[31] P. G. Ciarlet. Mathematical elasticity, vol iii, theory of shells. 2000.

[32] P. G. Ciarlet. *The finite element method for elliptic problems*, volume 40 of *Classics in Applied Mathematics*. Society for Industrial and Applied Mathematics (SIAM), Philadelphia, PA, 2002.

[33] P. G. Ciarlet and P.-A. Raviart. Interpolation theory over curved elements, with applications to finite element methods. *Comp. Meth. Appl. Mech. Eng.*, 1:217–249, 1972.

[34] M. Dambrine, D. Kateb, and J. Lamboley. An extremal eigenvalue problem for the Wentzell-Laplace operator. *Ann. Inst. H. Poincaré C Anal. Non Linéaire*, 33(2):409–450, 2016.

[35] C. Dapogny and P. Frey. Computation of the signed distance function to a discrete contour on adapted triangulation. *Calcolo*, 49(3):193–219, 2012.

[36] A. Demlow. Higher-order finite element methods and pointwise error estimates for elliptic problems on surfaces. *SIAM J. Numer. Anal.*, 47(2):805–827, 2009.

[37] A. Demlow and G. Dziuk. An adaptive finite element method for the Laplace-Beltrami operator on implicitly defined surfaces. *SIAM J. Numer. Anal.*, 45(1):421–442, 2007.

[38] F. Dubois. Discrete vector potential representation of a divergence-free vector field in three-dimensional domains: numerical analysis of a model problem. *SIAM J. Numer. Anal.*, 27(5):1103–1141, 1990.

[39] G. Duvaut. *Mécanique des milieux continus*. Éditions Dunod, 2001.

[40] G. Dziuk. Finite elements for the Beltrami operator on arbitrary surfaces. In *Partial differential equations and calculus of variations*, volume 1357 of *Lecture Notes in Math.*, pages 142–155. Springer, Berlin, 1988.

[41] G. Dziuk and C. M. Elliott. Finite element methods for surface PDEs. *Acta Numer.*, 22:289–396, 2013.

[42] D. Edelmann. Isoparametric finite element analysis of a generalized Robin boundary value problem on curved domains. *SMAI J. Comput. Math.*, 7:57–73, 2021.

[43] C. M. Elliott and T. Ranner. Finite element analysis for a coupled bulk-surface partial differential equation. *IMA J. Numer. Anal.*, 33(2):377–402, 2013.

[44] C. M. Elliott and T. Ranner. A unified theory for continuous-in-time evolving finite element space approximations to partial differential equations in evolving domains. *IMA Journal of Numerical Analysis*, 41(3):1696–1845, 2020.

[45] A. Ern and J.-L. Guermond. *Theory and practice of finite elements*, volume 159 of *Applied Mathematical Sciences*. Springer-Verlag, New York, 2004.

[46] L. C. Evans. *Partial differential equations*, volume 19 of *Graduate Studies in Mathematics*. American Mathematical Society, Providence, RI, 1998.

[47] K. Feng and Z.-C. Shi. *Mathematical theory of elastic structures*. Springer-Verlag, Berlin; Science Press Beijing, Beijing, 1996.

[48] D. Gallistl. An optimal adaptive FEM for eigenvalue clusters. *Numer. Math.*, 130(3):467–496, 2015.

[49] C. Geuzaine and J.-F. Remacle. *Gmsh Reference Manual*, 2024.

[50] S. Giani and I. G. Graham. A convergent adaptive method for elliptic eigenvalue problems. *SIAM J. Numer. Anal.*, 47(2):1067–1091, 2009.

[51] D. Gilbarg and N. S. Trudinger. *Elliptic partial differential equations of second order*. Classics in Mathematics. Springer-Verlag, Berlin, 2001. Reprint of the 1998 edition.

[52] G. R. Goldstein. Derivation and physical interpretation of general boundary conditions. *Adv. Differential Equations*, 11(4):457–480, 2006.

[53] P. Grisvard. *Elliptic problems in nonsmooth domains*, volume 69 of *Classics in Applied Mathematics*. Society for Industrial and Applied Mathematics (SIAM), Philadelphia, PA, 2011.

[54] H. Haddar. *Modèles asymptotiques en ferromagnétisme: couches minces et homogénéisation*. PhD thesis, Ecole des Ponts ParisTech, 2000.

[55] W. Han and B. Cockburn. *A Posteriori Error Analysis via Duality Theory: With Applications in Modeling and Numerical Approximations*. Advances in Mechanics and Mathematics. Springer, 2003.

[56] P. Hansbo and M. G. Larson. Finite element modeling of a linear membrane shell problem using tangential differential calculus. *Computer Methods in Applied Mechanics and Engineering*, 270:1–14, 2014.

[57] F. Hecht. New development in freefem++. *J. Numer. Math.*, 20(3-4):251–265, 2012.

[58] C.-J. Heine. *Isoparametric finite element approximation of curvature on hypersurfaces*. Citeseer, 2004.

[59] A. Henrot and M. Pierre. *Variation et optimisation de formes: une analyse géométrique*, volume 48. Springer Science & Business Media, 2006.

[60] T. J. Hughes. *The Finite Element Method: Linear Static and Dynamic Finite Element Analysis*. Dover Publications, 2000.

[61] C. Johnson. *Finite Element Methods: An Introduction*. Dover Publications, reprint of the 1987 edition edition, 2009.

[62] T. Kashiwabara, C. M. Colciago, L. Dedè, and A. Quarteroni. Well-posedness, regularity, and convergence analysis of the finite element approximation of a generalized Robin boundary value problem. *SIAM J. Numer. Anal.*, 53(1):105–126, 2015.

[63] A. V. Knyazev and J. E. Osborn. New a priori FEM error estimates for eigenvalues. *SIAM J. Numer. Anal.*, 43(6):2647–2667, 2006.

[64] B. Kovács and C. Lubich. Numerical analysis of parabolic problems with dynamic boundary conditions. *IMA J. Numer. Anal.*, 37(1):1–39, 2017.

[65] M. Lenoir. Optimal isoparametric finite elements and error estimates for domains involving curved boundaries. *SIAM J. Numer. Anal.*, 23(3):562–580, 1986.

[66] E. Luneville and J.-F. Mercier. Mathematical modeling of time-harmonic aeroacoustics with a generalized impedance boundary condition. *ESAIM Math. Model. Numer. Anal.*, 48(5):1529–1555, 2014.

[67] F. Nabet. Convergence of a finite-volume scheme for the cahn–hilliard equation with dynamic boundary conditions. *IMA Journal of Numerical Analysis*, 36(4):1898–1942, 2016.

[68] F. Nabet. An error estimate for a finite-volume scheme for the cahn–hilliard equation with dynamic boundary conditions. *Numerische Mathematik*, 149(1):185–226, 2021.

[69] J.-C. Nédélec. Curved finite element methods for the solution of singular integral equations on surfaces in R^3. *Comput. Methods Appl. Mech. Engrg.*, 8(1):61–80, 1976.

[70] B. Osting. Optimization of spectral functions of dirichlet–laplacian eigenvalues. *Journal of Computational Physics*, 229(22):8578–8590, 2010.

[71] C. Pierre. The finite element library Cumin, curved meshes in numerical simulations. *repository: https://plmlab.math.cnrs.fr/cpierre1/cumin*, hal-0393713(v1), 2023.

[72] Y. Saad. *Iterative Methods for Sparse Linear Systems: Second Edition*. Other Titles in Applied Mathematics. Society for Industrial and Applied Mathematics, 2003.

[73] R. Scott. Interpolated boundary conditions in the finite element method. *SIAM J. Numer. Anal.*, 12:404–427, 1975.

[74] J. Sokoowski and J.-P. Zolésio. Introduction to shape optimization: shape sensitivity analysis, 1992.

[75] A. D. Ventcel. Semigroups of operators that correspond to a generalized differential operator of second order. *Dokl. Akad. Nauk SSSR (N.S.)*, 111:269–272, 1956.

[76] A. D. Ventcel. On boundary conditions for multi-dimensional diffusion processes. *Theor. Probability Appl.*, 4:164–177, 1959.

[77] G. Vial. *Analyse asymptotique multi-échelle et conditions aux limites approchées pour un problème de couche mince dans un domaine à coin*. PhD thesis, Université Rennes 1, 2003.

[78] O. I. Yaman and F. L. Louer. An inverse parameter problem with generalized impedance boundary condition for two-dimensional linear viscoelasticity. *SIAM Journal on Applied Mathematics*, 81(4):1668–1690, 2021.

[79] O. C. Zienkiewicz, R. L. Taylor, and J. Z. Zhu. *The finite element method: its basis and fundamentals*. Elsevier, 2005.

[80] M. Zlámal. Curved elements in the finite element method. I. *SIAM J. Numer. Anal.*, 10:229–240, 1973.

[81] M. Zlámal. Curved elements in the finite element method. II. *SIAM J. Numer. Anal.*, 11:347–362, 1974.

UNIVERSITÉ DE PAU ET DES PAYS DE L'ADOUR

Titre : Prise en compte de conditions aux bords d'ordre élevé et analyse numérique de problèmes de diffusion sur maillages courbes à l'aide d'éléments finis d'ordre élevé.

Mot clés : Estimation d'erreur, conditions aux limites de Ventcel, maillages courbes, méthode des éléments finis, erreur géométrique, modèle d'élasticité, problème spectral.

Résumé : Cette thèse porte sur l'analyse numérique d'équations aux dérivées partielles impliquant des conditions de bord d'ordre élevé de type Ventcel en utilisant la méthode des éléments finis. Afin de définir l'opérateur de Laplace-Beltrami intervenant dans la condition au bord, le domaine est supposé lisse : ainsi le domaine maillé ne correspond pas au domaine physique initial, entrainant une *erreur géométrique*. Nous utilisons alors des maillages courbes afin de réduire cette erreur et définissons un *opérateur de lift* permettant de comparer la solution exacte définie sur le domaine initial et la solution approchée définie sur le domaine discrétisé. Nous obtenons alors des estimations d'erreur a priori, exprimées en termes d'erreur d'approximation par éléments finis et d'erreur géométrique. Nous étudions des problèmes avec termes sources et des problèmes spectraux ainsi que des équations scalaires et les équations vectorielles de l'élasticité linéaire. Des expériences numériques en 2D et 3D valident et complètent ces résultats théoriques, soulignant en particulier l'optimalité des erreurs obtenues. Ces simulations permettent également d'identifier une *super-convergence* des erreurs sur les maillages quadratiques.

Title: Consideration of high-order boundary conditions and numerical analysis of diffusion problems on curved meshes using high-order finite elements.

Keywords: Error estimation, Ventcel boundary conditions, curved meshes, finite element method, geometric error, elasticity model, spectral problem.

Abstract: This thesis focuses on the numerical analysis of partial differential equations involving high-order boundary conditions of the Ventcel type using the finite element method. To define the Laplace-Beltrami operator involved in the boundary condition, the domain is assumed to be smooth: thus, the meshed domain does not correspond to the initial physical domain, resulting in a *geometric error*. We then use curved meshes to reduce this error and define a *lift operator* that allows comparing the exact solution defined on the initial domain with the approximate solution defined on the discretized domain. We obtain a priori error estimates, expressed in terms of finite element approximation error and geometric error. We study problems with source terms and spectral problems, as well as scalar equations and vector equations of linear elasticity. Numerical experiments in 2D and 3D validate and complement these theoretical results, particularly highlighting the optimality of the obtained errors. These simulations also identify a *super-convergence* of the errors on quadratic meshes.